Horizontal vs. Vertical Tectonics: Analysis of Large-scale Structures Related to the Deformation History of the Archean Barberton Greenstone Belt

Dissertation

Zur Erlangung des akademischen Grades doctor rerum naturalium

(Dr. rer. nat.)

Vorgelegt dem Rat der Chemisch-Geowissenschaftlichen Fakultät der Friedrich-Schiller-Universität Jena

von M.Sc. (Geowissenschaften) Matthias Schmitz

geboren am 11.10.1988 in Ratingen

Gutachter:

1. Prof. Dr. Christoph Heubeck, Universität Jena
2. Prof. Dr. Kamil Ustaszewski, Universität Jena

Tag der Verteidigung: 10.07.2019

Selbstständigkeitserklärung

Ich erkläre, dass ich die vorliegende Arbeit selbstständig und unter Verwendung der angegebenen Hilfsmittel, persönlichen Mitteilungen und Quellen angefertigt habe.

Jena, den 09.12.2019

Table of Contents

Table of Contents i

List of Tables iv

List of Figures vi

List of Abbreviations vii

Zusammenfassung ix

Abstract 1

1 Introduction

1.1 Motivation 2

1.2 Onset of plate tectonics 3

2 Geological Setting

2.1 Kapvaal Craton 8

2.2 Barberton Granitoid-Greenstone Terrane 8

2.3 Stratigraphy 9

2.4 Structural Interpretations 12

3 Depth structure of the central Barberton Greenstone Belt from large-scale fold geometry

3.1 Introduction 20

3.2 Previous Investigations 21

3.2.1 Geological Setting 21

3.2.2 Fold Geometry 22

3.2.3 Ductile Strain 24

3.3 Methods 24

3.3.1 Field work 24

3.3.2 3D-modelling 28

3.4 Results 30

3.4.1 Stratigraphy and lithological units 30

3.4.2 Structures in Area 1 33

3.4.2.1 Regional fold structures 33

3.4.2.2 Faults 37

3.4.2.3 Subsurface data 37

3.4.2.4 3D Model 37

3.4.2.5 Paleocurrents 38

3.4.3 Structures in area 2 43

3.4.3.1 Regional fold structures 43

3.4.3.2 Faults 44

3.4.4 Summary of fold geometry 47

3.5 Discussion 47

3.5.1 Fold classification 47
3.5.2 Lithology control on fold style 48
3.5.3 Comparison between 3D model and 2D cross-section 50
3.5.4 Depth extent of folds 53
3.5.5 Synthesis 53
3.5.6 Quantification of the primary vertical extent of the folds 58 59
3.6 Conclusions 60
3.7 Acknowledgements 61
4 Structural geology and geochronology of the Malolotsha area, Eswatini, with implications on the deformation history and stratigraphy of the southwestern Barberton Greenstone Belt
4.1 Introduction 62
4.2 Geological framework 63
4.3 Methods 65
4.3.1 Geological mapping 65
4.3.2 Strain indicators 65
4.3.3 Radiometric age dating 67
4.4 Results 67
4.4.1 Lithological units 67
4.4.2 Structural units 72
4.4.2.1 Motjane Schist Belt 75
4.4.2.2 Ngwenya Syncline and subordinate folds 75
4.4.2.3 Malolotsha Syncline 80
4.4.2.4 Forbes Reef Anticline 80
4.4.3 Deformed conglomerate clasts 82
4.4.4 Results of age dating 82
4.5 Discussion 82
4.5.1 Structural evolution of the Ngwenya Syncline 82
4.5.2 Formation of the Malolotsha Syncline 87
4.5.2.1 Thrust complex 87
4.5.2.2 Stratigraphic continuity 87
4.5.2.3 Out-of-syncline thrusting 88
4.5.3 Relationship to adjacent granitoids and gneisses 90
4.6 Conclusions 92
4.7 Further research 92
4.8 Acknowledgments 92
5 Tectonic Evolution of the Barberton Granitoid-Greenstone Terrane – Integrating local studies into a regional model
5.1 Introduction 94
5.2 Geological framework 95
5.3 Suggested tectonic models 96
5.4 Methods 103
5.5 Results 103
5.5.1 Major lithostratigraphic units 103

5.5.2 Major folds 103
5.5.3 Major faults 116
5.5.4 Plutons and gneiss terranes 117
5.5.5 Contact relationships 118
5.5.6 Distribution of strain indicators 119
5.6 Structural domains 119
5.6.1 Subdivision into structural domains 119
5.6.2 Southwestern Domain 124
5.6.3 Southern Domain 127
5.6.4 Central Domain 127
5.6.5 Eastern Domain 131
5.6.6 Northern Domain 131
5.7 Discussion 135
5.7.1 Synthesis 135
5.7.2 Comparison of suggested tectonic models 137
5.8 Conclusions 139

Acknowledgments **141**

References **142**

Appendix

Appendix 1: Bedding planes 154
Appendix 2: Cleavage planes 162
Appendix 3: Fold axes 162
Appendix 4: Fold axial planes 163
Appendix 5: Foresets 164
Appendix 6: Deformed conglomerate clasts 165
Appendix 7: Orientation of major axes 167
Appendix 8: Results of U/Pb age dating 168
Appendix 9: Geological map of the BGGT 175

List of Figures

Figure 1.1 *Schematic sketch of the two principal different tectonic models* 3

Figure 1.2 G*eological features suggested to be indicative for the activity of plate tectonics* 4

Figure 1.3 *Th/Nb ratios of selected representative mafic rocks from Precambrian archives* 5

Figure 1.4 *Geodynamic models* 6

Figure 2.1 *Schematic map of the geology of the Kapvaal Craton* 9

Figure 2.2 *Overview map of the Barberton Granitoid-Greenstone Terrane* 10

Figure 2.3 *Principal tectonostratigraphic blocks in the Barberton Granite-Greenstone Terrain* 11

Figure 2.4 *Sketches of the suggested tectonic models* 15

Figure 2.5 *Comparison of deformation phases* 19

Figure 3.1 *Overview map of the Barberton Granitoid-Greenstone Terrane* 23

Figure 3.2 *Geometry suggested from surface geological mapping* 25

Figure 3.3 *Cross section of the Sheba Mine* 26

Figure 3.4 *Field photographs of the study area* 27

Figure 3.5 *Illustration of depth calculation* 29

Figure 3.6 *Field photographs of selected lithological* 32

Figure 3.7 *Geological map of study area 1* 34

Figure 3.8 *Structural map of study area 1* 36

Figure 3.9 *Detailed maps of hinge zones* 38

Figure 3.10 *Fold hinge geometry at Fairview Mine* 39

Figure 3.11 *3D model of area 1* 40

Figure 3.12 *Structurally restored paleocurrent orientations* 42

Figure 3.13 *Geological map of study area 2* 45

Figure 3.14 *Structural map of area 2* 46

Figure 3.15 *Fold geometry from surface data* 49

Figure 3.16 *Exposure of different structural levels of folds* 51

Figure 3.17 *Dependency between the depth of a synclines and the position of cross section* 52

Figure 3.18 *Illustrations of fold geometry implied from surface data* 54

Figure 3.19 *Illustrations of hypotheses addressing the unreasonable depth in 3D models* 56

Figure 3.20 *3D models of the hinge area of the Saddleback Syncline* 57

Figure 3.21 *Illustrations of hypotheses addressing the contradiction to geophysical data* 58

Figure 4.1 *Geological map of the BGB* *66*

Figure 4.2 *Field photograph of sampled outcrop* *71*

Figure 4.3 *Geological map of the southernmost BGB* *73*

Figure 4.4 *Field photographs* *74*

Figure 4.5 *Detailed Map of the Motjane Schist Belt* *76*

Figure 4.6 *Google Earth image of Ngwenya Syncline* *77*

Figure 4.7 *Detailed map of the Ngwenya Area* *78*

Figure 4.8 *Detailed Map of the Northern Ngwenya Syncline* *79*

Figure 4.9 *Detailed map of the Malolotsha Syncline* *81*

Figure 4.10 *Flinn diagrams of conglomerate clasts* *83*

Figure 4.11 *Simplified map of the study area* *84*

Figure 4.12 *Concordia diagram of sample 16-213* *85*

Figure 4.13 *Sketch showing the tectonic evolution of the Ngwenya area* *86*

Figure 4.14 *Comparison of three alternative cross sections of the Malolotsha area* *89*

Figure 4.15 *Semi-balanced cross-section of the Malolotsha Syncline* *90*

Figure 4.16 *Correlation of cross-sections drawn across the study area* *91*

Figure 5.1 *Overview map of the BGGT* *96*

Figure 5.2 *Sketches of suggested tectonic model and implied geometries* *99*

Figure 5.3 *Stereographic projections of structural features of the folds* *112*

Figure 5.4 *Map of plunge variability* *116*

Figure 5.5 *Structural elements of the BGGT* *120*

Figure 5.6 *Flinn diagrams showing strain distribution across the BGB* *122*

Figure 5.7 *Map showing distribution of strain indicators* *123*

Figure 5.8 *Subdivision of the BGB into five domains* *124*

Figure 5.9 *Stratigraphic units* *125*

Figure 5.10 *Map of the SW domain* *126*

Figure 5.11 *Map of the S domain* *128*

Figure 5.12 *Map of the C domain* *129*

Figure 5.13 *Map of the E domain* *132*

Figure 5.14 *Map of the N domain* *133*

List of Tables

Table 3.1 *Thickening factors derived from thickness variations* *48*

Table 3.2 *Quantification of possible depth reduction by suggested mechanisms* *59*

Table 3.3 *Exemplary calculation for a minimum and maximum depth for the depression* *60*

Table 4.1 *Measured length of conglomerate clasts* *68*

Table 5.1 *Map units of the study area* *104*

Table 5.2 *Summary of fold geometries* *105*

Table 5.3 *Plutons of the BGGT* *118*

Table 5.4 *Summary of clast axes ratios* *121*

List of Abbreviations

AGC	Ancient Gneiss Complex
AVF	Auber Villiers Fault
BGB	Barberton Greenstone Belt
BGGT	Barberton Granitoid-Greenstone Terrane
CD	Central Domain
ED	Eastern Domain
EMF	Eukalyptus Mill Fault
GGF	Granville Grove Fault
IF	Inyoka Fault
ISZ	Inyoni Shear Zone
KFZ	Kromberg Fault Zone
KSZ	Komati Shear Zone
KVT	Kaap Valley Tonalite
MF	Manhaar Fault
ND	Northern Domain
PCO	Partial Convective Overturn
SD	Southern Domain
SWD	Southwestern Domain
TTG	Tonalite, Trondhjemite, Granodiorite

Zusammenfassung

Die tektonischen Prozesse und die dafür verantwortlichen Kräfte und Mechanismen im Archaikum sowie der Zeitpunkt des Übergangs zur Plattentektonik im heutigen Sinne stellen eines der großen, nicht abschließend geklärten Fragestellung der frühen Erdgeschichte dar. Der Barberton Grünsteingürtel nimmt in dieser Debatte eine bedeutende Rolle ein, da er, zusammen mit der Pilbara Region in Australien, das wichtigste geologische Archiv des späten Paläoarchaikums (ca. 3,5 – 3,2 Ga) darstellt. In diesem Zeithorizont wird der Übergang von einem prä-plattentektonischen Szenario zur modernen Plattentektonik vermutet.

Die spezielle Geometrie des Barberton Grünsteingürtels zusammen mit seinem allgemeinen strukturellen Aufbau, insbesondere dem Faltungsstil, der stratigraphischen Abfolge und der Verteilung von Verformung innerhalb des Orogens, impliziert eine Entstehung durch tektonische Prozesse, die sich von heutiger Plattentektonik vor allem durch ausgeprägte vertikale Bewegungen anstelle von horizontaler Verkürzung unterscheidet.

Das spezielle Faltenmuster des zentralen Barberton Grünsteingürtels ist charakterisiert durch enge oder isoklinale Faltung von nordwestvergenten Synklinalen mit subvertikalen Schichtflächen und steil inwärts abtauchende Faltenachsen mit zwischenliegenden stark ausgedünnten oder kollabierten Antiklinalen und deutet eine deutlich größere Tiefenausdehnung der Falten an, als es irgendein plattentektonisches Szenario erklären könnte. Geophysikalische Untersuchungen, die eine deutlich geringere vertikale Ausdehnung des Grünsteingürtels implizieren, bilden vermutlich nur eine spätere Intrusion der Basis und nicht die ursprüngliche Geometrie des Barberton Grünsteingürtels ab.

Im Kern der Malolotsha Synklinale, die im Übrigen aus Gesteinen der jüngeren Moodies Gruppe aufgebaut ist, treten mächtige, alterierte, ultramafischer Vulkanite auf, die eigentlich nur aus der stratigraphisch ältesten Onverwacht Gruppe bekannt sind. Dies lässt sich entweder als tektonische Klippe durch eine großmaßstäbliche Überschiebung vor der Faltenbildung oder durch Heraushebung der älteren Onverwacht Gruppe entlang von steilgestellten Aufschiebungen mit entgegengesetztem Schersinn auf beiden Schenkeln der Falte erklären. Alternativ könnte die Abfolge ultramafischer Gesteine auch eine bisher unbekannte jüngere Einheit als die Moodies Gruppe darstellen, wie durch U/Pb-Datierung bestimmte Alter detritischer Zirkone aus verkieselten, felsischen, vulkanoklastischen Einheiten, die in die ultramafische Abfolge eingeschaltet sind, nahelegen. Für keine der genannten Hypothesen können jedoch alle Zweifel ausgeräumt werden.

Durch eine Zusammenstellung geologischer Daten aus dem gesamten Grünsteingürtel konnten wir seine komplexe und heterogene Deformationsgeschichte darstellen. Eine kritische Auseinandersetzung mit postulierten tektonischen Szenarios zeigt deutlich, dass keines dieser Szenarios unsere Daten widerspiegelt. Die räumliche und zeitliche Heterogenität der Deformation, das relative Absinken im Vergleich zu den umgebenden Plutonen sowie die insgesamt synklinale Struktur des Grünsteingürtels legen ein dynamisches, nicht plattentektonisches Szenario nahe, das durch vertikale Bewegung dominiert wurde. Lokale Subsidenz infolge von Faltung, Neigung und Absinken von mächtigen Grünsteinen von hoher Dichte in eine inkompetente granitische mittlere Kruste während partieller konvektiver Umwälzung bietet die beste Erklärung für die Rotation der gewaltigen Onverwacht Antiklinale, das charakteristische Faltenmuster und die räumlich und zeitlich heterogene Deformationsgeschichte des Barberton Grünsteingürtels.

Abstract

One of the major unresolved questions in Precambrian geology is the nature of tectonic processes during Earth's early history and the timing of the transition to modern-style plate tectonics. The Barberton Greenstone Belt (BGB) of South Africa and Eswatini features prominently in this discussion because it represents, along with the Pilbara region of Australia, the prime geological archive of the late Paleoarchean (ca. 3.5-3.2 Ga). This time period may mark the transition from a pre-plate tectonic setting to Phanerozoic-style plate tectonics.

The cuspate-lobate geometry of the BGB, together with its general structural make-up (defined by folding style, stratigraphic fill and strain distribution) appears to represent a non-actualistic Archean tectonic style characterized by vertical rather than horizontal displacements, as known from modern plate tectonics.

The distinctive folding pattern of the central BGB, characterized by tight or isoclinal, commonly northwestward verging synclines with subvertical bedding planes and steeply doubly-plunging fold axes with intervening thinned and faulted anticlines, implies a significantly larger vertical extent of the folds than suggested by any plausible plate-tectonic scenario. Geophysical data suggesting a shallow nature of the BGB may reflect subsequent intrusion of the BGB's base, not its initial geometry.

The presence of a thick succession of altered ultramafic volcanics, only known from the Onverwacht Group, in the core of the Malolotsha syncline, defined by the younger Moodies Group, either suggests major horizontal shortening by thrusting, resulting in a refolded klippe, or out-of-syncline-thrusting along (now vertical) reverse faults with opposing sense of displacement on both limbs. Alternatively, the ultramafic strata may represent a previously unknown stratigraphic unit postdating the Moodies Group, as suggested by limited U/Pb ages of detrital zircons derived from silicified felsic volcaniclastics interbedded with the ultramafic strata. Significant uncertainties remain for all three hypotheses.

A compilation of geological data from the entire greenstone belt demonstrates its heterogeneity and complex deformation history. A critical comparison of suggested tectonic settings to recent observations shows that no pure plate-tectonic scenarios are applicable. The temporal and spatial heterogeneity of deformation, the relative greenstone-down sense of shear along many of its contacts to the adjacent plutons, and the overall synclinal structure of the BGB emphasize a non-plate-tectonic setting dominated by vertical movements. Local subsidence due to folding, tilting and sagging of thick, dense greenstone regions into an incompetent granitoid middle crust during partial convective overturn plausibly explains the rotation of the enormous Onverwacht Anticline, the characteristic folding pattern and the temporally and spatially heterogeneous deformation history of the BGB.

1 Introduction

1.1 Motivation

During the Precambrian, the Earth differed significantly from its state in the Phanerozoic. The further we go back in Earth's history, the more pronounced many of these differences become. These include numerous environmental and biorelevant parameters, including atmospheric (Kasting, 1993; Catling et al., 2001; Tian et al., 2005; Lyons et al., 2014) and oceanic composition (Peck et al., 2001; Sleep, 2018), level of surface radiation (Pierson et al., 1993; Cockell & Horneck, 2001; Cnossen et al., 2007; Wassmann et al., 2010), fundamental material cycles (Sundquist & Broecker, 1985; Canfield & Raiswell, 1999; Canfield et al., 2000; Farquhar et al., 2000; Fischer et al., 2009), and the frequency and size of extraterrestrial impacts (Lowe & Byerly, 2018; Glikson & Pirajno, 2018). Although the last decades have seen significant progress in our understanding of the Earth's early history, the fragmentary nature of the geological record with age severly limits our knowledge.

One of the principal but poorly understood parameters in the workings of planet Earth is the rate and mechanism(s) of continental crust formation, represented by only very few well-preserved remnants of Archean crust. The presence of continental crust is crucial for many secondary parameters, such as material cycles, weathering, and nutrient delivery. It significantly affects the bio-, geo-, hydro-, and atmosphere (Chadwick et al., 1999; Goodwin, 2016). However, the timing of the onset of plate tectonics, which is the main continent-forming (and -destroying) process, at least since the Phanerozoic (van Kranendonk, 2011), is highly controversial (Shirey et al., 2008; Stern, 2008; Condie & Pease, 2009; van Kranendonk, 2010). While today the rate of growth and destruction of continental crust is balanced, there was a time of excess continental growth, principally by arc accretion and underplating between 3.0 and 2.7 Ga (Condie, 1986, 2000; Condie et al., 2011; Dhuime et al., 2012; Hawkesworth et al., 2013).

Authors opposing the existence of plate tectonics from the very beginning of our planet's history suggest a pre-plate tectonic regime based on a fixed or episodically mobile lithosphere, commonly referred to as "stagnant-lid" or "single-lid" (Reese et al., 1998; Dumoulin et al., 1999; Ernst, 2009; Debaille et al., 2013; Piper, 2013). Comparable to plate tectonics, these settings represent mechanisms of heat transfer from the hot interior to the colder exterior of the Earth, but in contrast to plate tectonics, which is largely based on thermal convection, pre-plate tectonic mechanisms transfer heat through a combination of conduction, mantle-plume focused magmatism, and periodic catastrophic overturn of the lithosphere (Solomatov & Moresi, 1997; Gerya, 2014; Bédard, 2018).

Most arguments relating to the activity of plate tectonics during the Archean are based on derived data and modelling assumptions, not on primary field data. The objective of this thesis is to add reliable and robust field data and first-hand interpretation of geological features to the debate. We chose the Barberton Greenstone Belt (BGB) in South Africa and Eswatini (former Swaziland) as the location of our field studies because this region represents one of the few well-preserved remnants of Paleoarchean lithosphere. Additionally, the BGB formed and was deformed between ca. 3.54 and 3.22 Ga, covering the most controversially discussed time period (see chapter 1.2). We investigated the large-scale structural geometry of the BGB, added data on the poorly investigated part of the BGB located in Eswatini, and re-examined the structural evolution of the entire BGB in order to compare it to suggested tectonic models. This approach is reflected in the structure of the thesis in its chapters 3, 4 and 5, respectively. Chapter 2 lays a foundation by providing an overview of the regional geology.

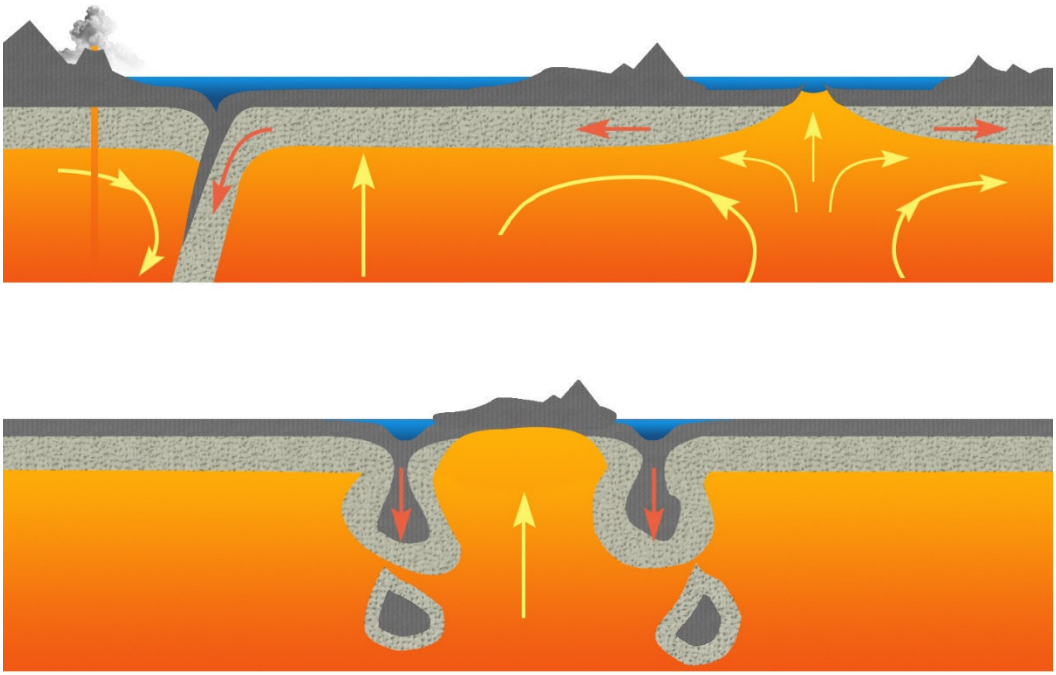

Fig. 1.1: Schematic sketch of the two principal different tectonic models applied to the early Earth in general and the BGB in particular. (a) Plate-tectonic setting, mainly driven by thermal convection with the formation of new crust at mid-oceanic ridges, horizontal movement of rigid plates and recycling of crustal material at subduction zones. (b) Pre-plate tectonic setting, mainly driven by contrast in temperature and consequently density and buoyancy of a cold lithosphere and an underlying hot asthenosphere, causing periodic overturns of the lithosphere back to the mantle.

1.2 Onset of plate tectonics

Pre-plate-tectonic hypotheses suggest that mantle temperatures, during the Earth's early history, were between 200-400° C higher than today (Polack, 1986; Martin, 1986; Kröner & Layer, 1992; Condie & Benn, 2006; Klein et al., 2017). This would result in a less dense, less viscous and less rigid lithosphere, which would be a poor conductor of stress (Moresi & Solomatov, 1998; Tackley, 1998). Only subsequent cooling of the Earth allowed rigid lithospheric plates with localized zones of high shear strain to form, marking the onset of plate tectonics. The onset of plate tectonic is defined by the appearance of structures and geometries, which rather reflect horizontally but vertically dominated movement. (Fig. 1.1). Thus, a common approach is the age dating and correlation of geological features characteristic of stable lithospheric plates, such as extensive sedimentary basins on stable cratons or large-scale brittle lithospheric deformation represented by rectilinear dike swarms (Cawood et al., 2018). These typically yield widely varying ages (Fig. 1.2).

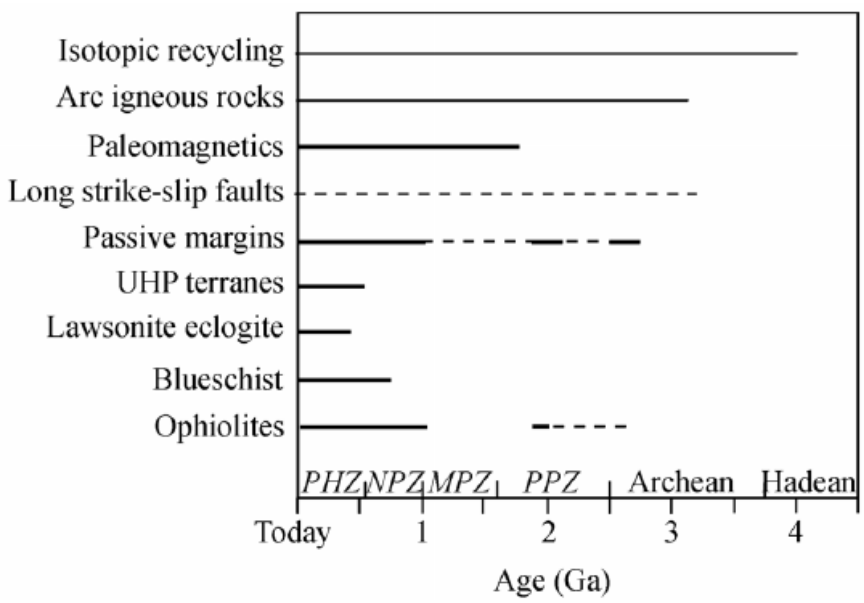

Fig. 1.2: Box diagram showing the occurrence of geological features suggested to be indicative for the activity of plate tectonics through time. PHZ= Phanerozoic, NPZ = Neoproterozoic, MPZ = Mesoproterozoic, PPZ = Paleoproterozoic. From Stern (2007).

Another approach to date the onset of plate tectonics is to use paleomagnetic data in order to constrain the movement of the lithosphere over time. Large variations in paleolatitude are not compatible with a pre-plate tectonic model. Cawood et al. (2006) and Evans & Pisarevsky (2008) analyzed paleomagnetic data from the Archean and Paleoproterozoic, concluding that plate tectonics was already active during that time due to the high variability in paleolatitude. However, their results remain doubtful, since some of the ages were later proven to be incorrect (Gumsley et al., 2017) or data were inconsistent with field observations by other authors (Layer et al., 1989). A follow-up study with a larger sample volume suggests that plate tectonics was active at least since the Neoarchean (Cawood et al., 2018).

A number of geochemical and petrological proxies can be used in order to identify a change in tectonic regime. Th/Nb ratios (Fig. 1.3) can be used as indicators of vertical or horizontal tectonic movement (Pearce, 2008) for the most important Archean and Paleoproterozoic locations. However, this diagram is inconclusive, since data points associated with vertical movements can be observed throughout. Furthermore, samples from the Pilbara Craton, which is widely accepted to have formed in a pre-plate tectonic setting (Collins et al., 1998), plots in the area associated with horizontal tectonic movement. Condie (2018) deployed a variety of geochemical proxies to conclude that the pre-plate tectonic setting changed to a modern style plate tectonic setting following a transitional period between 3 and 2 Ga. Van Kranendonk (2011) claims that plate tectonics commenced at 3 Ga due to eclogite inclusions in diamonds of that age, deducted from the common assumption, that eclogite is usually associated with subduction, a process directly linked to plate tectonics.

Another method to understand the mechanics and geometries of different geodynamic models, which has grown highly sophisticated in the past years, is geodynamical modelling. Modern linked geochemical-petrophysical models are not only able to reproduce geometries predicted by pre-plate tectonic hypothesis, but also able constrain the time at which the pre-plate tectonic regime switched to a modern-style plate tectonic regime. Such geodynamical models suggest ages from 3.2 to 2.5 for the onset of plate tectonics (Sizova et al., 2010; Laurent et al., 2014; Fischer & Gerya, 2016a, b). Geodynamical modelling can also be used to quantify the difference in heat flow that is required in order to change our modern tectonic regime to pre-plate tectonic setting (Fig. 1.4).

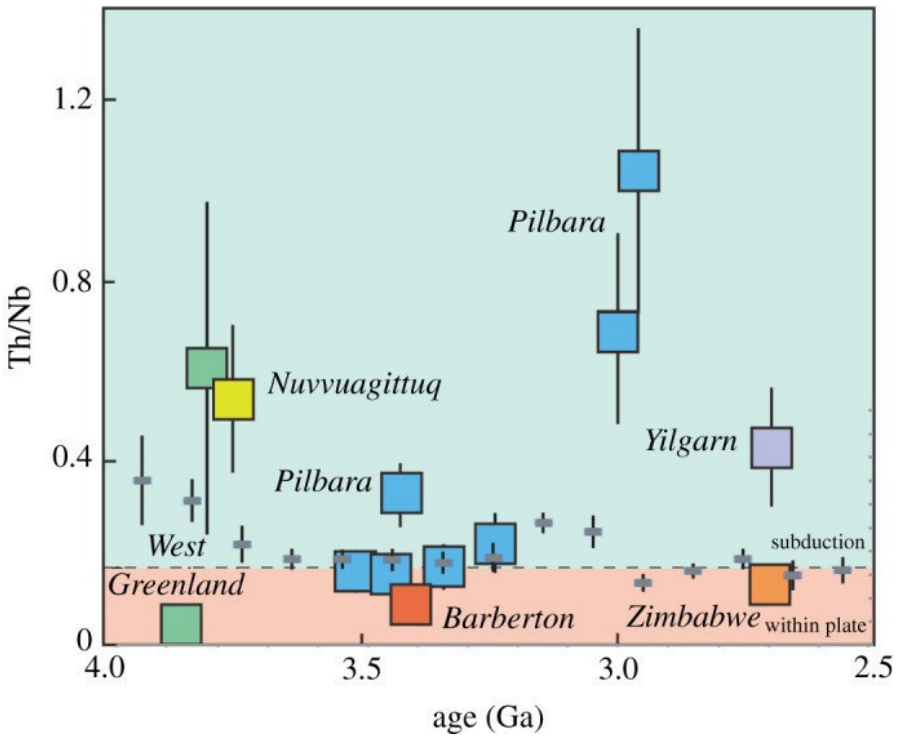

Fig. 1.3: Th/Nb ratios of selected representative mafic rocks from Precambrian archives over time. For explanation see text. From Keller & Schoene, 2018.

Metamorphic mineral assemblages can also be used to define the onset of plate tectonics because they provide a record of P-T conditions, allowing a calculation of heat flow within the crust at the time of their formation, which in turn is a function of tectonic environment. Brown & Johnston (2018) compiled P-T data, thermal gradients, and ages of mineral assemblages from c. 450 localities around the world. Their data suggest that plate tectonics commenced in the late Mesoarchean because this time period is marked by a significant change in thermal gradient of the metamorphic mineral assemblages. A later change in the tectonic setting in the Neoarchean marked the onset of deep subduction, as we know it from today. However, Stevens & Moyen (2007) reported a blueschist-facies metamorphic mineral assemblage, usually associated with the subduction of cold, oceanic crust (Cawood et al., 2018), from the Barberton Granitoid-Greenstone Terrane, which would indicate that plate tectonics was already active during the Paleoarchean.

Since the Barberton Granitoid-Greenstone Terrane (BGGT) is one of the crucial sites in the controversy about the onset of plate-tectonic, we decided to investigate the fold geometries, deformational history and mechanisms of the Barberton Greenstone Belt in order to gain new insights about the structural evolution of the BGGT and contribute to the understanding of the early Earth's evolution.

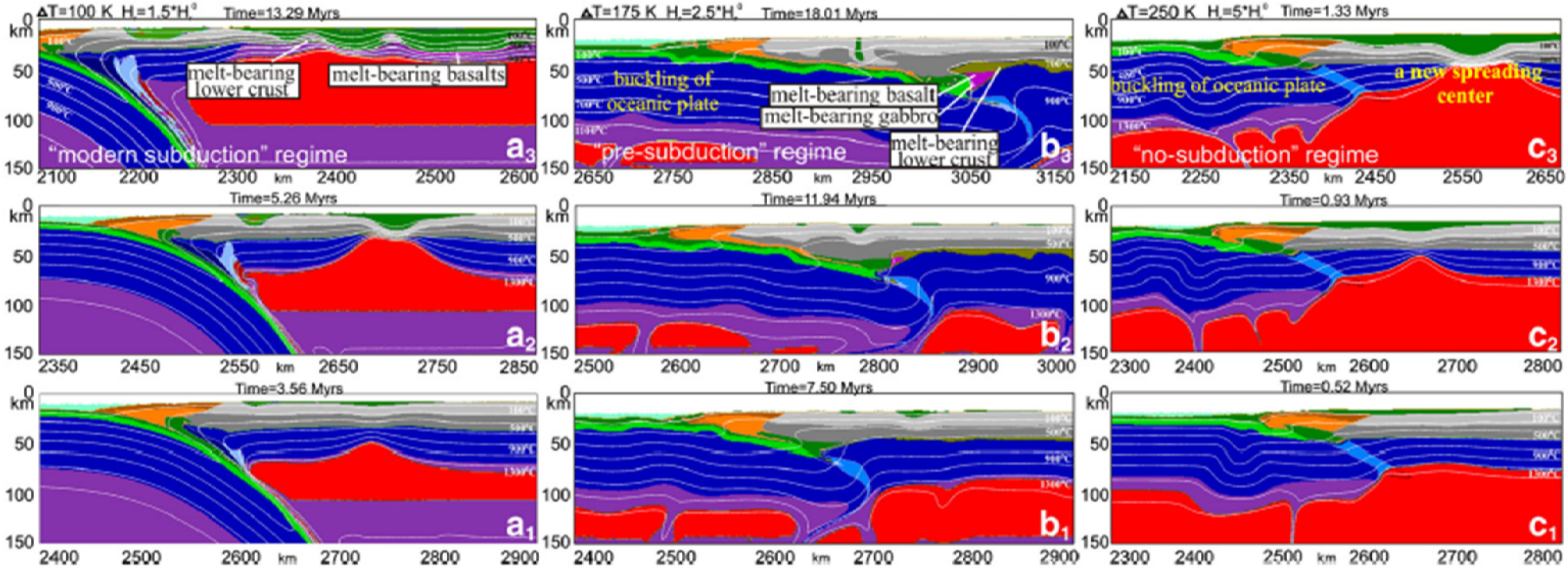

Fig. 1.4: Representative time-slice snapshots to show various stages during the evolution of a numerical experiments independently varying the upper-mantle temperature and the crustal radiogenic heat production (a, b, c). Experiments show three different tectonic regimes: (a) – ``modern subduction´´-regime (ΔT =0 – 175 K), (b) ``pre-subduction´´-regime (ΔT=175–250 K) and (c)— ``no-subduction´´-regime (ΔT≥250 K). Lower boundary of melt-bearing asthenospheric mantle (red) in (a) and (b) is located at depths of 100–150 km while in (c) this boundary extends to depths >200 km (i.e., below the base of the model). From Sizova et al., 2010.

2 Geological Setting

2.1 Kapvaal Craton

Cratons represent the old and stable cores of continents, which yield precious information about geological processes during the Earth's early history (van Kranendonk et al., 2002; Condie & Kröner, 2008). Besides the Pilbara Craton in Western Australia, the Kapvaal Craton in southern Africa represents the oldest well-preserved remnant of continental crust (Nelson et al., 1999; Eglington & Armstrong, 2004). It covers an area of approximately 12.000.000 km^2 and is bordered by the Zimbabwe Craton to the north, by Jurassic successions to the east and by Proterozoic orogens to the south and west. The complex basement of the Kapvaal Craton, which is overlain by a comparably simple cover, consists of gneisses, plutons of tonalitic, trondhjemitic and granodioritic (TTG) and granitic composition and supracrustal units, which are represented by greenstone belts (Tankard et al., 1982). Major greenstone belts in the basement of the Kapvaal Craton include the Giyani, Pietersburg, Murchison, Nondweni, Muldersdrif, Amalia, Kraaipan and Barberton greenstone belts (Nicoli et al., 2014). The latter is best suited for investigations on geological processes during the Archean because of its large size, excellent exposure, preservation and good accessibility.

2.2 Barberton Granitoid-Greenstone Terrane

The Barberton Greenstone Belt (BGB) makes up the Barberton-Makhonjwa Mountains, a southwest-northeast trending mountain range located in northeast South Africa and northwest Eswatini, formerly Swaziland. It covers an area of c. 40 by 120 km. Its highest mountain, Maid of the Mists, has an elevation of 1903 m. Parts of the mountain land became a UNESCO world heritage site in 2018 due to ``outstanding and unique universal value´´ as geological archive of the Archean.

The southwest-northeast striking BGB represents a complexly folded and faulted assemblage of volcanic and sedimentary. All greenstone belt strata show greenschist-grade metamorphic overprint (Xie et al., 1997; Toulkeridis et al., 1998). The metamorphic mineral assemblage comprises chlorite, epidote, serpentinite and fuchsite and gave the greenstone belt its name. Despite the metamorphic overprint, most primary sedimentary and volcanic structures are preserved due to widespread early silicification. Recrystallisation of the original matrix and cement is a common feature in sedimentary rocks, while igneous rocks of mafic composition have been altered to serpentinite or talcose schists (Byerly et al., 2018).

Together with a series of adjacent gneiss domes and plutons of TTG or granitic composition, the greenstone belt forms the Barberton Granitoid Greenstone Terrane (BGGT), which represents one of the oldest remnants of Archean crust (Anhaeusser, 2014). The TTG plutons can be subdivided into three petrogenetic groups comprising the Steynsdorp Gneisses in the south-east, which were emplaced at c. 3.61 Ga (TTG 1), followed by plutons south of the BGB in the Stolzburg Block, emplaced at c. 3.45 Ga (TTG 2) and plutons along the northwestern margin of the BGB, which formed between 3.28 and 3.25 Ga (TTG 3) (Moyen et al., 2018).

The contemporaneous and in part cogenetic supracrustal and magmatic successions within and outside the BGB allow a unique comprehension of crustal magmatic processes and the response of supracrustal processes in early Earth's history.

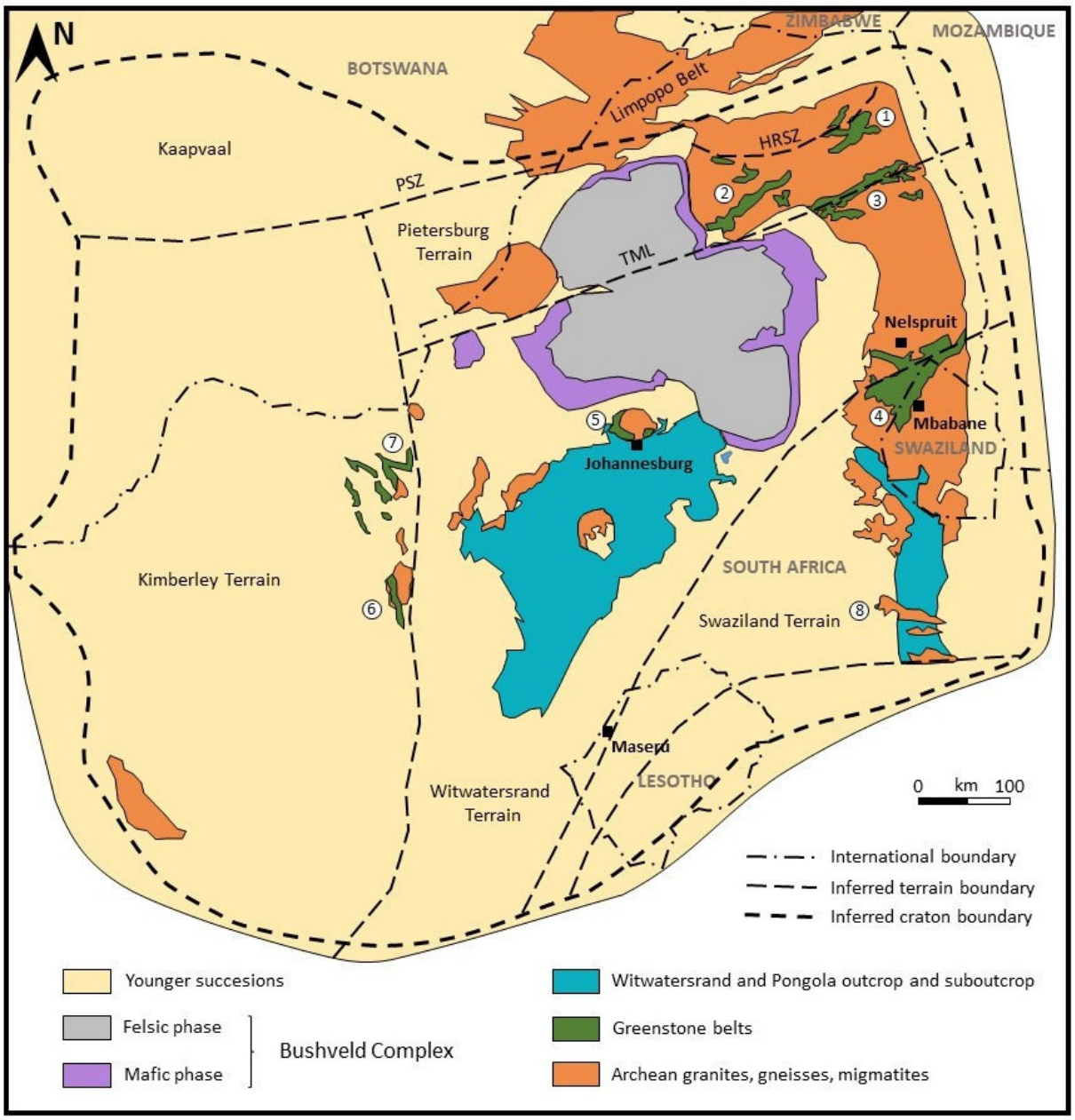

Fig. 2.1 Schematic map of the geology of the Kapvaal Craton including the major greenstone belts: (1) Giyani (2) Pietersburg (3) Murchison (4) Barberton (5) Muldersdrif (6) Amalia (7) Kraaipan (8) Nondweni. Modified from Eglington & Armstrong (2004).

2.3 Stratigraphy

The almost 16 km thick volcano-sedimentary succession of the BGB is termed the Barberton Supergroup (SACS, 1980) and is subdivided into three major groups, namely the Onverwacht, Fig Tree and Moodies Groups.

Early investigators interpreted the BGB stratigraphy as a simple, layer-cake volcano-sedimentary succession (Visser et al., 1956; Anhaeusser, 1975) folded into a complex synclinorium. Subsequent studies showed that the Barberton Supergroup represents a complex tectono-stratigraphic assemblage (Lowe & Byerly, 1999). The Inyoka Fault (IF), orientated parallel to the main southwest-northeast strike of the BGB, marks a major stratigraphic break and separates different facies

assemblages (e.g. Visser et al., 1956; Lowe & Byerly, 1999). The Granville Grove Fault (GGF) and Kromberg Fault Zone (KFZ) confine a triangular area in the southwest of the BGB, in which the oldest parts of the Barberton Supergroup are exposed. The complex tectonostratigraphy of the BGB has been subdivided variably into terranes, suites, blocks and domains (Lowe & Byerly, 1999, 2007; Kisters et al., 2010; de Wit et al., 2018; Byerly et al., 2018). In the following, we refer to the tectonostratigraphic model of Byerly et al. (2018), which subdivides the BGB into three blocks: The Kaap Valley, the Umuduha and the Songimvelo blocks (Fig. 2.3). A more detailed structural subdivision of the greenstone belt is discussed in chapter 5.

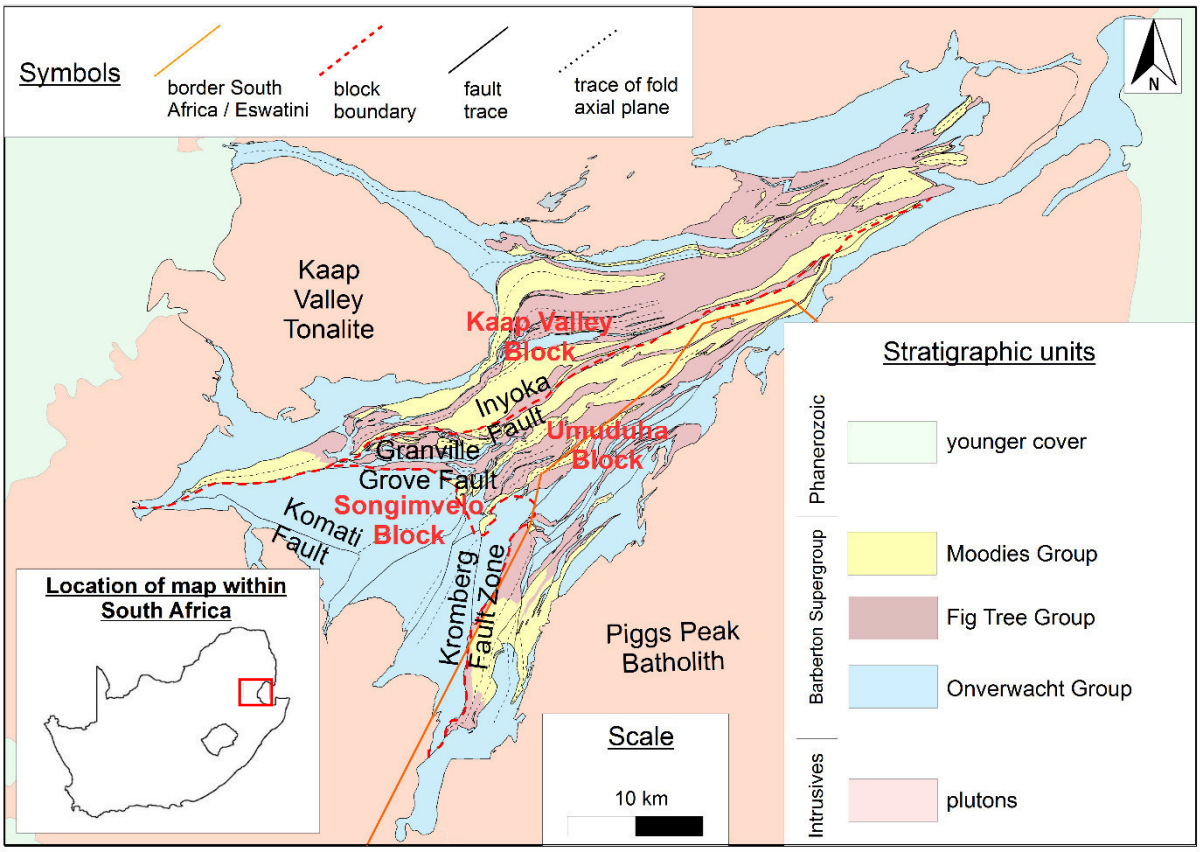

Fig. 2.2: Overview map of the Barberton Granitoid-Greenstone Terrane showing the location of major faults and block boundaries describ ed in the text.

The Onverwacht Group consists of mafic and ultramafic, mostly subaqueous volcanic rocks with minor chert (Lowe & Byerly, 2007 In the Songimvelo Block, the Onverwacht Group is subdivided into the older Theespruit and Sandspruit formations, which are exposed south of the Komati Fault, and the younger Komati, Hooggenoeg, Kromberg and Mendon formations, which are exposed north of the Komati fault. Only the uppermost part of this succession, the Mendon Formation, is present in the Umuduha Block, while the only formation of the Onverwacht Group in the Kaap Valley Block is the Weldevreden Formation, time-equivalent to the Mendon Formation (Byerly et al., 2018).

The overlying Fig Tree Group is made up mainly of (volcanoclastic) matrix-rich litharenites, conglomerates and chemical sediments deposited in a shallow- to deep-marine settings, and volcanic rocks of dacitic and andesitic composition. The Fig Tree Group is subdivided into the Auber Villiers Formation and the Mapepe Formation in Songimvelo and Umuduha blocks. In the Kaap Valley Block, the Fig Tree Group is subdivided into (oldest to youngest) the Ulundi, Sheba, Belvue Road and Schoongezicht formations (Heinrichs & Reimer, 1977; Lowe & Byerly, 1999; Byerly et al. 2018).

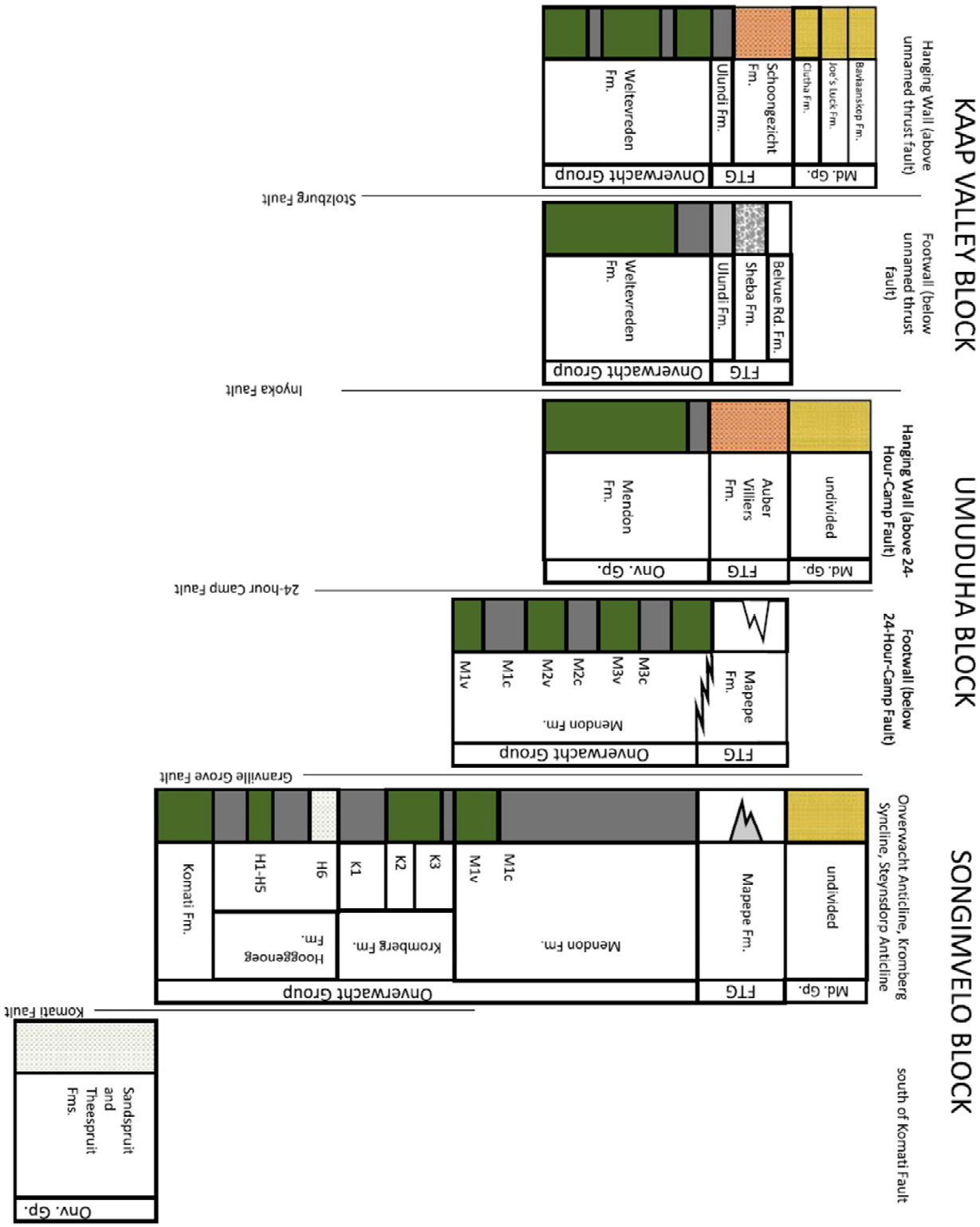

Fig 2.3: Principal tectonostratigraphic blocks in the Barberton Granite-Greenstone Terrain. The vertical extent of the stratigraphic columns does not indicate the thickness of the respective units. For the areal extent of the tectonostratigraphic blocks, see Fig. 2.2 From: Byerly et al. (2018).

The Moodies Group consists of quartz-rich matrix-poor sandstones, siltstones and conglomerates, deposited in terrestrial to shallow-marine settings, with subordinate Banded-Iron Formation (BIF) and volcanic units (Eriksson, 1977; Heubeck, 2019). Most authors do not provide a further subdivision. Anhaeusser (1976) suggested to subdivide this unit into the (oldest to youngest) Clutha, Joe's Luck and Baviaanskop formations in the northern part of the BGB.

2.4 Structural interpretations

Although, or perhaps because the structural framework of the BGB was described by many studies and authors, there is no general agreement about the mechanisms responsible for the formation and subsequent deformation of the greenstone belt. While the initial reason for geological investigations in the Barberton Mountain Land was the need of a better genetic understanding of the numerous gold deposits (e.g. Viljoen et al., 1969; Anhaeusser, 1972, 1976, 1986; de Ronde et al., 1991), most modern studies pursue a better understanding of Archean tectonic processes (e.g. van Kranendonk et al., 2009, 2014; Grosch & Slama, 2017; de Wit et al., 2018). Because of this intense research over decades, there exists a significant number of publications on the topic of the tectonic evolution of the BGGT.

The initial comprehensive analysis of BGB structure was conducted by Hall (1918), who was the first author to suggest that the complex structural evolution of the greenstone belt was influenced by the intrusion of various granites adjacent to the BGB. Later authors adopted the idea of the BGB being deformed by the syntectonically emplaced TTG plutons around the greenstone belt. Heam (1943) suggested that the arcuate shape of the Eureka and Ulundi synclines and other folds was caused by the intrusion of the Kaap Valley Tonalite. Van Eeden (1941) suggested that the refolding and bending of these folds were the result of the deflection of these structures by the *resistant buttress* which the Kaap Valley Tonalite (KVT) represented during the time of deformation. This interpretation is widely accepted today (e.g. Kisters et al., 2010; Heubeck & Lowe, 1994a), since the Kaap Valley Tonalite is dated at 3227±1 Ma (Kamo & Davis, 1994) and, thus, was already consolidated prior to the main deformational period (Fig. 2.5). However, major displacements between the KVT and the BGB occurred later.

The early investigators envisioned deformation of the BGB as the result of sagging and gravitational collapse in a tectonic setting dominated by vertical movement (Ramsay, 1963; Roering, 1965; Anhaeusser, 1976; Visser et al., 1956). The sagging of the greenstone belt was suggested to be associated with shortening and steep thrusting in the interior of the greenstone belt during one single deformational event. Hunter (1961) was the first author to suggest a multi-stage deformation history for the BGB, although his investigations were limited to the Eswatini part of the greenstone belt. His model for the tectonic evolution of the BGB comprises seven stages of alternating deformation, sedimentation and volcanism. He described the BGB as a geosyncline, basically a sedimentary basin, which subsides in specific phases and according to certain observational rules (Kay, 1951). Although this concept became seemingly obsolete with the acceptance of plate tectonics as the main driving force of crustal movement and mountain building (King & Young, 1977), the recognition of the complex structural framework of greenstone belt formation, induced by multiple events and/or mechanisms, was an important observation. Hunter's (1961) model shows significant similarities to later (and even modern) models (e.g. Anhaeusser 1981; van Kranendonk et al., 2014; Kröner et al., 2016).

Ramsay (1963) and Roering (1965) presented comprehensive structural studies of the main gold-producing area of the greenstone belt, situated in and near the Eureka and Ulundi synclines. Although they did not present new general models for greenstone belts deformation, they clearly documented several deformation events (Fig 2.5). Roering (1965) suggested, that the continuity of the northwestward directed stress during the deformation of the BGB indicates that the different

deformation events were linked or were perhaps even part of the same process. He envisioned the emplacement of the TTG plutons around the BGB as the main driving force behind the greenstone belt deformation. This relationship between the greenstone belts' deformation and the emplacement of the surrounding TTG plutons as well as the juxtaposition of the high-grade metamorphic terranes, which are represented by the plutons, and the low-grade metamorphic units of the greenstone belt led Roering (1965) to conclude that the deformation history of the BGGT was very different from modern orogenic belts. A uniformitarian approach could be used only with great caution.

During the 80s and 90s, these models of BGB tectonics were discarded in favor of actualistic models. The majority of these publications (Eriksson, 1980, 1982; de Wit, 1982, 1991; Lowe et al., 1985, 1999; Jackson et al., 1987; de Beer & Stettler, 1988; de Ronde et al., 1991, 1994; de Wit & Hart, 1993; de Ronde & de Wit, 1994; Heubeck & Lowe, 1994a) assumed or concluded that plate tectonics was already active during BGB formation and deformation. Hypotheses were supported by regional, low-resolution geophysical data indicating that the vertical extent of the greenstone belt was approximately 8 km, based on the density and resistivity contrast of the greenstones compared to the adjacent (and presumably underlying) TTG bodies (Darracott, 1975; Stettler & Plessis, 1988; de Beer & Stettler 1988, de Beer & Stettler, 2009).

A group of researchers envisioned the BGB stratigraphy as the result of subhorizontal thrusting and tectonic repetition of oceanic crust in an accretionary wedge, and implied that the primary stratigraphic thickness of the Onverwacht Group did not exceed a few 100 m (de Wit, 1982, 1991; de Wit et al., 1987, 2011; de Ronde et al., 1991, 1994; Jackson et al., 1987; Schoene et al., 2009; Schoene and Bowring, 2010). De Ronde & de Wit (1994) and de Wit & Hart (1993) suggested the first deformational event (D1, 3.55-3.45 Ga) to represent mid-ocean ridge-like processes with sea floor alteration, followed by island-arc- and trench-related processes (D2). They recognized in their studies the complete inventory of plate-tectonic elements, including oceanic crust, ophiolite complexes, black smokers, accretionary wedges, subduction zones, fracture zones, and island arc complexes, as well as (stratigraphically higher) "molasse-type" back-arc basins. Characterising perhaps best the spirit of these times were publications by Eriksson who, based on his sedimentary studies of Moodies strata, suggested the BGB to represent a passive continental margin (1979), a shelf rise (1980), or a foreland, foredeep- or retroarc basin (Eriksson et al., 1994; Jackson et al., 1987). Schoene et al. (2009) and Schoene and Bowring (2010) suggested, that the major deformation period (D3), contemporaneous with the deposition of the Moodies Group, was induced by the collision of several tectonic terranes and involved the closure of an ocean basin that had a doubly-vergent subduction zone (Fig. 2.4 a). Grosch & McLoughlin (2013), in an analysis of part of the Songimvelo Block, employ a ''proto-plate tectonic'' setting, supported by geochemical proxies and geochronological data.

Another group of researchers, principally including Lowe, Byerly, Heubeck, Kröner and their co-authors, envisioned the BGB as an assemblage of formerly adjacent or loosely related crustal blocks which had formed in oceanic-plateau and island-arc environments. Emplacement of TTG plutons during Moodies time led to the formation of a northwest-vergent fold-and-thrust-belt above a shallow detachment (Lowe et al., 1985, 1994, 2014; Kröner 1991; Kröner et al., 1996; Lowe & Byerly, 1999, 2007; Heubeck & Lowe, 1994a; Heubeck et al., 2013). Lowe et al. (1999) recognized six deformation phases (Fig. 2.5). Later, Lowe & Byerly (2007) noticed, that the earliest deformation event (D0), suggested by de Wit (1982, 1991) to represent the onset of major greenstone belt deformation, was confined to a small area in the southwestern BGB. Heubeck & Lowe (1994) drew the first semi-quantitative cross-section through the central BGB, combining their mapping results with available geophysical data (de Beer & Stettler, 1988). Lowe et al (1999; their Figs. 31, 32) provided map-based cross-sections through the central BGB, including the problematic structure of the vertically-plunging enormous Onverwacht Anticline, followed up by the most detailed map of the western-central part of

the BGB to-date and additional cross-sections (Lowe et al., 2012). This group was cautious regarding the vertical-vs.-horizontal tectonics controversy, generally avoided plate-tectonic terminology and was circumspect concerning the mechanisms causing the greenstone belt deformation. Nevertheless, the shallow detachment envisioned by Heubeck & Lowe (1994) and the tectonic terminology used to describe the associated structures are commonly associated with plate tectonics.

A third group, focusing on the southwestern margin of the BGB and following a tectonic-petrogenetic approach, also favored a plate-tectonic setting for the formation and subsequent deformation of the BGB. They suggested that the deformation of the BGB was caused by subduction (or very similar processes) along the Inyoni shear zone (Moyen et al., 2006, 2007; Kisters et al., 2003, 2010; Stevens & Moyen, 2007; Diener et al., 2005), followed by the extensional collapse of the resulting orogen and the formation of a core complex. A central element in their models is the Komati Shear Zone, interpreted as a major normal fault taking out c. 18 km of stratigraphic section and displacing bedding-parallel units of amphibolite-grade Sandspruit and Theespruit formations rocks in the footwall with greenschist-grade rocks (Komati Formation) in the hanging wall (Stevens et al., 2002; Dziggel et al., 2002, 2006, 2010; Kisters et al., 2003, 2010; Diener et al., 2005, Lana et al., 2010).

Lastly, based on structural-geology field work, reinterpretation of P-T paths and the observation of crustal contamination in even the oldest rocks of the BGB, van Kranendonk (2009) applied pre-plate-tectonic models from the Pilbara Craton in Western Australia (Collins et al., 1998; van Kranendonk & Collins, 1998; van Kranendonk et al., 2002, 2004, 2007) to the BGB. He suggested that the formation and most subsequent deformational events in the BGB were controlled by and consequence of *partial convective overturn* (PCO), a process driven by density inversion of thick, cold and dense (komatiitic) greenstones above hot, less dense and intermediate to felsic magmas in the middle crust (the latter having been generated by partial melting of the base of the (ultra-)mafic supracrustal stacks), resulting in periodic catastrophic overturns of the lithosphere back into the mantle (van Kranendonk et al., 2009, 2014). These models agree largely well with results of 3-D thermomechnical-chemical modelling (Fischer & Gerya 2016a, b, Sizova et al. 2018).

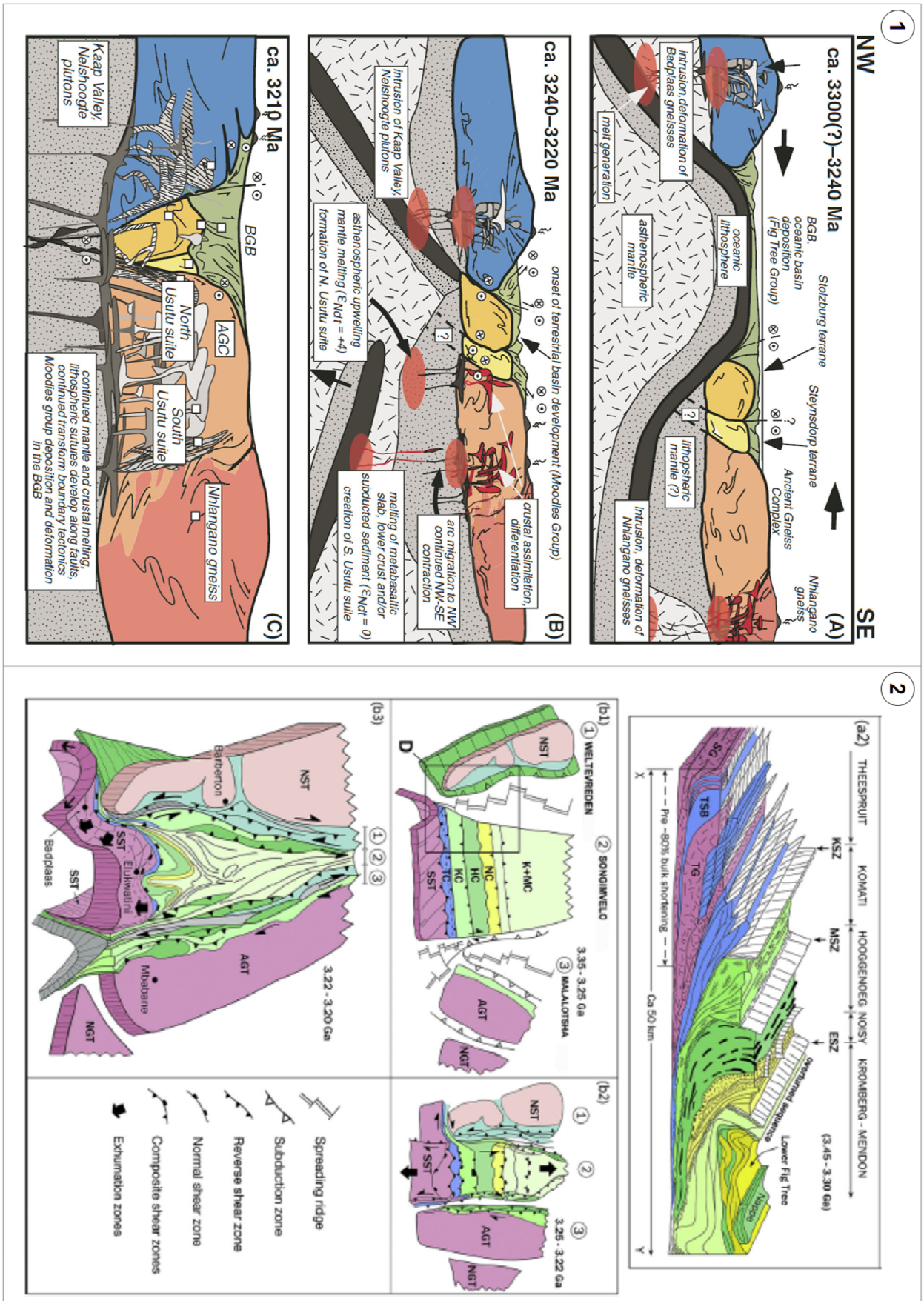
1
NW
SE
ca. 3300(?)–3240 Ma
(A)
BGB, oceanic basin deposition (Fig Tree Group)
Stolzburg terrane
Steynsdorp terrane
Nhlangano gneiss
oceanic lithosphere
asthenospheric mantle
melt generation
Intrusion,deformation of Badplaas gneisses
lithospheric mantle (?)
Ancient Gneiss Complex
Intrusion, deformation of Nhlangano gneisses
ca. 3240–3220 Ma
(B)
onset of terrestrial basin development (Moodies Group)
crustal assimilation, differentiation
arc migration to NW continued NW-SE contraction
melting of metabasaltic slab, lower crust and/or subducted sediment (εNdt = 0)
creation of S. Usutu suite
intrusion of Kaap Valley Nelshoogte plutons
asthenospheric upwelling mantle melting (εNdt = +4)
formation of N. Usutu suite
ca. 3210 Ma
(C)
BGB
AGC
North Usutu suite
South Usutu suite
Nhlangano gneiss
Kaap Valley Nelshoogte plutons
continued mantle and crustal melting, lithospheric sutures develop along faults, continued transform boundary tectonics
Moodies group deposition and deformation in the BGB
2
(a2)
THEESPRUIT
KOMATI
HOOGGENOEG
NOSY
KROMBERG - MENDON
KSZ
MSZ
ESZ
(3.45 - 3.30 Ga)
Pre ~80% bulk shortening
Ca 50 km
X
Y
SSC
TSB
TG
Lower Fig Tree
Upper Fig Tree
(b1)
WELTEVREDEN
SONGIMVELO
MALALOTSHA
3.35 - 3.25 Ga
K+NC
NC
HC
KC
TC
SST
NST
AGT
NGT
D
(b2)
3.25 - 3.22 Ga
(b3)
3.22 - 3.20 Ga
Barberton
Badplaas
Ehlwatini
Mbabane
Spreading ridge
Subduction zone
Reverse shear zone
Normal shear zone
Composite shear zones
Exhumation zones

3

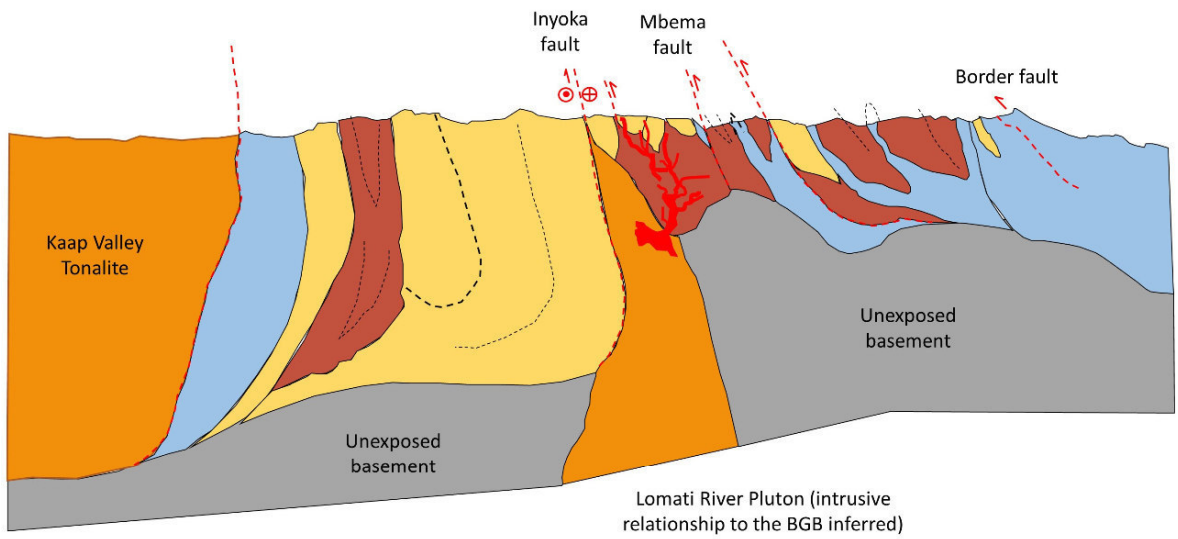
Inyoka fault
Mbema fault
Border fault
Kaap Valley Tonalite
Unexposed basement
Unexposed basement
Lomati River Pluton (intrusive relationship to the BGB inferred)

4

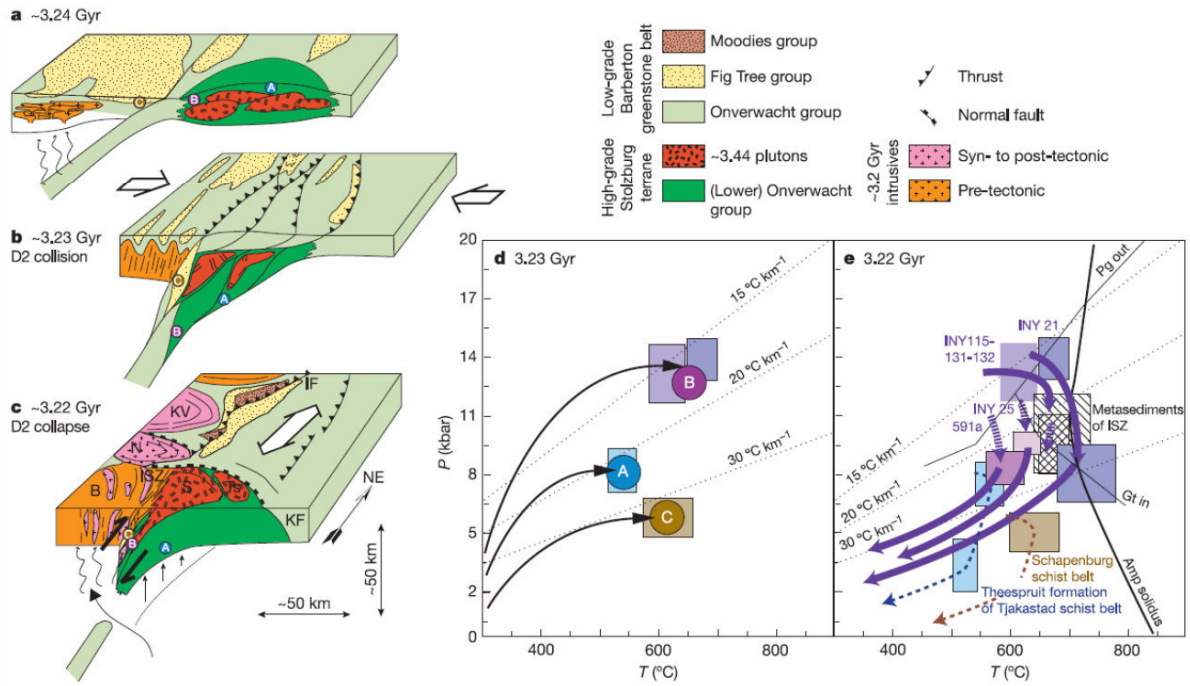
a ~3.24 Gyr
b ~3.23 Gyr
D2 collision
c ~3.22 Gyr
D2 collapse
IF
KV
N
ISZ
S
B
A
C
KF
NE
~50 km
~50 km
Low-grade Barberton greenstone belt
Moodies group
Fig Tree group
Onverwacht group
High-grade Stolzburg terrane
~3.44 plutons
(Lower) Onverwacht group
Thrust
Normal fault
~3.2 Gyr intrusives
Syn- to post-tectonic
Pre-tectonic
d 3.23 Gyr
e 3.22 Gyr
P (kbar)
T (°C)
15 °C km⁻¹
20 °C km⁻¹
30 °C km⁻¹
Pg out
INY 21
INY115-131-132
INY 25 591a
Metasediments of ISZ
Gt in
Schapenburg schist belt
Theespruit formation of Tjakastad schist belt
Amp solidus

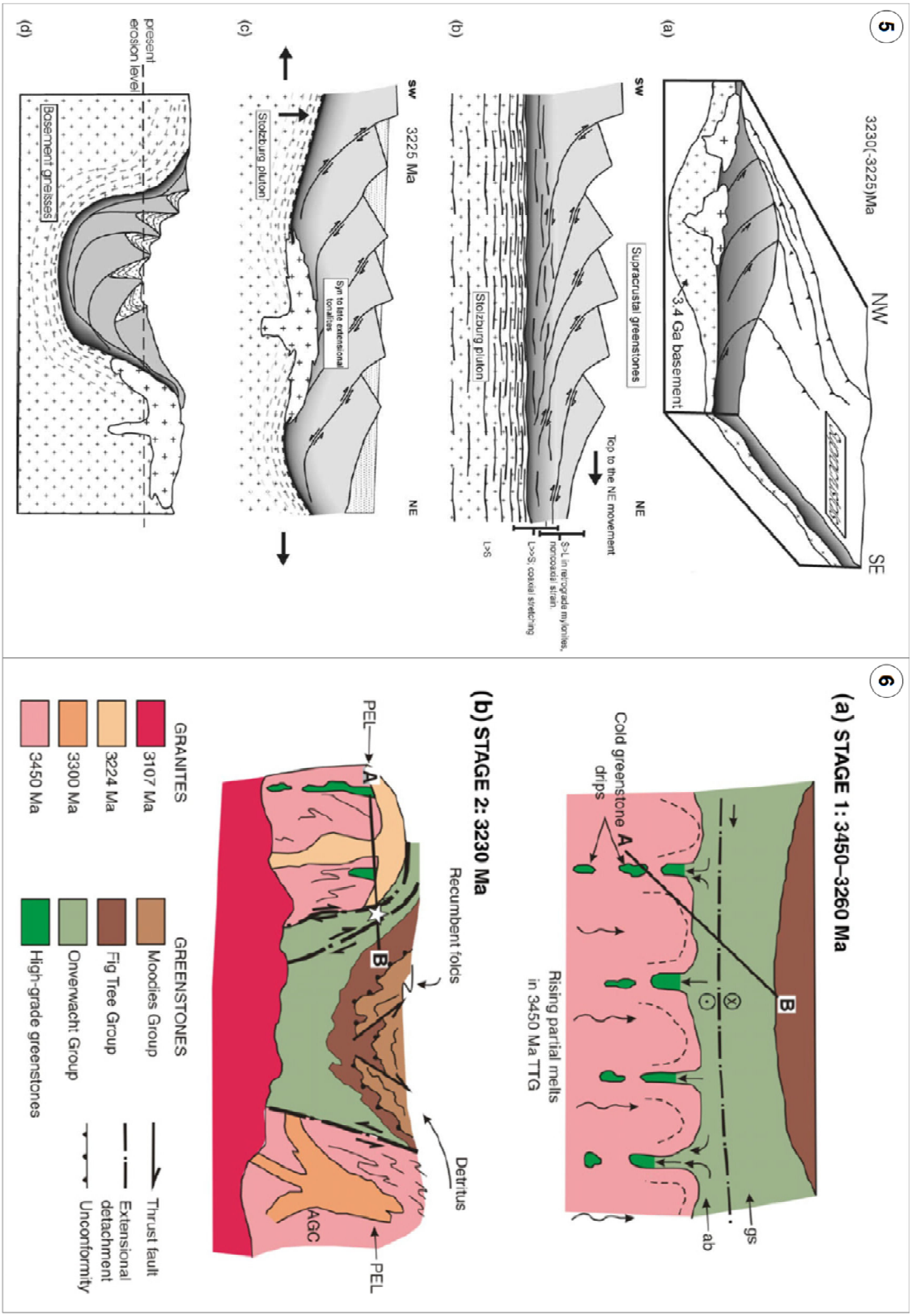

Fig. 2.4: Sketches of the suggested tectonic models for the formation and deformation of the BGB. (1) Constituents of the BGB merging at 3.30 and 3.22 Ga (Schoene & Bowring 2010). In this model, the BGB is formed by accretion above a doubly-dipping subduction zone. No vertical scale. (2) Geological evolution of the BGB (de Wit et al. 2017). The BGB is suggested to have formed by the amalgamation of three crustal blocks between 3.45 and 3.25 Ga, followed by subduction below the Ancient Gneiss Complex and exhumation of high-grade metamorphic terranes. The uppermost sketch shows the imbricated stratigraphy of Onverwacht Group units. (3) Cross-section through the west-central BGB by

Heubeck & Lowe (1994). The greenstone belt is envisioned as two inward-facing but consistently north-vergent fold-and-thrust-belts above shallow detachments, meeting at the Inyoka fault. (4) Tectonic and petrologic model of BGB evolution (Moyen et al., 2006). Sketches a – c show schematically subduction along the Inyoni Shear Zone and the subsequent collapse of the resulting orogen. Sketch e and f show P-T evolution in different parts of the BGB marked in the sketches to the left as A, B and C. (5) Greenstone belt evolution by formation of a core-complex (Kisters et al., 2003). Collapse of the collisional D2-orogen leads to the exhumation of high-grade metamorphic rocks and the formation of small-scale sedimentary basin in which Moodies Group sediments were deposited. (6) Partial Convective Overturn (van Kranendonk, 2011). Density contrast between cold and dense greenstones and the hot, buoyant mantle TTGs results in lithospheric overturn and sinking into the mantle. BGB deformation in this models is caused mainly by sagging during subvertical subsidence of greenstones and simultaneous rise of TTG plutons.

Next Page:

Fig. 2.5: Comparison of deformation phases suggested by various authors. Data compiled from Roering (1967), Anhaeusser (1976), de Ronde & de Wit (1994), Lowe & Byerly (1999a), Dirks et al. (2009), Lana et al. (2010) and Byerly et al (2018).

Deformational Events in the Barberton Greenstone Belt

Age	Stratigraphic Unit	Interpretations by authors					Emplacement of plutons
		Roering (1965)	Anhaeusser (1975)	De Ronde & De Wit (1994)	Lowe et al. (1999)	Byerly et al. (2018)	
c. 3.55 Ga	Lower Onverwacht Group			**D0:** ocean floor type metamorphism, decollement			TTG 1 c. 3.61 Ga
3.55 – 3.45 Ga	Lower Onverwacht Group			**D1:** subduction-accretion of island arcs	**D1:** local deformation on the western limb of the Onverwacht Anticline	**D1:** Extension associated with felsic magmatism	TTG 2 c. 3.45 Ga
3.230 – 3.226 Ga	Late- to post-Fig Tree Group	**Early trend**, deformation probably due to an orogey	**D1:** folding and thrusting of Onverwacht an Fig Tree Group strata	**D2:** subduction-accretion, thrusting, tight isoclinal folding	**D2:** Formation of Onverwacht and Steynsdorp anticlines in a SW-verging fold-and-thrust-belt	3.33 Ga Rifting **D2:** Formation of Onverwacht and Steynsdorp anticlines in a SW-verging fold-and-thrust-belt	
3.228 – 3.214 Ga	Moodies Group	**Main phase** deformation: Formation of NW-vergent folds and strike faults due emplacement of plutons	**D2:** formation of regional cleavage associated with emplacement of the Kaap Valley Tonalite	Early **D3:** formation of NW-verging fold-and-thrust belt, strike-slip activity	**D3:** basinal extension **D4:** basin inversion	**D3:** basinal extension **D4:** basin inversion, formation of doubly-plunging folds	TTG 3 c. 3.228 Ga
3.216 – 3.210 Ga	Post Moodies Group	**Montrose**, **Ulundi** and **Consort trends**: Formation of superimposed fabric and modification of earlier features	**D3:** strike-slip acitivity **D4:** formation of conjugate recumbant crenulation and chevron folds	Late **D3:** Shift from transpressional to transtensional regime **D4:** orogenic collapse, formation of core complex	**D5:** fold tightening, rotation to subvertical, strike-slip activity	**D5:** fold tightening, rotation to subvertical, strike-slip activity	
3.210 Ga	Late Post-Moodies Group	Dike emplacement, deformation must have ceased by this time					

3 Depth structure of the central Barberton Greenstone Belt from large-scale fold geometry

Schmitz, M.[1], Bieker, N.[2], Schlimme, M.[1], van Kranendonk, M. J.[3], and Heubeck, C.[1]

[1] Institut für Geowissenschaften, Friedrich-Schiller-Universität Jena, Burgweg 11, 07749 Jena, Germany

[2] Geographisches Institut, Christian-Albrecht-Universität zu Kiel, Ludwig-Meyn-Straße 14, 24118 Kiel

[3] School of Biological, Earth and Environmental Sciences, University of New South Wales, Kensington, NSW 2052, Australia

Abstract

The vertical extent of the Barberton Greenstone Belt, one of the archetypical Archean greenstone belts, has been used as a major argument in the debate about the nature of Archean pre-plate tectonic rates and mechanisms, dominated by vertical movements. Detailed field mapping and subsurface data indicates, that some large-scale fold structures in the Barberton Greenstone Belt extended (and possibly still extend) >20 km into depth, contradicting estimates of c. 8 km based on sparse legacy geophysical data. However, the large fold depth inferred by 3-D modelling appears unreasonable for several reasons. Most importantly, the inferred depth implies a higher stratigraphic thickness of units and predicts a high metamorphic grade of deep segments, both of which are not supported by field observations. In order to resolve these contradictions, we suggest (1) unit thickening by internal reverse faulting in synclines, (2) primary changes in stratigraphic thickness along strike of the fold axial planes due to syndeformational sedimentation and (3) different folding mechanisms, all of which are partially supported by field observations. Because folds generally plunge steeply, their vertical extent depends strongly on the position of the cross-section along strike of the fold axial plane.

3.1 Introduction

Granitoid-greenstone terranes represent the oldest cores of continental nuclei (Anhaeusser, 2014) and occur in the basement of most cratons. Greenstone belts represent Earth's oldest archives of supracrustal-plutonic interaction during continental growth (Bickle et al., 1980; Jackson et al., 1984). They usually occur between older, penecontemporaneous and younger voluminous tonalites, trondhjemites and granodiorites (TTG) and represent comparatively small and highly deformed remnants of formerly far more extensive volcanic and sedimentary units. The granitoid-greenstone terranes commonly show a radial cuspate-lobate geometry, in which the heterogeneous and mechanically less competent supracrustal lithologies (greenstones) are deformed between larger, more homogenous and mechanically more competent plutons. This particular geometry is widely interpreted as evidence of dominantly vertical tectonics, involving the down-sinking of denser greenstones into less dense intermediate lithosphere and the rise of hot and less dense, ultimately mantle-sourced TTGs (Chardon et al., 1996; van Kranendonk, 2011; Bedard, 2018).

There are several well investigated granitoid-greenstone terranes, such as the Yilgarn (Barley & Groves, 1990; Griffin et al., 2004; van Kranendonk et al., 2013) and Pilbara (Collins et al., 1998; van Kranendonk & Collins 1998; van Kranendonk et al. 2002, 2004, 2007) cratons in Western Australia, the Superior Province in Canada (Percival et al., 1994, 2004; Choukroune et al., 1997; Lin, 2005) and the North Atlantic Craton (Nutman & Collerson, 1991; Friend & Nutman, 2001; Windley & Garde, 2009). Among them, the Barberton Granitoid-Greenstone Terrane (BGGT) figures prominently in the debate about the style of Archean tectonic processes (e.g. de Wit, 1982; Hofmann, 2005; Moyen et al., 2006; van Kranendonk et al., 2009) because its size, low degree of deformation, excellent preservation and good accessibility has made it a type model of Archean tectonics (e.g. Anhaeusser, 1981).

Large-scale geometry and orogen depth is one of the major, controversially discussed issues in greenstone belt geology because it is a principal argument in the debate about the role of vertical vs. horizontal displacements in Early Archean tectonics. One school of thought envisions the BGB as a fold and thrust-belt (de Wit et al., 1992; Heubeck & Lowe, 1994a; Kisters et al., 2003; Lowe & Byerly, 2007); the other school as the result of vertical tectonics driven by some sort of density-viscosity instability (gravitational collapse of Anhaeusser, 1981, 1984; partial convective overturn of van Kranendonk et al. 2009, 2014).

The BGB features a distinctive large-scale fold pattern characterized by numerous km-scale, tight or isoclinal, commonly northwestward-verging synclines defined by volcanic and sedimentary strata. Bedding planes dip generally subvertically; fold axes plunge steeply to subvertically and commonly doubly. These folds show low to no strain except in the hinges and a lower-greenschist degree of metamorphism. Although the geometry of these peculiar folds has been described by numerous authors (Ramsay, 1963; Roering, 1965; Anhaeusser, 1984; Heubeck & Lowe, 1994a; Lowe & Byerly, 1999), none of them has considered systematically and semi-quantitatively their implications on the inferred depth of the greenstone belt. Our approach in this manuscript in resolving this issue is to extrapolate surface fold geometry into depth to provide insights in the deformation mechanism(s) during the dominant deformation phase of the BGB and to constrain 3-D depth, geometry and the tectonic setting during the final phase of greenstone belt (de-)formation.

3.2 Previous Investigations

3.2.1 Geological Setting

The BGB is part of the Barberton Granitoid-Greenstone Terrane in the eastern Kapvaal Craton. It is largely composed of plutons of tonalitic, trondhjemitic and granodioritic (TTG) composition, emplaced in three main phases at 3.61 Ga (TTG 1), at 3.45 Ga (TTG 2) and between 3.28 and 3.25 Ga (TTG 3) (Moyen et al., 2018). To the south-east, the BGB is bordered by a small segment of the Ancient Gneiss Complex (AGC), which consists of a variety of gneisses up to 3.644 Ga old (Kröner et al., 1988, 1989; van Schijndel et al., 2017).

The interior of the belt, between the plutons, represents a supracrustal succession of volcanic and sedimentary rocks, which is subdivided into three major groups (from oldest to youngest), the Onverwacht, Fig Tree and Moodies groups. Total stratigraphic thickness reaches 13-15 km. The Onverwacht Group (3.57 - 3.26 Ga) consists of mafic and ultramafic, mostly subaqueous volcanic rocks interbedded with minor chert (Byerly et al., 2018). The overlying Fig Tree Group (3.25 - 3.225 Ga) is made up mainly of volcanoclastic litharenites, conglomerates and chemical sediments deposited in a shallow- to deep-marine setting (Lowe & Byerly, 1999). The uppermost Moodies Group (3.224 - ca. 3.216 Ga) consists of quartzarenites, siltstones and conglomerates with subordinate jaspilites and volcanic rocks deposited in a terrestrial to shallow-marine setting (Heubeck, 2019). Furthermore, there is evidence of deltas in the Moodies Group, which prograde along strike from the margin towards the center of the fold (Stutenbecker et al., 2019).

The number and stated timing of deformation phases recorded in the BGGT varies among authors (e.g. Roering, 1965; Anhaeusser, 1975; de Ronde & de Wit, 1994; Lowe et al. 1999, Byerly et al., 2018). However, it is widely accepted that the first deformational event (D1) coincides with felsic magmatic activity around 3445 Ma (Lowe & Byerly, 2007), although some authors suggest, that an even older deformation event is recorded in the oldest stratigraphic units in the cores of the Onverwacht and Steynsdorp anticlines (De Wit et al., 1983; de Ronde & de Wit, 1994; Kröner et al., 1996; Kisters et al., 2003), followed by a period of rifting at c. 3.3 Ga (Byerly et al., 2018). The first large-scale deformation

event affecting the entire BGB (D2) occurred between 3.23 and 3.225 Ga (de Ronde & de Wit, 1994; Lowe et al., 1999; Kisters et al., 2003), resulting in the deformation, uplift and erosion of Onverwacht and the lower Fig Tree Group. The youngest and uppermost unit of the Fig Tree Group north of the Inyoka Fault, the Schoongezicht Formation (Lowe & Byerly, 1999), postdates this event and was deposited unconformably onto the D2 erosion surface, along with the subsequent Moodies Group (Lowe et al., 1999). D3 occurred contemporaneously with the deposition of the Moodies Group and resulted in the dominant SW-NE regional fold structural trend of the entire BGB. Two post-Moodies deformational events (D4 and D5) (Lowe & Byerly, 2007) modified the overall structure. Their ages are poorly constrained but must have occurred prior to the emplacement of an undeformed dike swarm at 3105 Ma (Kamo & Davis, 1994).

Even though all rocks exposed within the greenstone belt show at least greenschist metamorphic grade (Xie et al., 1997; Toulkeridis et al., 1998), most volcanic and sedimentary primary textures and structures are preserved, in part due to early silicification. However, recrystallisation of the original matrix and cement is a common feature in sedimentary rocks, while igneous rocks of mafic composition are widely altered to serpentinite or talcose schists (Byerly et al., 2018).

The SW-NE trending Inyoka Fault (IF) in the central BGB represents a major break marked by facies changes in all stratigraphic units across the fault (Heinrichs and Reimer, 1977; de Wit et al., 1991; Heubeck & Lowe, 1994a; Lowe et al., 1999; Lowe & Byerly, 1999; de Ronde and Kamo, 2000). Most other major faults in the BGB trend subparallel to the IF (e.g. the Moodies, Saddleback and Barbrook Faults). In contrast, in the southwestern part of the BGB, the trend of major faults changes, where the Granville Grove and Eucalyptus Mill faults trend E-W and the Kromberg Fault Zone approximately N-S (Fig. 3.1).

Sparse legacy geophysical data (Darracott, 1975; Stettler & Plessis, 1988; de Beer & Stettler, 1988) indicate that the vertical extent of the greenstone belt is about 8 km. At that depth, the dense and conductive, komatiite-dominated greenstone belt lithologies appear to be underlain subhorizontally by a less dense and resistive body, presumably of TTG composition (de Beer & Stettler, 2009). This geometry was interpreted by Heubeck & Lowe (1994) and by Kisters et al. (2003, 2010) as a potential shallow detachment below a fold-and-thrust belt with major horizontal shortening.

3.2.2 Fold geometry

The interior of the BGB is largely dominated by complex, tight to nearly isoclinally folded synclines of Fig Tree and Moodies rocks and intervening thinned, faulted anticlines of Onverwacht rocks (Fig. 3.2). Bedding planes of the synclines are usually subvertical; fold axes commonly plunge steeply inwardly (Fig. 3.2 d) at both ends of the folds while the plunge shallows towards their center. For that reason, the folds of the BGB were sketched as “canoe folds” by Lowe & Byerly (1999) and by Reimer (1971) (Fig. 3.2 b).

Ramsay (1963) conducted the first comprehensive structural analysis in the northwestern part of the BGB. He noted the unusual geometries of the folds and compiled a map showing the variations in fold axial plunge across his study area. Although Ramsay (1963) provided a sketch illustrating the canoe-shaped geometry of the Ulundi Syncline (consisting of Fig Tree Group strata) and the adjacent Eureka Syncline (consisting of Moodies Group strata) (his Fig. 32; Fig. 3.2 a), the latter with a consistently steep plunge of 40° and more, he did not elaborate their mechanism of formation. Roering (1965), following up on Ramsay’s work, concluded that the emplacement of the surrounding TTG plutons were the main force driving the formation of the observed folds, comparable to those adjacent to the batholiths of southern Rhodesia (Zimbabwe) which are draped by synclinal schist belts (Macgregor, 1951).

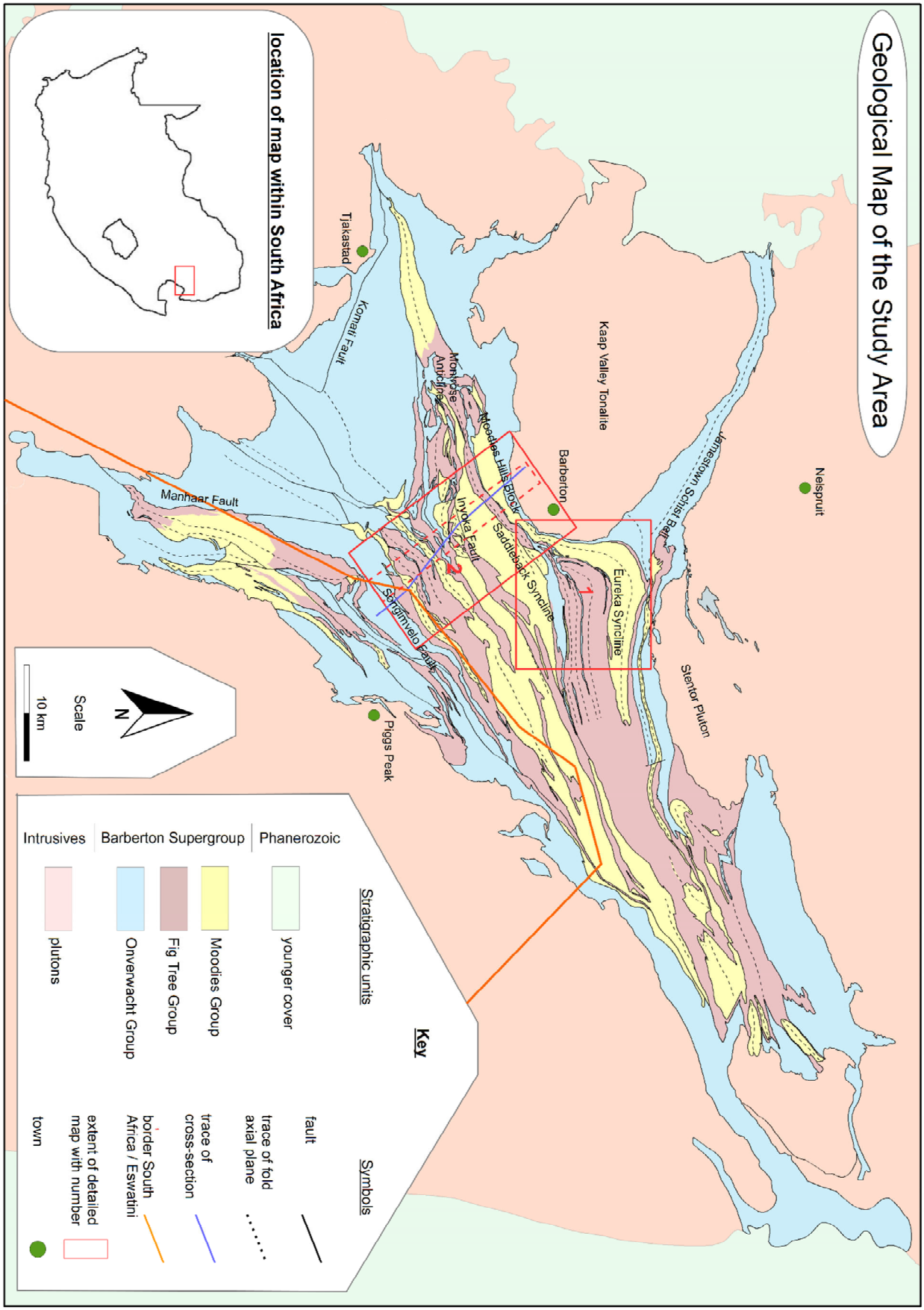

Fig. 3.1: Overview map of the Barberton Granitoid-Greenstone Terrane. For explanation see text. The red rectangles mark the two study areas.

Anhaeusser (1976) described folds from the Eureka Syncline and adjacent folds and pointed out differences between the open fold style of the competent, massive quartzose-sandstone formation of the Moodies Group and the tight folding of incompetent fissile shales and greywackes of the Fig Tree Group. He envisioned the folds to have formed as the result of dominantly vertical, gravity-driven deformation and the emplacement of diapiric TTG plutons (Fig 3.2 c).

Heubeck & Lowe (1994) and Lowe et al. (1999) described the fold style in the west-central part of the BGB. Lowe (1999) also sketched the unique "mushroom-style" of the Montrose Anticline (Fig. 3.2 d) in the northwestern BGB. Noting the absence of any strain indicators and small-scale deformation structures in the fold limbs of the central BGB despite the tight folding, Heubeck & Lowe (1994) suggested that folds formed by passive limb rotation.

3.2.3 Ductile strain

Strain distribution is heterogeneous across the BGB (Anhaeusser, 1984). Conglomerate clasts and volcanic lapilli represent the best strain markers in the greenstone belt (Reimer, 1967; Gay, 1969; Anhaeusser, 1969, 1976; Lamb, 1984; Daneel, 1987; Heubeck & Lowe, 1994a). Some authors assume initial non-spherical clasts and subhorizontal orientation. In many places, in particular on the thick fold limbs, abundant 2-D sedimentary structures (conglomerate clasts, desiccation polygons, silicified gypsum concretions, foresets, soft-sediment deformation features etc.) show virtually no strain (Heubeck & Lowe, 1994a). Prolate-oblate strain is high and widely distributed, however, along all margins of the BGB near the contacts to the gneissic plutons and near major fault zones (e.g. Inyoka Fault) within the BGB. The southern margin of the BGB appears to be dominated by prolate strain, indicating strong vertical stretching by an average factor of 2.7 (Lamb, 1984; Heubeck, 1994; see also chapter 4).

3.3 Methods

3.3.1 Field work

Throughout the central BGB, we collected structural and lithological data, measured major and minor fold axes (Fig. 3.4 c), and verified contacts.

Areas of Interest. We chose two representative areas in the central BGB for detailed investigation in order to take advantage of outcrop conditions and accessibility (Fig. 3.1). Area 1 is located near the northwestern margin of the greenstone belt and features two prominent fold structures, the Eureka and Saddleback synclines, as well as adjacent structures. This area represents one of the best investigated parts of the BGB (e.g. Ramsay, 1963; Roering, 1965; Anhaeusser, 1969, 1972, 1976, 1981, 1984; Gay, 1969; Fripp et al., 1980; Robb et al., 1986; Heubeck & Lowe, 1994a, b; Harris et al., 1995; Lowe et al., 1999; Lowe & Byerly, 1999; Dziggel et al., 2007, 2010; Dirks et al., 2009; Muyai et al., 2011).

Area 2 forms a wide strip across the strike of the central BGB. It includes the region through which Anhaeusser (1984), Jackson et al. (1987), de Beer et al. (1988), Heubeck and Lowe (1994), Lowe et al. (1999) and Lowe et al. (2012) drew or sketched regional cross-sections. It was chosen in order to compare and evaluate the assumptions of these cross sections, fold geometry and greenstone belt depth.

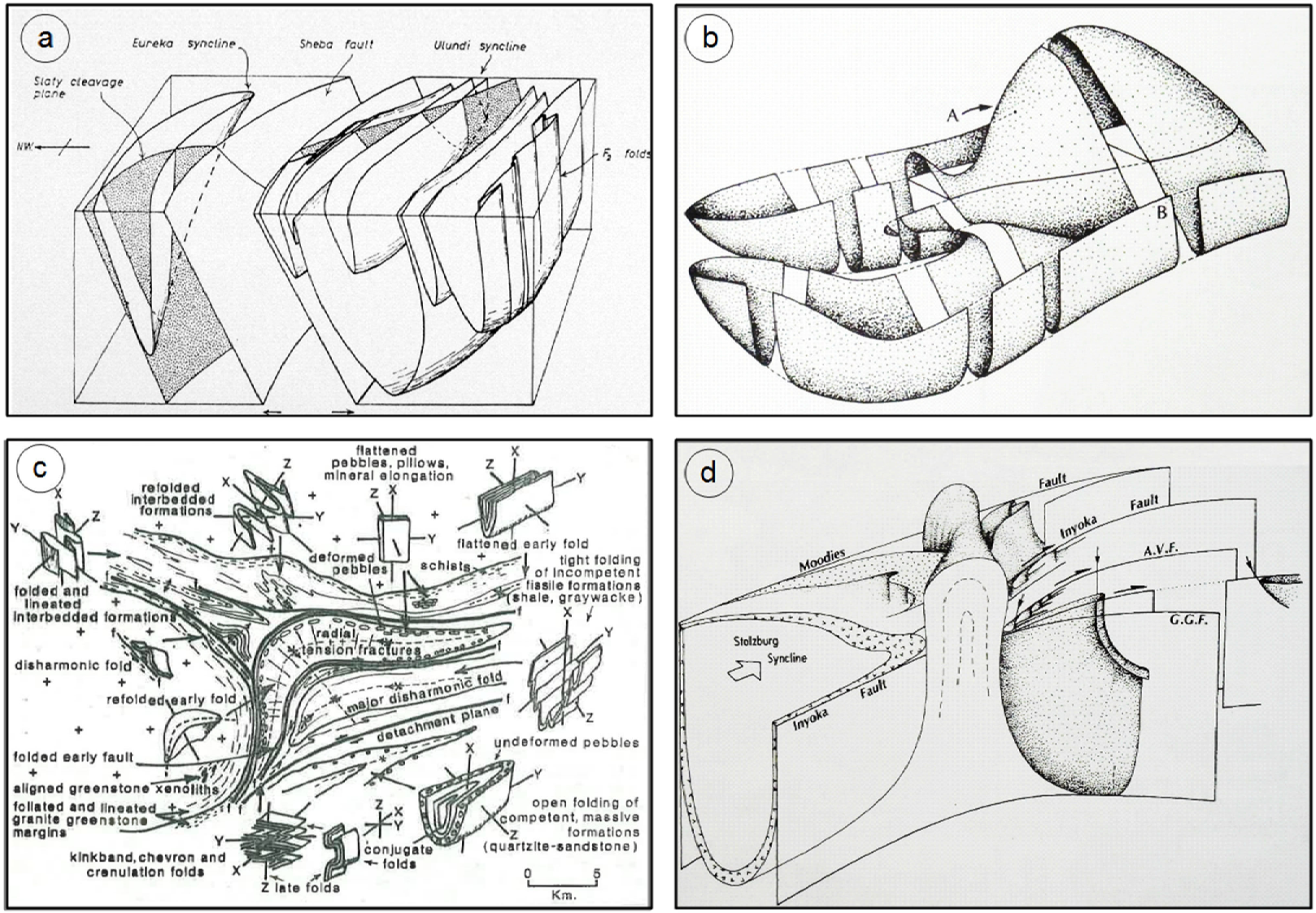

Fig. 3.2: Sketches of three-dimensional fold geometry suggested from surface geological mapping. (a) Northeastern part of study area 1 (Ramsay, 1963). (b) Canoe-shaped syncline (Lowe, 1999). (c) Eureka Syncline and adjacent structures (northern part of study area 1) with exemplary structural features (Anhaeusser, 1975). (d) Montrose Anticline, example of a mushroom-shaped anticline between a series of canoe-shaped synclines in the western BGB (Lowe, 1999).

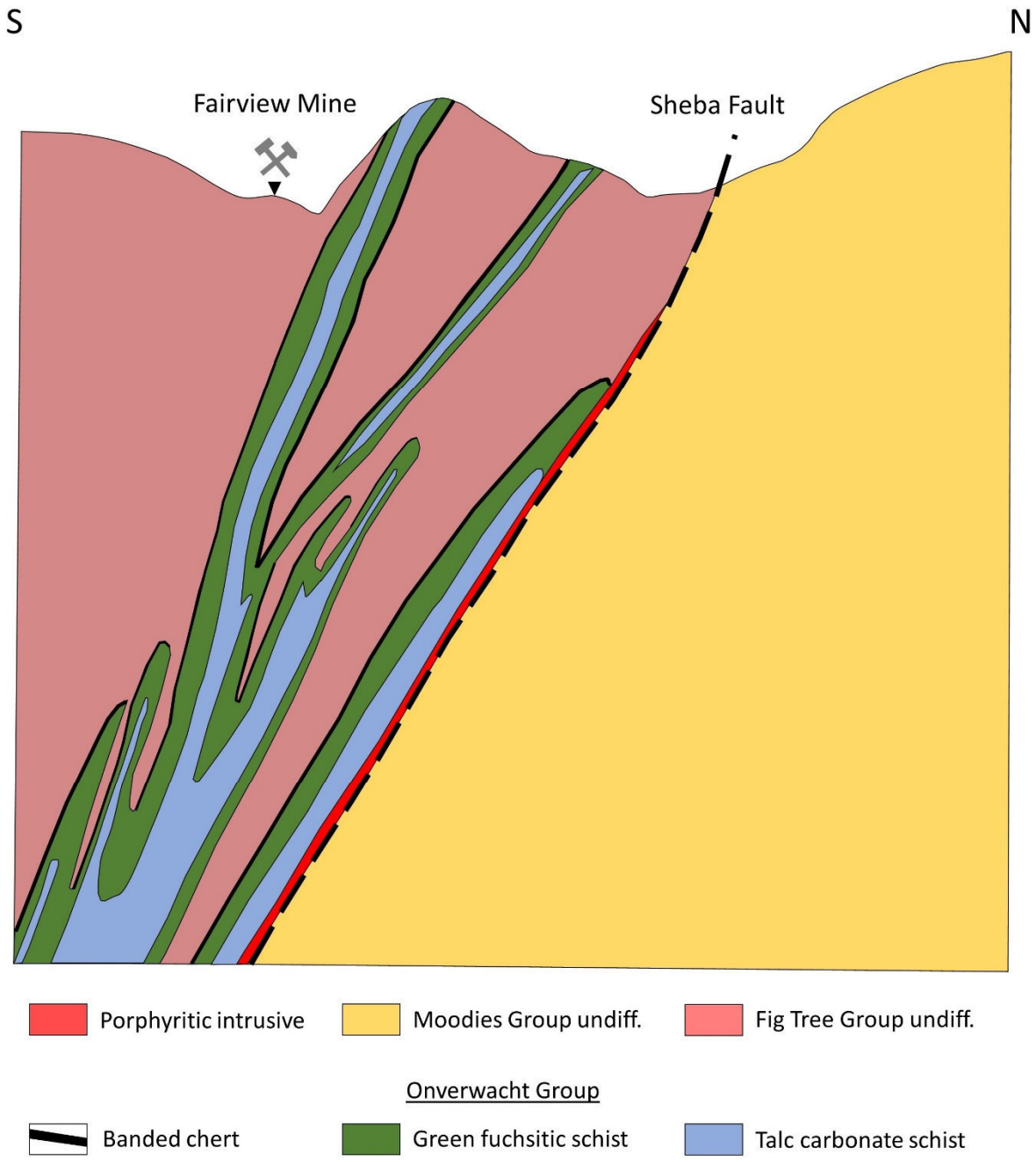

Fig. 3.3: Cross section of the Sheba Mine area (occupying the complex Sheba Anticlinorium between Eureka and Ulundi Synclines), showing several narrow and tightly folded anticlines principally composed of talcose and silicified ultramafic rocks of the Onverwacht Group (data provided by Barberton Mines).

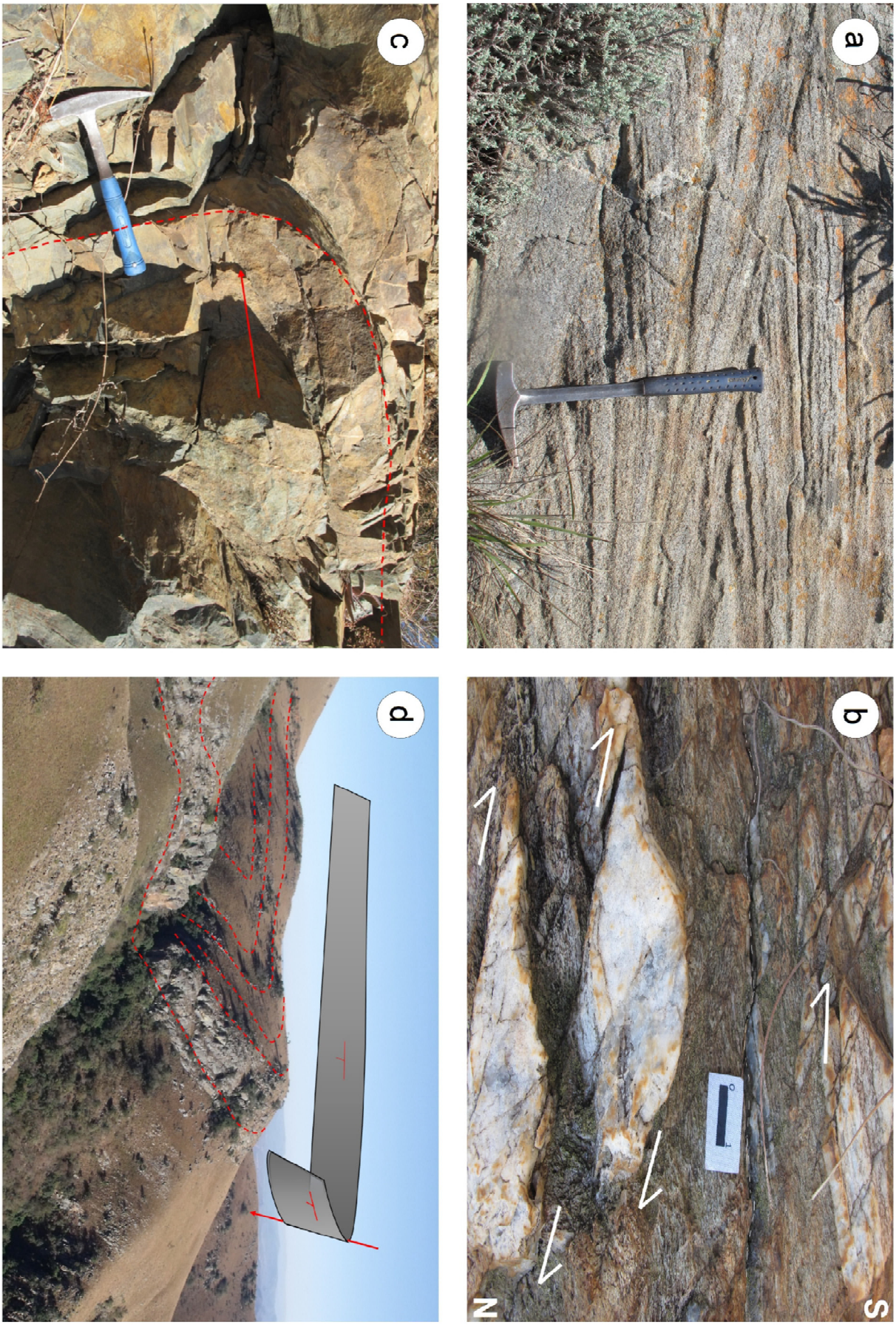
c
a
d
b
N
S

Fig. 3.4: Field photographs of the study area. See Fig. 3.7 for locations. (a) Foresets in Moodies Group sandstone from the Saddleback Syncline. (b) Kinematic indicators on bedding plane (dashed white line) in the Eureka Syncline. σ-clasts indicate sinistral shear sense, up to the south-movement and relative uplift of the interior parts of the syncline along bedding planes. (c) Parasitic fold in the Eureka Syncline (d) Hinge of the Dycedale Syncline. Dashed red lines indicate the trace of the respective bedding planes while the grey plane with red bedding symbols visualizes the general orientation of the bedding planes in the hinge area. The steeply plunging fold axis of the Dycedale Syncline is represented by the red arrow.

We excluded the very large Onverwacht Anticline in the far southwestern BGB from consideration, even though it forms the largest and highest-relief fold structure of the BGB. The at-depth extension of this enormous, subvertically plunging structure with its limb thicknesses of ~ 10 km (Lowe & Byerly, 2007) is in unresolved conflict with the geophysically suggested depth of ~8 km for the BGB derived from a traverse only c. 10 km to the northeast. Virtually all other of the numerous large-scale folds in the central BGB, in contrast, are similar in size and style throughout the belt, in particular those involving substantial thicknesses of Moodies strata.

Subsurface structural data from Sheba and Fairview Mines (see Fig. 3.7 for location) enabled us to extend surface data to depth (Fig. 3.10).

Paleocurrents. Because syndeformational sedimentation may have contributed to primary thickness variation and fold geometry, we measured foreset orientation in sandstones of the Moodies Group (Fig. 3.4 a) and restored paleocurrent directions in order to determine the direction of sediment transport. Readings were taken from units regardless of their stratigraphic position. In order to correct the readings, we first removed fold axis plunge by rotating data around a vector perpendicular to strike of the fold axial plane and then removed the inclination of the bedding plane by rotating the data around a vector parallel to the strike of the fold axial plane. See the Appendix 5 for measured data and the structurally corrected values in Area 1. Paleocurrent orientations of Area 2 are available in Heubeck & Lowe (1994).

Thickness ratios of hinges/limbs. We measured the thicknesses of stratigraphic units perpendicular to strike of bedding planes on the limbs and in the hinge area of the Eureka, Dycedale and Saddleback synclines, which contain heterogeneous lithologies including numerous marker units. Measurements were taken only where stratigraphic units could clearly be traced from the limb through the hinge zone. Measured sections for limbs (l-l') and hinges (h-h') are marked in Fig. 3.7.

3.3.2 3D-modelling

We compiled map data and generated three-dimensional models in study area 1 by extending surface bedding plane dips, axial plane orientations, and fold axial plunges to depth, using the software Move by PetEx. Because fold axes plunge steeply to (sub-)vertically, we took fold hinge geometry in map view as a predictor of hinge geometry at depth in cross section, an inference supported by observations in deep mines along the northern margin of the BGB (Fig. 3.10). Our initial model uses three simplifying assumptions: (1) Single-layer thickness remains constant; (2) strain is – on map-scale – accommodated homogeneously; (3) fold axial plunge and limb dip values remain constant with depth; they do not change significantly from their surface values. In the latter assumption, we were guided by the impossibility to keep strata thicknesses constant when reducing fold plunge in the subsurface, for example in efforts to create "canoe folds".

The three-dimensional geometry of plunging folds (Fig 3.5) includes the depth of the synclinal “keel” (the enveloping surface). This depth z can be calculated by

$$z = \cos(\beta) * \tan(\alpha) * y$$

in which z represents the depth of the fold envelope, y the horizontal distance along the fold axial trace from the envelope - surface intersection to the calculated point, α is the plunge of the fold axis, and ß equals 90° minus the dip angle of the fold axial plane. This equation returns the true vertical depth of a point (depression) on a line (fold axis) on an inclined plane (fold axial plane).

Where surface fold plunge changed measurably (>10°) downplunge, we recalculated depths for different segments of that fold, using individual plunge values for each segment.

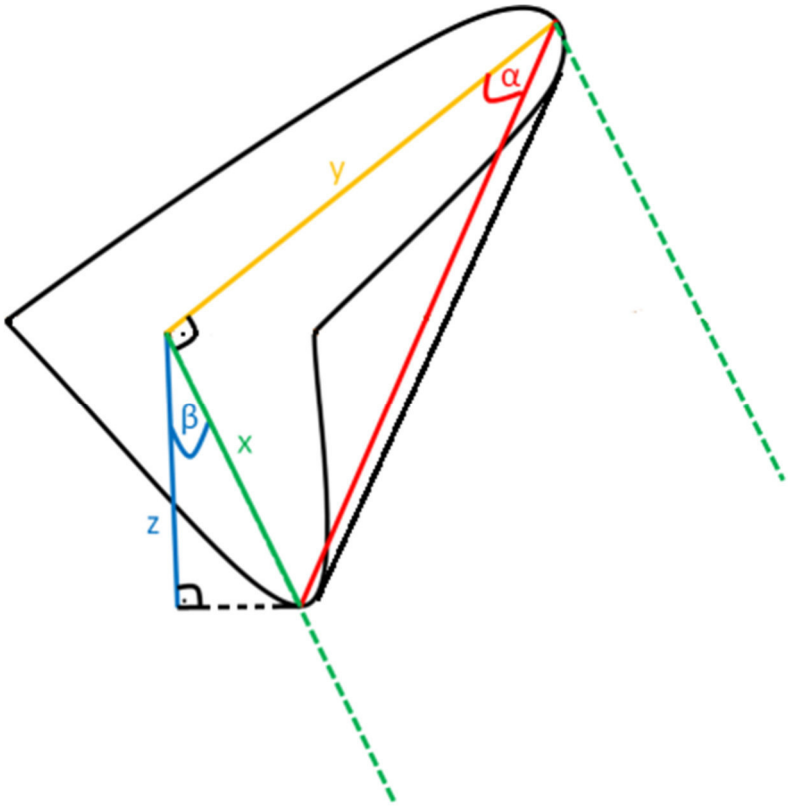

Fig. 3.5 Illustration of depth calculation used in three-dimensional modelling. Black lines represent the three-dimensional synclinal geometry. The inclined fold axial plane is marked by the dashed green lines. The yellow line (y) marks the fold axial trace of the fold, the red line the subsurface fold axis with the angle of its plunge (α).

3.4 Results

3.4.1 Stratigraphy and lithological units

In the following, the lithological units in the two study areas are briefly described in stratigraphic order. Abbreviations in parentheses refer to unit names used on the maps (Figs 3.7 and 3.13).

Onverwacht Group:

Mafic and ultramafic volcanics (on_um)

Undifferentiated altered volcanic rocks, varying from talc and serpentinite to dolomite.

Talcose schist (on_tc)

Talcose schists (Fig. 3.6 a) are interpreted as alteration product of mafic and ultramafic volcanic rocks of the Onverwacht Group (Lowe et al., 2012). The schists are medium- to coarse-grained and show a strong foliation. Their color ranges from dark grey and brownish-red to pink. Due to their poor weathering resistance, they generally form low elevations and provide few or no outcrops.

Chert (on_bc)

Layers of alternating black-and-white cherts with single-bed thickness of up to 40 cm interbedded with altered Onverwacht Group volcanic rocks. The cherts are weathering-resistant and form excellent marker horizons.

Fig Tree Group:

Conglomerate (ft_c)

Polymict clast- or matrix-supported conglomerate consisting of well-rounded pebble to cobble clasts in a coarse-grained sandy-shaly lithic matrix. Clast composition shows little variability and consists mainly of cherts and dacitic feldspar porphyries.

Greywacke (ft_gw)

Brownish-grey to red, medium- to coarse-grained volcanoclastic sandstone (Fig. 3.6 b) composed largely of lithic fragments of sedimentary and volcanic provenance and chert.

Fine-grained Sediment (ft_fg)

Brown to red ferruginous siltstones and shales. This incompetent lithology shows commonly parasitic folds.

Jaspilite (ft_j)

Up to 12 cm thick beds of hematitic jaspilite alternating with chert, shale or tuffaceous sediments (Fig. 3.6 d), including marker beds. Internal deformation and parasitic folds are common.

Moodies Group:

Conglomerate (md_c)

Mostly clast-supported cobble conglomerate consisting of a medium- to coarse-grained quartzose matrix and well-rounded polymict clasts of chert varieties, felsic and intermediate volcanics, quartzites, silicified ultramafic volcanic rocks and rare jaspilite (Fig. 3.6 e).

Quartz-rich sandstones (md_q)

Medium- to coarse-grained, medium- to thick-bedded, quartzose, commonly cross-bedded, quartz-cemented, weathering-resistant and mechanically highly competent sandstone (Fig. 3.6 f).

Sandstone (md_s)

Medium- to coarse-grained sandstone, consisting mainly of quartz, feldspar and rare lithic fragments. Due to its high weathering resistance, this unit forms topographic highs.

Fine-grained Sediments (md_fg)

Shale and siltstones of the Moodies Group with usually well-developed cleavage, but poor outcrops due to their low weathering resistance.

Jaspilite (md_j)

Magnetic shale and hematitic jaspilite with common internal deformation and parasitic folds, providing good marker units due to its characteristic appearance and high weathering resistance.

Amygdaloidal lava (md_b)

Basaltic lava, mostly altered to chlorite, albite and/or carbonate. Not very resistant against weathering and erosion.

Kaap Valley Tonalite (kvt)

Large (35 km * 30 km), coarse-grained hornblende-biotite-plagioclase tonalite pluton with several compositionally and texturally distinct phases and minor mafic enclaves. The originally intrusive contact against the greenstone belt (Moyen et al., 2018) is structurally modified by major displacement (de Ronde & Kamo, 2000). Zircon crystallization ages cluster within analytical error around 3229 Ma (Moyen et al., 2018), which implies a syntectonic emplacement of the pluton during late Fig Tree Group time.

Doleritic Dikes (dol)

Mafic dikes with an ophitic fabric consisting mainly of plagioclase and pyroxene. Dikes cross-cut folds and faults and were thus emplaced post-deformationally. The dikes weather recessively in the BGB and form ridges in the Kaap Valley Tonalite.

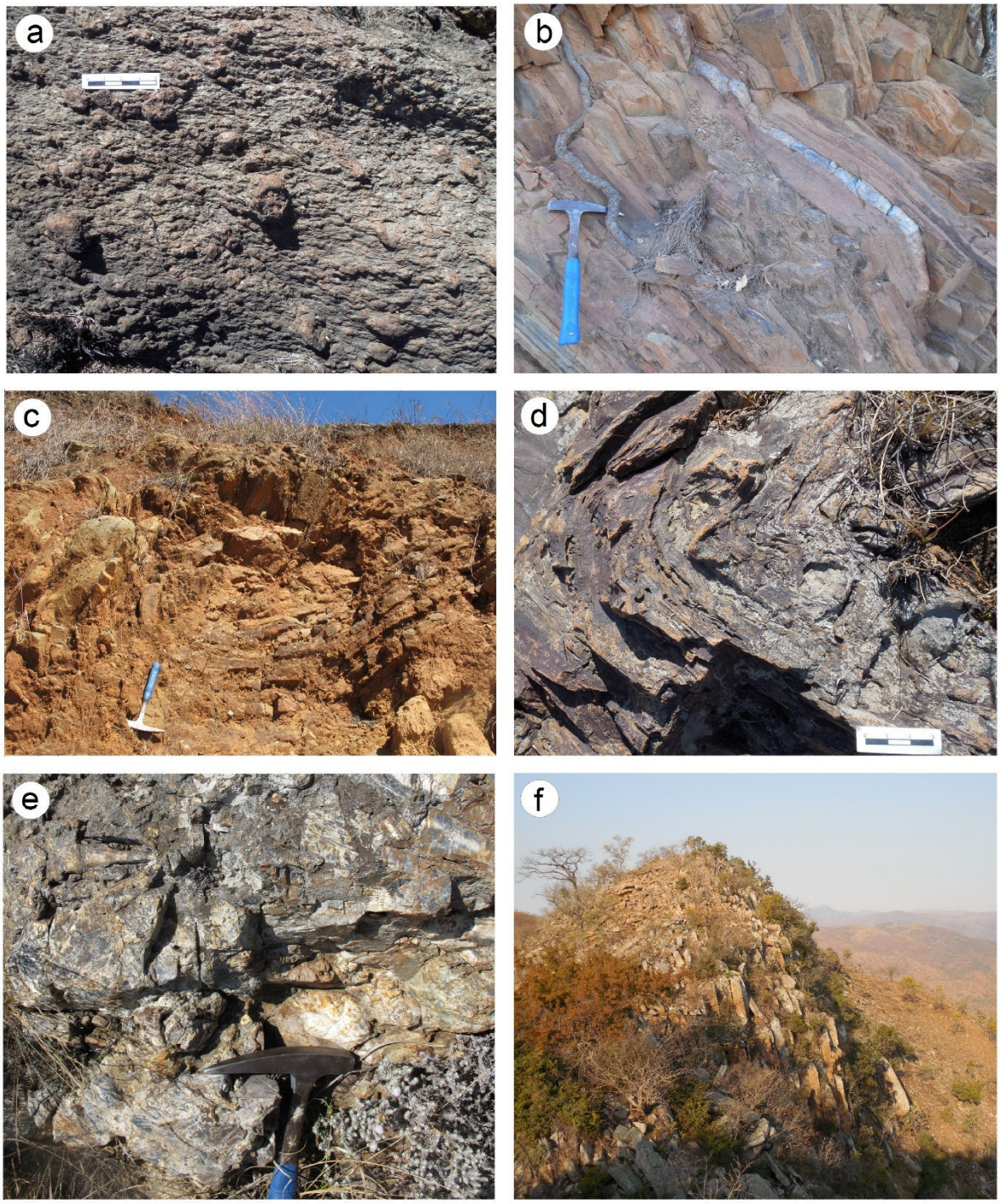

Fig. 3.6: Field photographs of selected lithological units. For explanation see text. See Figs. 3.7 and 3.13 for locations. (a) Talcose schist of the Onverwacht Group. This unit represents the alteration product of mafic and ultramafic volcanic rocks. (b) Greywackes from the Fig Tree Group. (c) Fine-grained volcanoclastic sediments of the Fig Tree Group. This incompetent unit consists of finely laminated beds, which show a significant amount of internal folding. (d) Jaspilite from the Fig Tree Group. A lot of internal deformation, irregular bedding and slumping can be observed in this unit. (e) Conglomerate of the Moodies Group. The clasts consist mainly of cherts and minor volcanic rocks. (f) Quartz-rich sandstone of the Moodies Group. Representing one of the most weathering resistant units, these sandstones commonly form high ridges and can be used as marker units.

3.4.2 Structures of area 1

3.4.2.1 Regional fold structures

Jamestown Schist Belt

Anhaeusser (1972) provides a detailed description of the Jamestown Schist Belt, an SE-NW trending, elongate synclinal structure of altered mafic and ultramafic volcanics interbedded with minor chert units between major plutons. It extends from the northwestern corner of area for c. 15 km to the NW (Fig. 3.1) and is bordered by the Kaap Valley Tonalite to the west, the Nelspruit Batholith to the north and the Berlin and Stentor plutons to the east.

The Jamestown Schist Belt comprises a number of minor folds such as the Handsup Fold and the Woodstock Anticline. Its synclinal axis coincides with the axis around which the Eureka Syncline and adjacent folds were refolded.

Eureka Syncline

The arcuate, 27 km long Eureka Syncline (Fig. 3.7) is one of the dominant synclines of the BGB. It consists mainly of competent quartzose sandstone, incompetent fine-sandy siltstone and subordinate lithologies, including conglomerate and jaspilite, of the Moodies Group. Up to 500 m thick Fig Tree strata are preserved along its outer northern margin. The Eureka Syncline is tightly folded and plunges moderately to steeply. Its limbs reach a maximum of c. 3.2 km stratigraphic thickness, of which 3 km consist of Moodies Group strata (Anhaeusser, 1976). The overall SW-NE-trending structure is refolded about an SE-NW tending fold axial trace defining the Jamestown Schist Belt, so that its synclinal axis is arcuate and changes its strike from N-S to E-W. The southern and eastern limbs are generally overturned. The axial plane dips east and south, respectively. Bedding planes generally dip steeply towards the east and to the south, respectively. The eastern hinge zone is offset by several minor brittle faults trending perpendicular to the strike of the fold axial plane.

Towards the southwest, in the vicinity of Barberton, the Eureka Syncline narrows and the strike of the fold axial plane changes from N-S to E-W as it is refolded. The structure continues towards the SW but faulting along its northern margin (Moodies Fault) has removed its south-facing northern limb and the fold axis so that only the overturned, north-facing southern limb is preserved. This area is known as the Moodies Hills Block. The stratigraphy and petrography of the Eureka Syncline – Moodies Hills combination is generally well investigated (e.g. Lowe et al., 1999; Hessler & Lowe, 2006; Heubeck et al., 2013; Bontognali et al., 2013; Homann et al., 2015; Nabhan et al., 2016).

The fold axis of the Eureka Syncline consistently plunges steeply (between 67° and 40°) inwards. The maximum depression occurs close to the R 40 outside Barberton. Southwest of the R 40, minor old axes plunge steeply towards the north, none shallower than 40°.

Along the northern margin of the Eureka Syncline, the Lily Fault separates the Eureka Syncline from the Jamestown Schist Belt. To the south, the Sheba Fault Zone separates it from the Ulundi Syncline. The western margin of the Eureka Syncline lies in places less than 300 m from the Kaap Valley Tonalite (KVT), its northern margin only ca. 500 m from the Stentor Pluton.

Ulundi Syncline and associated folds

The Ulundi Syncline lies adjacent to the Eureka Syncline (Fig. 3.7). It is mapped for c. 20 km along strike of the fold axial plane, but may extend further to the east. The Ulundi Syncline comprises c. 2.3 km thick strata mainly of incompetent greywackes, siltstones and cherts of the Fig Tree Group. The overall geometry resembles that of the Eureka Syncline with subvertical bedding, an overturned southern

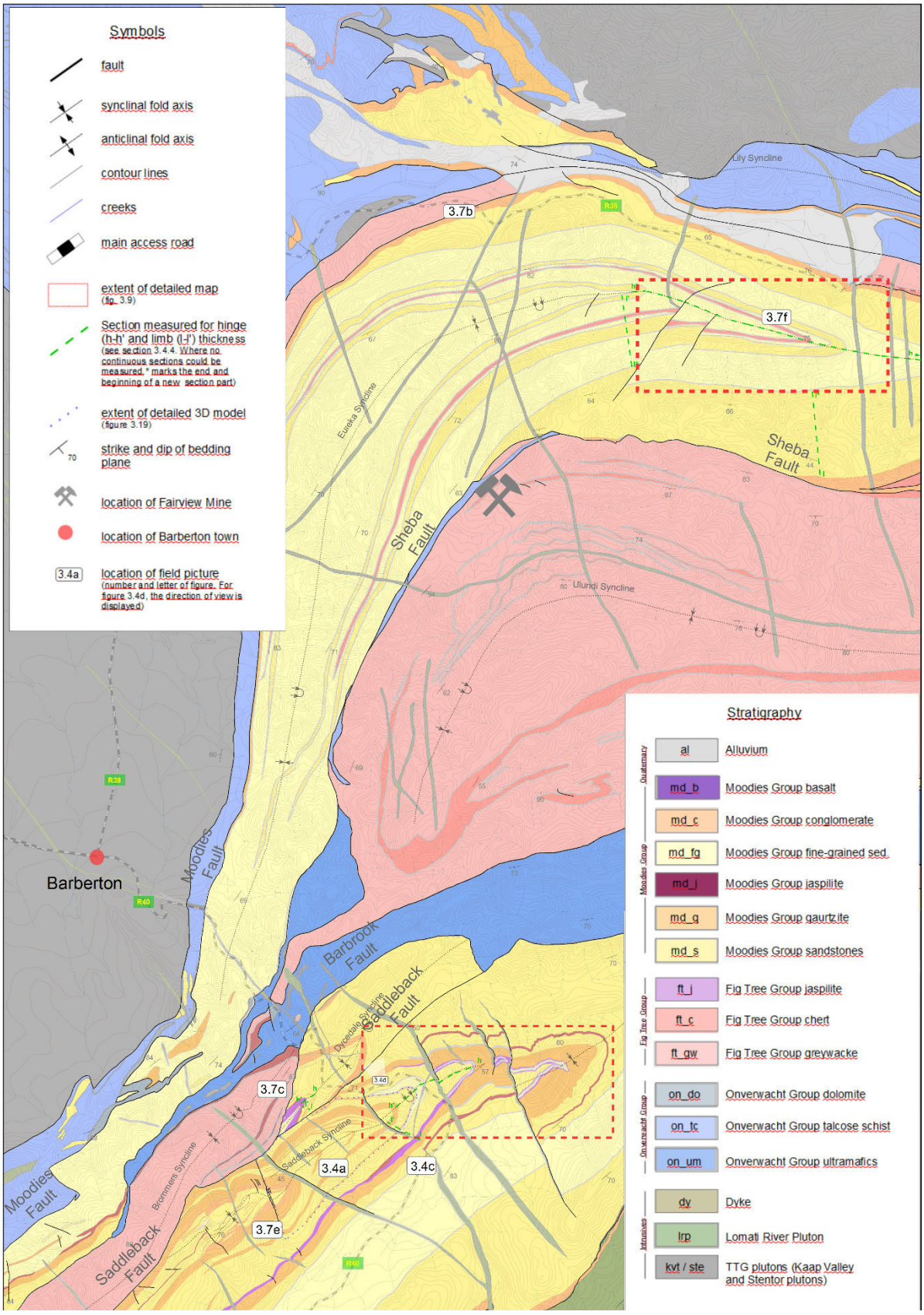

Fig. 3.7: Geological map of study area 1. For explanation see text. Location is shown in Fig. 3.1.

limb, and an arcuate fold axis refolded about the same fold axis as the Eureka Syncline. Its double inward plunge (69° at the eastern, 56° at the southern margin) shallows to 16° and becomes horizontal towards the center of the syncline (3°).

South of the Ulundi Syncline, two minor, unnamed synclines in Fig Tree Group strata show a similar geometry as the Ulundi Syncline. Fold axes plunge steeply at their northeastern and southwestern ends and shallow down-plunge. Axial planes of both synclines dip towards the south, with overturned southern limbs.

Brommers Syncline

The Brommers Syncline is a narrow syncline (c. 20 x 1.5 km) south of Barberton, consisting of competent greywacke, incompetent fine-grained ferruginous sediment and brittle chert of the Fig Tree Group (Fig. 3.7). Bedding planes dip steeply southeast; the southern limb of the syncline is overturned. The fold axial plane strikes northeast-southwest and the fold axis plunges moderately (43°) towards the southwest. An eastward plunge at its western end (Lowe et al., 2012), outside the study area, defines a double plunge. The incompetent units show abundant minor folding. The Brommers Syncline is separated by the Barbrook Fault from the Moodies Hills Block to the north and by the Saddleback Fault from the Dycedale and Saddleback synclines to the south.

Dycedale Syncline

The Dycedale Syncline is a small remnant of a formerly larger syncline consisting of Moodies Group rocks, covering an area of only ca. 4 km by 1 km. Its fold axial plane strikes northeast-southwest; its southeastern limb is overturned. Bedding planes generally dip steeply to the southeast. The fold axis of the Dycedale Syncline plunges steeply (mean 47°) towards the southwest. The Dycedale Syncline is truncated by the Barbrook Fault to the north and the Saddleback Fault to the south.

Saddleback Syncline

The Saddleback Syncline is the dominant feature in the southern part of study area 1. It reaches ca. 28 km NE-SW and consists mainly of competent quartz-rich sandstone, incompetent fine-grained sediment, and subordinate lithologies, including conglomerate and jaspilite, all of the Moodies Group. Like many other folds in the area, its northeast-southwest trending fold axis plunges steeply (c. 60°) towards the southwest. Its steeply dipping southern limb reaches great thickness of up to 3.5 km and is overturned. Similar to the Eureka Syncline, the fold axis is truncated obliquely by the bounding fault to the north (the Saddleback Fault), so that only the overturned southern limb is preserved for the westernmost 20 km of its length. Numerous brittle faults approximately perpendicular to the strike of the fold axial plane offset the hinge zone (Fig. 3.9), partially repeating hinge stratigraphy (Engelhardt, 2012). The overturned southern limb of the Saddleback Syncline exposes the complete thickness of the Moodies Group and several hundred meters of conformably underlying Schoongezicht volcanics and volcaniclastics.

The Saddleback Syncline is marked by the Saddleback Fault separates the Saddleback Syncline from the Dycedale and Brommers Synclines. Towards the west, the Saddleback Syncline extends to the Montrose Anticline, outside the study area (Fig. 3.1). The Inyoka Fault defines the southern boundary of the Saddleback Syncline.

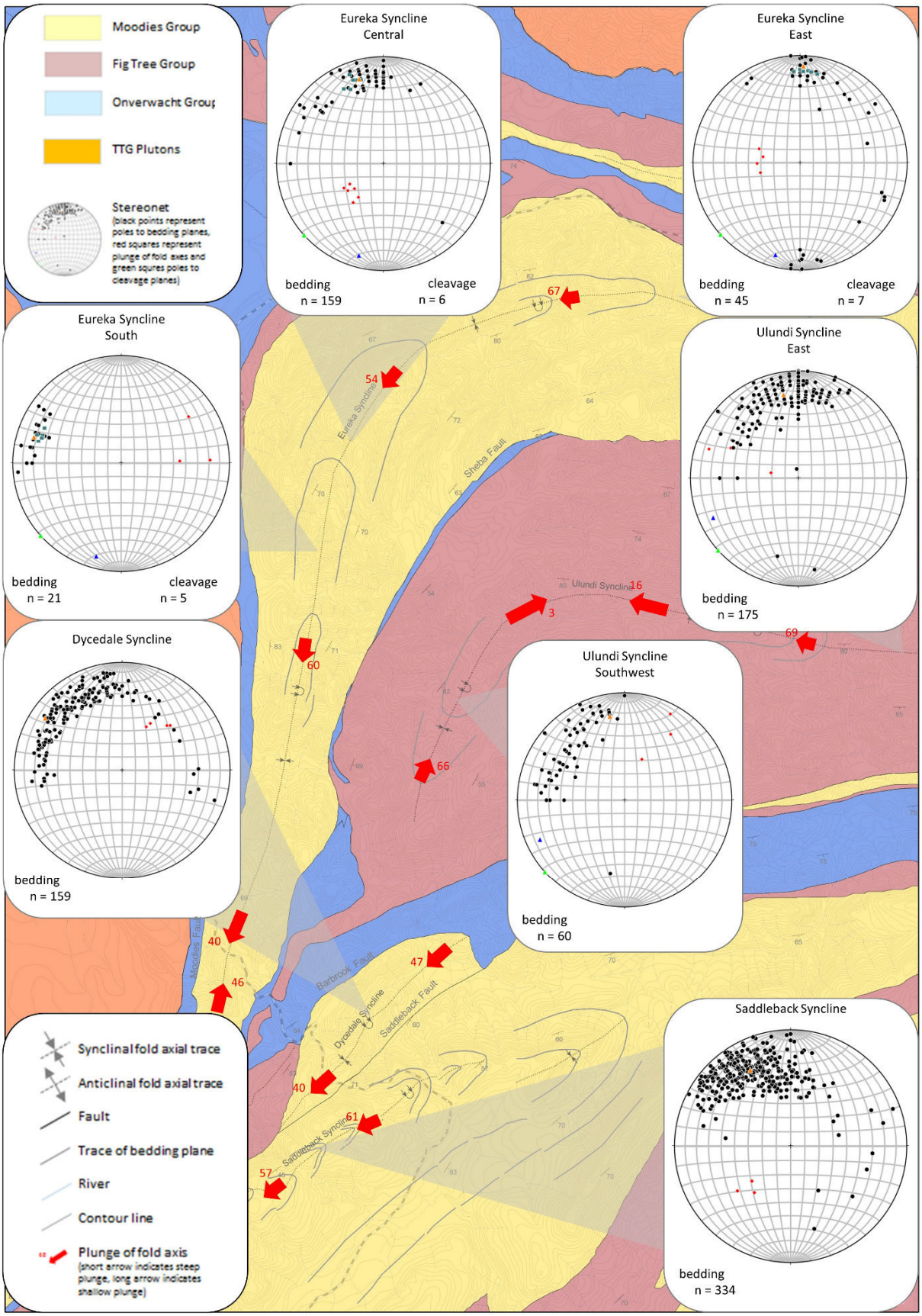

Fig. 3.8: Structural map of study area 1

3.4.2.2 Faults

Strike Faults

All major faults in the study area strike subparallel to the orientation of the fold axial planes. The dominant faults include the Lily Fault, which separates the Jamestown Schist Belt from the Eureka Syncline and represents the northeastern prolongation of the Moodies Fault, the Sheba Fault, which separates the Eureka Syncline from the Ulundi Syncline, the Barbrook Fault, which separates the Dycedale from the Brommers Syncline, and the Saddleback Fault, which separates the Saddleback Syncline from the Brommers and Dycedale synclines (Fig. 3.8). The Moodies and Saddleback Faults truncate the fold axes of the southwardly adjacent synclines (Eureka and Saddleback Synclines, respectively).

While the Barbrook and Saddleback faults strike SW-NE, the Lily and Sheba faults are as arcuate as the adjacent folds, due to late refolding of the original fold axes (Lowe et al., 1999). Displacement along mostthese faults is up-to-the-north (e.g Lowe et al., 2012).

Internal Faults

Many folds in the study area show minor internal faults perpendicular to the strike of the respective fold axial planes (Figs. 3.7, 3.13). These faults mostly occur in the hinge zone of the folds and usually terminate within the limbs. They show seemingly strike-slip displacement and top-to-the-southwest displacement in map view. The common NNW-SSE striking dolerite dikes of ca. 2967 Ma age (Olson et al., 2010) occasionally follow the weaknesses created by these internal faults.

3.4.2.3 Subsurface data

Barberton Mines provided subsurface data from several levels of Fairview Mine (Fig. 3.7 for location), located at the complex transition from the Eureka Syncline to the Ulundi Syncline (Fig. 3.3). Those allowed us to trace fold axial geometry from the surface to ca. 1.6 km depth. Chert beds of the Swartkoppie Formation (a local term for strata of the Onverwacht Group) were used as a marker horizon to determine fold geometry. Fold axial plunge and fold style does not significantly change with depth (Fig. 3.10).

3.4.2.4 3D Model

The 3D-model of the study area shows variable fold geometries. While Onverwacht Group strata form narrow and tightly folded anticlines or highly sheared fault zones, Fig Tree Group strata appear to form synclines with the characteristic canoe-shaped geometry (section 3.2.2). The large synclines filled by Moodies Group strata dominate the 3D model. Due to their large length and consistently high plunge values along the fold axis, they are inferred to extend to much greater depth than the other fold types. For better visualization of the model, a 3D pdf file showing the 3D model of area 1 is provided in the supplementary data.

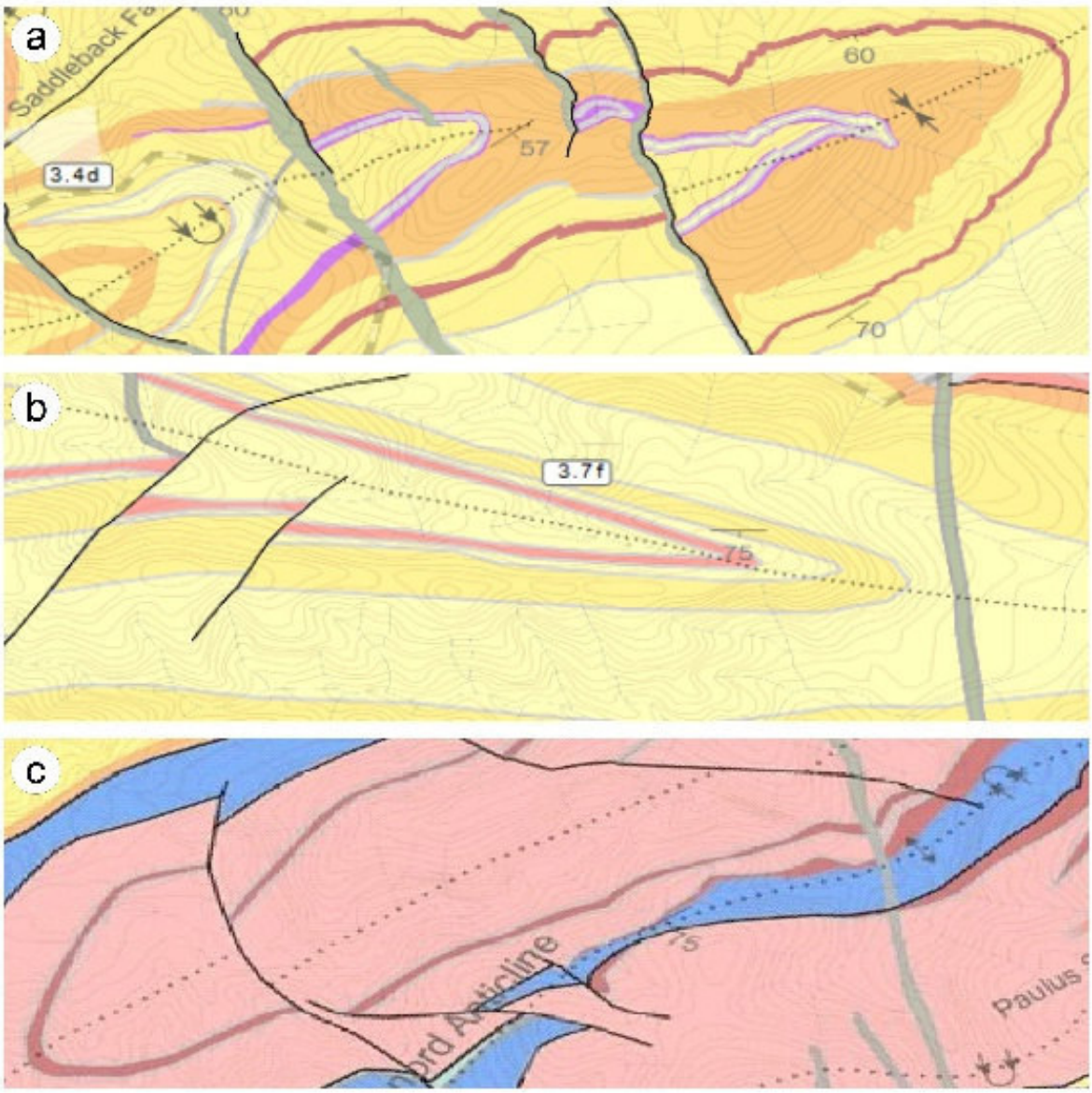

Fig. 3.9: Detailed maps of hinge zones offset by minor faults. (a) Map of the hinge zone of Saddleback Syncline. See Fig. 3.7 for location. (b) Map of hinge zone of the Eureka Syncline. See Fig. 3.7 for location. (c) Map of the hinge zone of the Manzimnyama Syncline. See Fig. 3.13 for location.

3.4.2.5 Paleocurrents

Overall, sediment transport within the Moodies Group occurred parallel to the strike of the fold axial planes. It appears to be mostly directed towards the northeast and, importantly, independent of fold axis plunge direction (Fig. 3.12). A second, less pronounced trend is transport perpendicular to the strike of the fold axial plane, which can be observed in data collected near Elephant's Kloof and, to a smaller extent, at many other locations. These findings are consistent with paleocurrent data presented by Heubeck & Lowe (1994b).

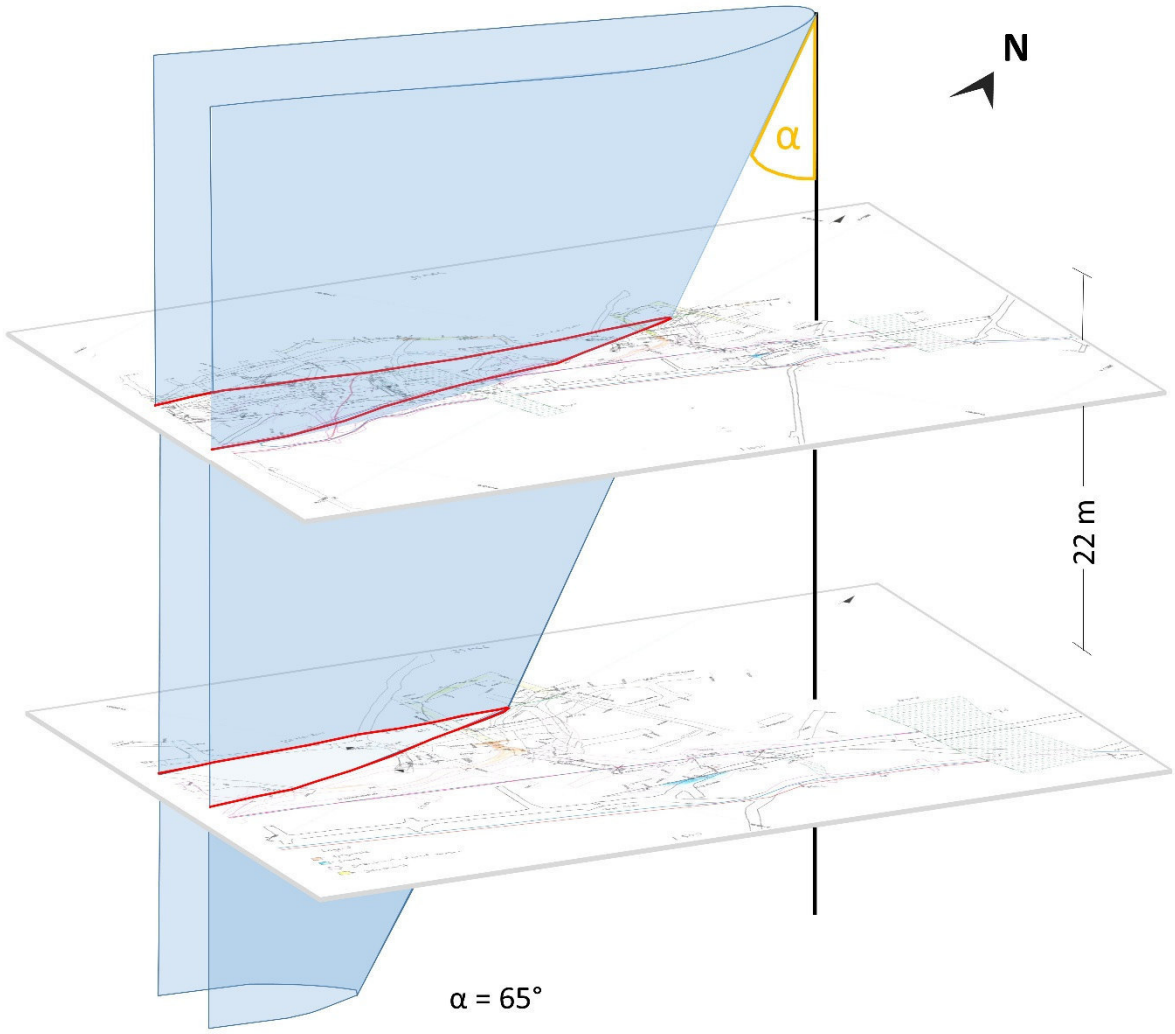

Here Fig. 3.10

Fig. 3.10: Fold hinge geometry at Fairview Mine. The geometry of the fold mapped at different levels (red lines), spaced 22 m apart, allows to trace the plunge of the fold axis underground. Note that fold axial plunge does not change with depth.

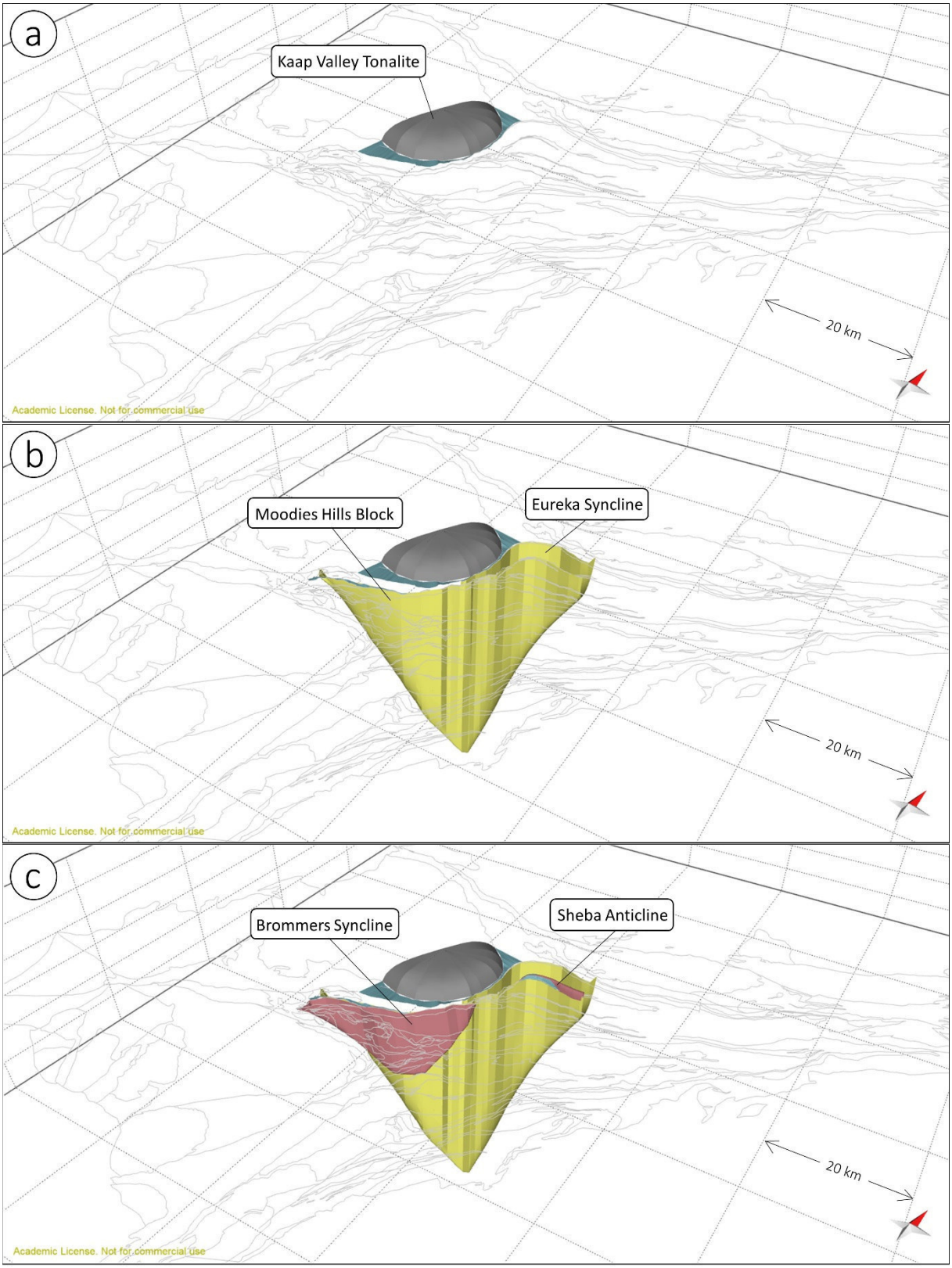
a
Kaap Valley Tonalite
20 km
Academic License. Not for commercial use
b
Moodies Hills Block
Eureka Syncline
20 km
Academic License. Not for commercial use
c
Brommers Syncline
Sheba Anticline
20 km
Academic License. Not for commercial use

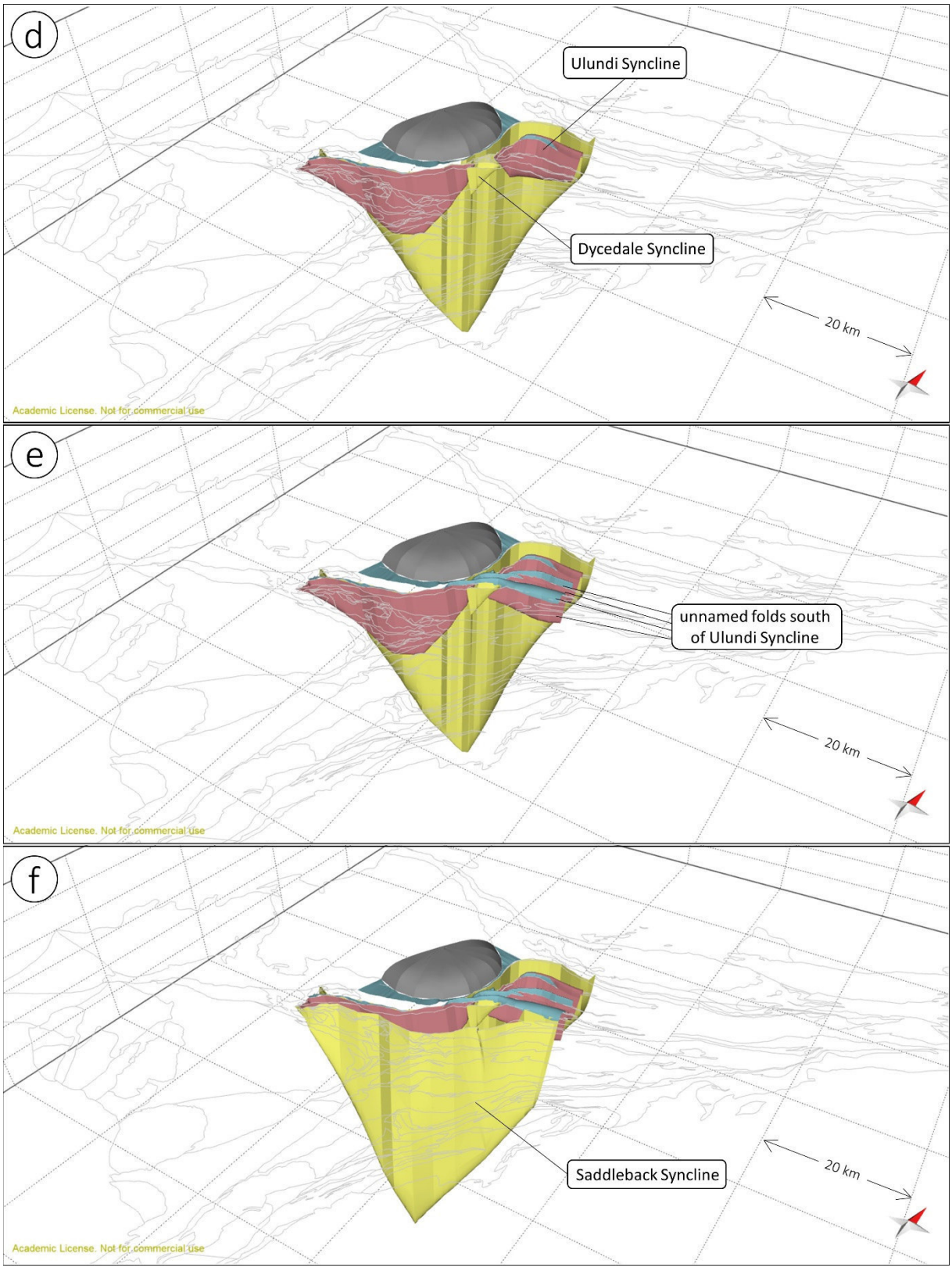

Figure 3.11: 3D model of area 1. The red arrow indicates north. Blue colored folds represent Onverwacht Group strata, red Fig Tree Group and yellow Moodies Group. The Kaap Valley Tonalite is colored grey. For a better view of the model, see the 3D pdf in the supplementary data.

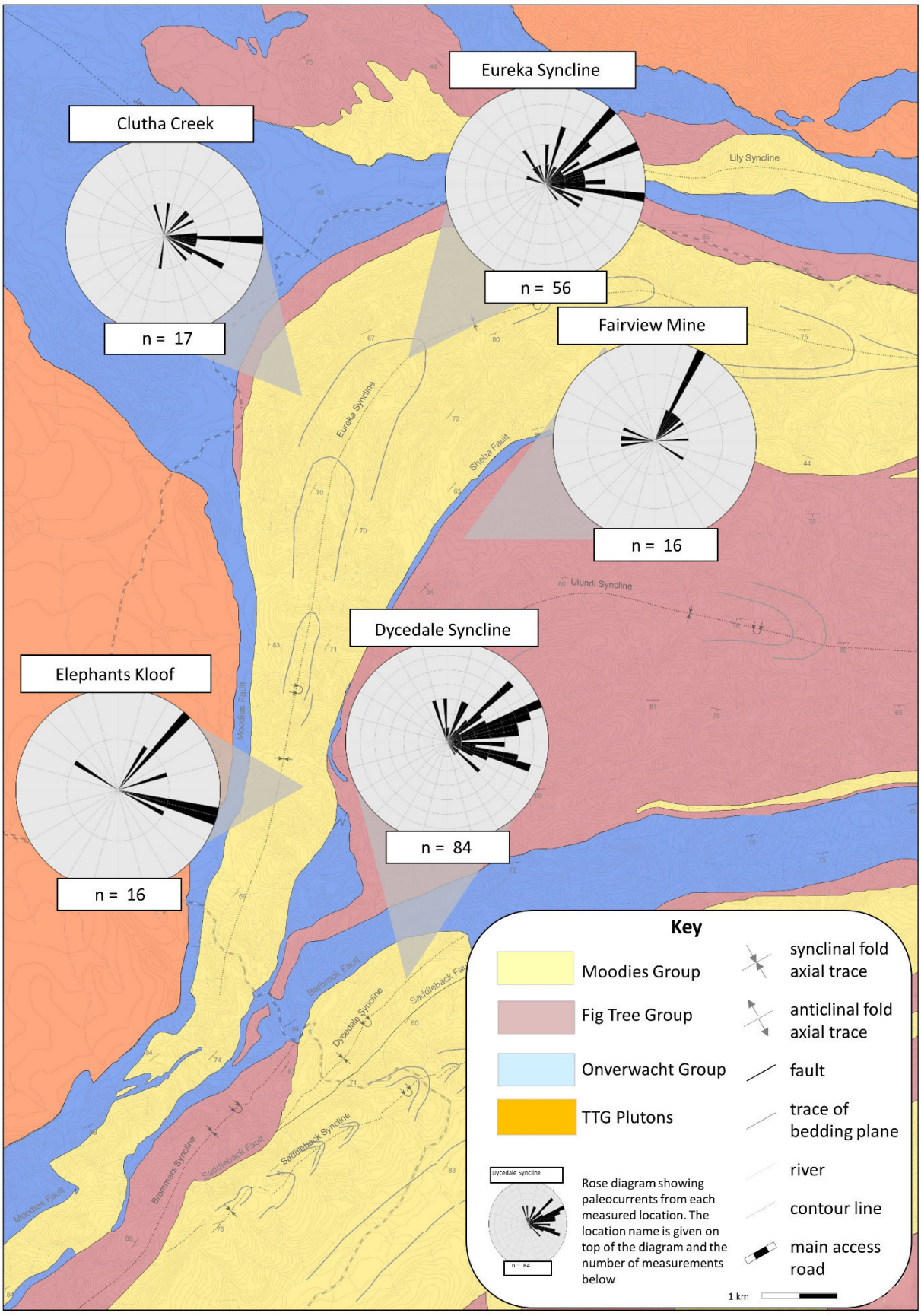

Fig. 3.12: Structurally restored paleocurrent orientations from study area 1 is directed towards the northeast. For explanation, see text.

3.4.3 Structures in area 2

3.4.3.1 Regional fold structures

Area 2 overlaps partially with area 1 and includes the following additional structures.

Maid-of-the-Mists, Heemstede and Angle Station Syncline

These three synclines (Fig. 3.13), each a few km long and involving ca. 1 km thick Moodies strata, form part of a belt of Moodies strata immediately south of the Inyoka Fault. They are arranged en-echelon and are separated by brittle, hydrothermally altered and subvolanically intruded faults, which probably accommodated only of minor shortening.

The Maid-of-the-Mists Syncline is an in map view ovoid, east-west striking syncline, c. 3.5 km long. Its southern limb is overturned only in the eastern part of the syncline, while its western part is upward-facing. The doubly plunging fold axis shows plunge values between 36° and 49°. The syncline is separated from the Heemstede Syncline to the northeast by a series of unnamed splay faults subparallel to the Inyoka Fault, while the 24-Hour-Camp-Fault separates it from deformed Fig Tree and Onverwacht strata to the south.

The poorly exposed Heemstede Syncline is tightly folded and shows an overturned southern limb. Bedding planes are steeply inclined to the south or southwest. In its eastern part, the fold axis plunges steeply (52°) to the east; in its western part, to the west (57°). It is thus one of few examples of a syncline with a bidirectionally outwardly plunging fold axis, apparently away from an up-plunge culmination in the center of the fold. The seemingly arcuate shape of the central fold axial trace in map view is an artifact of a deep valley (Lowe et al., 2012).

The Angle Station Syncline strikes NNE-SSW. It has an overturned eastern limb and a fold axis moderately (35-46°) plunging towards the NE. It is bordered by the Heemstede Syncline to the west and the Masenjane Block to the west, both of which are separated from the Heemstede Syncline by unnamed faults.

The The Heights Syncline is a narrow (1.6 km wide), NE-SW striking and c. 14 km long syncline with an overturned southeastern limb. Its fold axis plunges doubly at about 45°; its maximum depression lies in the northeasternmost third of the syncline, outside of the study area. The syncline consists of quartzites and subordinate conglomerates of the Moodies Group. It is terminated to the north by the Kromberg Fault Zone, while an unnamed fault separates the it from the Manzimnyama Syncline to the south.

Loenen Anticline

The Loenen Anticline is a narrow anticline consisting of talcose and serpentinite schists of the Onverwacht Group. It strikes approximately NNE-SSW to ENE-WSW. It shows an overturned northwestern limb. Its fold axis plunges towards the northeast. The Loenen Anticline is bordered by the The Heights Syncline to the north and the Manzimnyama Syncline to the south.

Manzimnyama Syncline

The Manzimnyama Syncline is an elongated, NNE-SSW- to NE-SW-striking syncline filled by greywacke, fine-grained siliciclastic sediment and BIF of the Fig Tree Group. It shows an overturned southeastern limb and steeply inclined bedding planes. The fold axis plunges 42° to 45° to the northeast; a possible depression or culmination is not known. The Manzimnyama Syncline shows a number of minor faults perpendicular to the strike of the fold axial plane with up-to-the-southwest displacement and a minor strike-slip component (Figs. 3.9, 3.13). The Manzimnyama Syncline is separated from the The Heights

Syncline to the north by the Loenen Anticline and by the Schoonoord Anticline from Paulus's Syncline to the south.

Schoonoord Anticline

The Schoonoord Anticline is a narrow anticline consisting of altered mafic volcanic rocks of the Onverwacht Group, which strikes approximately NNE-SSW to ENE-WSW. It shows an overturned northwestern limb and its fold axis plunges towards the northeast. Although it can be traced along strike of the fold axial plane for c. 9 km, its width is only 100 - 350 m. The Schoonoord Anticline is bordered by the Manzimnyama Syncline to the north and the Paulus Syncline to the south.

Paulus Syncline

Paulus Syncline is a tightly folded syncline consisting of conglomerate, greywacke, siltstone and BIF of the Fig Tree Group. It strikes generally NNE-SSW to ENE-WSW and shows an overturned southeastern limb. Its fold axis trends northeast and plunges at c. 50° in that direction. Regional mapping indicates that the Paulus Syncline is doubly-plunging; in its northeastern part, outside the study area, the fold axis plunges 45° - 50° towards the southwest. It is bordered by the Schoonoord Syncline to the north and the Songimvelo Syncline to the south.

Songimvelo Syncline

The Songimvelo Syncline consists of quartzites and conglomerates of the Moodies Group. It is strongly refolded so that the strike of the fold axial plane varies between SSW and E. The syncline shows an overturned southern limb and a large variability in the steepness of bedding planes (28° to 83°). It is one of few examples of a syncline with an outwardly plunging fold axis; the culmination lies in the western part of the fold. It is separated by an unnamed fault from the Paulus Syncline to the north and by the Songimvelo Fault from a minor syncline consisting of Fig Tree strata to the south.

3.4.3.2 Faults

Strike Faults

As in study area 1, all major faults strike parallel to the orientation of the fold axial traces of the adjacent folds. Most of the folds are fault-bounded. Only the faults north of the Inyoka Fault are named with the exception of the Songimvelo Fault. North of the Inyoka Fault, major faults include the Moodies Fault, marking the northern boundary of the Moodies Hills Block, the Barbrook Fault, which separates the Brommers Syncline from the Dycedale Syncline and the Saddleback Fault, which separates the Saddleback Syncline from the Brommers and Dycedale synclines. The Inyoka Fault, which represents the boundary between the Saddleback Syncline and the folds adjacent to the south, is commonly referred to as a suture zone (Viljoen & Viljoen, 1969), separating two different terranes marked by changes in sedimentary facies (Lowe & Byerly, 1999) and distinct petrographic composition (Lowe & Byerly, 2007).

Internal Faults

Similar to study area 1, internal faults occur in the hinge zone of the folds (Figs. 3.9, 3.13). The internal faults show strike-slip and up-to-the-northeast displacement in map view. The NNW-SSE striking dikes, which can be observed all across the BGB, are commonly emplaced along such internal faults. Additionally, faults at an angle of c. 45° to the strike of the fold axial plane occur in the Manzimnyama Syncline (Fig. 3.13).

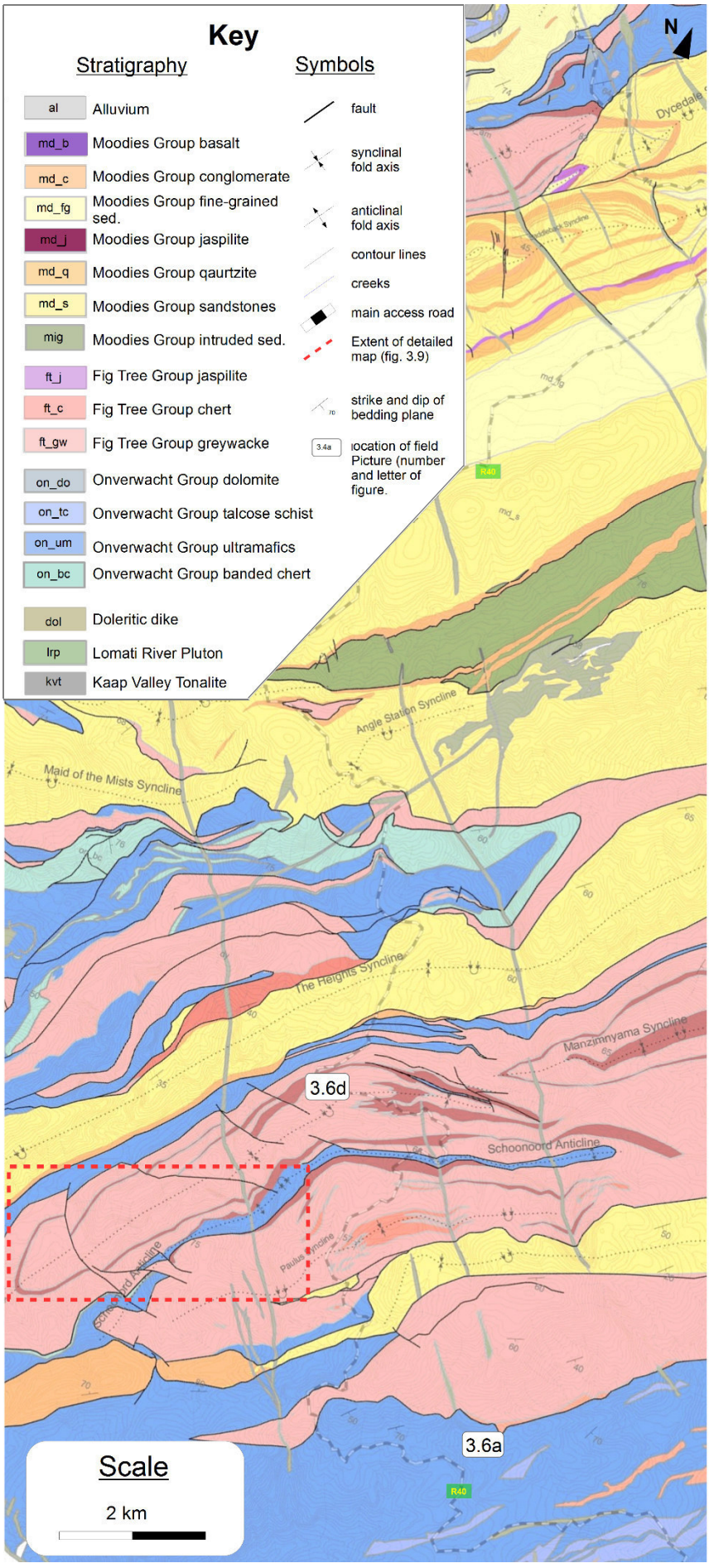

Fig. 3.13: Geological map of study area 2.

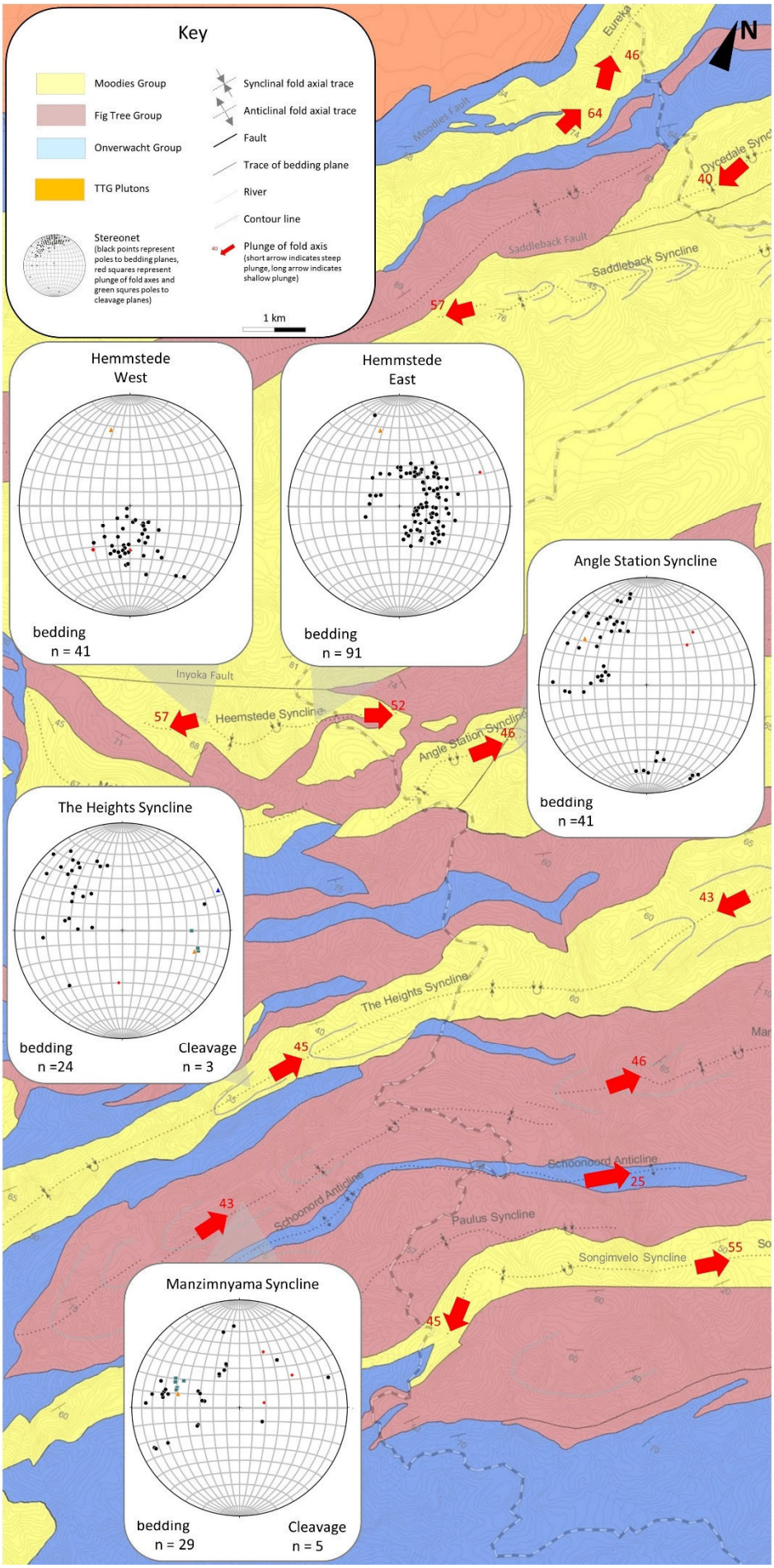

Fig. 3.14: Structural map of area 2.

Folds in both study areas share, with few exceptions, numerous properties. Well-developed anticlines are rare. Where they are present, their core is usually taken up by highly incompetent talcose or serpentinized ultramafic volcanics and minor chert units of the Onverwacht Group (Fig. 3.3). Synclines are always composed of Fig Tree or Moodies Group strata, which mainly consist of variably competent greywacke or highly competent quartzose siliciclastica, respectively. Despite of the commonly tight folding, almost no internal deformational features and strain markers can be observed.

Bedding planes are generally steeply inclined to subvertical in the central part of the BGB. The fold axial plane of most folds is inclined to the S or SE and, thus, the southern limbs of synclines are commonly overturned. Cleavage planes defined by mineral elongation is usually oriented parallel to the fold axial plane. Schistosity can best be observed in fine-grained sediments of the Fig Tree Group and, to a lesser extent, of the Moodies Group. Competent units, such as the thick quartzose sandstones of the Moodies Group, show virtually no strain except in the hinges of the synclines. Fold axes plunge moderately to subvertically and mostly inward, while anticlines show, where preserved, outwardly plunging fold axes. Many fold axes are slightly to strongly arcuate (most strongly those of the Eureka and Ulundi Synclines) due to refolding of the originally SW-NE-oriented fold axes around the circular competent plutons adjacent to the BGB.

Fold axes are obliquely truncated by faults subparallel to the strike of the greenstone belt in the Moodies Hills, the Dycedale and the Saddleback synclines. Internal faults perpendicular to the strike of the fold axial planes are common and displace the down-plunge part of the fold on top of the up-plunge part of the fold with subordinate strike-slip movement.

Incompetent lithologies, such as fine-grained sedimentary rocks, increase markedly in thicknesses in the fold hinges (e.g. Saddleback or Eureka synclines; Fig. 3.7) while competent lithologies, such as Moodies sandstones and conglomerates, show little thickness variation there. Thick homogenous strata, such as the greywackes of the Ulundi Syncline, appear to show little or no hinge thickening. While the thickening factor (ratio of hinge thickness to limb thickness) reaches nearly a value of 5 in the Eureka Syncline (Table 3.1), but is strongly lithology-dependent: Fine-grained sediments (md_fg) in the Eureka Syncline show a thickening factor of nearly 10, more competent sandstones thicken little (values between 1.3 and 2.4). Thicknes variations in the Saddleback and Dycedale Synclines show a lower but similar trend (Table 3.1). Fine-grained sediments (md_fg) commonly show the highest hinge to limb-thickness ratio, while conglomerates (md_c), jaspilite (md_i), basalt (md_b) and, to a lesser extent, sandstones (md_s) show little hinge thickening.

3.5 Discussion

3.5.1 Fold classification

Relative limb thinning and hinge thickening (Fig. 3.9) identifies folds of the central BGB as Class 2 folds of Ramsay (1967). The steep to moderate plunge (up to 60°) does not shallow along trend in the Eureka, Saddleback and Dycedale synclines, suggesting their considerable depth (Fig. 3.15 d).

These highly non-cylindrical folds resemble large sheath folds (Cobbold & Quinquis, 1980), common in metamorphic terranes, where most deformation occurs by processes that permit high strain and extensive ductile flow by unidirectional shear (Skjernaa, 1989; Alsop & Holdsworth, 1999, 2006). However, the paucity of structures indicating penetrative deformation and the negligible strain implies that one or several different mechanism have shaped these folds. Thus, the term *sheath fold* should not be applied.

Thickness variations within folds of the Central Barberton Greenstone Belt				
Fold	**Stratigraphic Unit**	**Thickness Limb**	**Thickness Hinge**	**Ratio Hinge / Limb**
Eureka Syncline	md_s	70 m	170 m	2,42
	md_fg	280 m	850 m	3,04
	md_j	70 m	130 m	1,86
	md_fg	50 m	260 m	5,2
	md_s	170 m	230 m	1,35
	md_fg	460 m	4590 m	9,98
	md_s	1300 m	5230 m	4,02
	total	**2400 m**	**11460 m**	**4,78**
Saddleback Syncline	md_q	110 m	120 m	1,09
	md_s	180 m	320 m	1,78
	md_c	10 m	10 m	1
	md_fg	10 m	190 m	19
	md_s	190 m	770 m	4,05
	md_i	20 m	20 m	1
	md_fg	20 m	20 m	1
	md_i	20 m	20 m	1
	total	**560 m**	**2030 m**	**3,63**
Dycedale Syncline	md_b	60 m	80 m	1,33
	md_s	30 m	100 m	3,33
	md_c	10 m	10 m	1
	md_s	380 m	1130 m	2,97
	md_c	100 m	100 m	1
	total	**580 m**	**1420 m**	**2,44**

Table 3.1: Thickening factors derived from thickness variations within folds of the central Barberton Greenstone Belt. See Fig. 3.7 for traces of measured sections.

3.5.2 Lithology control on fold style

Folds cored or principally composed of different lithologies in map view differ systematically in their 3-D geometry (Figs. 3.7, 3.8, 3.11, 3.13, 3.14). While plunges in Fig Tree synclines shallow and, thus, form “canoe-synclines” (Figs. 3.2, 3.15b), plunges in Moodies synclines appear to remain steep. The resulting folds are deep and resemble flattened cones (Fig. 3.15d).

There are a at least three possible explanations for this observation:

(1) Both styles represent temporally distinct deformation phases. Onverwacht and lower Fig Tree Group strata were deformed during D2 prior to onset of Schoongezicht Formation and Moodies Group deposition (Lowe et al., 1999; Lowe & Byerly, 1999; Byerly et al., 2018). If so, one could argue, that structures of the earlier deformation phase should be tighter and more strongly deformed than the younger, D3- and D4-deformed Moodies Group (and Schoongezicht Formation) strata, which is not the case. However, bending stresses in canoe folds (e.g. Cobbold & Quinquis, 1980; Skjernaa, 1989) are actually higher because plunge changes continuously, while plunge appears largely invariable along fold axis trend in folds cored by Moodies strata, which provides an explanation for the steeper plunging folds consisting of younger and less deformed strata.

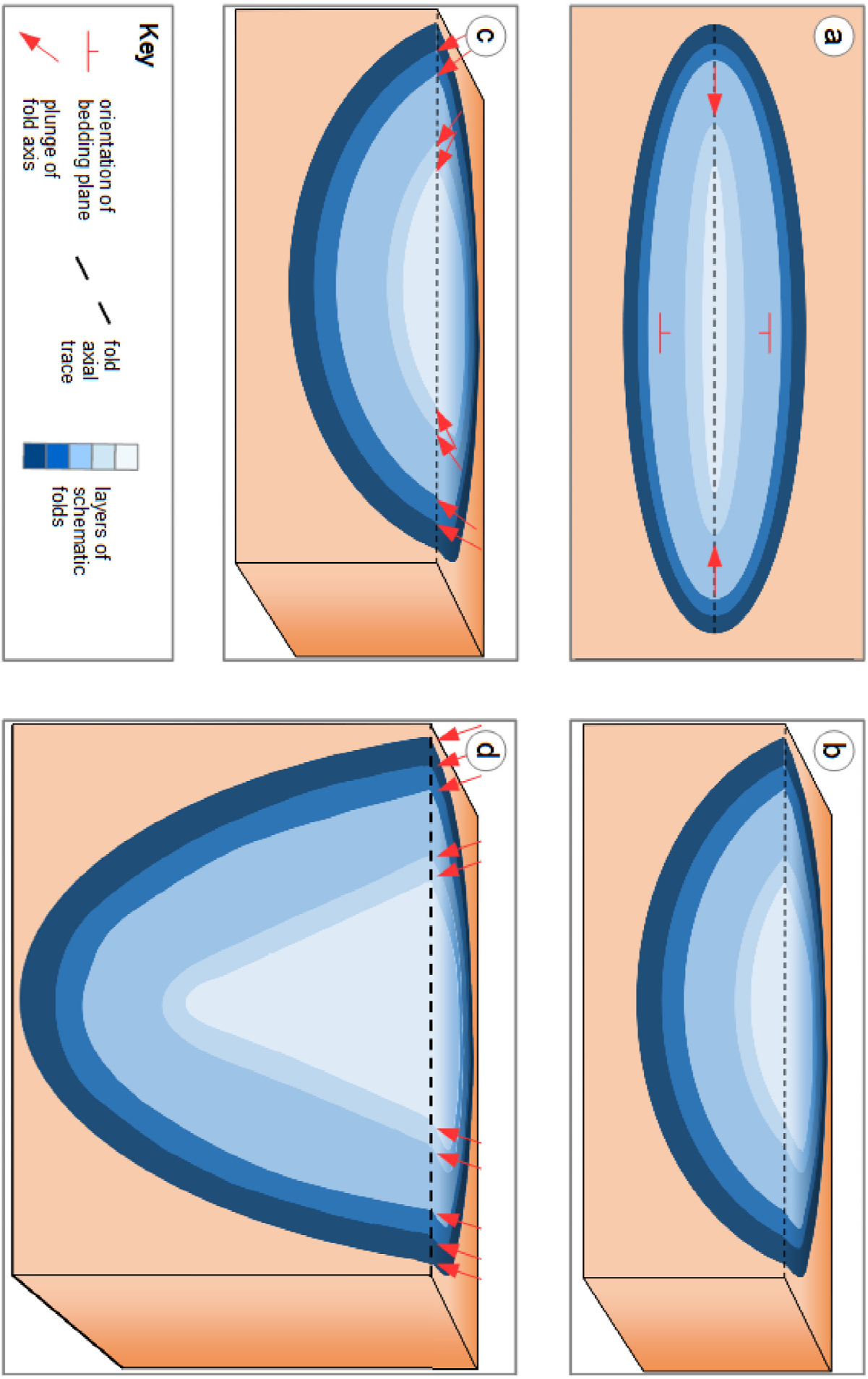
a
b
c
d
Key
orientation of bedding plane
plunge of fold axis
fold axial trace
layers of schematic folds

Fig. 3.15: Map view (a) and block diagrams (b, c, d) of schematic BGB synclines. Cross sections front faces of block diagrams represent fold axial planes, here simplified as vertical. Red arrows indicate orientation of fold axial plunge. (a) Schematic syncline of the BGB in map view. (b) Geometry of "canoe-syncline'', as described by previous investigators (Fig. 3.2). (c) Orientation of fold axial plunges along strike of the fold axial plane inferred from the ''canoe-shape'' geometry: Fold axial plunge is steep at the far ends and shallows towards synclinal center. The resulting syncline in cross section is relatively shallow. (d) Implications of constant bidirectional plunge of fold axis along strike of axial plane, as observed in the majority of major synclines consisting of Moodies Group strata in the central BGB. This geometry predicts a much greater depth of the synclinal depression.

(2) Deformation geometry depends not only on tectonic parameters but also on lithological properties of the deformed units (Fischer & Jackson, 1999). Fig Tree and Moodies Groups differ significantly in their lithological composition. While the Fig Tree Group consists mainly of incompetent lithologies, the Moodies Group is largely composed of competent quartzites and conglomerates. This may result in changing fold axial plunge in the easily deformable Fig Tree strata compared to constant fold axial plunge in stiff and rigid Moodies Group strata.

(3) The fold pattern in map view may represent different structural levels exposed at the surface. If D3 affected both deformed Fig Tree and undeformed Moodies strata by buckling, Fig Tree strata would represent the limbs and lower levels of such synclines, Moodies strata their cores and upper parts. Exposed lower structural levels would then tend to show a shallower fold axis plunge axis (Fig. 3.16).

3.5.3 Comparison between 3D model and 2D cross section

In the effort to derive a meaningful depth structure of the central BGB, information derived from synclinal trends is more important than limb thickness in cross section because the former yields a continuous constraint of quantitative data for up to 20 km (along the traces of the Saddleback and Eureka Synclines), the latter for not more than 3.6 km (the maximum stratigraphic thickness of Moodies strata on the overturned limb of the Saddleback Syncline). In addition, the degree of bending of these limbs at depth is virtually unconstrained, whereas variation in fold plunges can be measured. (Figs. 3.5, 3.17).

Heubeck and Lowe (1994a), in an early attempt to sketch depth geometry of the BGB, estimated the minimum depth of the synclines along a Barberton-to-Piggs Peak transect through the central BGB in a purely 2-D approach by assuming flexural-slip bending and constant stratigraphic thickness (approach by Dahlstrom (1969)) along the line of section, constrained by limb thickness only. This approach did not take into account the variable and commonly steep fold plunges of the synclines crossed by the line of section.

This is not so much of a problem for the ''canoe-shaped'' synclines of Fig Tree Group strata because these are shorter and plunge shallows towards their center. Their depth, thus, does not vary significantly along strike of the fold axial plane; depths derived from the 3D model do not differ greatly from those derived from the 2D-cross section. Moodies Group synclines, on the other hand, show large differences in depth along strike due to their continuously plunging fold axes and, thus, large differences between depth inferred from the 3D model and those from the 2-D cross-section. The true depth of a Moodies fold into depth in a cross section strongly depends on the position of the 2-D cross section along strike of the fold axial plane (Fig. 3.17).

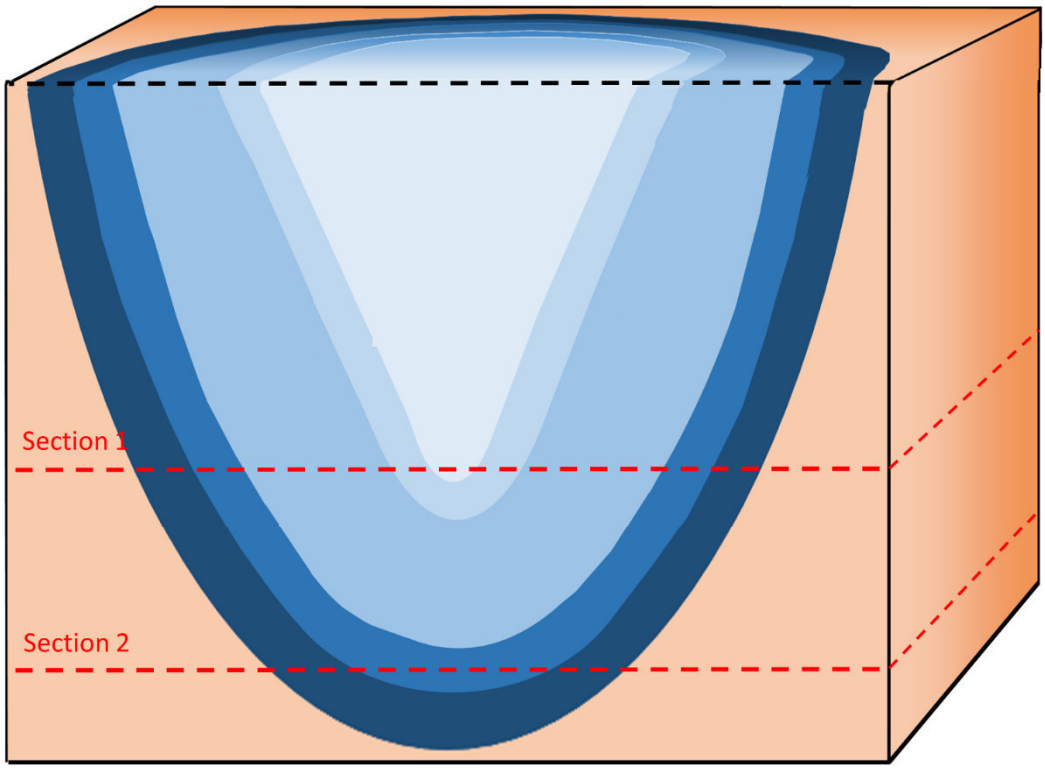

Section 1:

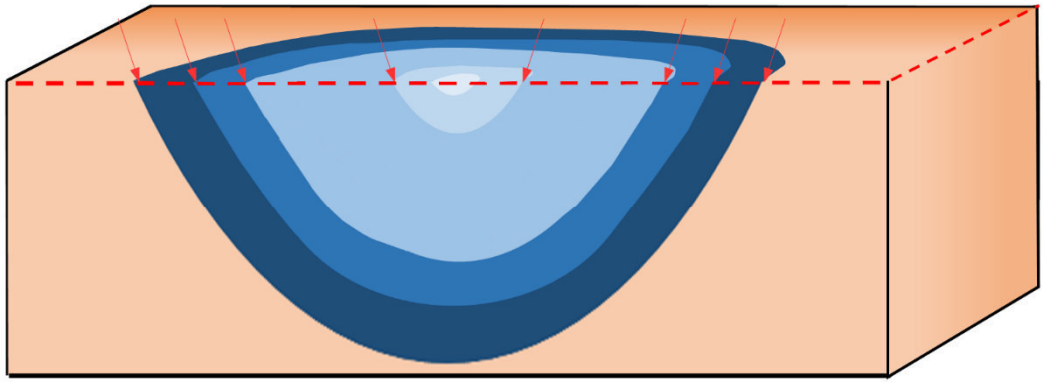

Section 2:

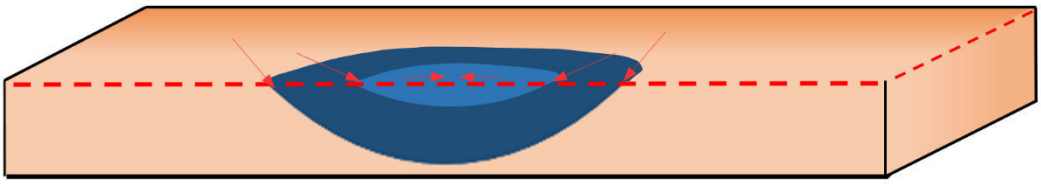

Fig. 3.16: Exposure of different structural levels of folds in the central BGB and its effect on fold geometry. Darker layers represent older stratigraphic units. The dashed red lines show sections at two different levels through the fold. Section 1 shows a flattened sheath-fold geometry at a higher structural level; section 2 shows a canoe geometry at a deeper structural level of the fold.

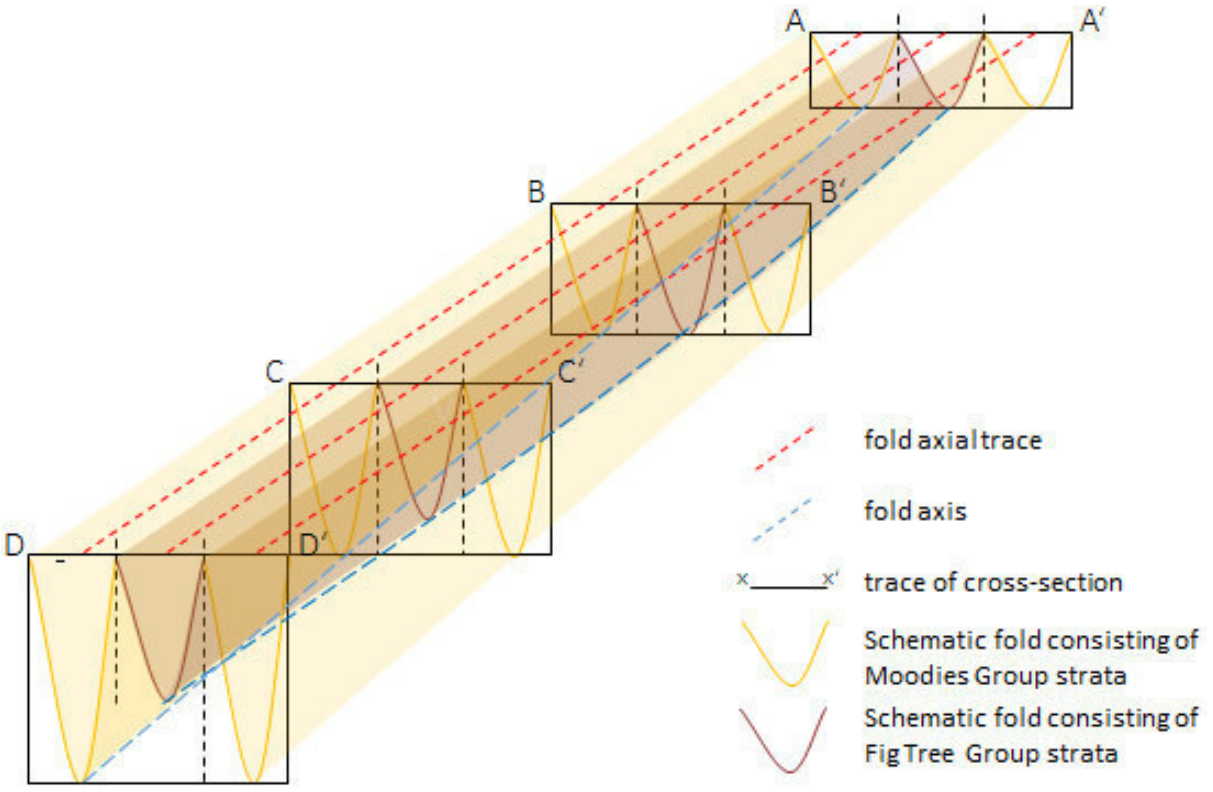

Fig. 3.17: Illustration of the dependency between the depth of a synclines' hinge in cross-section and the position of the cross section along strike of the fold axial plane. Four simplified cross-sections show the geometry of schematic synclines of Moodies and Fig Tree Group strata. The depth of the hinge increases down-plunge, especially in the synclines consisting of Moodies Group strata because of their constant steep fold axial plunge along strike of the fold axial plane.

3.5.4 Depth extent of folds

Two arguments bear on the depth of folding in the central BGB.

(1) Constant steep plunges of the fold axes of Moodies synclines in outcrop suggest their constancy also at depth, which is also confirmed by limited subsurface data from Fairview Mine. 3-D modelling and cross section construction shows that fold hinges consistently plunge at values between 50° (Eureka Syncline) to 60° (Saddleback Syncline) for many km and involve strata with little recognizable ductile strain. Folds thus must extend to 25 - 30 km depth (Figs. 3.5, 3.15 d).

(2) Synclines filled by Moodies Group strata are likely underlain by Fig Tree and/or Onverwacht Group rocks of unknown thickness, which would extend any Moodies Group syncline's depth further.

Arguments to counterargue such inferred large depths include:

(1) Rocks involved in folding at this scale would show a significant change in metamorphic grade with depth. This should be observable along fold axis trend but is not the case.

(2) If hinge thickening was not taken into account, the original sedimentary thickness of Moodies strata, measured along the trend of the fold axes of the Saddleback and Eureka Synclines, would be about one order of a magnitude larger than the observed thickness of < 3.6 km on the limbs (Anhaeusser, 1969; Heubeck and Lowe 1994b). It thus appears unreasonable to apply hinge thicknesses and plunge values at face value.

(3) If the thickness of the Moodies Group had originally been significantly larger than preserved, the underlying Fig Tree Group should show a higher metamorphic grade because of deeper burial. This is not the case.

3.5.5 Synthesis

A reasonable hypothesis resolving these contradictions must take into account the sustained steep plunge of the fold axes along strike of the fold axial plane, the stratigraphic thickness of the units contained in the respective folds, the uniform metamorphic grade across the greenstone belt, the information from syndeformational sedimentary fill and variability of primary stratigraphic thickness, the degree of hinge thickening and limb thinning, and constraints by geophysical data.

Hypotheses addressing the disparity between measured stratigraphic thickness and depth implied from fold geometry and 3D modelling include:

(1) Folding of strata with high competence contrasts would create similar, not parallel folds (Johnson & Pfaff, 1989), leading to a significant higher thickness in the hinge compared to the thickness measured on the limbs (Table 3.1) resulting in a larger depth of the folds' depressions.

(2) Prolate-oblate ductile strain along the basin margins was significant, indicating that clasts were stretched subvertically on average by a factor of 2.7 (chapter 4, see appendix for measured values). Fold margins sagged vertically relative to the rising plutons along all BGB margins, extending its original stratigraphic depth to greater values than implied by primary stratigraphic thickness. Most prolate strain is concentrated along the southernmost part of the BGB in Eswatini (chapter 4), possibly indicating a large-scale asymmetry of late BGB deformation.

margins, extending its original stratigraphic depth to greater values than implied by primary stratigraphic thickness. Most prolate strain is concentrated along the southernmost part of the BGB in Eswatini (chapter 4), possibly indicating a large-scale asymmetry of late BGB deformation.

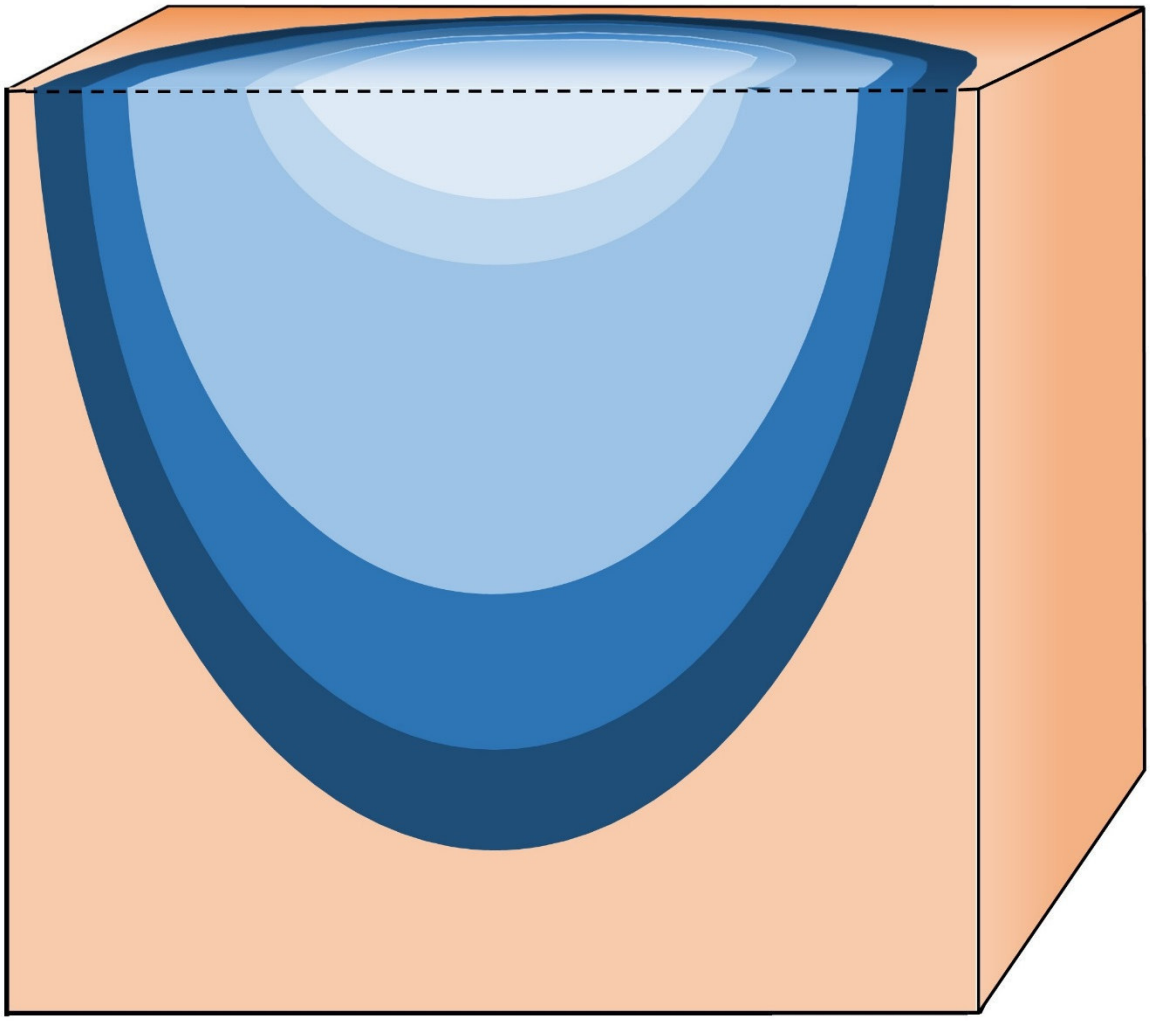

Here FIg. 3.18

Fig. 3.18: Illustrations of hypotheses addressing the contradiction between measured stratigraphic thickness and depth implied from fold geometry and 3D modelling. Both similar folding (hypothesis (1)) and later vertical stretching (hypothesis (2)) imply a similar geometry, in which the thickness of each unit increases with depth, resulting in larger vertical extent of the fold, than the stratigraphic thickness would imply. For key, see Fig. 3.21.

Hypotheses addressing the unreasonable depth inferred from fold geometry and 3D modelling include:

(3) Fold amplitude could be significantly reduced if primary stratigraphic thickness of units thinned towards the synclinal interior (Fig. 3.19 a). Although some alluvial-fluvial-deltaic Moodies units thin towards its center, such as the Lomati Delta Complex (Stutenbecker et al., 2019) of the Saddleback Syncline, this process runs counter to the commonly observed trend that sediments shed into a depression initially thicken towards the center (e.g. Duebendorfer & Wallin, 1991; Lüning et al., 1998; Teson & Teixell, 2008) because the largest accommodation space and lowest slope exist near and in the basin center, favoring deposition there. In any case, the data from the Lomati Delta Complex thins by obly c. 300 m over c. 7 km length.

The contribution of syntectonic sedimentation is difficult to quantify: Ideally, strata in the core of the syncline should lie horizontal and be underlain by numerous packages bound by progressive unconformities. These have been observed but are rare (Heubeck, 2019). Strata in the synclinal cores are subvertical, suggesting the erosion of higher structural levels many km thick.

(4) The minor faults perpendicular to fold axial plane strike may have been active as core-of-syncline-up faults. This would reduce the true depth of the fold (Fig. 3.19 b). The up-faulted fold interior would expose strata of a similar stratigraphic level as the down-faulted side because a structurally lower level of the same stratigraphic unit would have been brought to the surface (Fig. 3.20). Thus, vertical displacements on such faults would be difficult to recognize at the surface unless they crosscut marker units.

Additional faults of that type may be hidden in locations that are now occupied by the numerous NW-SE trending dolerite dikes. There may be many more unrecognized faults with no recorded vertical displacements perpendicular to the folds' trend. This hypothesis is supported by observed strike-slip displacement along some dikes in the study area (Figs. 3.7, 3.13). Although we made no field observations to support this hypothesis, structural analyses from underground mines imply the presence of reverse faults perpendicular to the folds' strike, which were reactivated as transtensional faults after the compressional regime during the deformation of the BGB had ceased at c. 3015 Ma (Dirks et al., 2009, 2013).

(5) The σ-clasts visible on some bedding planes of Moodies Group synclines suggest uplift of more central parts of the fold relative to more marginal layers suggesting, that reverse faulting along bedding-parallel, possibly listric fault planes ("out-of-syncline-thrusting") has taken place. This would repeat stratigraphic sections in map view, raise the synclinal core and reduce the depth of the depression (Fig. 3.19 c). Secondly, the apparent paucity of incompetent, fine-grained sediments in the Moodies Group may be because they preferentially accommodated the distributed faulting.

However, these kinematic indicators of ductile deformation (including also tension gashes, s-c fabric, rotated clasts and slickensides) are all rare, both in the competent sandstones and incompetent siltstones on Moodies synclinal limbs. They may have been eroded but there are no indications from subsurface exposures either. The poor documentation of fine-grained strata in synclines consisting of Moodies Group strata in the study area could alternatively be explained by poor exposure and coverage by pine plantations of these easily erodible units.

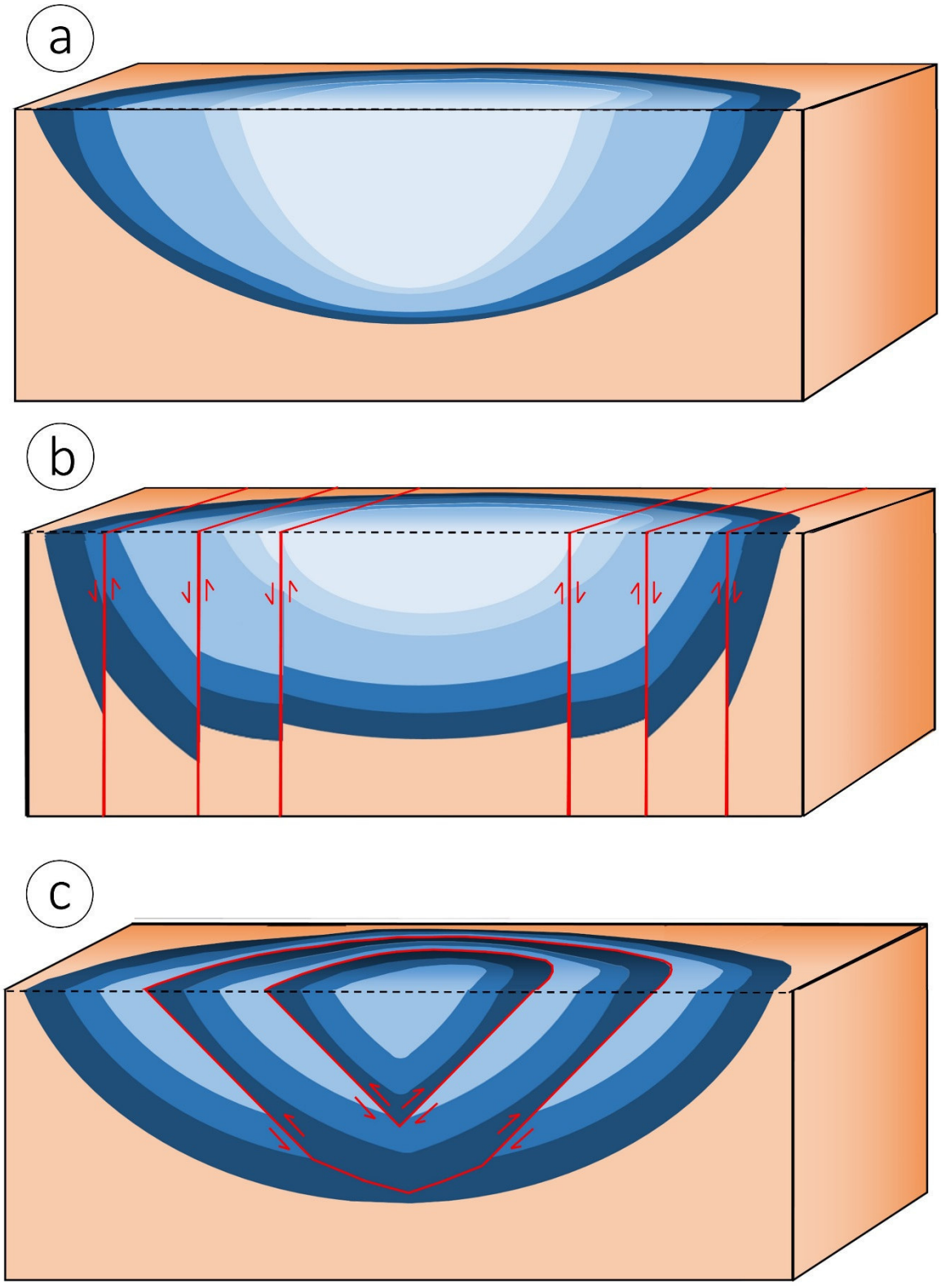

Fig. 3.19: Illustrations of hypotheses addressing the unreasonable depth inferred from fold geometry and 3D modelling. (a) Decreasing primary stratigraphic thickness towards the center of the fold (along strike) leads to a significantly reduced vertical extent of the fold. (b) Faults perpendicular to the trend of the fold axis causing uplift of the more central segments (along strike) of the fold and, thus, reducing its depth. (c) Fault planes parallel to bedding (flexural slip) causing uplift of more central parts (core) of the fold, reducing its depth. For key, see Fig. 3.21.

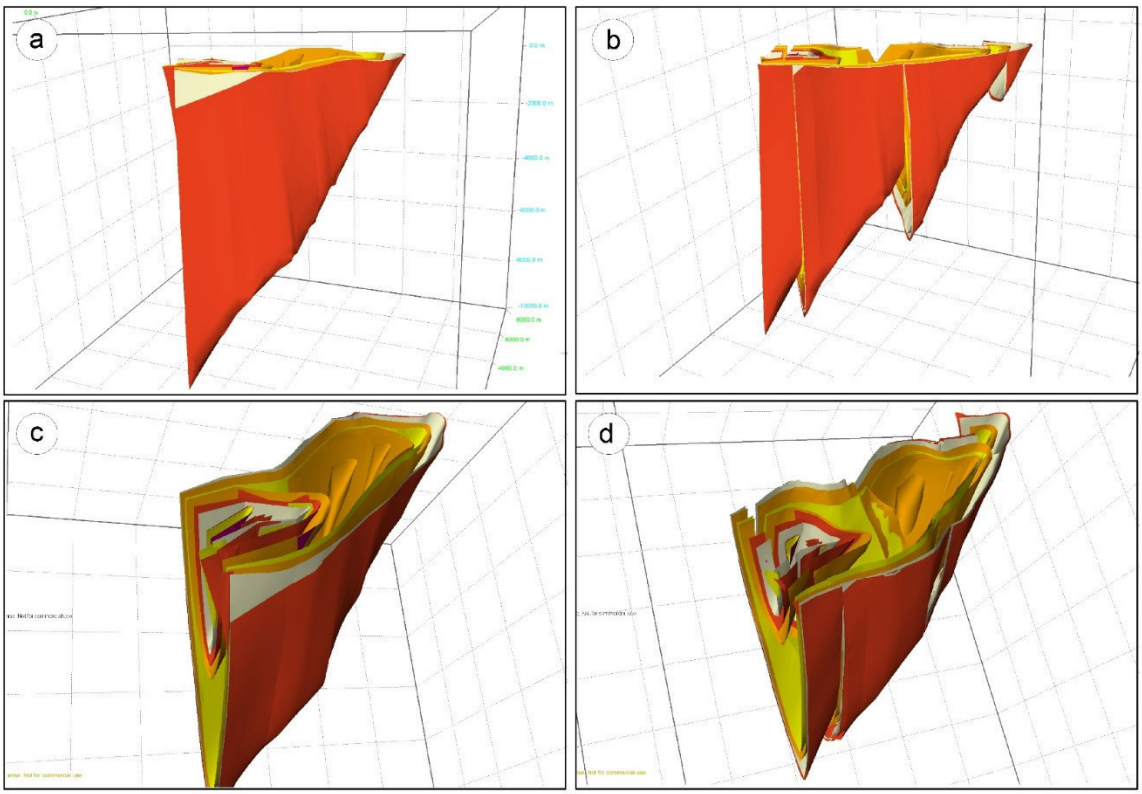

Fig. 3.20: 3D models of the hinge area of the Saddleback Syncline (see Fig. 3.7 for location) showing the effect of reverse faults perpendicular to fold trend on surface geometry and fold depth. Dikes are not displayed in this model. (a) Side (cross-sectional) view displacements restored. (b) Side view of the hinge area of the Saddleback Syncline with reverse faults. The depth of the fold section is significantly reduced by uplift along the fault planes. (c) Oblique view of the fold shown in (a). (d) Oblique view of the faulted fold shown in (b). Surface stratigraphy in map view is repeated in each up-faulted block along fold axis trend, recognizable only by marker units. If this happened in a thick uniform section, structural repetition would remain unrecognized.

Hypotheses addressing the contradiction between the shallow depth implied from legacy geophysical data and the great depth implied by stratigraphic thickness and fold geometry include:

(6) The BGB could be floored by a shallow subhorizontal detachment at a depth between 5 and 15 km, as suggested by Heubeck & Lowe (1994a), Kisters et al. (2003) and Moyen et al. (2006). Such a detachment could truncate all structures at depth. (Fig. 3.21 a).

(7) In the Yilgarn Craton in Western Australia, where a similar geometrical problem arose, Drummond et al. (2000) suggested, that the base of the greenstone belts was intruded by plutons (Fig. 3.21 b). Such intrusive contacts exist in the Tjakastad area (Fig. 3.1), where the base of the BGB is exposed (Kröner et al., 1996; Dann, 2000; Kisters et al., 2010), although the age of intrusion there is ca. 3420 Ma (pre-D2), not post D4. However, TTG emplacement in the BGGT is multi-generational and it can be reasonably assumed, that the base of the greenstone belt was also intruded by different generations of plutons.

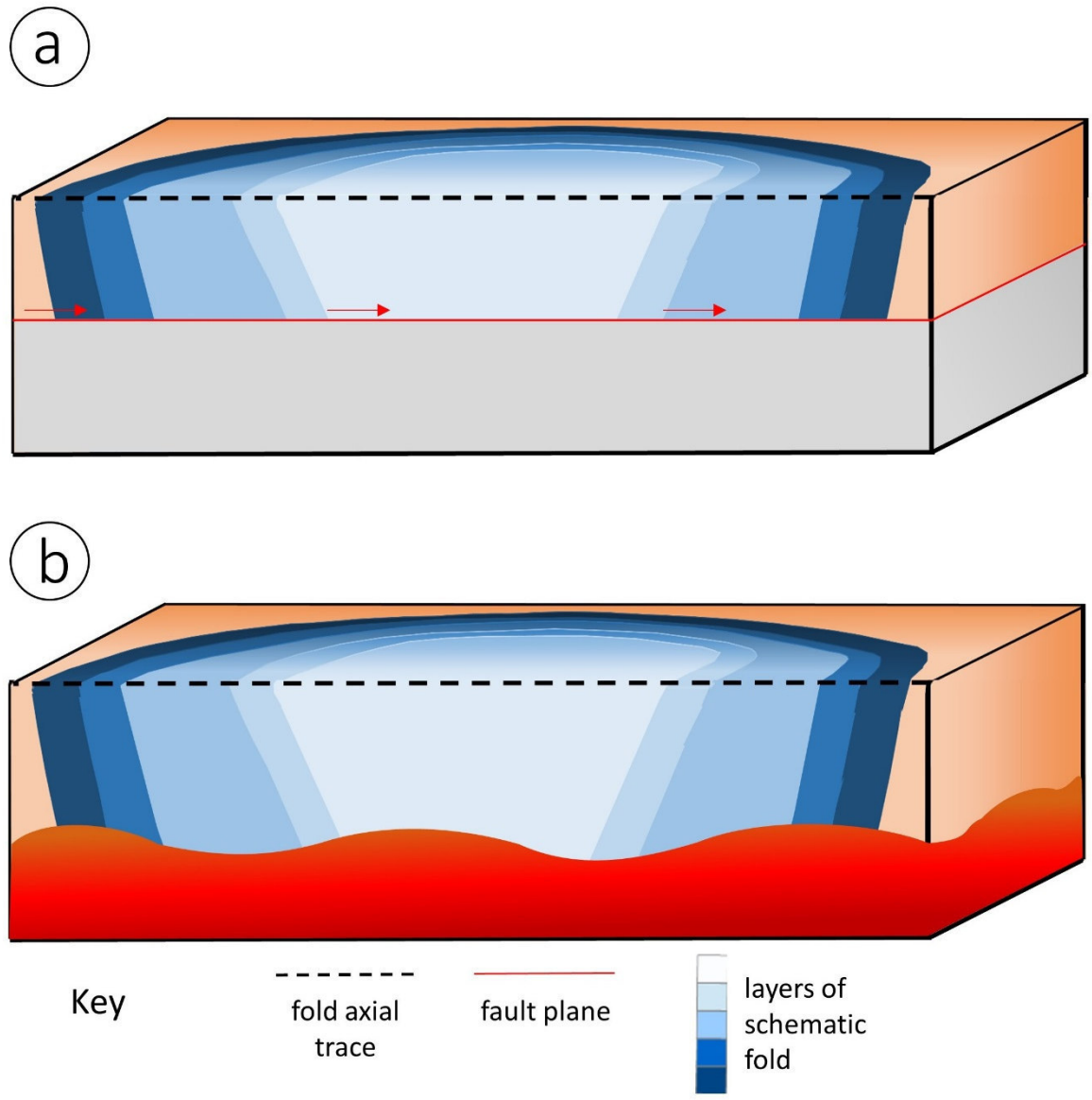

Fig. 3.21: Illustrations of hypotheses addressing the contradiction between the depth implied from legacy geophysical data and depth implied by stratigraphic thickness and fold geometry. (a) Shallow detachment (hypothesis (6)), as suggested by Heubeck & Lowe (1994a), Kisters et al. (2003), Moyen et al. (2006) and de Beer and Stettler (2009). (b) Intrusion of plutons at shallow depth, which modified the original geometry of large-scale folds in the BGB.

3.5.6 Quantification of the primary vertical extent of the folds

Hypothesis (1) (hinge thickening) and, locally, hypothesis (2) (ductile stretching) contribute to explain the great inferred depth of the synclines. If the mean hinge thickening factor is approximately 5, any thickness projections derived from hinge data should be reduced to 20% of the uncorrected estimate.

Ductile stretching, indicated by conglomerate clasts, would increase thickness by values between 0 (unstrained clasts in the interior of the central BGB) and 2 – 3 (margins near contacts to plutons).

Hypotheses (3) (variations in primary thickness), (4) and (5) (up-faulting) serve to explain the difference between the depth predicted by inferred fold geometry from surface data (Fig. 3.15) and the geometry suggested by hypotheses (1; hinge thickening) and (2; ductile strain). Primary thickness variations during syntectonic sedimentation cannot account for large discrepancy in the estimates of fold depth.

Because the vertical displacement along potential faults is unknown and their number cannot be reliably quantified, out-of-syncline thrusting is a poorly constrained mechanism.

We suggest that the combination of hypotheses (4) and (5) in their entirety has to compensate the remaining difference between the depth inferred from stratigraphic thickness measured on the limbs, modified by hypotheses (1) and (2) and the depth inferred from cross-section drawing and 3D modelling.

Quantification of possible depth reduction by suggested mechanisms				
Hypothesis	Mechanism	vertical extent		
		max.	min.	estimate
1	hinge-thickening	4,78 x strat. thickness	2,44 x strat. thickness	3,63 x strat. thickness
2	postdepositional subvertical stretching	2,7 x strat- thickness	0	locally 2,7, in most parts 0
3	primary strat. thickness variations	54,8 m depth /km along strike	0	54,8 m depth /km along strike
4	down-plunge upfaulting		no qunatification possible	
5	out-of-syncline-thrusting		no qunatification possible	
6	intrusion of base			c. 8 km
7	shallow detachment			c. 8 km

Table 3.2: Quantification of possible depth reduction by suggested mechanisms.

Table 3.3 shows estimates of the minimum and maximum vertical extent of the Eureka Syncline. We chose this structure because it has the largest discrepancy in depth estimate but also the most data and well-constrained geometry and stratigraphy.

To estimate the depth of the Eureka Syncline's depression, we followed two alternative approaches: (1) We used the plunge equation of section 3.3.2, obtaining a hypothetical depth of 37 km. We then attempted to reduce that unreasonable depth by accounting for minor (5%) primary thickness reduction towards the basin center (hypothesis (3)), obtaining a depth of 35.2 km.

(2) We used the minimum depth estimate by Heubeck (1994a for the Saddleback Syncline), which assumes parallel folding and is based on the dip of the bedding planes combined with the stratigraphic thickness of the synclinal limbs (Dahlstrom, 1969), obtaining a depth of 7 km. We adjusted that unreasonably low depth by accounting for hinge thickening by adding c. 10 km (factor of 4.78, suggested by our observations from the Eureka Syncline (hypothesis (1)) multiplied with the limb thickness of 2.1 km = 10.083 km), obtaining a depth of 17 km (Table 3.3). We did not modify the depth estimate for hypothesis (2) because the Eureka Syncline was mainly affected by oblate strain and only subordinate vertical stretching.

The difference between the estimated maximum (approach 1) and minimum (approach 2) depths of the syncline's depression is the very substantial distance of c. 18 km. Possibly, this discrepancy is accountable by the total vertical (core-up) displacement at limb-parallel and/or limb-perpendicular faults described in hypotheses (4) and (5). To reduce the maximum depth of 35 km to a depth of 17 km would require a fault of c. 85 m vertical displacement every 125 m along strike of the fold axial plane.

Overall, our first-order estimate suggests that the synclinal depth of the Eureka Syncline is 26±9 km.

Estimated depth of the Eureka Syncline		
Approach	**Implied depth**	
Plunge equation	37 km	Maximum
Modified by hyp. 3	35 km	
Modified by hyp. 4 + 5	?	
Synthesis	26±9 km	
Modified by hyp. 4 + 5	?	
Modified by hyp. 1	17 km	
Dahlstrom Approach	7 km	Minimum

Table 3.3: Exemplary calculation for a minimum and maximum depth for the depression of the Eureka Syncline. See text for explanation.

3.6 Conclusions

(1) Previous analyses did not adequately consider the consequences of steep and sustained fold axial plunge (e.g. Ramsay, 1963; Roering, 1965; Lowe et al., 1999).

(2) The 3-D geometry of major regional folds in the central BGB consisting of Moodies Group strata resembles best those of subhorizontally flattened cones. It is likely a result of syndepositional stratigraphic thickness variation, diffuse limb thinning and hinge thickening, in particular in fine-grained and incompetent strata during syn- or early postdepositional synclinal sagging and late brittle “out-of-syncline” thrusting. All these mechanisms indicate a dominantly vertically oriented displacement.

(3) Maximum depth of folds in 2-D cross section depends highly on the availability of plunge information which may be distant from the cross section trace. This crucial information may be difficult to reliably be projected onto the section because some folds change plunges (Fig Tree cored structures) while the plunge of others (Moodies-cored structures) remains constant.

(4) The original depth of the greenstone belt likely exceeded the 8 km implied by legacy geophysical data significantly. The change in density and resistivity measured at that depth is best explained by later intrusions of plutons.

(5) Due to the complex geometry, the large number of contributing factors and the lack of detailed seismic data, we cannot give a precise depth for the respective folds. However, by estimating the contribution of every factor involved, it is possible to give a minimum and a maximum depth for the folds’ depressions.

(6) Synclines in the BGB had reached significant depth. They sagged strongly during formation and were filled, at least in part, syndeformationally. Postfill deformation included vertical stretching but also hinge thickening and out-of-syncline thrusting, strongly modifying original synclinal shapes. Because perhaps the upper two-third structural levels of the BGB have been eroded and only deep-level remnants are preserved, variations with depth are difficult to estimate. BGB snyclines may have reached mid-crustal depth (ca. 20 km). They were likely largely resorbed by late plutonism, accounting for “shallow-BGB” geophysical data.

3.7 Acknowledgments

The authors express their gratitude towards Barberton Mines for providing structural data, and to Barberton Tourism, Dusty Tracks and Barberton NTT Toyota for advice, support and logistical help, respectively. Sappi allowed the use of private forest roads. Funding by the DFG-SPP 1833 ``Building a Habitable Earth´´ made this study possible.

4 Structural geology and geochronology of the Malolotsha area, Eswatini, with implications on the deformation history and stratigraphy of the southwestern Barberton Greenstone Belt

Schmitz, M.[1], Linnemann, U.[2], Fugmann, P.[3], van Kranendonk, M.[4] and Heubeck, C.[1]

[1] Institut für Geowissenschaften, Friedrich-Schiller-Universität Jena, Burgweg 11, 07749 Jena, Germany

[2] Senckenberg Naturhistorische Sammlungen Dresden Museum für Mineralogie und Geologie, Sektion Geochronologie, Königsbrücker Landstraße, 159 D-01109, Dresden, Germany

[3] L.A. Géologie, Pétrologie et Géochimie (B20), Université de Liège, Sart Tilman, Liege 4000, Belgium

[4] School of Biological, Earth and Environmental Sciences, University of New South Wales, Kensington, NSW 2052, Australia

Abstract

The tectonic evolution of the Barberton Greenstone Belt has been suggested to include major horizontal shortening in the Malolotsha area, strongly contradicting the suggested pre-plate-tectonics setting, which is dominated by vertical movement. This hypothesis is based on the presence of a thick succession of altered ultramafic volcanics, only known from the Onverwacht Group, in the core of the Malolotsha syncline, defined by the younger Moodies Group. In this study we reexamine the scarce structural studies of the area conducted to date and present the results of our own detailed field mapping in the Malolotsha area, U/Pb zircon dating and additional structural information derived from the remnants of the Ancient Gneiss Complex adjacent to the greenstone belt. We suggest a deformation history for the southern part of the Barberton Greenstone Belt which comprises a first deformational event after deposition of the Fig Tree Group (D2), pervasive deformation contemporaneous to the deposition of the Moodies Group, which is recorded both in the greenstone belt and adjacent gneisses (D3), followed by post-Moodies deformation (D4) and eventually the exhumation of high-grade metamorphic terranes and their juxtaposition next to greenschist-grade greenstone belt strata. The geological history recorded by the stratigraphy of the Malolotsha Syncline and the origin of the thick ultramafic succession in its core remains unclear because stratigraphic age and structural relationships are not well defined. We suggest, that this peculiar structure represents either (1) a folded tectonic klippe, (2) a younger unit of ultramafic volcanics conformably overlying the Moodies Group or (3) that it was formed by out-of-syncline thrusting of Onverwacht Group strata during continuous shortening.

4.1 Introduction

The origin and development of continental crust is pivotal to weathering and linked to the development, if not the origin, of life. However, no Hadean and only few Archean strata record the interaction of surface, crustal and mantle processes involved in this process. These archives are represented by greenstone belts, volcano-sedimentary successions, surrounded by plutonic or metamorphic rocks (Anhaeusser, 2014). The best exposed and preserved greenstone belts, which contributed significantly to our understanding of the early Earth, are located in the Pilbara Craton of Western Australia and the Kapvaal Craton of South Africa and Eswatini (formerly Swaziland).

The Barberton Greenstone Belt (BGB) of the Kapvaal Craton and represents one of the key areas for Archean research. One of the major unresolved questions is the origin of the peculiar, cuspate-lobate geometry and the nature of the overall synclinal structure of the BGB. While one group of researchers maintains the idea of active plate tectonics during the Archean (de Wit, 1982, 1991; de Wit et al., 1987, 2011, 2018; de Ronde et al., 1991; de Wit & Hart, 1993; de Ronde & de Wit, 1994; Stevens et al., 2002;

Dziggel et al., 2002, 2006, 2010; Moyen et al., 2006, 2007; Kisters et al., 2003, 2010; Diener et al., 2005; Stevens & Moyen, 2007; Schoene et al., 2009; Schoene & Bowring, 2010; Lana et al., 2010, 2011), another group suggests that higher mantle temperature, resulting higher degree of partial melting and reduction in mantle viscosity governed a pre-plate tectonic mechanism through the rise of hot and buoyant, mantle-derived melt and the concurrent sinking of the overlying cold and dense (ultra-)mafic greenstones (Solomatov & Moresi, 1997; Reese et al., 1998; Dumoulin et al., 1999; Ernst, 2009; van Kranendonk et al., 2009, 2014; van Kranendonk, 2011, Debaille et al., 2013; Piper, 2013; Gerya, 2014; Bédard, 2018).

While there is general agreement on the tectonic evolution of the Pilbara Craton, the structural geology of the BGB is still topic of debate. Most relevant studies were conducted in its central part (e.g. Anhaeusser, 1976; de Wit, 1982; Nocita & Lowe, 1990; de Ronde et al., 1991, 1992; Heubeck & Lowe, 1994a, b; Lowe, 1994; Byerly et al., 1996; Lowe et al. 1999; Lowe & Byerly, 1999) because of better access, continuous stratigraphic sequence and perceived less deformation compared to its margins. In particular, the Eswatini part of the BGB has received only little attention (Urie, 1965; Jackson & Robertson, 1983; Lamb 1984; Lamb & Paris, 1988; Schoene & Bowring 2008). Archean contributions from Eswatini focused largely on the Ancient Gneiss Complex (Hunter, 1957, 1961, 1970; Hunter et al., 1978; Carlson et al., 1983; Barton et al., 1983; Jackson, 1984; Hunter & Wilson, 1988; Jackson et al., 1987; Kröner et al., 1988, 2014), an early- to mid-Archean terrane comprising granitoids, multiply deformed orthogneisses and interlayered amphibolites, to the southwest of the BGB (Hoffmann & Kröner, 2018). The stratigraphy and structural geology of the BGB in Eswatini was addressed to-date only by Lamb (1984), Jackson et al. (1987), Lamb & Paris (1988) and Lana et al. (2011).

In an important, but widely overlooked hypothesis, Lamb (1984) postulated significant sub-horizontal shortening in the Malolotsha region of the Eswatini BGB, which is in strong contrast to the vertically-dominated deformation style suggested in numerous studies from the South African part of the BGB (Anhaeusser, 1981, 1984; van Kranendonk et al., 2009, 2014; van Kranendonk, 2011). We here follow up on this controversy to gain new insights into the structure of this poorly understood part of the BGB by means of additional detailed field mapping and age dating.

4.2 Geological framework

The BGB strikes generally SW-NE and covers an area of approximately 10,000 km^2. The surrounding TTG bodies were mostly emplaced contemporaneously with its protracted 450 Ma-long formation and subsequent deformation history. The TTG plutons can be subdivided into three petrogenetic groups, ranging from 3.51 Ga (TTG 1) and 3.48 Ga (TTG 2) to 3.28 and 3.22 Ga (TTG 3) (Moyen et al., 2018). Likewise, the greenstone belt stratigraphy is subdivided into three groups, which are, from oldest to youngest, the Onverwacht Group, which mainly consists of largely subaqueously deposited mafic and ultramafic volcanic rocks and cherts (Byerly et al., 2018), the Fig Tree Group, composed of volcanoclastic and chemical sediments, such as chert, jaspilite and barite (Lowe & Byerly, 1999), and the Moodies Group, which largely consists of quartz-rich siliciclastics and subordinate volcanics (Heubeck, 2019).

The central BGB is dominated by tightly and isoclinally folded synclines, which are commonly overturned to the northwest, while anticlines are thinned, faulted and missing entirely in many parts of the greenstone belt. Synclines consist of Fig Tree and Moodies Group strata, while the anticlines are almost exclusively represented by Onverwacht Group rocks. Synclinal fold axes generally plunge steeply inwards, while the anticlinal fold axes generally plunge steeply outwards (chapter 3). This style extends to other parts of the BGB but is less well pronounced there or modified by processes that occurred along the BGB margins.

The SW-NE trending Inyoka Fault (IF) in the central greenstone belt represents a major break marked by facies changes in all stratigraphic units across the fault (Heinrichs and Reimer, 1977; de Wit et al., 1992, Heubeck & Lowe, 1994a, b; Lowe et al., 1999; Lowe & Byerly, 1999; de Ronde and Kamo, 2000) and most of the faults of the BGB strike (sub)parallel to the IF. However, the E-W striking Granville Grove Fault and the N-S striking Kromberg Fault represent exceptions to this main orientation and mark the boundaries of the oldest exposed strata of the greenstone belt. All stratigraphic units older than c. 3.3 Ga are confined to the area between these Granville Grove Fault and the Kromberg Fault Zone.

A number of models have been suggested for the tectonic evolution of the BGB (chapter 2) to account for its complex, multi-stage deformation history. Here, we follow the deformation phase terminology (D1 –D5) suggested by Lowe & Byerly (1999, 2007) and Byerly et al. (2018). The first deformation event (D1) coincides with felsic magmatic activity around 3445 Ma (Lowe & Byerly, 2007) and was followed by a period of crustal extension, responsible for the formation of the basin, in which units of the Fig Tree Group were deposited (Byerly et al., 2018). D2, between 3230 and 3225 Ma (de Ronde & de Wit, 1994; Lowe et al., 1999; Kisters et al., 2003), represents the first deformation event that affected the entire BGB and resulted in the deformation, uplift and erosion of Onverwacht and the lower Fig Tree Group (Mapepe Formation). Beginning in upper Fig Tree Group time (ca. 3.230 – 3225 Ma) and continuing into Moodies Group time (ca. 3225 – 3217 Ma), D3 created significant accommodation space which was filled syntectonically (Byerly et al., 2018) by strata of the Moodies Group. D4 represents late syn- to post-Moodies deformation of the greenstone belt, resulting in the folding of upper Fig Tree and Moodies Group strata (as well as previously deformed Onverwacht and lower Fig Tree Group strata), and in the inversion of the Moodies basins. These folds were subsequently modified by a poorly constrained later deformational event (D5), including strike-slip displacement along previously emplaced faults and further steepening of earlier structures (Byerly et al., 2018).

Although the entire greenstone belt was subject to multiple deformation events and regional greenschist-grade metamorphism (Xie et al., 1997; Toulkeridis et al., 1998), primary structures and sedimentary textures are well preserved, probably because of early silicification. Recrystallisation of the original matrix and cement is common in sedimentary rocks, while igneous rocks of mafic composition are widely carbonatized, serpentinized or altered to talcose schists (Byerly et al., 2018). Along the northwestern margin, greenstone belt strata adjacent to TTG plutons show tectonically thinned contact-metamorphic aureoles (Robb et al., 1986). Metamorphic fabric at the BGB margins indicates a normal, greenstone-down pluton-up sense of shear (Anhaeusser, 1984; Kisters et al., 2003; Lana et al., 2011. The primary contact relationship between the Ancient Gneiss Complex (AGC) and the BGB in the southern part of the greenstone belt is largely obliterated or obscured by ductile shearing, younger intrusions of granitoid composition at c. 3.14 – 3.1 Ga (Schoene & Bowring, 2010) or plantation and soil cover.

The AGC represents a chronologically complex and heterogeneous Paleoarchean crustal unit containing a variety of gneisses that vary in age from c. 3666 to 3200 Ma (Hoffmann & Kröner, 2018). The last deformational event recorded in the AGC at or shortly after c. 3220 Ma coincides with the deformational event contemporaneous to Moodies Group deposition and deformation (D3). Most authors consider these deformational events to be related (Kröner et al., 1989; Kamo & Davis, 1994; Dziggel et al., 2002; Brown, 2015), although the original contact between the BGB and AGC has, except for the short sections to the Phophonyane and Malolotsha inliers subsequently been intruded and obliterated by the Piggs Peak and Mpuluzi batholiths at c. 3.1 Ga (Fig. 4.3).

Contacts between the Phophonyane and the Malolotsha Inlier to the BGB have been interpreted as transtensional shear zones with dextral shear sense (Schoene et al., 2008; Schoene & Bowring, 2010; Lana et al., 2010, 2011) along which the AGC was uplifted relative to the BGB (Lana et al., 2011).

Because the structural information from the AGC and the two BGB-AGC contact regions are rather limited, structural and stratigraphic information from the BGB margins must be used to infer the deformational history along the southern margin of the BGB.

Geographically, the BGB in Eswatini can be subdivided into three regions: The northern area corresponds to the Sondeza Range and is comprised of rugged mountains that trend across the border. It largely consists of steeply dipping and folded strata of the Moodies Group. BGB rocks in the central area, near the town of Piggs Peak, largely consist of strongly deformed and disrupted slivers of serpentinized ultramafic rocks. Interbedded cherts indicate very high flattening and subvertical stretching strain. The area is almost entirely forested. The southern area, studied by Lamb (1984) and Lamb & Paris (1988), extends from the Komati River to Ngwenya and Motjane. It represents a complex assemblage of folded and faulted rocks of Onverwacht, Fig Tree, and Moodies Group rocks. Strata are best exposed in the northern part of this region; exposure decreases south of Ngwenya and is poor near Motjane.

We focused on the northern part of the southern area between the Komati River and Forbes Reef due to its excellent outcrop situation and the well-preserved structural features in order to reexamine the structural evolution of the southern part of the BGB..

4.3 Methods

4.3.1 Geological mapping

We conducted detailed geological mapping based on 1:25,000-scale map sheets by Hunter (1969), Urie (1970), and Bennett (1971). Despite its superb lithological detail, these maps provide no structural interpretation and lack cross sections and stratigraphic facing indicators. The authors had to do without a geochronological framework and had no or only very limited knowledge of the regional structural geology and stratigraphy in adjacent South Africa. Our mapping, thus, focused on identifying fault traces, fold axes, stratigraphic facing indicators, kinematic indicators and age dating.

4.3.2 Strain indicators

We measured the major, intermediate and minor diameter and the orientation of the long axis of 142 conglomerate clasts at 15 localities. Strain was not calculated with reference to a unit ellipsoid but with respect to the three diameters of an average undeformed Moodies Group conglomerate clast (axes-ratios of 1.26 / 1 / 0.8; Heubeck and Lowe, 1994a). Strain data from Heubeck & Lowe (1994a) served to compare our finding to results of previous investigations and to build a more robust database.

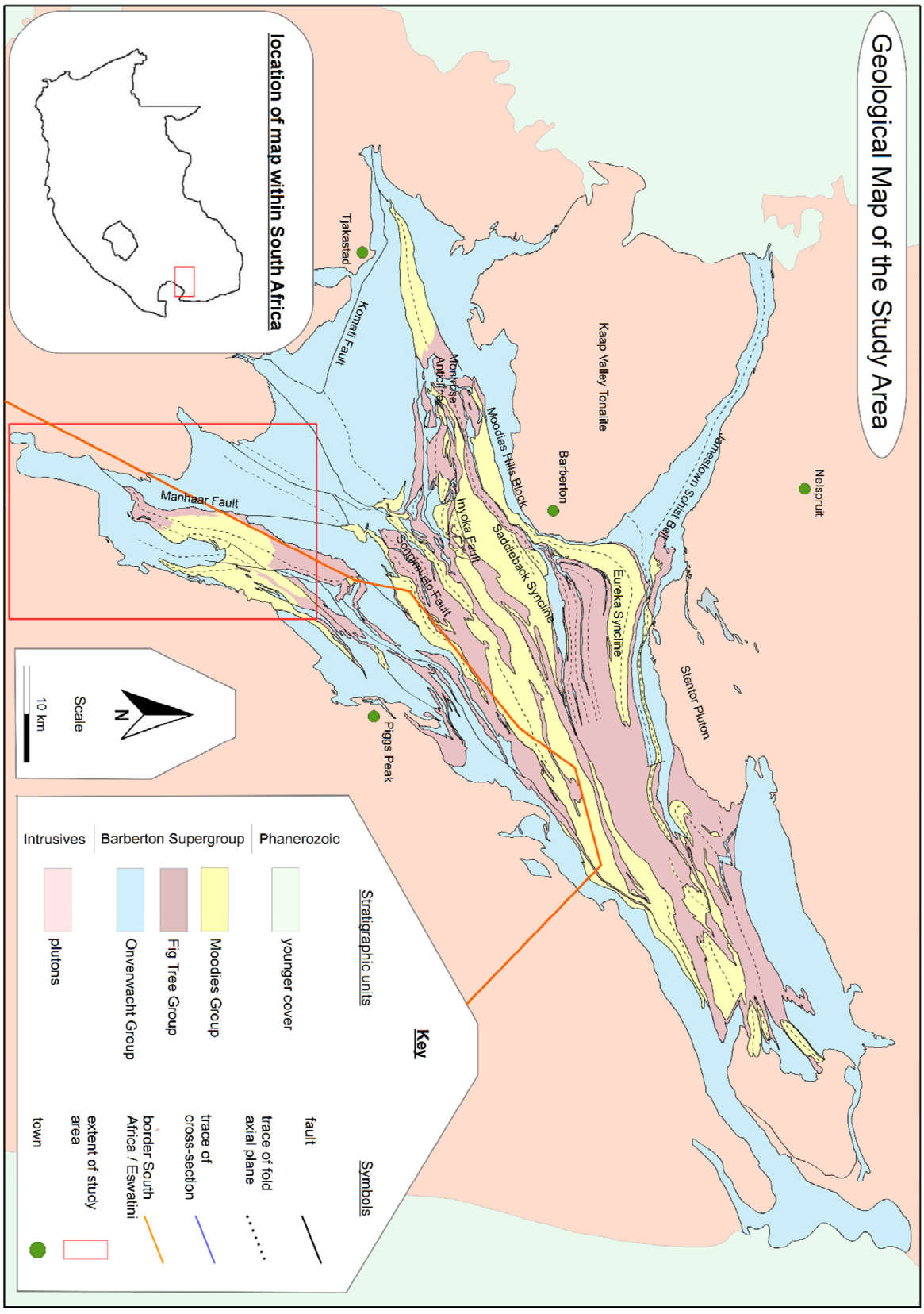

Fig. 4.1: Geological map of the BGB. Inset shows location of map in South Africa; the red rectangle marks the investigated area. See text for explanation.

4.3.3 Radiometric age dating

Thin silicified metavolcanic beds in the core of the Malolotsha Syncline are interbedded with thick talcose schists and were sampled for U-Pb dating. Of three location sampled, only sample 16-213 (Fig. 4.2a) yielded zircons suited for dating, which were extracted using standard mineral separation techniques. Out of a total of c. 400 zircons, 239 were dated. Zircons were mounted in epoxy resin, polished to expose their centers, and imaged using a scanning electron microscope (SEM) and cathodoluminescence (CL) prior to analysis. Zircons were analyzed for U, Th, and Pb isotopes by LA–ICP–MS at the Museum für Mineralogie und Geologie (GeoPlasma Lab, Senckenberg Naturhistorische Sammlungen Dresden, Germany), using a Thermo-Scientific Element 2 XR sector field ICP-MS coupled to a New Wave UP-193 Excimer Laser System. Each analysis consisted of approximately 15 s background acquisition followed by 30 s data acquisition, using a laser spot-size of 25 and 35 µm, respectively. Approximation of terrestrial lead isotope evolution by a two-stage model was carried out if necessary. Raw data were corrected for background signal, common Pb, laser-induced elemental fractionation, instrumental mass discrimination, and time-dependant elemental fractionation of Pb/Th and Pb/U using an Excel® spreadsheet program developed by Axel Gerdes (Institute of Geosciences, Johann Wolfgang Goethe-University Frankfurt, Frankfurt am Main, Germany) (Krautz et al. 2018).

4.4 Results

4.4.1 Lithological units

We identified the following lithostratigraphic units (from oldest to youngest) and a complex remnant of the AGC at the eastern margin of the Malolotsha Syncline:

Malolotsha Inlier

This remnant of the AGC covers an area of c. 6 x 0.5 km east of the Malolotsha Syncline. It contains gneisses representing the earliest phase of TTG pluton emplacement at 3644 ± 4 Ma and subsequent reworking and intrusion by further magmatism between c. 3.5 and 2.9 Ga (Compston & Kröner, 1988; Kröner et al., 1989). Most of the rock is characterized by a porphyritic and medium-grained granodiorite containing up to 6 x 2 cm-sized feldspar crystals, which defines a later phase of magmatism. The Malolotsha Inlier shows a marked northeast trending fabric, defined by mineral alignment. We observed dikes of granitic composition, which clearly crosscut the fabric.

Onverwacht Group

Strata assigned to the Onverwacht Group include talcose schists, phyllites and banded cherts. Where mafic and ultramafic volcanics were variably altered, including serpentinite and dolomite. Talcose schists are medium- to coarse-grained, show strong foliation, are dark grey and brownish-red to pink and form topographic depressions with few or no outcrops (Fig. 4.4 d). Phyllites and show strong foliation defined by mineral alignment (mica and actinolite, respectively). Banded cherts consists of black and white cherts and represent well traceable marker units due to their high weathering resistance.

Calculation of strain magnitude from deformed conglomerate clasts

Structural Unit	Data Point	Reading	X	Y	Z	X:Y	Y:Z	X'	Y'	Z'	X':Y'	Y':Z'	X':Y'	K	average X'	average Y'	average Z'
Ngwenya Syncline South	1	1	7	1,8	1,4	3,89	1,29	5,56	1,80	1,75	3,09	1,03	1,41	3,00	1,99	0,80	0,71
		2	1,9	0,4	0,3	4,75	1,33	1,51	0,40	0,38	3,77	1,07	3,17	3,53	1,11	0,45	0,40
		3	1,3	0,4	0,2	3,25	2,00	1,03	0,40	0,25	2,58	1,60	2,58	1,61			
		4	3	1,2	0,7	2,50	1,71	2,38	1,20	0,88	1,98	1,37	1,98	1,45			
		5	1	0,2	0,1	5,00	2,00	0,79	0,20	0,13	3,97	1,60	3,97	2,48			
		6	1,6	0,9	0,5	1,78	1,80	1,27	0,90	0,63	1,41	1,44	1,32	0,98			
		7	5,6	2,2	1,8	2,55	1,22	4,44	2,20	2,25	2,02	0,98	2,06	2,07			
		8	1,4	0,3	0,2	4,67	1,50	1,11	0,30	0,25	3,70	1,20	2,38	3,09			
		9	2,4	0,5	0,4	4,80	1,25	1,90	0,50	0,50	3,81	1,00	3,81	3,81			
		10	1,9	0,3	0,2	6,33	1,50	1,51	0,30	0,25	5,03	1,20	3,77	4,19			
		11	2,5	0,8	0,4	3,13	2,00	1,98	0,80	0,50	2,48	1,60	2,18	1,55			
		12	2,2	0,4	0,3	5,50	1,33	1,75	0,40	0,38	4,37	1,07	2,83	4,09			
		13	2,8	1,8	1,4	1,56	1,29	2,22	1,80	1,75	1,23	1,03	1,17	1,20			
		14	1,8	0,4	0,3	4,50	1,33	1,43	0,40	0,38	3,57	1,07	3,57	3,35			
	2	15	1,2	0,4	0,3	3,00	1,33	0,95	0,40	0,38	2,38	1,07	1,90	2,23			
		16	2,7	1,2	0,9	2,25	1,33	2,14	1,20	1,13	1,79	1,07	1,65	1,67	2,31	1,16	1,05
		17	7	3,5	2,8	2,00	1,25	5,56	3,50	3,50	1,59	1,00	1,63	1,59	1,00	0,50	0,46
		18	1,8	0,9	0,3	2,00	3,00	1,43	0,90	0,38	1,59	2,40	2,04	0,66			
		19	2,4	0,9	0,4	2,67	2,25	1,90	0,90	0,50	2,12	1,80	2,38	1,18			
		20	3,1	0,5	0,4	6,20	1,25	2,46	0,50	0,50	4,92	1,00	5,24	4,92			
		21	1,5	0,4	0,2	3,75	2,00	1,19	0,40	0,25	2,98	1,60	3,44	1,86			
		22	5,3	1,9	1,5	2,79	1,27	4,21	1,90	1,88	2,21	1,01	2,13	2,18			
		23	1,2	0,4	0,32	3,00	1,25	0,95	0,40	0,40	2,38	1,00	3,17	2,38			
		24	1,7	1,1	0,8	1,55	1,38	1,35	1,10	1,00	1,23	1,10	1,12	1,12			
		25	3,4	2,3	1,8	1,48	1,28	2,70	2,30	2,25	1,17	1,02	1,21	1,15			
		26	1,8	0,3	0,2	6,00	1,50	1,43	0,30	0,25	4,76	1,20	3,37	3,97			
		27	3,2	1,5	1,1	2,13	1,36	2,54	1,50	1,38	1,69	1,09	1,69	1,55			
		28	3,6	0,9	0,7	4,00	1,29	2,86	0,90	0,88	3,17	1,03	3,09	3,09			
		29	3,6	1,3	1	2,77	1,30	2,86	1,30	1,25	2,20	1,04	2,26	2,11			
No 53 from Heubeck & Lowe 1994	3	30	1,4	0,3	0,2	4,67	1,50	1,11	0,30	0,25	3,70	1,20	3,17	3,09			
Ngwenya Syncline North	4		2,1	1	0,69	2,10	1,45	1,67	1,00	0,86	1,67	1,16	3,17	1,44	1,00	0,48	0,33
(formerly Masali Syncline)		31	8,2	2,6	2,1	3,15	1,24	6,51	2,60	2,63	2,50	0,99	2,12	2,53	2,96	1,84	1,59
		32	0,6	0,3	0,2	2,00	1,50	0,48	0,30	0,25	1,59	1,20	1,19	1,32	1,00	0,62	0,54
		33	0,5	0,2	0,1	2,50	2,00	0,40	0,20	0,13	1,98	1,60	2,38	1,24			
		34	0,8	0,3	0,1	2,67	3,00	0,63	0,30	0,13	2,12	2,40	3,17	0,88			
		35	1,2	0,4	0,2	3,00	2,00	0,95	0,40	0,25	2,38	1,60	2,65	1,49			
		36	0,4	0,2	0,1	2,00	2,00	0,32	0,20	0,13	1,59	1,60	1,06	0,99			
		37	5	1	1,2	5,00	0,83	3,97	1,00	1,50	3,97	0,67	2,65	5,95			
		38	12	8,1	5,9	1,48	1,37	9,52	8,10	7,38	1,18	1,10	1,21	1,07			
		39	7,1	5	2,6	1,42	1,92	5,63	5,00	3,25	1,13	1,54	1,11	0,73			
	5	40	1,5	0,3	0,2	5,00	1,50	1,19	0,30	0,25	3,97	1,20	2,58	3,31			
		41	1,2	0,9	0,4	1,33	2,25	0,95	0,90	0,50	1,06	1,80	1,06	0,59	2,95	1,20	0,90
		42	6,4	2,3	1,4	2,78	1,64	5,08	2,30	1,75	2,21	1,31	1,90	1,68	1,00	0,41	0,30
		43	8,6	2	1,3	4,30	1,54	6,83	2,00	1,63	3,41	1,23	3,57	2,77			
		44	0,5	0,3	0,2	1,67	1,50	0,40	0,30	0,25	1,32	1,20	1,32	1,10			
		45	1	0,3	0,2	3,33	1,50	0,79	0,30	0,25	2,65	1,20	3,97	2,20			
Malolotsha Syncline	6	46	0,9	0,2	0,1	4,50	2,00	0,71	0,20	0,13	3,57	1,60	3,17	2,23			
		47	2,4	1,9	1,4	1,26	1,36	1,90	1,90	1,75	1,00	1,09	3,17	0,92	1,75	1,80	1,88
		48	1,2	0,9	0,9	1,33	1,00	0,95	0,90	1,13	1,06	0,80	2,70	1,32	1,00	1,03	1,07
		49	1,1	1	0,7	1,10	1,43	0,87	1,00	0,88	0,87	1,14	3,44	0,76			
		50	2,3	1,9	1,8	1,21	1,06	1,83	1,90	2,25	0,96	0,84	1,59	1,14			
		51	3,7	3	2,2	1,23	1,36	2,94	3,00	2,75	0,98	1,09	3,17	0,90			
		52	3,5	2,8	2,7	1,25	1,04	2,78	2,80	3,38	0,99	0,83	2,38	1,20			
		53	2,4	1,9	1,3	1,26	1,46	1,90	1,90	1,63	1,00	1,17	3,57	0,86			
		54	1,4	1,2	1,1	1,17	1,09	1,11	1,20	1,38	0,93	0,87	5,56	1,06			
		55	1,6	1,3	0,9	1,23	1,44	1,27	1,30	1,13	0,98	1,16	0,90	0,85			

	7	56	2,5	2,1	2	1,19	1,05	1,98	2,10	2,50	0,94	0,84	3,97	1,12				
		57	2,7	2,2	1,5	1,23	1,47	2,14	2,20	1,88	0,97	1,17	5,16	0,83	2,24	2,23	2,21	
		58	3,5	3,3	3,1	1,06	1,06	2,78	3,30	3,88	0,84	0,85	2,91	0,99	1,00	1,00	0,99	
		59	2,1	1,8	1,3	1,17	1,38	1,67	1,80	1,63	0,93	1,11	3,70	0,84				
		60	2,2	1,7	1,2	1,29	1,42	1,75	1,70	1,50	1,03	1,13	4,37	0,91				
		61	2,8	2,2	2,2	1,27	1,00	2,22	2,20	2,75	1,01	0,80	4,76	1,26				
		62	3,6	3,2	2,2	1,13	1,45	2,86	3,20	2,75	0,89	1,16	2,18	0,77				
		63	1,2	0,7	0,5	1,71	1,40	0,95	0,70	0,63	1,36	1,12	2,58	1,21				
		64	2,2	1,6	1,5	1,38	1,07	1,75	1,60	1,88	1,09	0,85	2,38	1,28				
		65	3,1	1,9	1,4	1,63	1,36	2,46	1,90	1,75	1,29	1,09	8,73	1,19				
	8	66	4,8	3,7	2,8	1,30	1,32	3,81	3,70	3,50	1,03	1,06	0,85	0,97				
		67	8,5	7,6	4,7	1,12	1,62	6,75	7,60	5,88	0,89	1,29	3,17	0,69	2,50	2,95	2,53	
		68	2,3	1,9	1,4	1,21	1,36	1,83	1,90	1,75	0,96	1,09	1,98	0,88	1,00	1,18	1,01	
		69	2,3	1,6	1,2	1,44	1,33	1,83	1,60	1,50	1,14	1,07	1,19	1,07				
		70	1,4	4	3	0,35	1,33	1,11	4,00	3,75	0,28	1,07	2,38	0,26				
		71	2,5	2,4	1,5	1,04	1,60	1,98	2,40	1,88	0,83	1,28	2,58	0,65				
		72	1,9	1,5	1,1	1,27	1,36	1,51	1,50	1,38	1,01	1,09	5,16	0,92				
		73	1,9	1,4	1,1	1,36	1,27	1,51	1,40	1,38	1,08	1,02	2,81	1,06				
		74	7,2	6,7	4,6	1,07	1,46	5,71	6,70	5,75	0,85	1,17	4,27	0,73				
		75	2,3	1,9	1,4	1,21	1,36	1,83	1,90	1,75	0,96	1,09	2,76	0,88				
		76	2,4	1,9	1,3	1,26	1,46	1,90	1,90	1,63	1,00	1,17	3,17	0,86				
Forbes Reef Syncline North	9	77	1,9	1,5	1	1,27	1,50	1,51	1,50	1,25	1,01	1,20	2,78	0,84				
		78	10,5	4	3,2	2,63	1,25	8,33	4,00	4,00	2,08	1,00	2,51	2,08	7,83	2,03	1,93	
		79	2	0,5	0,4	4,00	1,25	1,59	0,50	0,50	3,17	1,00	7,94	3,17	1,00	0,26	0,25	
		80	15	4	3,2	3,75	1,25	11,90	4,00	4,00	2,98	1,00	3,70	2,98				
		81	7,1	1,4	1	5,07	1,40	5,63	1,40	1,25	4,02	1,12	4,76	3,59				
		82	14,5	2	1,6	7,25	1,25	11,51	2,00	2,00	5,75	1,00	5,16	5,75				
		83	9,6	1,4	1	6,86	1,40	7,62	1,40	1,25	5,44	1,12	3,49	4,86				
		84	12,1	1,8	1,3	6,72	1,38	9,60	1,80	1,63	5,34	1,11	1,59	4,82				
		85	9,7	0,9	0,4	10,78	2,25	7,70	0,90	0,50	8,55	1,80	1,76	4,75				
		86	10,4	1,9	1,2	5,47	1,58	8,25	1,90	1,50	4,34	1,27	2,45	3,43				
	10	87	7,8	2,4	2,1	3,25	1,14	6,19	2,40	2,63	2,58	0,91	1,29	2,82				
		88	8,1	1,6	1,2	5,06	1,33	6,43	1,60	1,50	4,02	1,07	1,85	3,77	6,79	1,31	0,96	
		89	9,8	1,4	1,1	7,00	1,27	7,78	1,40	1,38	5,56	1,02	2,38	5,46	1,00	0,19	0,14	
		90	13,1	2,6	2	5,04	1,30	10,40	2,60	2,50	4,00	1,04	1,80	3,84				
		91	6,8	0,8	0,3	8,50	2,67	5,40	0,80	0,38	6,75	2,13	2,58	3,16				
		92	9,7	1,1	0,7	8,82	1,57	7,70	1,10	0,88	7,00	1,26	2,98	5,57				
		93	6,3	1,1	0,5	5,73	2,20	5,00	1,10	0,63	4,55	1,76	2,98	2,58				
		94	7,4	1,2	0,6	6,17	2,00	5,87	1,20	0,75	4,89	1,60	2,98	3,06				
		95	7,6	1,1	0,4	6,91	2,75	6,03	1,10	0,50	5,48	2,20	2,98	2,49				
		96	9,2	1,3	0,6	7,08	2,17	7,30	1,30	0,75	5,62	1,73	2,98	3,24				
No. 56 from Heubeck & Lowe 1994	11	97	7,5	0,9	0,3	8,33	3,00	5,95	0,90	0,38	6,61	2,40	2,98	2,76				
No. 57 from Heubeck & Lowe 1994	12		2,02	1	0,49	2,02	2,04	1,60	1,00	0,61	1,60	1,63	2,98	0,98	1,00	0,63	0,38	
Forbes Reef Syncline South	13		1,55	1	0,44	1,55	2,27	1,23	1,00	0,55	1,23	1,82	2,98	0,68	1,00	0,81	0,45	
		98	11,7	2	1,5	5,85	1,33	9,29	2,00	1,88	4,64	1,07	3,73	4,35	4,11	1,33	1,03	
		99	9	1	0,5	9,00	2,00	7,14	1,00	0,63	7,14	1,60	6,35	4,46	1,00	0,32	0,25	
		100	4,5	1,5	1,1	3,00	1,36	3,57	1,50	1,38	2,38	1,09	5,21	2,18				
		101	6	1	0,6	6,00	1,67	4,76	1,00	0,75	4,76	1,33	2,58	3,57				
		102	5	1,5	0,9	3,33	1,67	3,97	1,50	1,13	2,65	1,33	7,62	1,98				
		103	8	4	2,6	2,00	1,54	6,35	4,00	3,25	1,59	1,23	3,97	1,29				
		104	2,5	1	0,6	2,50	1,67	1,98	1,00	0,75	1,98	1,33	4,55	1,49				
		105	3	1	0,5	3,00	2,00	2,38	1,00	0,63	2,38	1,60	2,12	1,49				
		106	3,5	0,5	0,2	7,00	2,50	2,78	0,50	0,25	5,56	2,00	3,65	2,78				
		107	6,5	1	0,6	6,50	1,67	5,16	1,00	0,75	5,16	1,33	2,65	3,87				
		108	4	1	0,7	4,00	1,43	3,17	1,00	0,88	3,17	1,14	2,51	2,78				
		109	2	0,5	0,3	4,00	1,67	1,59	0,50	0,38	3,17	1,33	2,50	2,38				
		110	5,5	2	1,2	2,75	1,67	4,37	2,00	1,50	2,18	1,33	3,77	1,64				
		111	3,5	1	0,6	3,50	1,67	2,78	1,00	0,75	2,78	1,33	2,08	2,08				

	14	112	3	1	0,5	3,00	2,00	2,38	1,00	0,63	2,38	1,60	3,57	1,49			
		113	4	2	1,2	2,00	1,67	3,17	2,00	1,50	1,59	1,33	2,15	1,19	4,05	1,70	1,36
		114	5	1,5	0,8	3,33	1,88	3,97	1,50	1,00	2,65	1,50	2,98	1,76	1,00	0,42	0,34
		115	4	3	2,3	1,33	1,30	3,17	3,00	2,88	1,06	1,04	2,65	1,01			
		116	3,5	1	0,4	3,50	2,50	2,78	1,00	0,50	2,78	2,00	2,20	1,39			
		117	3	0,5	0,3	6,00	1,67	2,38	0,50	0,38	4,76	1,33	1,79	3,57			
		118	9	3,5	2,6	2,57	1,35	7,14	3,50	3,25	2,04	1,08	5,56	1,90			
		119	3,5	1	0,4	3,50	2,50	2,78	1,00	0,50	2,78	2,00	5,56	1,39			
		120	6	2	1,2	3,00	1,67	4,76	2,00	1,50	2,38	1,33	3,97	1,79			
		121	2,5	1	0,5	2,50	2,00	1,98	1,00	0,63	1,98	1,60	4,37	1,24			
		122	7	2	1,3	3,50	1,54	5,56	2,00	1,63	2,78	1,23	4,23	2,26			
		123	3	1	0,6	3,00	1,67	2,38	1,00	0,75	2,38	1,33	3,17	1,79			
		124	4	1,5	1,1	2,67	1,36	3,17	1,50	1,38	2,12	1,09	2,22	1,94			
		125	11	3	2,1	3,67	1,43	8,73	3,00	2,63	2,91	1,14	2,38	2,55			
		126	8	1,5	0,9	5,33	1,67	6,35	1,50	1,13	4,23	1,33	1,50	3,17			
	15	127	3	1	0,6	3,00	1,67	2,38	1,00	0,75	2,38	1,33	2,57	1,79			
		128	5,5	2,5	1,6	2,20	1,56	4,37	2,50	2,00	1,75	1,25	3,81	1,40	3,02	1,53	1,35
		129	3,5	2	1,6	1,75	1,25	2,78	2,00	2,00	1,39	1,00	1,39	1,39	1,00	0,51	0,45
		130	3,5	2	1,4	1,75	1,43	2,78	2,00	1,75	1,39	1,14	1,39	1,22			
		131	6	2,5	1,9	2,40	1,32	4,76	2,50	2,38	1,90	1,05	1,90	1,81			
		132	5	1,5	1,1	3,33	1,36	3,97	1,50	1,38	2,65	1,09	2,65	2,43			
		133	2	0,5	0,3	4,00	1,67	1,59	0,50	0,38	3,17	1,33	3,17	2,38			
		134	3,5	1,5	0,9	2,33	1,67	2,78	1,50	1,13	1,85	1,33	1,85	1,39			
		135	3	1,5	0,8	2,00	1,88	2,38	1,50	1,00	1,59	1,50	1,59	1,06			
		136	3	2	1,5	1,50	1,33	2,38	2,00	1,88	1,19	1,07	1,19	1,12			
		137	3	1	0,7	3,00	1,43	2,38	1,00	0,88	2,38	1,14	2,38	2,08			
		138	3	1	0,6	3,00	1,67	2,38	1,00	0,75	2,38	1,33	2,38	1,79			
		139	4,5	2	1,2	2,25	1,67	3,57	2,00	1,50	1,79	1,33	1,79	1,34			
		140	4,5	1,2	1,1	3,75	1,09	3,57	1,20	1,38	2,98	0,87	1,79	3,41			
		141	5	1,3	1,2	3,85	1,08	3,97	1,30	1,50	3,05	0,87	1,79	3,52			
		142	2	0,5	0,3	4,00	1,67	1,59	0,50	0,38	3,17	1,33	1,79	2,38			

Table 4.:1 measured length of conglomerate clasts. For explanation see text. Locations of data points are shown in Fig. 4.11.

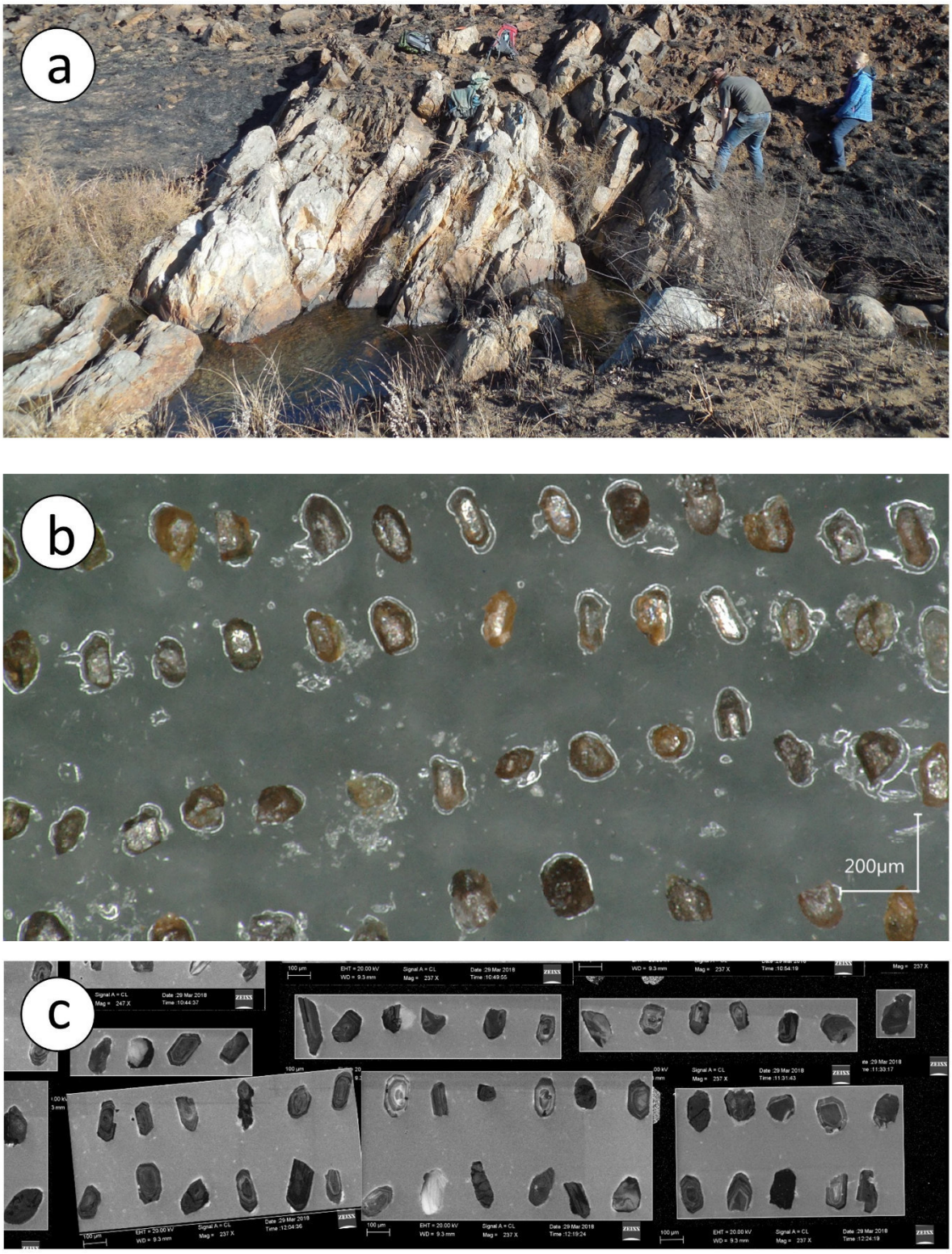

Fig. 4.2: (a) Field photograph of sampled outcrop. For location see Fig.4.3. (b) Microscopy image of extracted zircons. (c) CL-images of selected dated zircons from sample 16-213.

Fig Tree Group

Strata assigned to the Fig Tree Group include conglomerates, greywackes, fine-grained sediments and jaspilites. Fig Tree conglomerates consist of well-rounded clasts ranging in size between 0.5 and 15 cm in a coarse-grained matrix of lithic fragments. Clast composition shows little variability and comprises mainly cherts and dacites. Greywackes are medium- to coarse-grained and consist largely of lithic fragments; they locally contain dacitic tuff. Fine-grained sediments are laminated, commonly ferruginous and show abundant parasitic folds. Jaspilites consist of up to 12 cm thick, conspicuous red to pink beds of hematitic jaspilite. Jaspilite beds alternate with chert, shale or tuffaceous sediments. We observed abundant internal deformation within this unit; parasitic folds are common (Fig. 4.4e).

Moodies Group

Strata assigned to the Moodies Group include clast-supported conglomerates, sandstones and fine-grained sediments. Conglomerate consist of well-rounded clasts, 0.5 to 18 cm in diameter, in a quartzose medium- to coarse-grained matrix. Clast composition includes chert, felsic volcanics and minor jaspilite, sandstone and ultramafic volcanic rocls. Quartzites are medium- to coarse-grained and are dominated by monocrystalline quartz grains and in places abundant chert grains; they are quartz-cemented. Fine-grained sediments of the Moodies Group consist largely of siltstone and are generally poorly exposed. Jaspilites consist of magnetic shale and red hematitic jaspilite, showing abundant internal deformation and parasitic folds.

Younger intrusives

Younger intrusive bodies in the study area comprise the Piggs Peak and Mpuluzi batholiths, the Ushushwana Complex and a swarm of doleritic dikes. The Piggs Peak and Mpuluzi batholiths are of granitoid composition and intruded the southern and eastern flank of the BGB at c. 3.1 Ga (Kamo & Davis, 1994). The Ushushwana Complex is an igneous complex, largely mafic in composition, which is not associated with the primary formation of the BGGT. It intruded the TTG plutons and the Motjane Schist Belt at c. 2671±18 Ma (Walraven & Pape, 1994). The mafic dike swarm shows an ophitic fabric and consists mainly of plagioclase and pyroxene. They crosscut folds and faults and were emplaced post-dating the deformation.

4.4.2 Structural units

The study area (Fig. 4.1, 4.3) can be subdivided into 5 structural units, each of which are – at first order - represented by a major fold and bounded by major subvertical faults. In the following, these structural units are described from southwest to northeast.

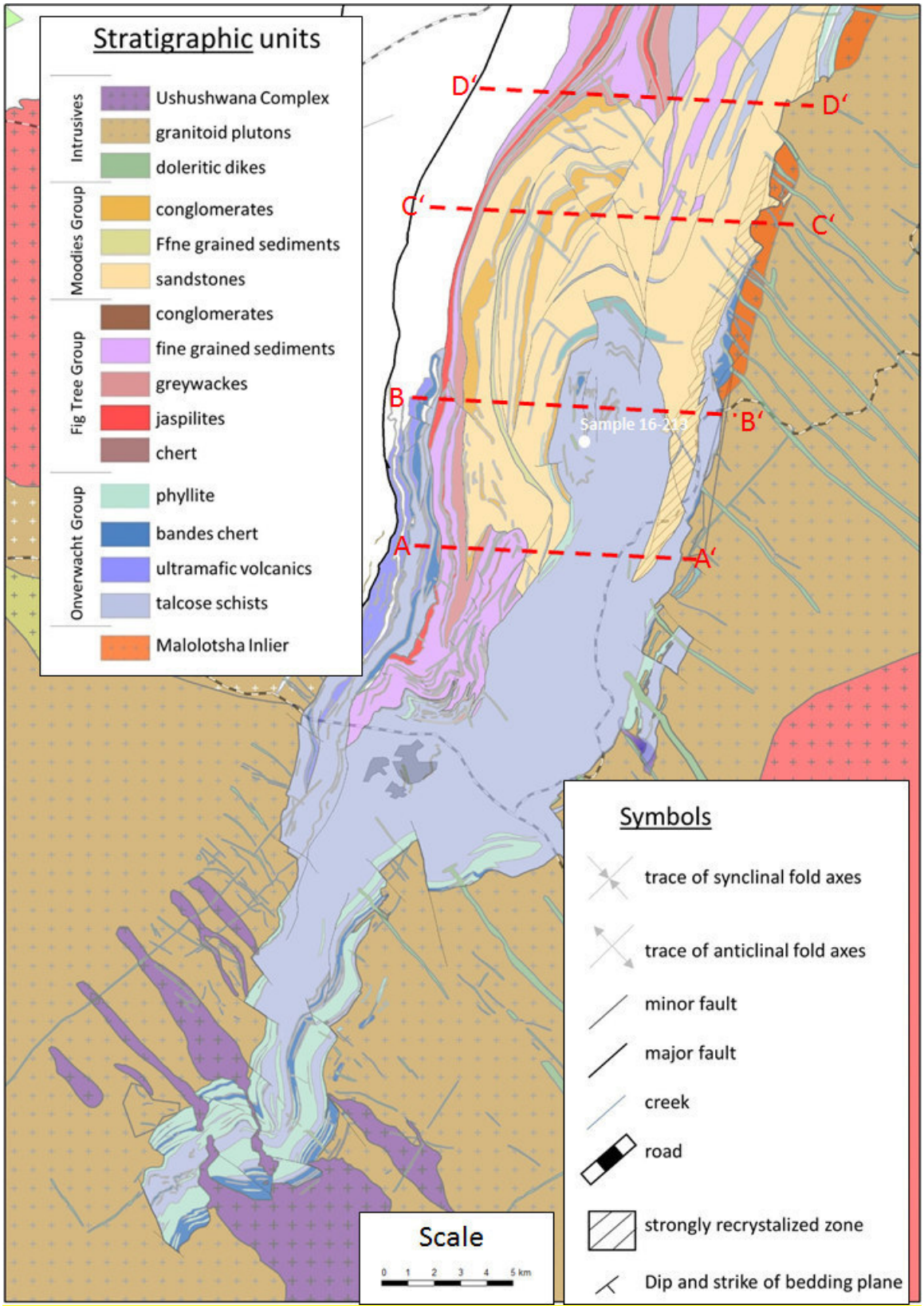

Fig. 4.3: Geological map of the southernmost BGB (outline shown in Fig.4.1). The map shows data compiled from authors mentioned in section 4.3.1 and our own mapping in 2017 and 2018. Cross section A-A' refers to Fig.4.15. For description of units, see text.

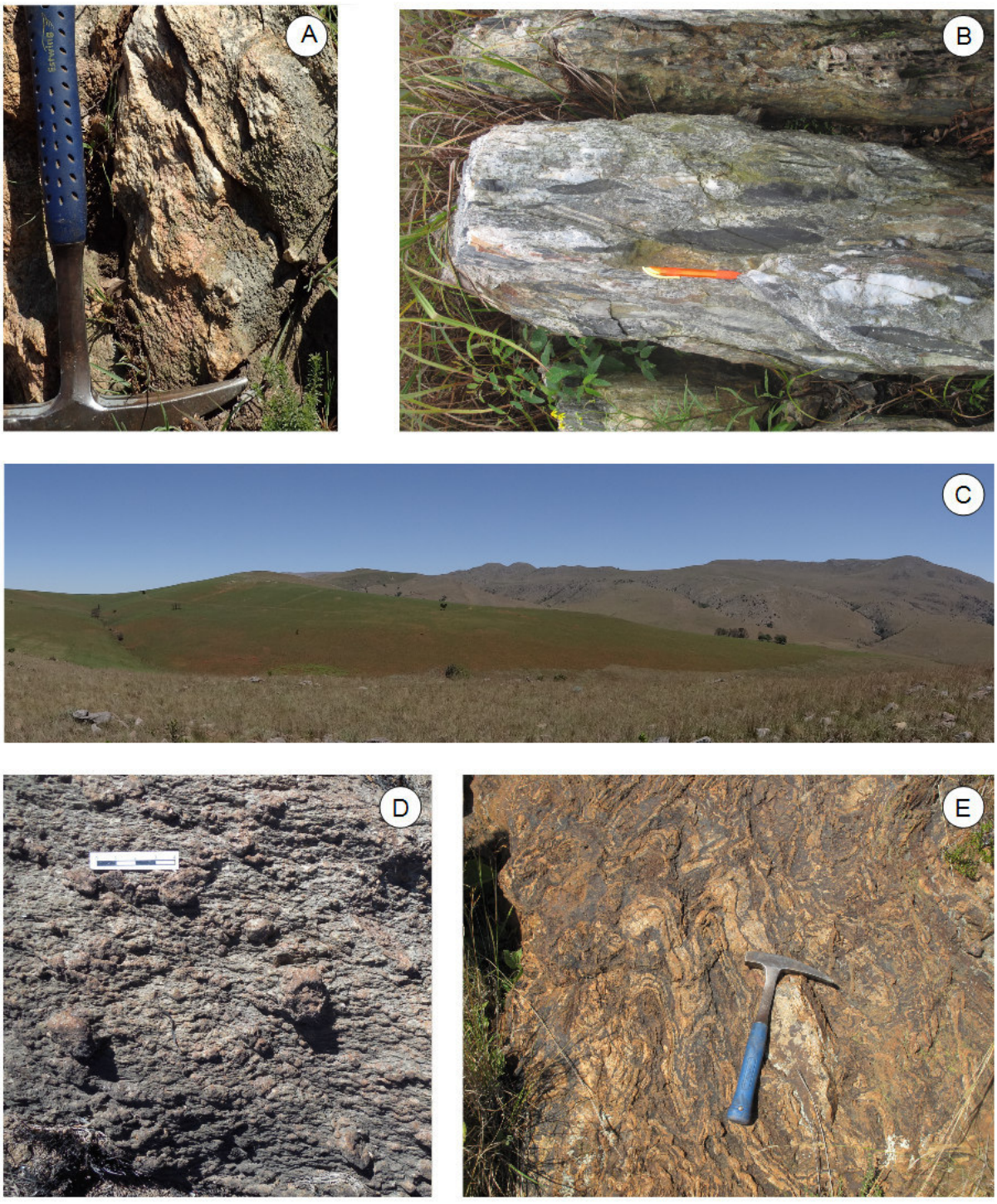

Fig. 4.4: Field photographs. (A) Massive quartzite of the Moodies Group from the eastern margin of the Forbes Reef Anticline. (B) Elongate clasts in conglomrates of the Moodies Group from the Ngwenya Syncline. Major, intermediate and minor axis were measured to obtain strain values. (C) Overview of the central Malolotsha Syncline. The talcose schist in the center of the syncline can clearly be recognized by the low topographic relief in between the hills consisting of Moodies Group rocks and by the different color of the grass. (D) Talcose schist of the Onverwacht Group. (E) Internally strongly deformed ferruginous sediments of the Fig Tree Group.

4.4.2.1 Motjane Schist Belt

The Motjane Schist Belt (Fig. 4.5) is the southernmost extent of the BGB and can be traced for ca. 7 km along its north-trending strike. Its E-W extent in the north (5 km) narrows to not more than a few hundred meters to the south. It is bordered by the Piggs Peak Batholith to the east and south and to the west by the Mpuluzi Batholith. The schist belt connects to the north with the Ngwenya and Malolotsha synclines and their subordinate folds.

The Motjane Schist belt represents a north-plunging synclinorium that is overturned to the northwest (Jackson & Robertson 1983). It consists mainly of mafic and ultramafic volcanic rocks, which have been altered to talcose and serpentinite schists, and minor beds of black and white banded chert, all assigned to the Onverwacht Group (Bennett, 1971). The schist belt generally shows a greenschist-facies metamorphic grade, but rocks adjacent to the margins are characterized by amphibolite facies conditions. This high-grade assemblage becomes more dominant towards the SW, where the schist belt is refolded around a NW-striking axis (Jackson & Robertson, 1983). In this area, the Motjane Schist Belt is intruded by the Ushushwana Complex, a crescent-shaped plutonic body consisting of medium-grained quartz-gabbro and coarse-grained pyroxenite (Hunter, 1970), dated at 2815 Ma (Hoffmann & Kröner, 2018).

4.4.2.2 Ngwenya Syncline and subordinate folds

The north-plunging Ngwenya Syncline (Fig. 4.7) represents the dominant structure of the western part of the study area. It is bounded by the Manhaar Fault to the west and the Mhlamgampepa Fault to the east, which truncates the synclinal fold axis and cuts off minor folds to the east. The Ngwenya Syncline can be traced for about 15 km along strike. It is topographically prominent because it includes resistant Moodies quartzites and forms, north of the former Ngwenya iron ore mine, the steepest slopes of the entire Barberton-Makhonjwa Mountain range. The interlimb angle in the south (where the Ngwenya Syncline extends into the Motjane Schist Belt) is very small, making the fold almost isoclinal, but increases towards the north where the fold opens. The eastern limb is mostly overturned.

In the south, the syncline deforms strata of the Fig Tree Group, comprising greywackes, fine-grained ferruginous sediments, jaspilites and conglomerates. In the north, it includes mainly quartzose sandstones and conglomerates of the Moodies Group. The contact between the two groups appears conformable in the hinge zone of the Ngwenya Syncline. However, Moodies strata east of the central Ngwenya Syncline unconformably overlap and truncate the Ngwenya Anticline and the Rashale Syncline, both expressed in ferruginous sand- and siltstone which appear as lithological equivalent to Mapepe Formation (lower Fig Tree Group) strata in South Africa.

Unique in the study area, Moodies strata above this unconformity show a basal conglomerate about 80 m thick. Overlying sandstones are in places gravelly but appear to lack marker units such as jaspilites or the widespread Moodies lava. Regional silicification, fracturing, and has obscured bedding and sedimentary structures in many places.

The fold axial trace of the north-plunging Ngwenya Syncline is truncated by the convex-to-the west, steeply dipping Mhlamgampepa Fault. It reappears, south-plunging, further north (Fig 4.8), where Lamb (1984) named this the Masali Syncline.

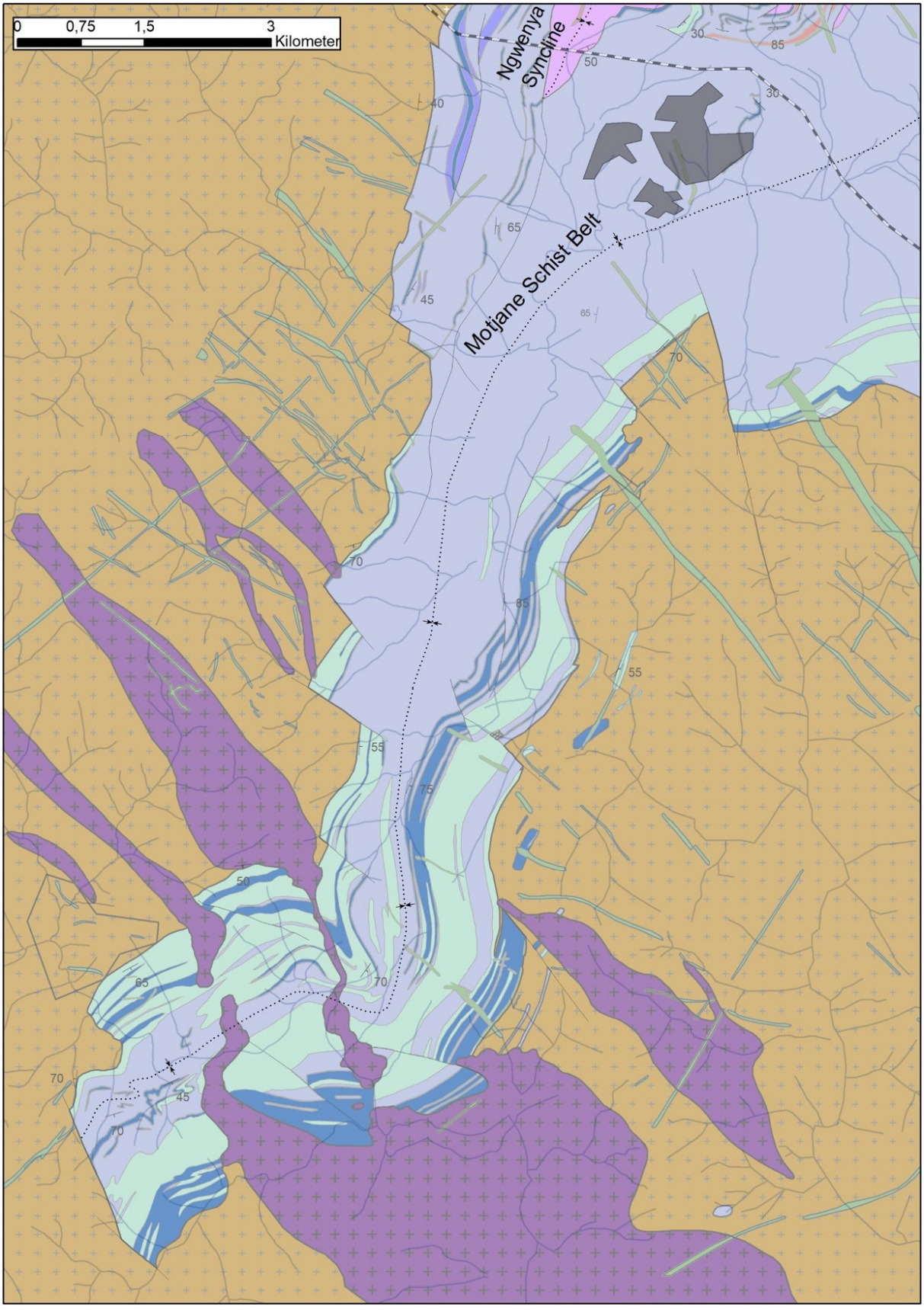

Fig. 4.5: Detailed Map of the Motjane Schist Belt. For key and location, see figure 4.3.

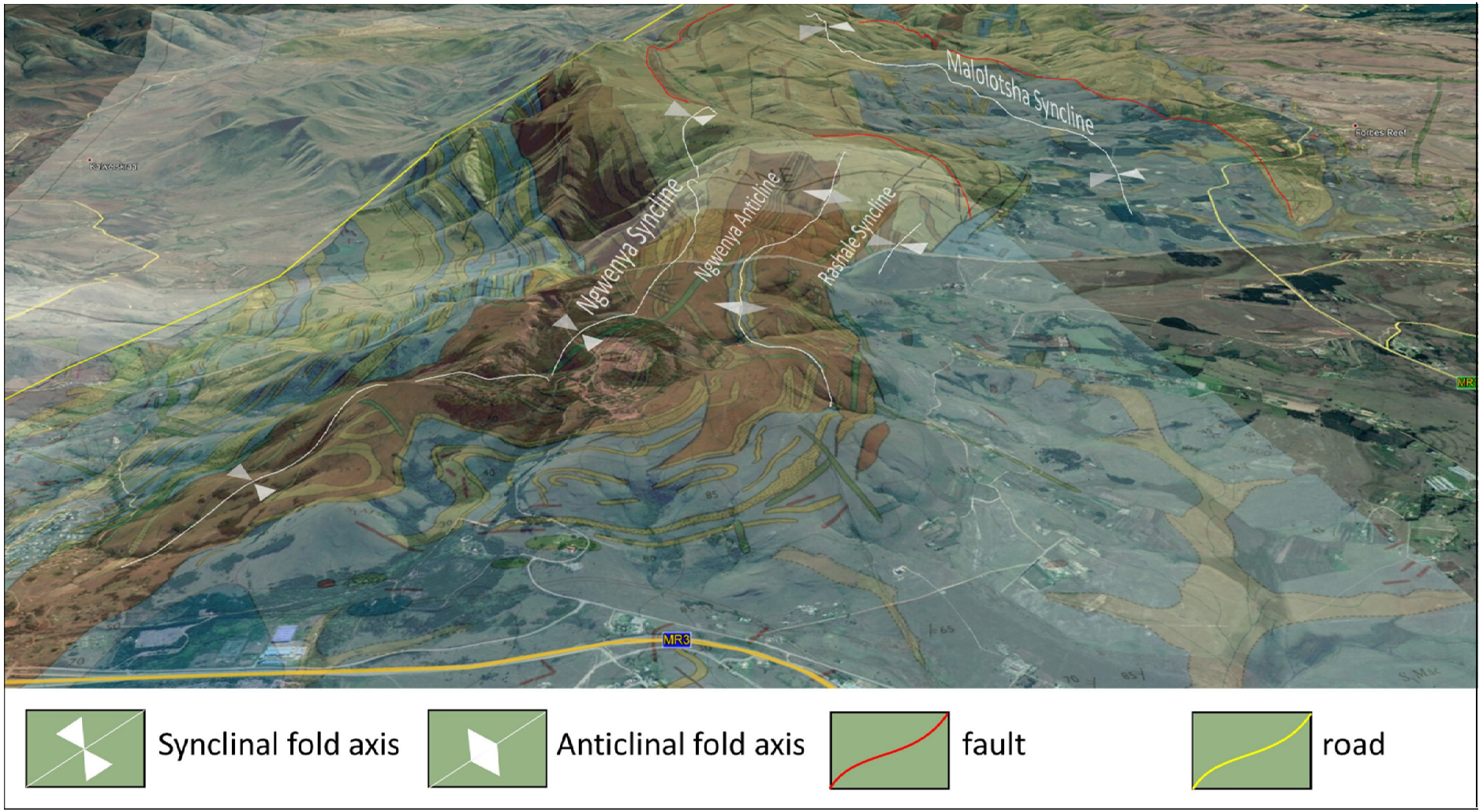

Fig. 4.6: Geological Map of the study area displayed on elevation model by Google Earth.

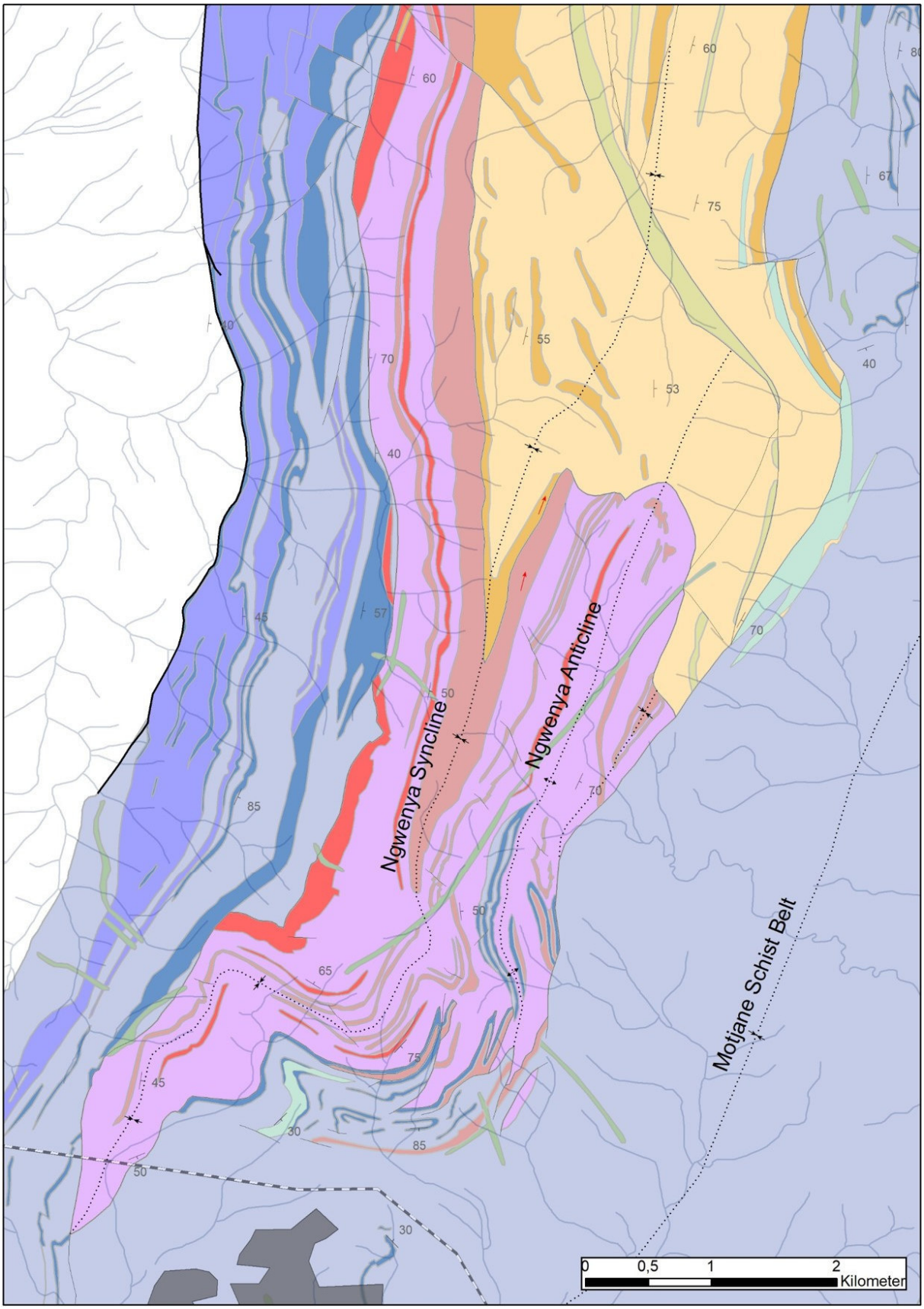

Fig. 4.7: Detailed map of the Ngwenya Area. For key, see figure 4.3.

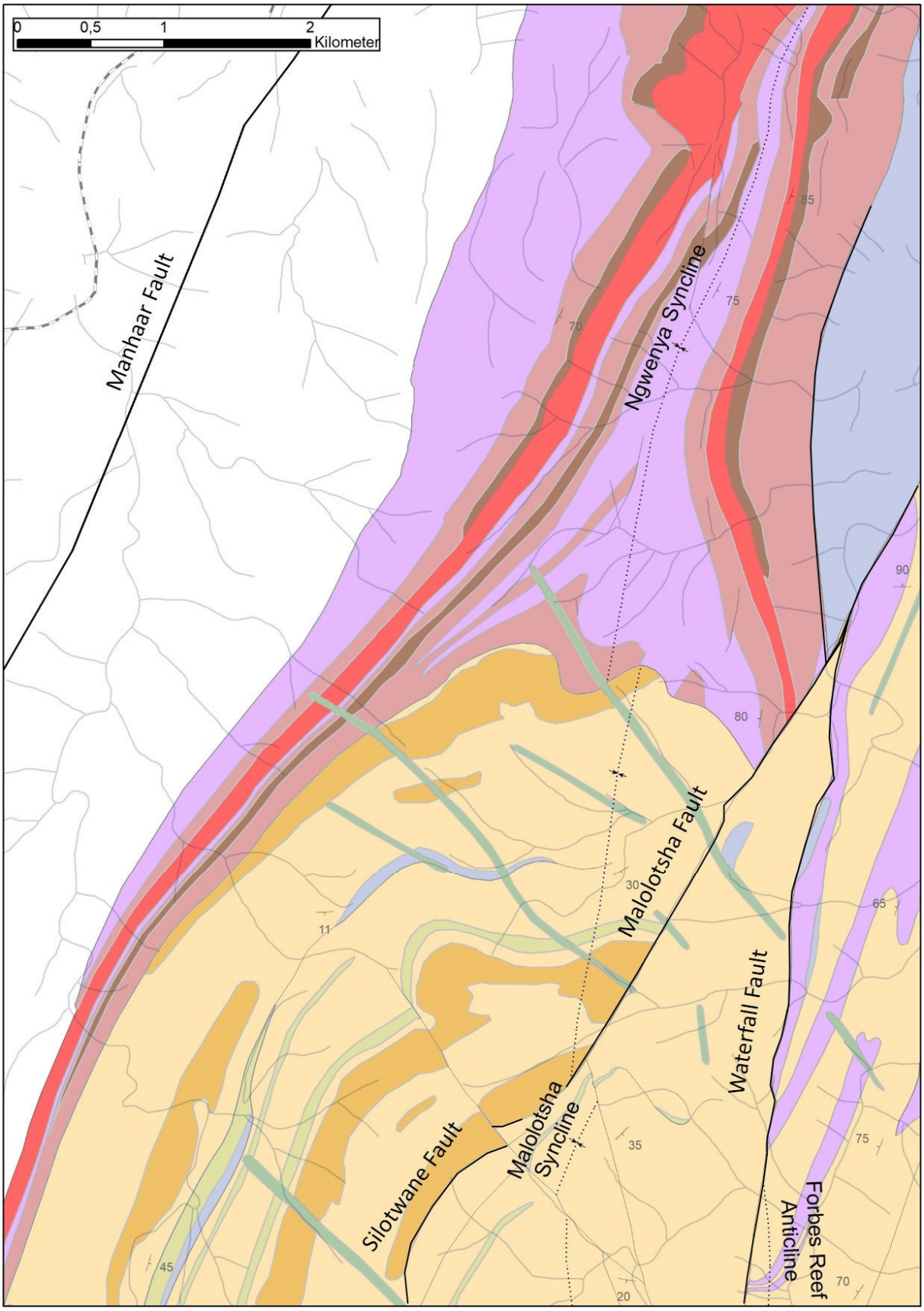

Fig. 4.8: Detailed Map of the Northern Ngwenya Syncline, formerly Masali Syncline. For key, see figure 4.3.

4.4.2.3 Malolotsha Syncline

The Malolotsha Syncline (Fig. 4.9) is the largest and dominant structure of the study area. It is southward plunging (c. 30°), isoclinal and upright, and consists of talcose schists in the core and quartzose siliciclastics on the limbs, which are two rheologically strongly contrasting lithologies. The dip of bedding planes in siliciclastic rocks and the dip of foliation in talcose schists are steep on the limbs (55-80°) but generally 30° or shallower in the hinge zone.

The core of the syncline consists of talcose schists, which presumably represent altered mafic and ultramafic volcanic rocks with a thickness of c. 1.5 km. Several chert beds (on_ch), probably representing silicified ignimbrites and ash-fall tuffs, can be traced for usually a few hundred meters. They show tight folding on map scale. Phyllites and greenschists occur in the contact area between the talcose schist and the quartzose siliciclastics and, to a lesser extent, in the synclinal core (Fig. 4.9).

The synclinal core is surrounded by thick-bedded, commonly cross-bedded, in places gravelly, quartz-rich sandstones and minor conglomerates of the Moodies Group with a total thickness of c. 1.5 km. Shale-draped ripples, desiccation cracks in thin shales, and shallow but wide erosional scours clearly indicate a subaerial deposition. Sedimentary structures consistently show facing up-directions towards the core of the syncline. Locally, these beds are interbedded with elongate areas of talcose schists, reaching several 100 m in length and 20-100 m in thickness. Their stratigraphic relationship to adjacent quartzose sandstones is unresolved. The degree of recrystallization and fracturing is moderate to high.

The Malolotsha Syncline is fault-bounded to the north, east and west. Its continuation to the south appears continuous with talcose schists of the Onverwacht Group in the Motjane Schist Belt (Fig. 4.5). The fault closest to the synclinal core occurs at the contact between the talcose schists and the quartzites of the Moodies Group. The Silotwane Fault truncates talcose schist within Moodies Group strata and marker beds (md_c, md_fg) to the north. The Silotwane Fault is truncated to the south by the Mhlamgampepa Fault. Both the Silotwane and Mhlamgampepa faults are cut off by the Malolotsha Fault in the north (Fig. 4.11).

4.4.2. Forbes Reef Anticline

The Forbes Reef Anticline east of the Malolotsha Syncline is located between the Black Mpuluzi and Waterfall faults (4.11). It is nearly isoclinally folded and overturned to the east. The anticline extends for c. 20 km in NNE-SSW direction and reaches its maximum E-W extent of c. 4 km in the central part of the fold. Bedding planes generally dip steeply (60-85°) and the eastern limb is overturned. In the southern part of the anticline, east of the core of the Malolotsha Syncline, the Forbes Reef Anticline is narrow and consists entirely of quartzites of the Moodies Group. The degree of alteration increases markedly in its eastern limb, within a few hundred meters to the contact to the Piggs Peak Batholith. Sedimentary structures become obliterated and the quartzarenites are strongly sheared and mylonitised (Fig. 4.8, shaded area).

Northward, the western limb and then the axis of the Forbes Reef Anticline are truncated by the Waterfall Fault. Relative displacements along this fault indicate a sinistral shear sense (Fig. 4.11). The preserved thickness of the east limb increases and outcrop widens towards the north, where it consists of a complex sequence of interbedded Fig Tree and Moodies strata with minor talcose schists. This might indicate a tectonic stack. Along the eastern margin of the anticline, the granitoid complex of the Malolotsha Inlier is in contact with the strata of the Forbes Reef Anticline.

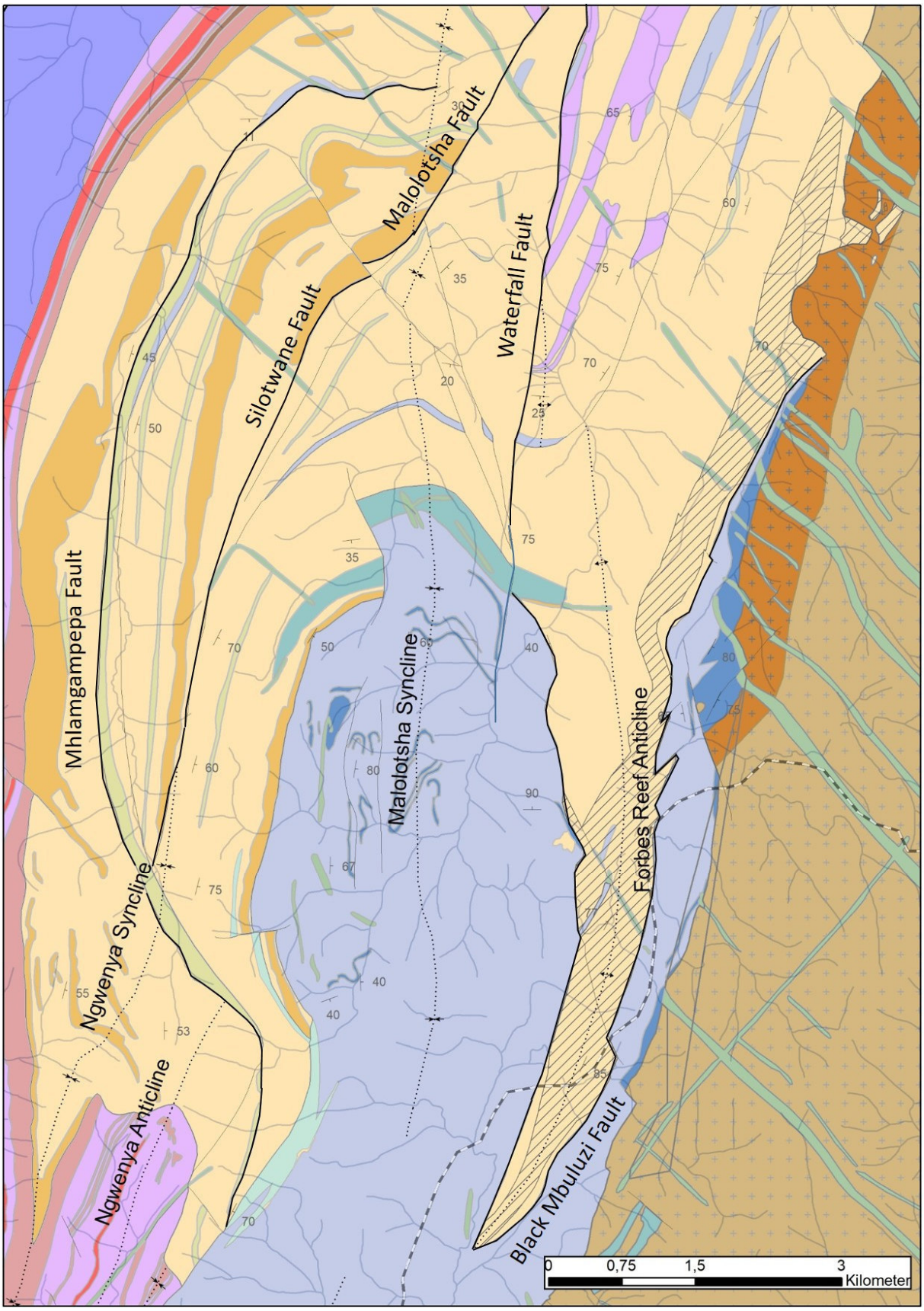

Fig. 4.9: Detailed map of the Malolotsha Syncline and Forbes Reef Anticline. For key, see figure 4.3.

4.4.3 Deformed conglomerate clasts

Depending on their deformation pattern, strained clasts in the study area can be subdivided into three major groups. These correspond to the western part of the study area (locations 1 - 5), the Malolotsha Syncline (locations 6 - 8), and the eastern margin of the Forbes Reef Anticline (locations 9 - 15).

Most clast populations are dominated by prolate strain (Fig. 4.10). This trend is most pronounced in the west, where pure L-tectonites are common. In the central part of the study area, conglomerate clasts are estenially undeformed. Along the eastern margin of the study area, the clasts show a strong of prolate strain (Fig. 4.10).

Long axes of clasts generally trend parallel to the plunge of the nearest major fold axis (Fig. 4.11). The plane of flattening coincides with the bedding plane.

4.4.4 Results of age dating

The majority of analyzed zircons are bipyramidal in shape and show oscillatory zoning (Fig.4. 2c). Ages of dated zircons from sample 16-213 range between 3078 and 3560 Ma. 62 grains are between 95 and 105 % concordant. The youngest coherent cluster within this group (n= 10) shows a concordant age of 3220±12 Ma (Fig. 4.12). We interpret that cluster to represent the depositional age of the unit.

4.5 Discussion

4.5.1 Structural evolution of the Ngwenya Syncline and subordinate folds

Because the Ngwenya area (Fig. 4.7) comprises excellent outcrop conditions and exposes the complete stratigraphic succession (Lamb & Paris, 1988), this region is best suited for understanding the structural pattern of the study area. The contact between the Onverwacht Group surrounding the Ngwenya Syncline and Fig Tree Group at the western margin of the fold is clearly fault-bounded. Even though the Onverwacht strata crop out poorly, the contact clearly truncates units of the Fig Tree Group (Fig. 4.6) on both limbs of the Ngwenya Syncline.

The contact between the Fig Tree Group and the overlying Moodies Group is well exposed in the axial zone of the Ngwenya Syncline and the Ngwenya Anticline as well as in the Masali Syncline. The angular unconformity between these two groups represents uplift, deformation and erosion of Fig Tree Group strata during D2 prior to deposition of Moodies Group units. This unconformable contact to the overlying Moodies Group is well documented from other parts of the greenstone belt (e.g. Lowe & Byerly, 1999, 2007). Large-scale regional refolding incorporating Fig Tree and overlying Moodies Group strata during (D3, D4) or following (D5) Moodies time (c. 3224-3218 Ma) created the present folding pattern (Fig. 4.13)

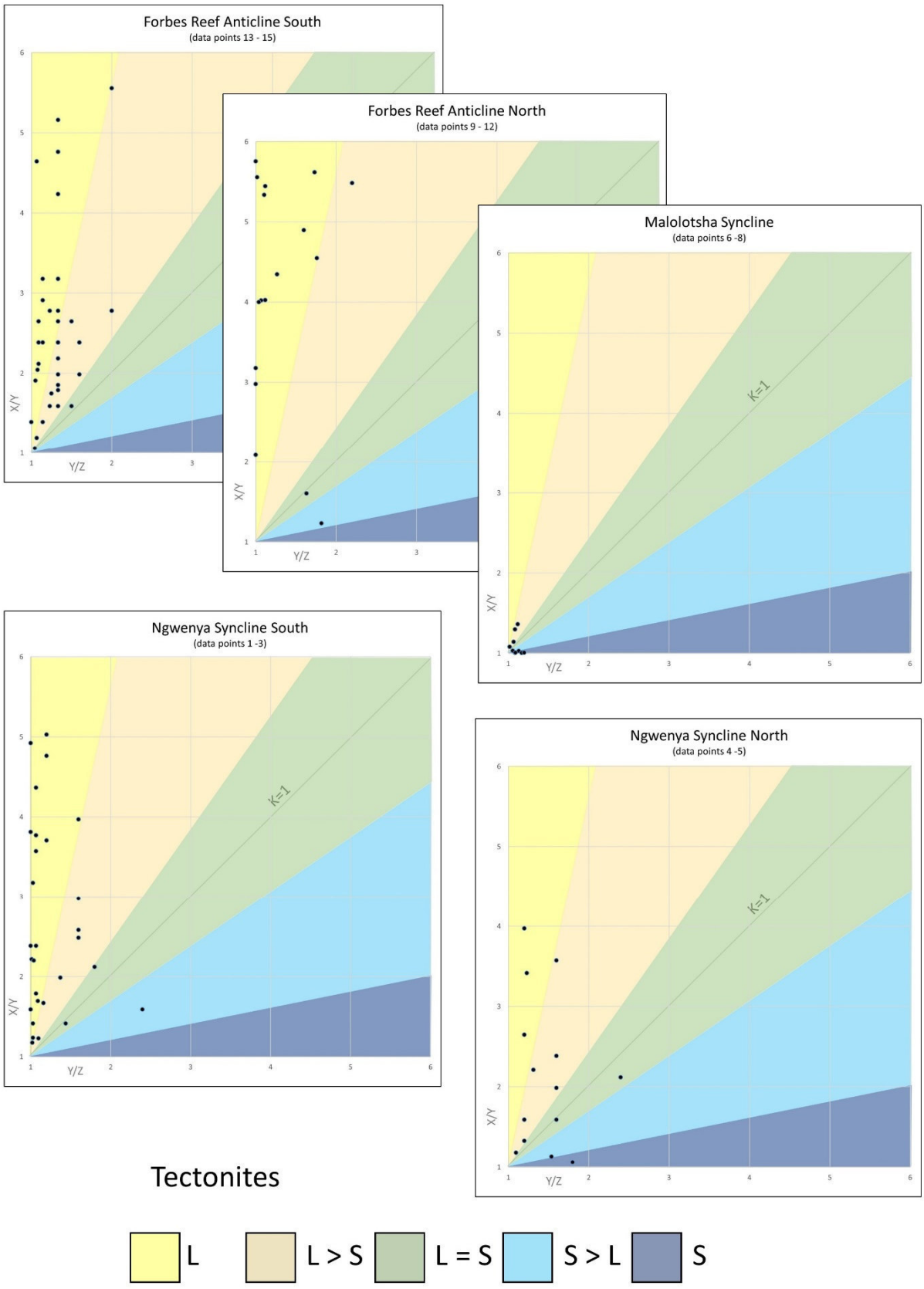

Fig. 4.10: Flinn diagrams of conglomerate clasts. Data from Table 4.1. Fig. 4.11 shows the location of data points and strain distribution throughout the study area.

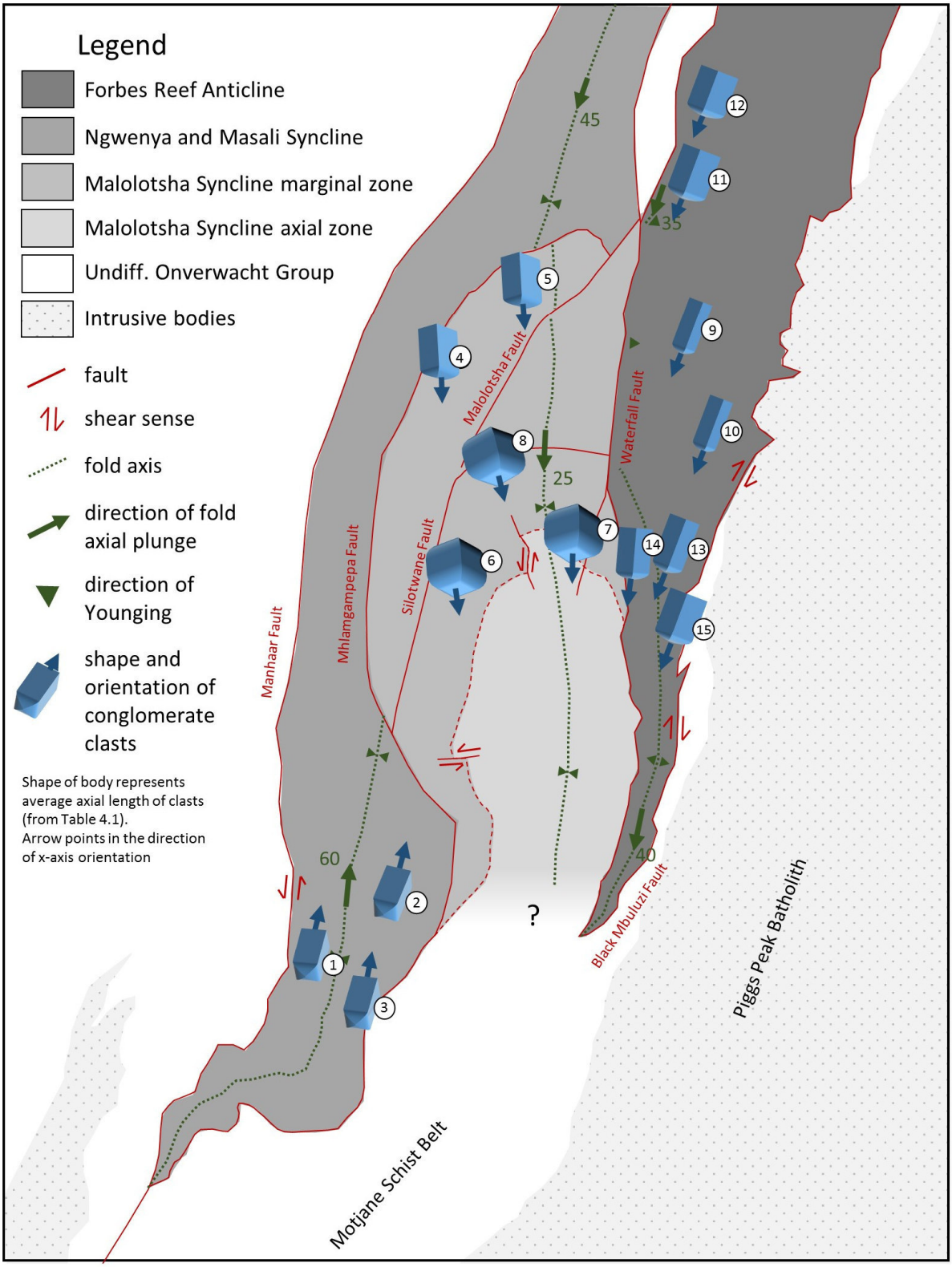

Figure 4.11: Simplified map of the study area showing subdivision into different fault-bounded blocks and structural features.

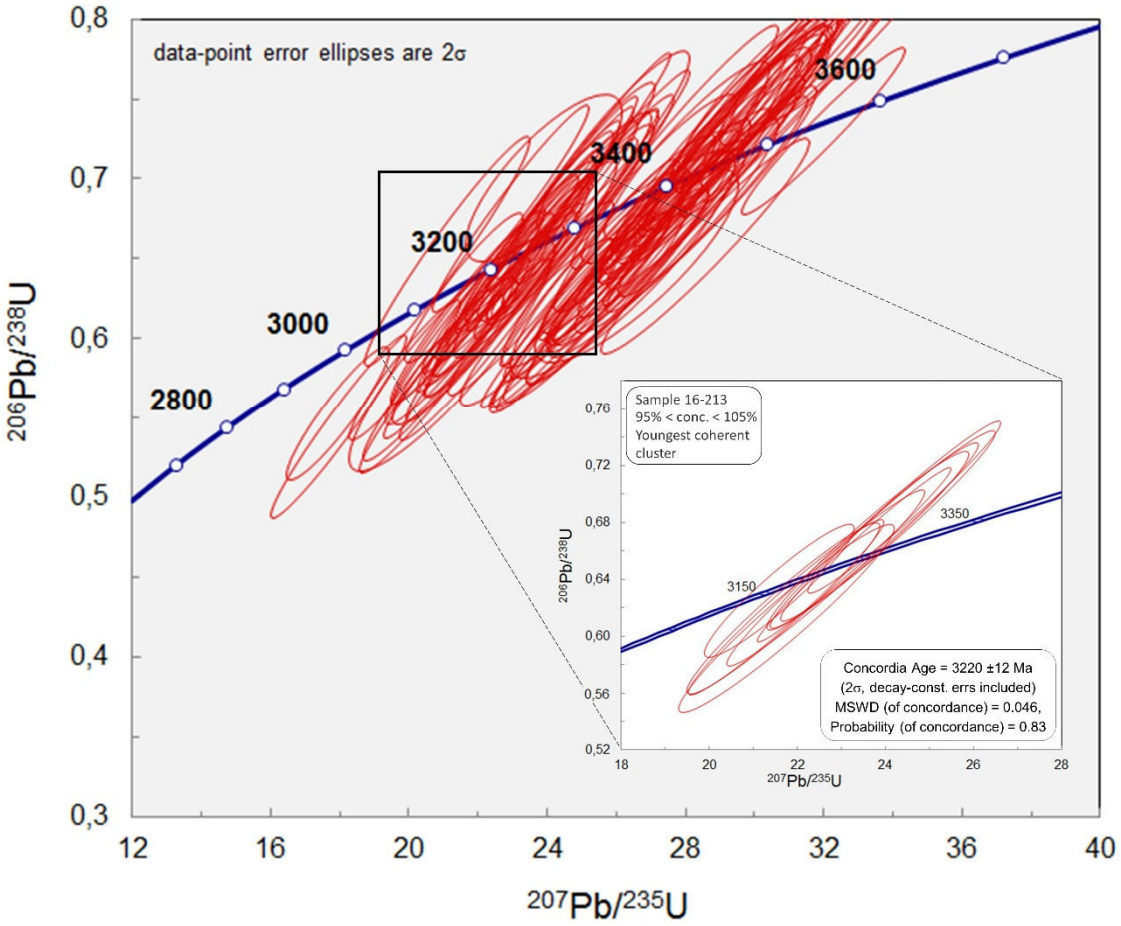

Fig. 4.12: Concordia diagram of sample 16-213 (silicified metavolcanic bed from the central Malolotsha Syncline). Insert shows youngest coherent cluster of concordant zircon ages. See Fig. 4.3 for sample location.

The refolding of the southwesternmost part of the Ngwenya Syncline around a northwest-trending axial trace (Fig. 4.6), which can also be observed in the Motjane Schist Belt, can be explained by one of the following hypotheses: (1) The refolding of the southernmost part of the synclines is a result of rotation due to shearing and lateral displacement along the Manhaar Fault (de Wit et al., 2018), suggesting a sinistral sense of movement along that fault, contrary to the sense of movement observed at the Black Mbuluzi Fault along the eastern margin of the Forbes Reef Anticline (Fig. 4.11). (2) Alternatively, refolding may have been induced by the later emplacement of the Ushushwana Complex. However, this trend is not observable in Onverwacht strata exposed immediately west of the Manhaar Fault (Fig. 4.5).

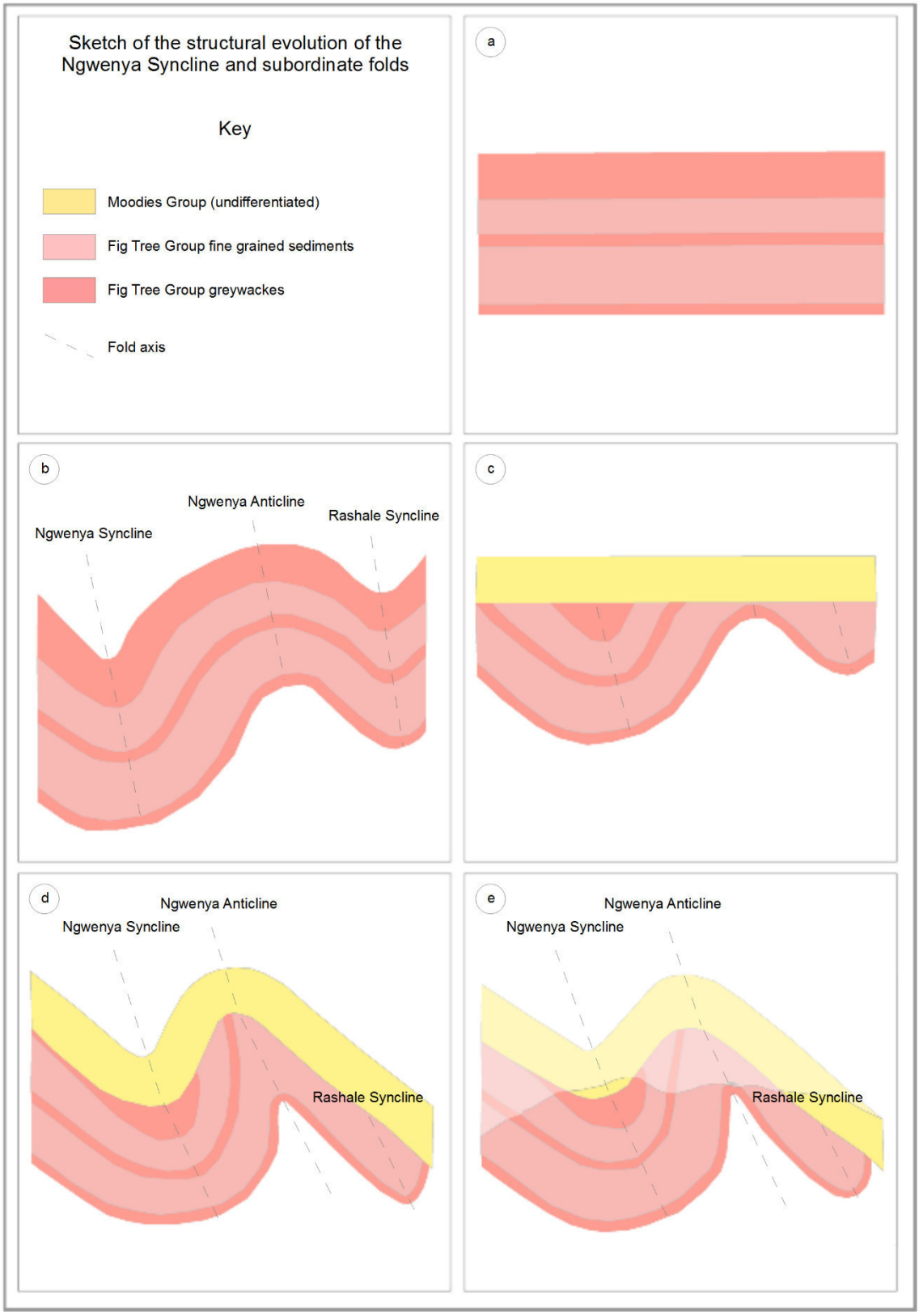

Fig. 4.13: Sketch showing the tectonic evolution of the Ngwenya area. (a) Deposition of the Fig Tree Group. (b) D1 deformation leads to the west-vergent folding and uplift of Fig Tree Group strata. (c) Moodies strata are deposited unconformably on top of the Fig Tree Group. (d) D2 deformation folds Moodies strata in large syn-and anticlines, along with the previously folded Fig Tree Group. (e) Erosion exposes different levels of the complex fold structure.

The Masali Syncline was described by Lamb (1984) as a south-plunging, tight to isoclinal NNW-trending syncline. Our inspection, however, shows that it rather represents the northern continuation of the Ngwenya Syncline because jaspilite marker beds on its western limb can be traced continuously to the Ngwenya Syncline. Only its eastern limb and the fold axis are truncated by the Mhlamgampepa Fault. (Fig. 4.11).

The stratigraphy of the Fig Tree Group in the Ngwenya and Masali Synclines differs significantly. Small-scale facies variation in the Mapepe Formation (Drabon et al., 2019) are well known and do not support the interpretation that the Ngwenya and Masali synclines formed as two distinct structures.

4.5.2 Formation of the Malolotsha Syncline

The superposition of altered ultramafic rocks, known only from the c. 3.57 to 3.27 Ga old Onverwacht Group, above strata of the c. 3.22 Ga old Moodies Group is unique throughout the BGB. Three mutually exclusive hypotheses (Fig. 4.15) may explain the formation of this complex structure.

4.5.2.1 Thrust complex

Lamb (1984), recognizing the unusual lithologic sequence, interpreted the structure as a result of thrusting of Onverwacht Group strata over Moodies Group strata, followed by folding of both (Lamb, 1984; Lana et al., 2011). To account for the ca. 5 km stratigraphic juxtaposition, Lamb (1984) postulated major sub-horizontal shortening above a shallowly eastward dipping thrust plane (Fig. 4.15a). Several problems arise related to this interpretation:

(1) Northwestward thrusting should result in folds of a uniform sense of vergence. However, the Forbes Reef Anticline is overturned to the east while the Ngwenya Syncline is overturned to the west, while the Malolotsha Syncline shows no vergence.

(2) There is ample evidence that Moodies Group strata were folded syndepositionally (Heubeck et al., 2013, 2016; Byerly et al., 2018; Stutenbecker & Heubeck, 2019). Therefore, it appears unlikely that Onverwacht Group strata were thrusted on top of Moodies Group strata prior to folding of the Moodies Group. In addition, deformation is usually initially accommodated ductily (by folding) before brittle deformation (by faulting) sets in (e.g. Gibson & Gray, 1985; Avigad et al., 2001), contradicting the suggested order of deformation in this model.

(3) The age data of sample 16-213 from the talcose schists in the central part of the Malolotsha Syncline is not compatible with an Onverwacht Group age, but represents a standard Moodies Group age (e.g. Heubeck et al., 2013).

4.5.2.2 Stratigraphic continuity

The youngest coherent cluster of concordant zircons from a silicified ignimbrite (sample 16-213) yields a crystallization age of 3220 ± 12 Ma, interpreted as age of deposition (Fig. 4.12). Although the silicified volcanoclastic beds cannot be mapped continuously around the synclinal core and are in places tightly folded, they follow the stratigraphy and parallel the foliation in the talcose schists. The lack of cross-

cutting relationships and paucity of truncations makes their structural insertion into a stack of ultramafic rocks unlikely. Their ages can, thus, be reasonably interpreted to represent the age of the over- and underlying talcose schists.

This finding implies that altered ultramafic strata in the core of the syncline are not older but younger than the underlying sandstones, plausibly inferred to represent the Moodies Group. Talcose ultramafic strata in the core of the syncline are interpreted to be in stratigraphic, not structural, contact with the underlying quartz-rich sandstones and may represent a stratigraphic unit above the Moodies Group (Fig. 15 b). The sheared contact between the two units is easily explained by flexural slip due to the strongly contrasting rheological properties (Damasceno et al., 2017). However, doubts remain related to this hypothesis as well:

(1) The age of sample 16-213 coincides with a major deformation event of the BGB (D3) at c. 3220 Ma (De Ronde & de Wit, 1984; Lowe et al., 1999; Lana et al., 2011). The obtained age may represent a metamorphic age instead of a depositional age (Dong et al. 2017). ``Concordia-parallel´´ Pb loss due to metamorphic or hydrothermal overprint is well known from other Moodies samples (Heubeck et al., 2013) and may lead to a misinterpretation of the true depositional age (Zeh et al., 2008, 2013; Cabral et al., 2012; Zeh & Gerdes 2012).

(2) Talcose schists younger than uppermost Onverwacht Group are documented nowhere else in the BGB.

4.5.2.3 Out-of-syncline thrusting

The talcose schists in the core of the syncline may have been squeezed up and out along reverse faults with opposite sense of displacement on the eastern and western contacts of the talcose schists to the quartzitic sandstones. These developed during D3 (Fig. 4.15 b) due to ESE-WNW-directed shortening (Fig. 4.15 b, c) and were subsequently steepened. Further shortening eventually made the Malolotsha Syncline into a complex structure of three fault-bounded blocks (Fig. 4.11). This model is consistent with deformation contemporaneous to the deposition of the Moodies Group and explains the different fold vergences of the adjacent synclines.

The shortcomings of this model are:

(1) Due to the poor outcrop in the synclinal core, no evidence for the existence of reverse faulting along the talcose schist / quartzite contact can be documented.

(2) The true three-dimensional geometry of the southward-plunging Malolotsha Syncline must involve some N-S directed shortening as well.

(3) The sparse geochronological data do not conform with this hypothesis.

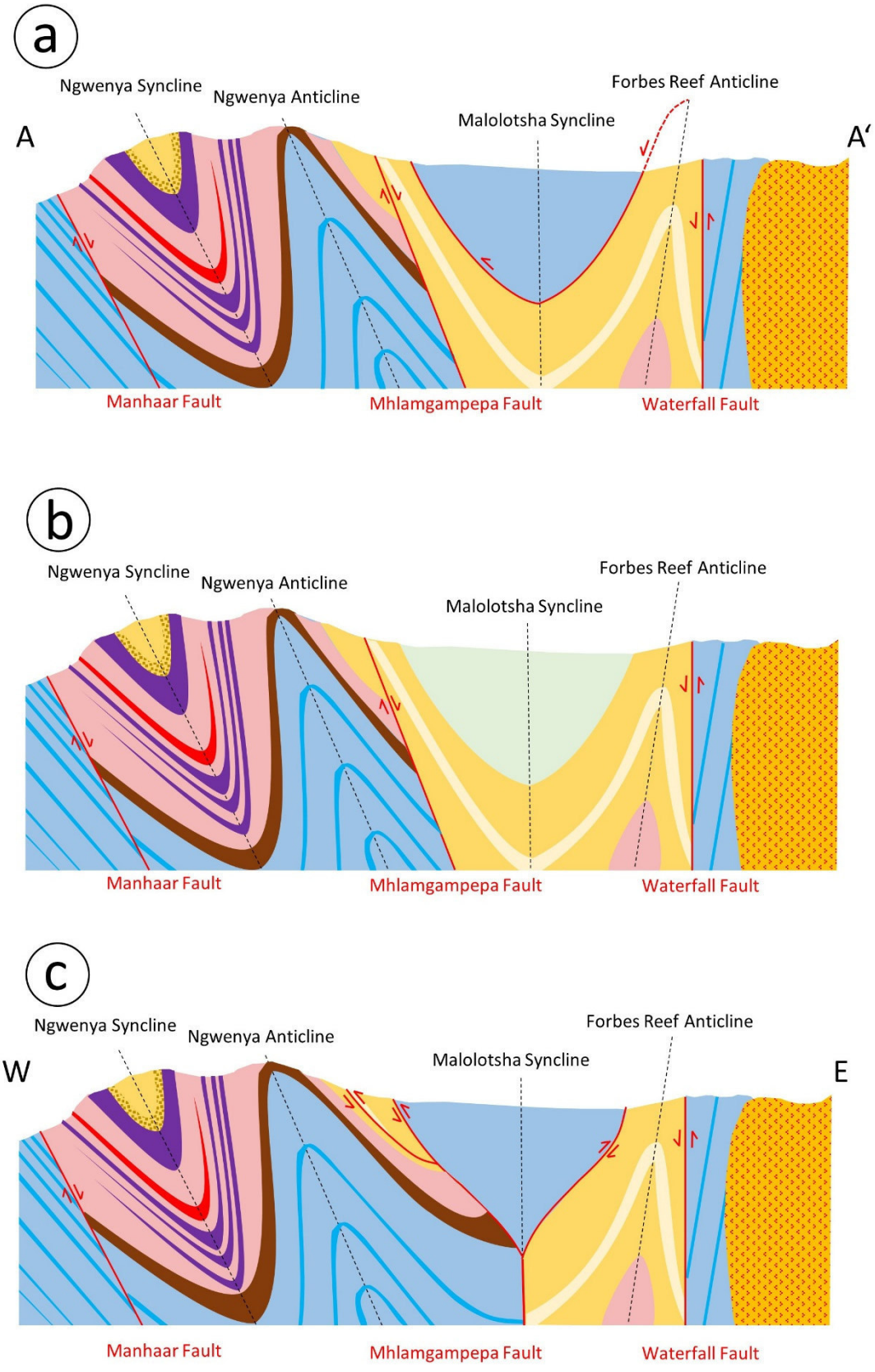
a
Ngwenya Syncline
Ngwenya Anticline
Malolotsha Syncline
Forbes Reef Anticline
A
A'
Manhaar Fault
Mhlamgampepa Fault
Waterfall Fault
b
Ngwenya Syncline
Ngwenya Anticline
Malolotsha Syncline
Forbes Reef Anticline
Manhaar Fault
Mhlamgampepa Fault
Waterfall Fault
c
Ngwenya Syncline
Ngwenya Anticline
Malolotsha Syncline
Forbes Reef Anticline
W
E
Manhaar Fault
Mhlamgampepa Fault
Waterfall Fault

Fig. 4.14 – Comparison of three alternative cross sections illustrating subsurface relationships and inferred formation mechanisms of the Malolotsha Syncline region. Cross sections are drawn along the line marked in Fig. 4.3 A to A'. (a) The core of the Malolotsha Syncline represents a folded klippe and folding occurred after thrusting of Onverwacht Group strata on top of Moodies Group strata. (b) The core of the Malolotsha Syncline represents a younger, conformable overlying unit on top of the Moodies Group. (c) The core of the Malolotsha Syncline was up-faulted along two reverse faults with opposing sense of shear on both limbs of the Malolotsha Syncline.

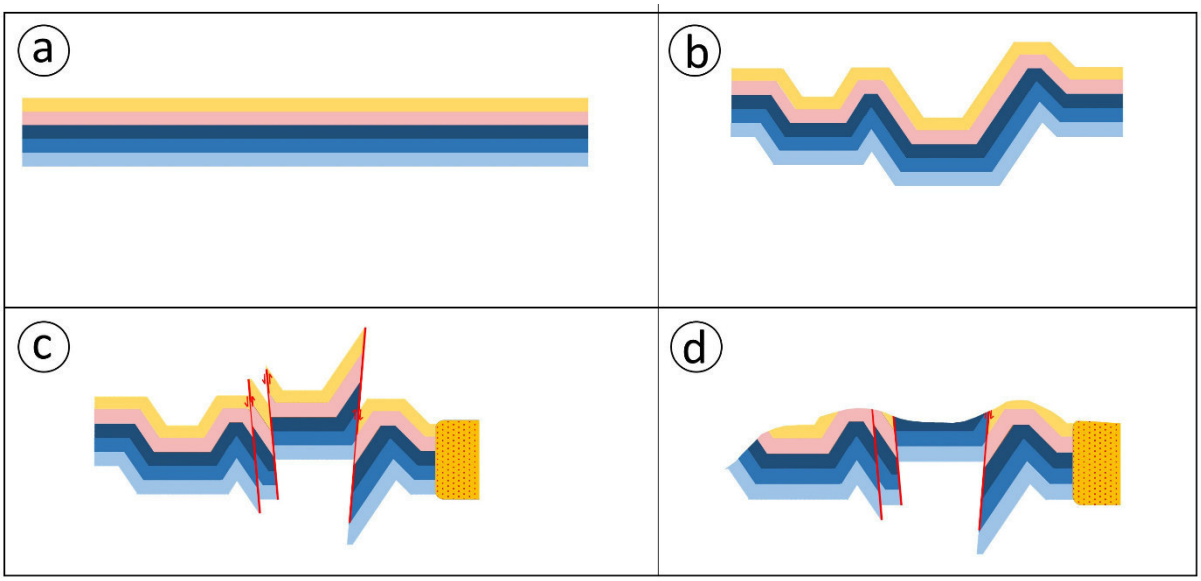

Fig. 4.15: Semi-balanced cross-section sketches illustrating out-of-syncline thrusting in the center of the Malolotsha Syncline. Sketches are drawn approx. from A to A' (Fig. 4.3) (a) Situation prior to deformation. Pre-Moodies deformation is not shown (see Fig. 4.13). (b) Ductile D3 deformation leads to folding. (c) Brittle D3 deformation leads to faulting and the ''squeez-out'' of the central Malolotsha Syncline. (b) and (c) may have happened contemporaneously but are shown here as two subsequent processes for clarity. (d) Erosion results in the present-day surface pattern.

4.5.3 Relationship to adjacent granitoids and gneisses

(1) D3 represents the last pervasive deformation that affected both the BGB and the adjacent plutons. Both the Malolotsha and Piggs Peak inliers at the southeastern flank of the BGB (Schoene et al., 2008; Schoene & Bowring, 2010; Lana et al., 2010, 2011) and the plutons and gneisses along the southern margin of the BGB (Kröner et al. 2018) record a major tectonometamorphic event at c. 3.2 Ga. Later BGB deformations (D4, D5) are not recorded.

(2) D5 (D4 of de Ronde & de Wit (1984)) involves exhumation of the Malolotsha Inlier along an extensional fault at the eastern margin of the BGB (Lana et al. 2011). Exhumation and juxtaposition of high-grade metamorphic terranes next to lower-greenschist-facies strata of the BGB, thus, occurred here significantly later compared to the southern margin where an extensional detachment exhumed deeper crustal levels at c. 3230-3225 Ma (D2, Kisters et al., 2003).

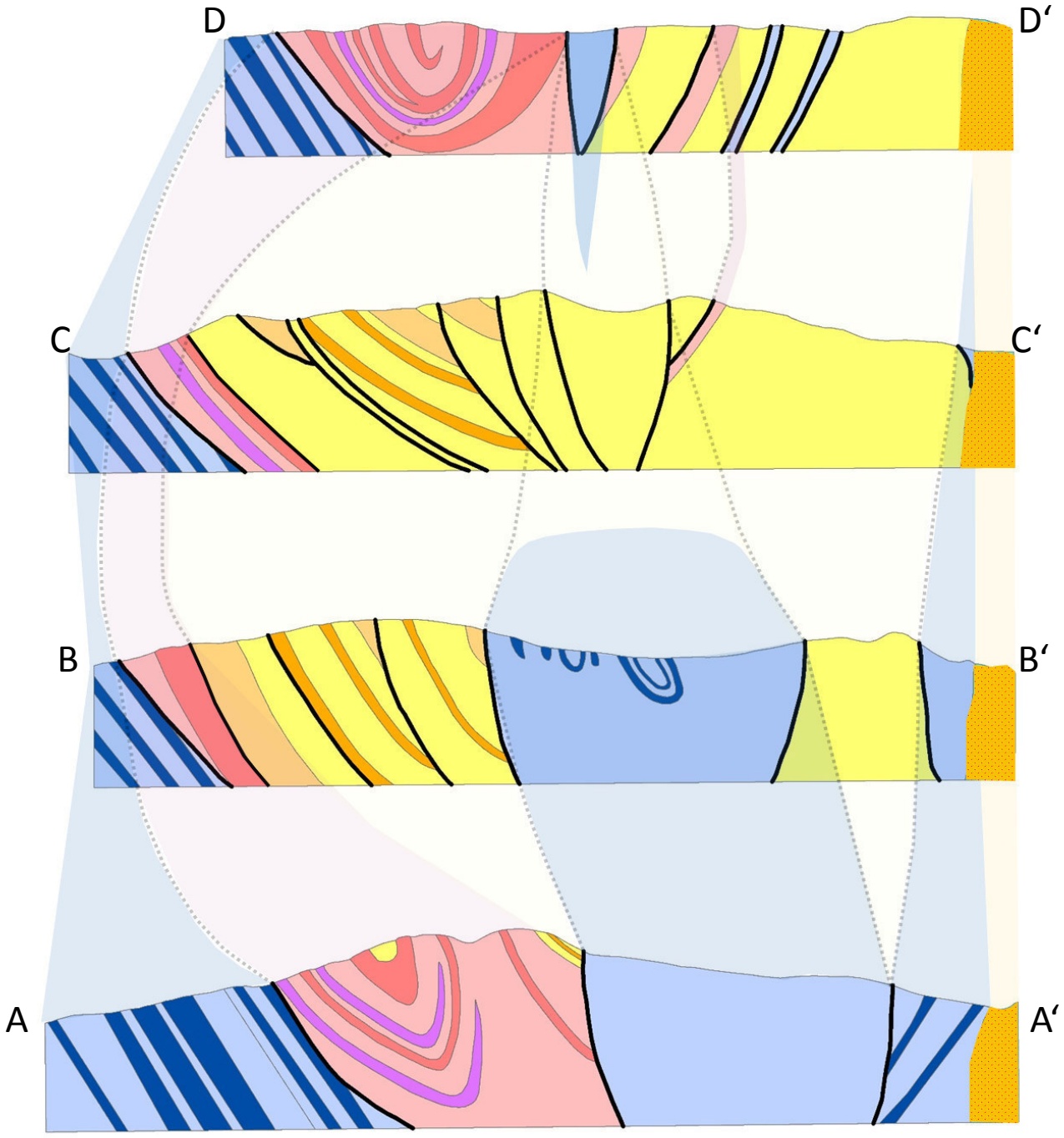

Fig. 4.16: Correlation of cross-sections drawn across the study area. For location of the cross section traces, see Fig. 4.3.

(3) The metamorphic overprint along the eastern margin of the greenstone belt represents a contact-metamorphic aureole induced by the emplacement of the Piggs Peak Batholith. Foliation along the eastern margin of the Forbes Reef Anticline shows a dextral shear sense, also observed by de Wit et al. (2018) and Schoene et al. (2008). It might have been the result of a space problem due to the emplacement of plutons southwest of the greenstone belt or may have been caused by strike-slip movement postdating the main phase of deformation in the BGB (Schoene et al., 2010).

4.6 Conclusions

D2 (c. 3230 Ma) represents the first record of complex deformation in the southernmost part of the BGB. It resulted in the angular unconformity between the Fig Tree Group and overlying Moodies Group strata observable in the Ngwenya Syncline. D3 occurred contemporaneous with the deposition of the (upper) Moodies Group and was the last pervasive deformation event, also recorded in the structural fabric of gneisses of the Malolotja and Piggs Peak inliers. D3 and D4 folded Moodies Group strata and tightened D2 folds. D4 inverted the Moodies basins (Lowe et al., 1999) and D5 exhumed high-grade gneisses along extensional faults on the eastern margin of the BGB.

The Ngwenya and Masali synclines are the southern (Ngwenya) and northern (Masali) segments of the same complex structure of imbricated synclinal limbs.

Three hypotheses may explain the unique structure of the Malolotsha Syncline: (1) a folded klippe, (2) a unit of ultramafic volcanics conformably overlying Moodies Group sandstones, or (3) out-of-syncline reverse faulting of Onverwacht Group strata during continuous shortening in WNW-ESE direction. Hypotheses (1) and (2) are mutually exyclusive but both may be modified by hypothesis (3). All models face serious counterarguments.

4.7 Further research

Investigating the relationship of the talcose schists in the core of the Malolotsha Syncline and the underlying quartzose sandstones will remain an important geologic task. Either hypothesis (1 – 3) has profound implications on the stratigraphy and tectonic evolution of the BGB. Future studies should sample and age-date additional beds of silicified volcaniclastics. Geochemical parameters of the talcose schists should be compared to altered ultramafic rocks from other parts of the BGB. A detailed study of the contact zone between the talcose schists and the quartzose sandstones may demonstrate the existence of a shear zone and its kinematics. Finally, a detailed investigation of the elongate strips of altered ultramafic rocks interbedded with the quartzose sandstones on the northern limb of the Malolotsha Syncline should demonstrate their tectonic (imbricated thrust sheets) or stratigraphic (lava flows) nature.

4.8 Acknowledgments

This study was funded by the SPP 1833 ``Building a habitable Earth´´ of the DFG. The Eswatini National Trust Commission granted access to the Malolotsha Nature Reserve and supported our work. The author would like to express his gratitude towards Linda Gosniak and Maik Schlimme for assistance in the field and data processing.

5 Tectonic Evolution of the Barberton Granitoid-Greenstone Terrane – Integrating local studies into a regional model

Abstract

The Barberton Greenstone Belt features prominently in the debate about Archean tectonic processes because it provides a detailed geological record of the transitional time period (c. 3.53 – 3.2 Ga) from pre-plate tectonic mode to modern-style plate tectonics. A variety of actualistic and non-actualistic, in part contradictory tectonic settings, including gravitational collapse, terrane accretion, foreland basins, continental rifting, doubly-vergent subduction zones and partial convective overturn have been proposed. In this study, we critically review these scenarios, compile a greenstone-belt-wide digital geological map by combining published data with our own observations and compare our findings to geometries and structures implied by the different models. While most previous studies focused on particular segments of the Barberton Greenstone Belt, we aim at providing a comprehensive analysis of the entire region. We examine the effects and timing of the deformation events (D1 – D5) in different parts of the greenstone belt and provide a new subdivision of the belt into five domains, based on differences in deformation geometry. We conclude that none of the published models can account for all of the structural features nor sufficiently explain the heterogeneity of deformation patterns across the greenstone belt. The partial convective overturn model, despite minor weaknesses and oversimplifications, appears to be suited best to explain the unusual fold geometry of the greenstone belt and the orientation of the enormous Onverwacht Anticline. We suggest that local subsidence caused by gravitationally induced sinking of dense greenstones into hot and buoyant felsic lithosphere, resulting in passive block rotation, is responsible for the tilting of the Onverwacht Anticline and accounts to a high degree for the formation of the particular fold style of the Barberton Greenstone Belt.

5.1 Introduction

Some type of pre-plate tectonic setting has been suggested for the Earth's early history. Plate tectonics did not operate during at least part of the Archean due to a significantly higher heat flow, resulting in a less dense and more buoyant mantle (Reese et al., 1998; Dumoulin et al., 1999; Ernst, 2009; Debaille et al., 2013; Piper, 2013; Bedard, 2018; Sleep, 2018). Instead, Archean tectonics was dominated by vertical movements induced by subsidence of dense and thick, cold and mechanically competent piles of mafic-volcanic rocks (greenstones) and the more or less simultaneous diapiric rise of hot and buoyant intermediate to felsic plutons that originated from the partial melting of basaltic/gabbroic lower crust.

The Barberton Greenstone Belt (BGB) is one of the key areas for that debate because the critical time period of about 3.2 Ga, which is thought to mark the onset of modern-style plate tectonics (Cawood et al., 2018), is recorded in its strata. The controversy and purported evidence for either tectonic regime is reflected in a large number of publications on its tectonic evolution. They can be divided into a plate-tectonics m (de Wit, 1982, 1991; de Wit et al., 1987, 2011; de Ronde et al., 1991, 1994; Jackson et al., 1987; Kisters et al., 2003, 2010; Moyen et al., 2006, 2007; Stevens & Moyen, 2007; Diener et al., 2005; Schoene et al., 2009; Schoene & Bowring, 2010) and a pre-plate-tectonics "camp" (Ramsay, 1963; Roering, 1965; Anhaeusser, 1981, 2001, 2014; van Kranendonk et al., 2009, 2014; van Kranendonk, 2011) while a minority of publications does not draw a final conclusion about the tectonic

mechanisms operating during the Archean (e.g Lowe, 1994, Lowe et al., 1999; Lowe & Byerly, 2007; Byerly et al., 2018).

An agreement is impeded by numerous controversies over the interpretation of structures (e.g., recumbent folds), contacts (stratigraphic or structural) and rock types (Kromberg Formation "zebra rocks"; origin of cherts). Additionally, although most publications focus on only a small part of the BGB, many tend to deduce implications for the entire BGB, for all greenstone belts, or even for terrestrial tectonics.

We here provide a BGB-wide synthesis of available data to view synoptically BGB tectonics. We also critically review tectonic models and compare them to data we collected. Of course, the level of detail provided in this study cannot reach that of more specialized investigations from parts of the greenstone belt; generalizations and simplifications are unavoidable.

5.2 Geological framework

The Barberton Greenstone Belt (BGB) forms, together with adjacent plutons and gneisses, the Barberton Granitoid-Greenstone Terrane (BGGT). Most rocks of the BGGT have experienced regional metamorphism ranging from lower-greenschist facies to amphibolite facies. Foliation in fine-grained rocks and gneissic fabrics in plutonic rocks are widespread. Strictly speaking, these are metamorphic rocks. However, they are, for historical reasons and for clarity, commonly described using the terminology of their protoliths. An exception is made for the Ancient Gneiss Complex (AGC), which represents a complex assemblage of various gneisses, intercalated greenstone remnants and intrusive bodies (Kröner et al., 2019).

The plutons surrounding the BGB are mainly composed of tonalites, throndhjemites and granodiorites (TTG) and were emplaced in three generations: at c. 3.61 Ga (TTG1), at c. 3.45 (TTG2) and between 3.28 and 3.25 Ga (TTG3) (Moyen et al., 2018). Along most or all of its southeastern margin, the BGB was likely originally bordered by the AGC. Of it, only small remnants remain in contact to the BGB because of the subsequent intrusion by the Piggs Peak and Mpuluzi batholiths have covered or intruded the original contact relationships (Lana et al., 2010, 2011; Murphy, 2015). The AGC consists of a variety of gneisses up to 3.644 Ga in age (Kröner et al., 1988, 1989; van Schijndel et al., 2017). Several younger plutons of granitoid composition, truncating deformed greenstone belt strata, were emplaced around the BGB and postdate clearly the deformation of the greenstone belt (Heubeck et al., 1993; Kisters & Anhaeusser, 1995)

Strata of the greenstone belt represent a volcano-sedimentary supracrustal sequence and are subdivided into three major stratigraphic groups, including (from oldest to youngest) the Onverwacht, Fig Tree and Moodies Groups with a total stratigraphic thickness of up to about 15 km. The Onverwacht Group ranges from 3.57 to 3.26 Ga in age and consists of mafic and ultramafic volcanic rocks with minor chert, deposited mainly in subaqueous environments (Byerly et al., 2018). The overlying Fig Tree Group ranges in age between 3.26 and 3.225 Ga and comprises mostly volcanoclastic and minor chemical sediments deposited in shallow- to deep-marine settings (Lowe & Byerly, 1999). The Moodies Group ranges between 3.224 and 3.216 Ga in age and consists mainly of quartz-rich sandstones and subordinate conglomerates, siltstones, jaspilites and volcanic rocks (Heubeck, 2019).

The c. 350 Ma-long history of the BGB includes a number of deformation phases to which various authors have applied different nomenclature and interpretations. In the following, we will use the classification of deformation events (D1 to D5) of Byerly et al. (2018).

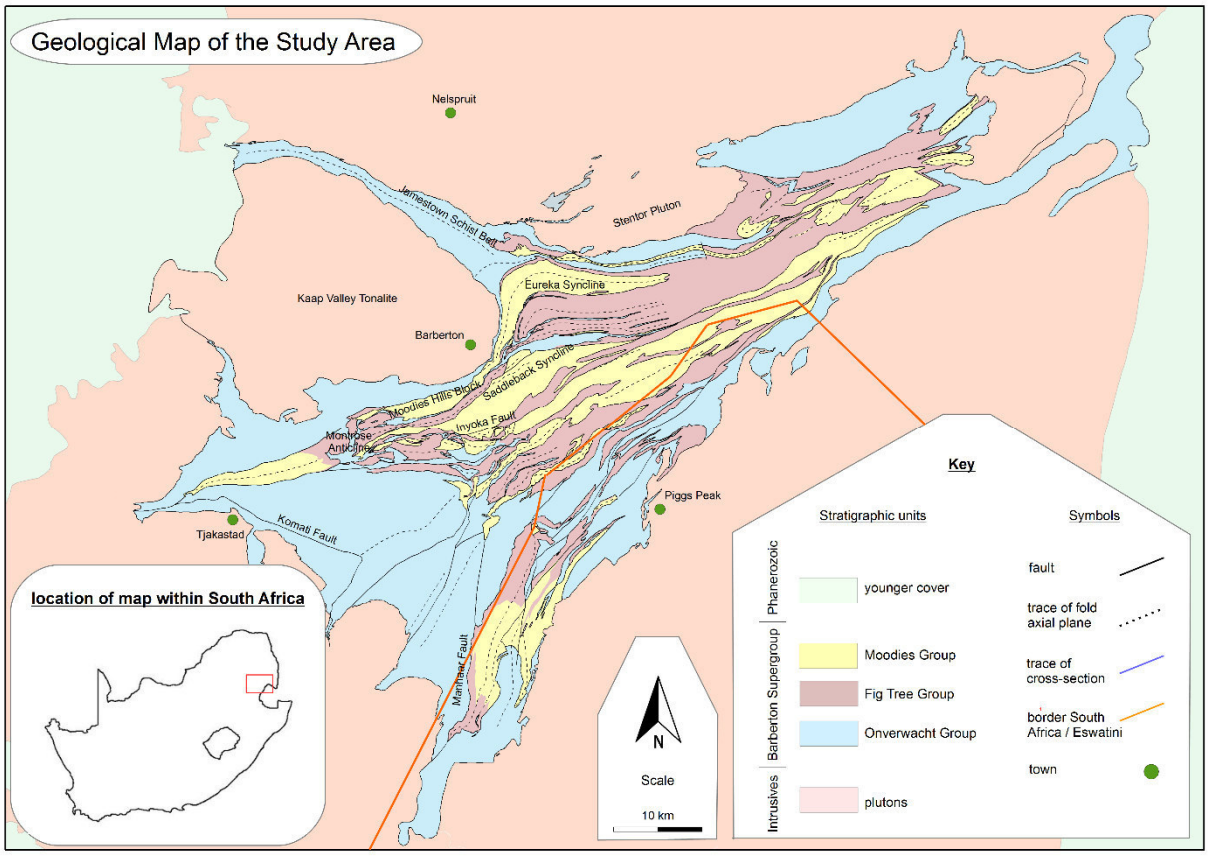

Fig. 5.1: Overview map of the BGGT.

Although some authors suggested an even earlier deformational event (D0 of de Ronde & de Wit 1994), D1 represents the earliest deformational event recorded regionally in the BGB, coinciding with felsic magmatic activity around 3445 Ma (Lowe and Byerly, 2007) and local uplift and erosion (Noisy Formation of Grosch et al., 2011). At c. 3300 Ma, a period of rifting commenced (no phase name assigned), which accommodated the units of the lower Fig Tree Group. This was followed by D2, the first deformational event recorded across the entire greenstone belt. It deformed, uplifted and eroded Onverwacht and lower Fig Tree Group strata (Mapepe Formation south of the Inyoka Fault; Belvue Road, Sheba and Ulundi formations north of it). D3 represents the creation of syndepositional accommodation space for Moodies Group strata in extensional basins while D4 deformed these and underlying units during late syn- and early post-Moodies Group time (Byerly et al., 2018; Heubeck, 2019). These structures were subsequently modified by a later deformational event (D5) which is poorly constrained in time (Lowe et al., 1999).

The entire greenstone belt was subjected to greenschist-grade metamorphism (Xie et al., 1997; Toulkeridis et al., 1998). However, primary sedimentary and volcanic structures are widely well preserved because of early silicification. Recrystallisation of the original matrix and cement is a common feature in sedimentary rocks while igneous rocks of mafic composition have been altered to serpentinite or talcose schists (Byerly et al., 2018).

5.3 Suggested tectonic models

A large number of studies on the tectonic evolution of the BGB exist. This is due to its considerable size which allows regional correlation, its unusual geometry and deformation patterns, the exceptional preservation of its rock types and good exposure. Studies were also driven by the need to understand the structurally controlled gold deposits (Anhaeusser, 1969; Otto et al., 2007; Dirks et al., 2013). Most publications can be assigned to one of the following groups:

(1) Early studies showed already that the deformation pattern of the BGB differed significantly from that of Proterozoic and Phanerozoic orogens. Anhaeusser (1976) emphasized the overall synclinal structure (Fig. 5.2a) of the BGB and argued that the distribution of strain markers, the refolding of primary structures around plutons, the disharmonic internal folding and the radial tension fractures indicated that deformation of the greenstone belt was mainly driven by ''gravitational collapse''. The steep inclination of strata and the juxtaposition of high-grade metamorphosed plutons to lower-greenschist facies supracrustal BGB rocks led other authors to conclude that the BGB was not deformed by simple horizontal shortening. Early studies concluded that uniformitarian approaches had to be used with great caution (Ramsey, 1963; Roering, 1965).
The gravitational collapse model invoked sagging of dense greenstone belt strata and the contemporaneous diapiric rise of the adjacent TTG plutons. It implies mainly vertical displacement, decoupled deformation of the greenstone belt from that of the surrounding plutons, and predicts a large vertical extent and a general synclinal structure of the greenstone belt.

(2) Another group of researchers envisioned the BGB as a plate tectonic assemblage of terranes which accreted during the formation and subsequent deformation of the greenstone belt along major fault zones (Fig. 5.2b), based mainly on geochemical proxies and field relationships (de Wit, 1982, 1991; de Ronde et al., 1991, 1994; de Wit & Hart, 1993; de Ronde & de Wit, 1994; Grosch et al., 2009, 2011, 2012; de Wit et al., 2017). Schoene & Bowring (2010) suggested doubly-verging subduction zones being responsible for the accretion and amalgamation of the different terranes.
This model involves many features indicative of plate tectonics, such as ophiolites, trenches, accretionary prisms, magmatic arcs, fore- and backarc basins. It postulates the identifiable presence of terranes, numerous sutures, subduction zones and the presence of tectonic index minerals, significant horizontal displacements, and a low vertical extent of the greenstone belt.

(3) Other researchers also have suggested plate-tectonic settings of the BGB mainly based on the reconstruction of paleoenvironments from sedimentary rocks of the Fig Tree and Moodies groups (Fig. 5.2c). Eriksson, in part with co-authors, proposed a number of different settings, including continental margin (1980), continental rift (1982), or foreland basin (Jackson et al. 1987).
Each of these models carry their own tectonic and sedimentary implications, such as unidirectional thrusting and the exhumation of older strata with time, the formation and sediment fill of a forebulge as the result of lithospheric flexure for a foreland basin, or large-scale listric normal faults and unidirectional sediment transport for a passive continental margin, respectively. They all predict a low vertical extent of the BGB.

(4) Some of the most comprehensive and detailed studies on the BGB (Lowe et al. 1985, 1999, 2014; Kröner et al., 1991, 1996; Lowe & Byerly, 1999, 2007; Heubeck & Lowe, 1994a; Heubeck et al., 2013, 2016; Byerly et al., 2018) did not clearly favor either dynamic model. These authors only occasionally use models and terminology associated with plate tectonics (e. g. Heubeck & Lowe, 1994a; Lowe et al., 1999) and terrane tectonics (Lowe, 1994). Some publications from this group interpret the BGB as a fold-and-thrust belt above a shallow detachment (Heubeck & Lowe, 1994), based on field geologic mapping, analysis of fold geometry, and interpretation of low-resolution geophysical data (de Beer & Stettler, 1988). These models predict unidirectional thrusting, major horizontal shortening and a low vertical extent of the greenstone belt (Fig. 5.2d).

(5) Another group favoring plate tectonic mechanisms for the formation and subsequent deformation of the BGB applied petrogenetic approaches and largely documented findings from the southwestern part of the greenstone belt (Moyen et al. 2006, 2007, 2018; Kisters et al. 2003, 2010; Diener et al., 2005; Stevens & Moyen, 2007; Lana et al., 2010, 2011). They suggest that subduction occurred along the Inyoni Shear Zone, followed by orogenic collapse and exhumation of high-grade metamorphic terranes as a core complex (Fig. 5.2e).
This model implies the presence of a subduction zone and associated mineral assemblages, the exhumation of high-grade metamorphic terranes along very shallow normal faults, major horizontal shortening and a low vertical extent of the greenstone belt.

(6) Transferring his concepts and findings from the Pilbara region of northwestern Australia (Collins et al., 1998; van Kranendonk & Collins, 1998; van Kranendonk et al., 2002, 2004, 2007), van Kranendonk (2011) suggested a pre-plate tectonic setting (Fig. 5.2e) for the tectonic evolution of the BGB, mainly based on field relationships and reinterpretation of p-T paths. This partial convective overturn (PCO) model emphasizes vertical displacement and employs density-driven inversion of thick, cold and dense (komatiitic) lavas composing the bulk of the greenstone belt above hot, less dense and intermediate to felsic magmas in the middle crust, resulting in periodic overturns of the lithosphere back to the mantle (van Kranendonk et al., 2009, 2014; Kröner et al., 2016; Hoffmann & Kröner, 2018).

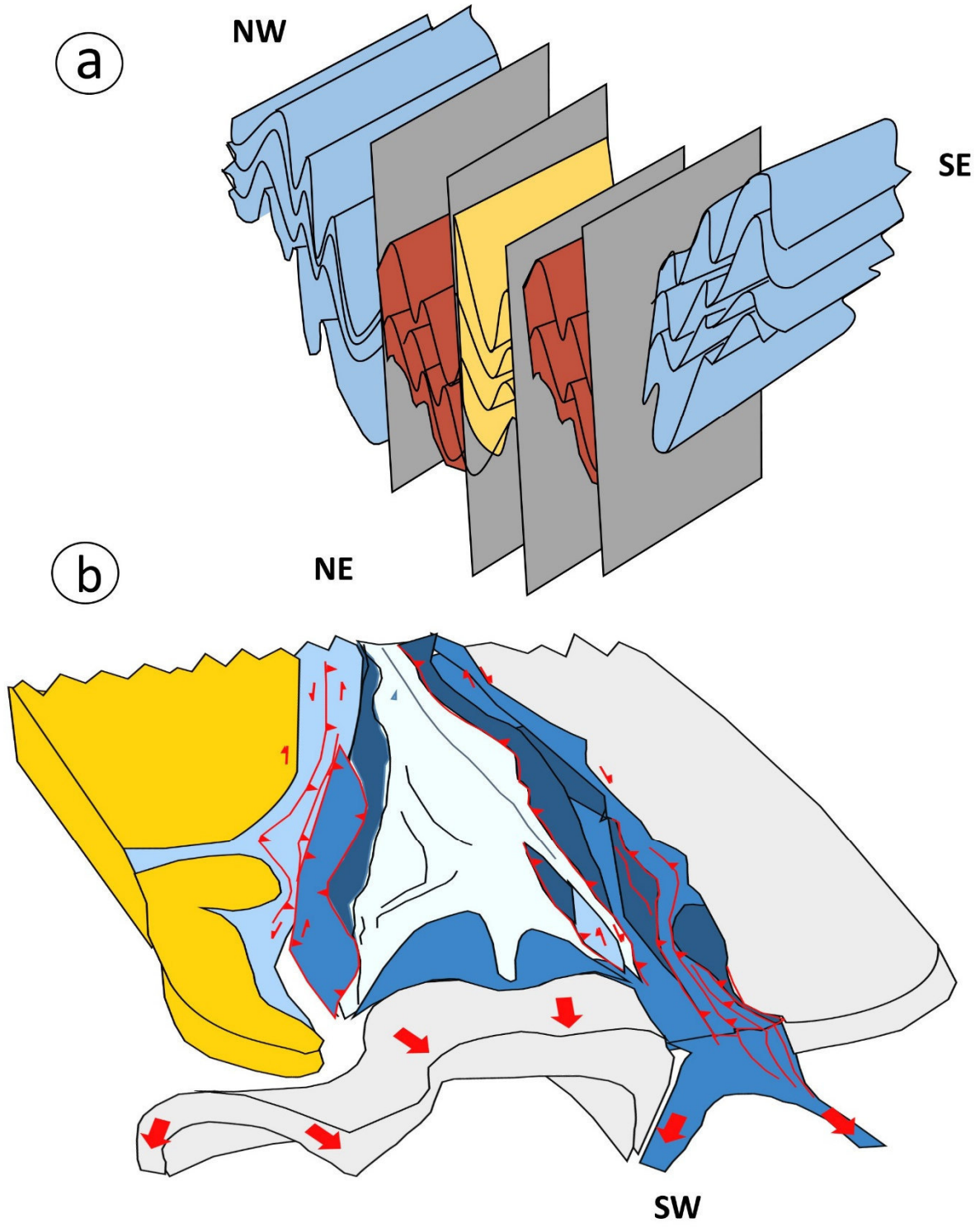
a
NW
SE
b
NE
SW

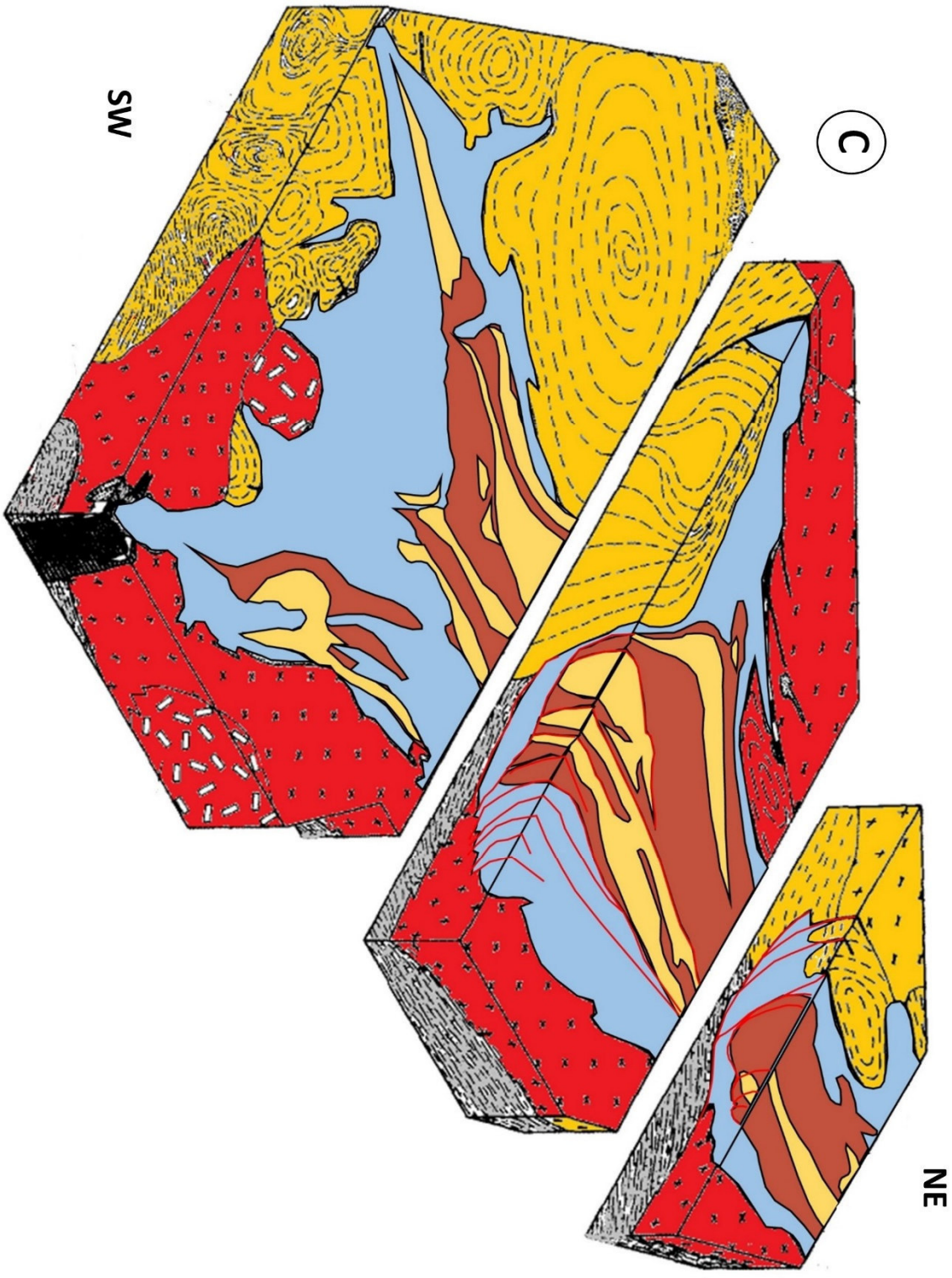
SW
C
NE

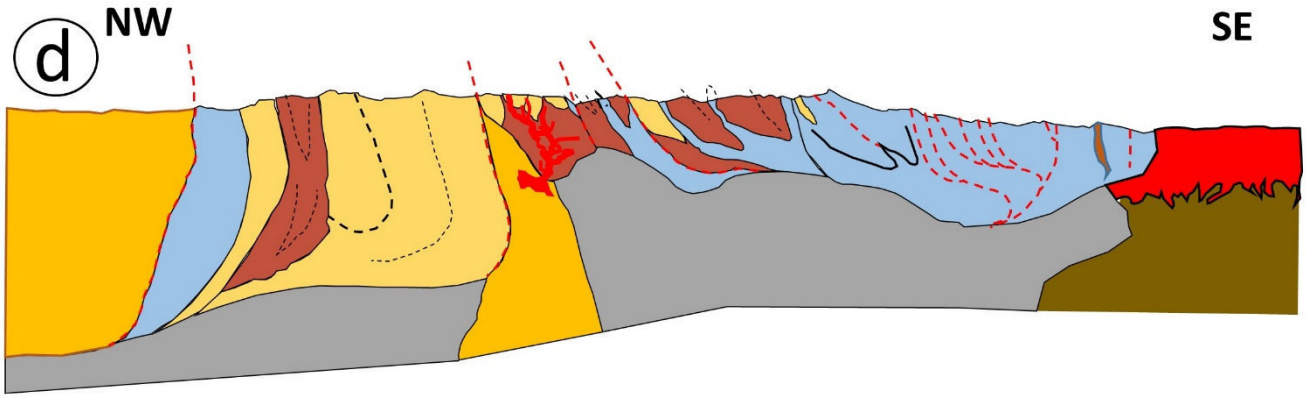
d
NW
SE

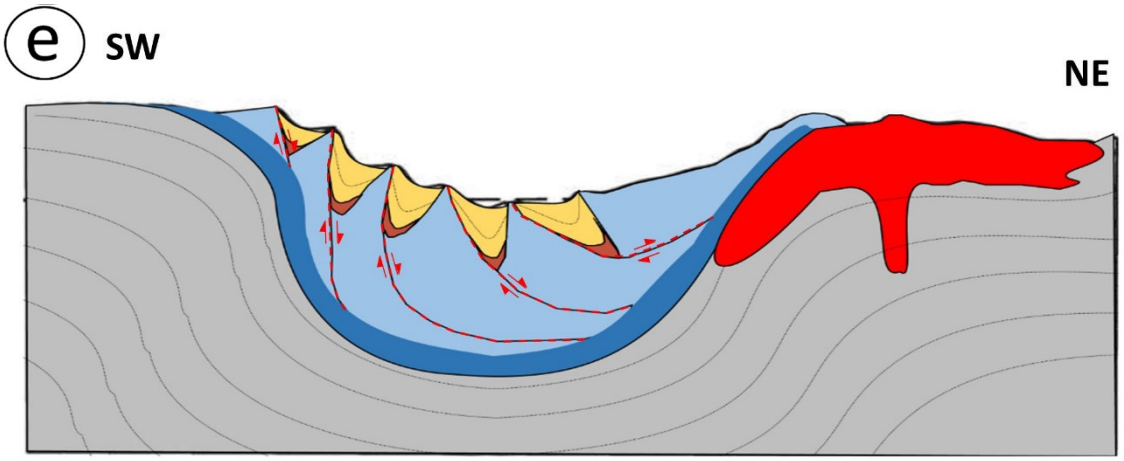
e
SW
NE

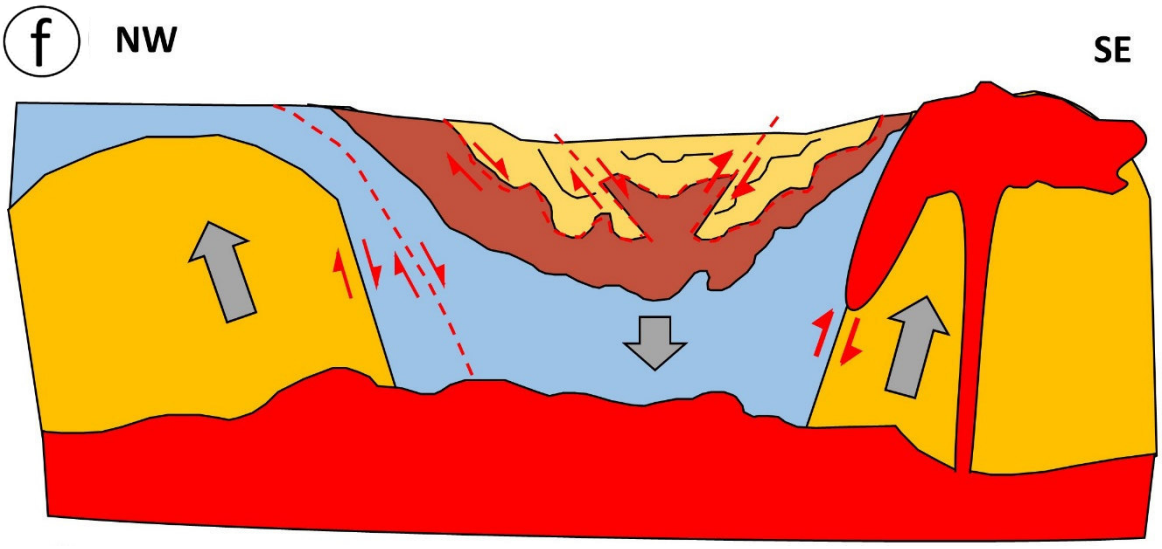
f
NW
SE

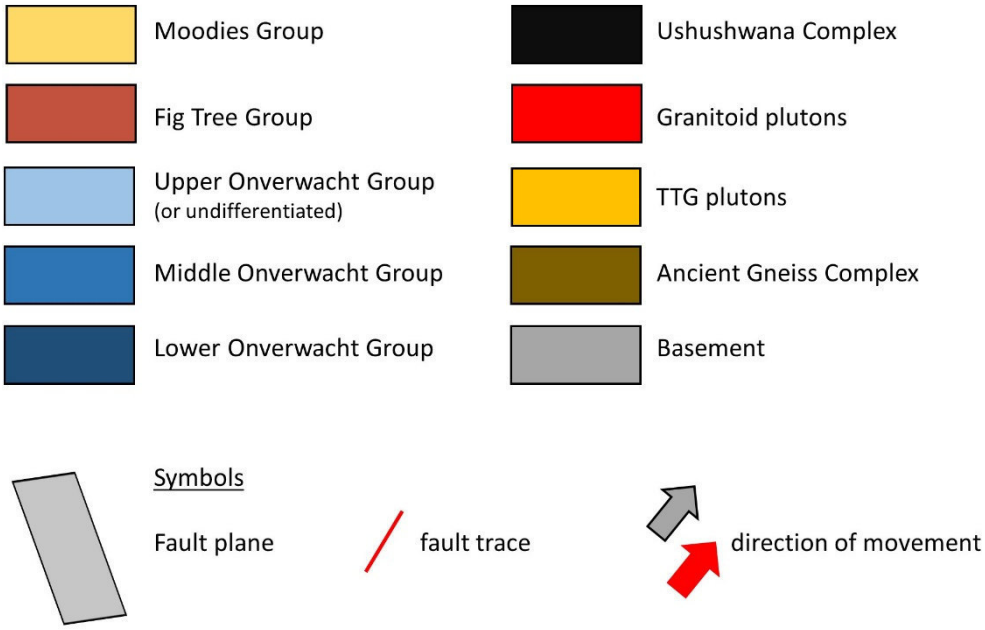

Fig. 5.2: Sketches of suggested tectonic model and implied geometries. (a) Gravitational collapse model by Anhaeusser (1975): This model emphazises the general synclinal geometry of the BGB with the oldest units (Onverwacht Group) close to the margins and the youngest units (Moodies Group) in the core. Faulting takes place mainly at or parallel to the fold axial planes of collapsed anticlines. (b) Terrane-accretion model by de Wit et al. (2018): Different terranes accreted at doubly-verging subduction zones, which also caused the emplacement of syn- and post-deformational plutons. (c) Foreland basin model by Jackson et al. (1987): This model envisions the sedimentary units of the BGB (Fig Tree and Moodies groups) as deposits of a foreland basin resulting from crustal shortening. Orientation of fault planes implies tectonic transport mainly to the northwest in this model. (d) Fold-and-thrust-belt model by Heubeck & Lowe (1994a): Similar to (c), the central BGB represent a fold-and-thrust-belt above a shallow detachment in accordance with geophysical data. (e) Core complex model by Kisters et al. (2003): In this model, the BGB represents a collapsed orogeny after initial accretion. Large-scale extensional fault separate single blocks of Onverwacht Group strata and create accommodation space for the deposition of the younger sedimentary units. (f) Partial convective overturn model by van Kranendonk (2011): Movement in this model is mainly vertical due to density-driven sagging of greenstones and diapiric rise of hot and buoyant felsic crust. The sedimentary units of the BGB are interpreted as the fill of the resulting subsiding basin.

The PCO model predicts sagging of greenstone belt strata contemporaneous with diapiric rise of adjacent plutons, radial orientation of fold axial plunges and mineral elongation lineations towards a central ''zone of sinking'', dominantly vertical movements, subordinate horizontal displacements and a large vertical extent of the greenstone belt. This model also includes periods of extension during the initial stage of the overturn, followed by a period of compression, as the greenstones converge above the zone of sinking (van Kranendonk, 2011).

5.4 Methods

We digitized geological information from the maps of Anhaeusser (1969, 1976, 1981), Anhaeusser & Robb (1990), Belcher & Kisters (2003), Bennett et al. (1971), Byerly et al. (2018), de Ronde & Kamo (2000), de Wit et al. (1987, 2011), Diener et al. (2005), Dziggel et al. (2002, 2010), Furnes et al. (2010), Heubeck et al. (1993, 2016), Heubeck & Lowe (1994), Hunter et al. (1969), Kisters et al. (2003, 2010), Kohler (2003), Kröner et al. (1996, 2009), Lana et al. (2010, 2011), Lamb (1984), Lowe et al. (1999), Lowe & Byerly (1999, 2007), Lowe et al. (1999, 2012), Moyen et al. (2006, unpublished data), Ramsey (1963), Robb et al. (1986), Roering (1965), Urie et al. 1970), van Kranendonk et al. (2009, 2014), Visser et al. (1956), Ward (2000), Wiestraat et al. (2005) and merged them into a single, detailed map of the BGB. Because many authors used different stratigraphic units, we simplified and harmonized units (Table 5.1), adapting them to the stratigraphic units by Lowe & Byerly (1999), Lowe et al. (2012) and Byerly et al. (2018).

We conducted additional mapping in order to validate the quality of the maps and lithological units, to fill gaps and to add information to existing maps (e.g. plunge of fold axes, orientation of fold axial planes, orientation of cleavage planes). A major product of this study is the creation of a new map (Appendix), showing the entire BGGT in both countries, in color and much greater detail than all prior maps of the same scale. Map quality strongly varies with the availability and precision of data. Additional geologic mapping is necessary to improve and standardize the quality of this map.

Strain indicators: We compiled ratios of axes-length of deformed conglomerate clasts throughout the greenstone belt, using both our own measurements (Chapter 4) and data of Gay (1969), Reimer (1967), Anhaeusser (1969, 1976), Lamb (1984), Daneel (1987) and Heubeck & Lowe (1994). The original clast shape was assumed to be 1.26 / 1 / 0.8, following the argumentation of Heubeck & Lowe (1994) (Appenidx VI).

5.5 Results

5.5.1. Major lithostratigraphic units

We subdivided the greenstone belt strata and surrounding plutonic bodies into a total of 55 units (Table 5.1).

5.5.2 Major folds

A total of 38 major folds were identified in the BGB. Table 5.2 lists their geometry, stratigraphic units and stereographic orientation (Fig. 5.3). In the following, the major, SW-NE striking folds are referred to as F1 folds. The axes, at which the fold axial plunge of F1 folds changes (culminations or depressions of F1 folds), are termed F2 folds. They are generally oriented perpendicular to F1 fold axes. Younger folds, which refold F1 folds around a vertical axis, are termed F3 folds. Although F3 represents a younger deformation superimposed on F1 and F2 folds, F1, 2 and 3 do not imply a strict chronological sequence because F1 and F2 may have occurred simultaneously and do not correspond to deformational events D1, 2 and 3. Because F1 folds are defined by all stratigraphic units of the BGB, they must postdate all sedimentation and likely correspond to D4 (see section 5.7.1).

Map units			
Group	**Formation**	**Abbreviation**	**Description**
Younger Units		ph	Phanerozoic cover
Moodies Group	(undifferentiated)	M_fg	Fine-grained sediment
		M_j	Jaspilite
		M_s	Quartz-rich sandstone
		M_q	Quartzite
		M_cg	Conglomerate
		M_b	Basalt
Fig Tree Group	**Schoongezicht Formation**	FSc_gw	Greywacke
(North of Inyoka Fault)		FSc_cg	Conglomerate
		FSc_fg	Fine-grained sediment
	Belvue Road Formation	FB_gw	Greywacke
	Sheba Formation	FSh_c	Chert
		FSh_gw	Greywacke
	Ulundi Formation	FU_c	Chert
		FU_fg	Fine-grained sediment
		FU_cg	Conglomerate
		FU_gw	Greywacke
Onverwacht Group	**Weldevreden Formation**	OW_am	Amphibolite
(North of Inyoka Fault)		OW_vc	Volcanoclastic rocks
		OW_do	Dolomite
		OW_c	Chert and silicified ash
		OW_uc	Ultramafic complex
		OW_um	Mafic and ultramafic volcanic rocks
Fig Tree Group	**Auber Villiers Formation**	FA_ts	Tuffaceous sandstone
(South of Inyoka Fault)		FA_d	Dacite
	Mapepe Formation	FM_fg	Fine-grained sediments
		FM_j	Jaspilites and banded iron formation (BIF)
		FM_cg	Pebble to cobble conglomerate with chert clasts
		FM_gw	Dacitic, tuffaceous greywackes and lithic sandstones
Onverwacht Group	**Mendon Formation**	OM_tc	Talcose schists
(South of Inyoka Fault)		OM_ph	Phylite
		OM_se	Sericite
		OM_c	Chert and silicified ash
		OM_um	Mafic and ultramafic volcanic rocks
	Kromberg Formation	OKr_c	Chert and silicified ash
		OKr_pc	Pyrocalstic rocks, tuffs and lapillistones
		OKr_um	Mafic and ultramafic volcanic rocks
	Hoogenoeg Formation	OH_s	Dacitic sandstone with local fine-grained cherty ash layers
		OH_cg	Dacite-clast conglomerates and breccias
		OH_um	Basalts, Pillowbasalts and komatiites
		OH_d	Intrusive and extrusive igneous rocks of dacitic composition
		OH_r	Peridotites and pyroxenites of the Rosentuin Ultramafic Complex
	Komati Formation	OKo_um	Mafic and ultramafic volcanic rocks
		OKo_tc	Talcose schists
		OKo_c	Chert and silicified ash
	Theespruit Formation	OT_um	Mafic and ultramafic volcanic rocks
	Sandspruit Formation	OS_um	Mafic and ultramafic volcanic rocks
Intrusive units	**Intra-greenstone belt intrusives**	dol	doleritic dyke
		fel	felsic intrusive
		lri	Lomati River Intrusive
		per	Peridotite
		mig	Stockwerk of subvolcanic mafic dikes and sills
	Greenstone belt-external intrusives	GMS	Granitoid plutons
		TTG	TTG plutons
		AGC	Remnants of the Ancient Gneiss Complex

Table 5.1: Map units of the study area.

Overview of selected representive fold structures of the Barberton Greenstone Belt

Name	Lithology	Domain	Boundaries	Overturned	Fold axis	Reference	Data	Comment
Amo Syncline	Moodies Group (mostly quartzites and conglomerates)	E	N: Mac Mac Fault, E: Amo Fault, S: Barbrook Fault, W: Shale and Metagreywackes of the Sheba Fm (unknown syncline)	no	plunges towards NE (60° - 73°)	most comprehensive work: Kohler 2003	dip data by Kohler 2003 and the author	
Angle Station Syncline	Moodies Group (mostly sandstones and quartzites)	C	NW: Heemstede Syncline (seperated bay unnamed fault), E: Makonjwa Block (seperated bay unnamed fault), S: Minor folds consisting of FT and Onv rocks, W: Maid of th Mists Syncline	to the northwest	°plunges towards NE (35 -50°)	best mapped by Lowe et al. 2012	dip data by the authors	Named after a cableway station
Big Buffalo Syncline	Moodies Group (mostly quartzites and conglomerates)	E	N: Adonachi Fault, E: truncated by Salisbury Kop Pluton, S: Barbrook Fault, W: Amo Fault	to the northwest	plunges towards NE (40° - 75°, steeper plunges in the W)	most comprehensive work: Kohler 2003	dip data by Kohler 2003 and the author	Dominant feature of the NE part of the BGB
Brommers Syncline	Fig Tree Group (Sheba Fm Greywackes and Ulundi Fm shales)	N	N: Moodies Hills Block (seperated by Sheba Fault), E: Dycedale Syncline (seperated by Barbrook Fault), S: Saddleback Syncline (seperated by Saddleback Fault), W: Montrose Anticlinorium	to the northwest	plunges SW (60°), plunges NE at ist western end (40° - 50°)		dip data by the author	Many parasitic folds and wavy bedding
Duurstede Syncline	Moodies Group	C	S: Vooruitzicht Anticline, N: Duurstede Anticline	no	plunges towards NE (46°)			little litholigal variability and internal structures
Duurstede Anticline	Moodies Group	C	S: Duursetde Syncline, N. Makhonjwa Block	no	plunges towards NE (42°)			little litholigal variability and internal structures
Devils Bridge Syncline	Moodies Group	C	N: Paulus Syncline, E: Fig Tree Group rocks, S: Border Post Syncline, seperated by Songimvelo Fault, W: Steynsdorp Anticline, separated by Manhaar Fault	to the northwest	plunges towards NE (30° - 40°)	Best described in Heubeck & Lowe 1994	data by Heubeck & Lowe 1994 and the authors	
Dycedale Syncline	Moodies Group	N	N: Onverwacht rocks (Weldevreden Fm, seperated by Barbrook Fault), S: Saddleback Syncline (seperated by Saddleback Fault), W: Brommers Syncline (Seperated by Barbrook Fault)	to the northwest	plunges towards SW (50° - 65°)	best described in Heubeck et al. 2016	dip data by the authors	

Eureka Syncline	Moodies Group (mainly sandstones and conglomerates)	N	N: Jamestown Schist Belt (Seperated by Lily Fault), E: Undifferentiated rocks of FT, S: Ulundi Synclne (seperated by Sheba Fault) W: continues along a thin (100 m wide) compressed belt into Moodies Hills Block)	to the northwest	plunges in the eastern part to the W and in the western part to the S (45° - 60°)	Best described in Anhaeusser 1974	dip data by Anhäusser 1974, Ramsey 1963 and the author	Refolded fold axis, hosts major hydrothermal gold deposits, dominant feature of the northwestern part of the BGB
Forbes Reef Anticline	Moodies and Fig Tree Group, subordinate Onverwacht Group strata	S	N: Ntaba Mhlope Syncline, E: Piggs Peak Batholith, S: Motjane Schist Belt, W: Malolotsha Syncline	to the east	plunges towards S (25° -30°)		data by Lamb (1984) and the authors	contact metamrophic overprint due to emplacement of adjaden Piggs Peak Batholith
Heemstede Syncline	Moodies Group	C	N: Saddleback Syncline (seperated by Inyoka Fault), E: Angle Station Syncline (seperated by unnamed fault), SW: Maid of the Mists Syncline	to the northwest	plunges towards WSW in the western part (30° - 40°) and ENE in the eastern part	mapped by Lowe et al. 2012	dip data by the author	Seemingly arcuate fold axis in map view is effect of topography
Himbanyathi Syncline	Moodies Group (Mainly quartzites and conglomerates with minor shales)	NE	N: Barbrook Fault, S: Inyoka Fault	in places overturned to the northwest	plunges ENE (10° - 20°) west of Amo Fault and SW (30°) east of Amo Fault	most comprehensive work: Kohler 2003	dip data by Kohler 2003 and the author	
Igwalagwala Syncline	Moodies Group	E	surrounded by undiff. Fig Tree Group strata	no	plunges slightly to the NE (5°)	most comprehensive work: Kohler 2003	dip data by Kohler 2003 and the author	Probably Continuation of the Amo Syncline
Jamestown Schist Belt	Onverwacht Group (Mainly mafic and ultramafic schists)	N	NE: Nelspruit Nuite, SE: Stentor Pluton, S: Eureka Syncline (seperated by Lily Fault), W. Kaap Valley Pluton	no	plunges towards SE (10° - 20°)	most comprehensive work: Anhaeusser 1971	dip data by Anhaeusser 1971	Synclinal Structure

Kromberg Syncline	Onverwacht Group (Mainly mafic and ultramafic volcanics	W	N: Kromberg Fault Zone, E: Stenysdorp Anticline (seperated by Kromberg Fault), S. Dalmein Pluton, W: Onverwacht Anticline	fold axis overturned (plunge > 90°)	plunges towards SW 60° - 85°)	well described by Vennemann & Smith 1999, De Wit et al. 2011	dip data by Vennemann & Smith 1999, De Wit et al. 2011, Lowe et al. 2012	synformal anticline, type section of the Kromberg Fm (Onverwacht Group)
Lily Syncline	Moodies Group (Mainly quartzites and conglomerates) west of the Louieville Fault and Fig Tree Group (shales and Metagreywackes) east of it	N	N: Scotsman Fault, S: Lily Fault (western part), Southern Fault (eastern part)	to the northwest	plunges towards E (30° - 40°)	well described by Anhaeusser 1969 (western part) and Kohler 2003 (eastern part)	dip data by Anhaeusser 1969 and Kohler 2003	
Maid of the Mists Syncline	Moodes Group	W	N: Heemstede Syncline, E: Angle Station Syncline, S: Unnamed fold consisting of FT and Onv rocks, W: Powerline Road Syncline	to the northwest	inward plunging	no detailed description so far, best mapped by Lowe et al. 2012	dip data by Lowe et al. 2012 and the author	named after the highest mountain of the BGB
Makonjwa Block	Moodies Group	C	N: Saddleback Syncline (Seperated by Inyoka Fault, E: Vorrutzicht Syncline, S: Unnamed Fold consisting of Fig Tree rocks (Mapepe Fm and minor Auber Villiers Fm)	to the northwest	plunges towards NE	no detailed description so far, very poorly understood,	dip data by the author and Visser 1956	
Malolotsha Syncline	Moodies Group (mainly quartzarenites and conglomerates) and Onverwacht Group (talcous schists)	S	N: Undifferentiated Onverwacht Group rocks, E: Piggs Peak Batholith, S: Undifferentiated Onverwacht Group rocks, W: Ngwenya Syncline	no	plunges towards SSW (30°)	best described by Lamb 1984	dip data by Lamb 1984 and the author	unclear relationship between Moodies and Onverwacht Group in the center of the syncline

Manzimnyama Syncline	Fig Tree Group (litharenites and finegrained sediments of the Mapepe Fm)	C	NW: The Heights Syncline, E: unnamed fold consisting of Onv. And FT group rocks, S: Schoonoord Anticline	to the northwest	plunges towards NE (50° - 60°)	best mapped by Heinrichs & Reimer 1977	dip data by Lowe et al. 2012 And the author	
Montrose Anticlinorium	Onverwacht and Fig Tree groups rocks	N	N: Many small-scale folds consisting of FT (Sheba and Ulundi Fm) and Onv. (Weldevreden Fm), E: Brommers Syncline, S: Granville Grove Fault, W: Stolzburg Syncline	no	plunges steeply outwards	best mapped by De Ronde & Kamo 2000 and Lowe et al. 2012	data from De Ronde & Kamo 2000 and Lowe et al. 2012	no longer mappable due to pine and eucalyptus plantations
Moodies Hills Block	Moodies Group	N	N: Moodies Fault, E: Euereka Syncline, S: Brommers Syncline (seperated by Sheba Fault), W: Montrose Anticlinorium	?	plunges towards E (50 - 60°)	best mapped by Lowe et al. 2012	data from Lowe et al. 2012 and the author	only northern limb preserved, basically continuation of the Eureka Syncline, but traditionally counted as an own unit
Motjane Schist Belt	Onverwacht Group	S	N: Malolotsha Syncline, E: Piggs Peak Batholith, S + W: Mpuluzi Batholith	no	unknown	best described by Jackson & Robertston 1983	data by Jackson & Robertson (1983) and Bennetton et al. 1971	Synclinal structure
Nelshoogte Schis Belt	Onverwacht Group	N	N + E: Kaap Valley Tonalite, S: Stolzburg Syncline, W: Nelshoogte Pluton	no	inward plunging	best described by Anhaeusser 2001	data by anhaeusser 2001	Synclinal structure
Ngwenya Syncline	Moodies and Fig Tree groups	S	N: Undifferentiated Onverwacht Group rocks, E: Ngwenya Anticline, S: Motjane Schist Belt , W: Steynsdorp Anticline, separated by Manhaar Fault	to the west	northern part plunges SSW (30°), southern part plunges NNE (60° - 70°)	well described by Lamb 1984	data from Lamb 1984 and the author	hosts major ironoxide deposits
Ngwenya Anticline	Moodies and Fig Tree groups	S	N + E Malolotsha Syncline, S: Motjane Schist Belt, W: Ngwenya Syncline	to the west	plunges towards NNE (60°-70°)		well described by Lamb 1984	data from Lamb 1984 and the author
Ntaba Mhlope Syncline	Moodies and Fig Tree groups	S	surrounded by undiff. Onverwacht Group strata	to the northwest	doubly inwardly plunging		data from the authors	

Onverwacht Anticline	Onverwacht Group	W	N: central region (seperated by Granville Grove Fault), NE: The Heights Syncline (seperated by Inyoka Fault), E: Kromberg Syncline, S: Theespruit Pluton, NW: Stolzburg Syncline (seperated by Inyoka Fault)	no	plunges very steeply towards NE (80° - 90°)	Described in many studies, starting with Viljoen & Viljoen 1969, most comprehensive one by Lowe et al 1999 and Lowe 1994	data from Lowe et al. 2012	Dominant feature of the SW part of the BGB, contains the type section of most Onverwacht formations and c. 10 km stratigraphic thickness in total
Paulus Syncline	Fig Tree Group (Mapepe Fm)	C	NW: Schoonoord Anticline, SE: Devils Bridge Syncline (minor syncline defined by Moodies Group rocks)	to the northwest	plunges towards E east of the R 40 and west of it towards W	mapped by Heubeck & Lowe 1994	data from Heubeck & Lowe 1994, Lowe et al. 2012 and the author	
Powerline Road Syncline	Moodies Group	W	N: Minor fold defined by Onv. rocks (Weldevreden Fm), E: Maid of the Mists Syncline, SW: Minor Folds of FT rocks (Auber Villiers Fm), bounded to the N, E and S by the 24-Hour-Camp Fault	no	plunges moderatly towards the centre of the elliptical syncline	mapped by Lowe et al. 2012		
Saddleback Syncline	Moodies Group	N	N: Brommers and Dycedale synclines (seperated by Saddleback Fault), E: Undifferentiated rocks of FT, S: Heemstede Syncline (seperated by Inyoka Fault)	to the northwest	plunges SW (40 - 60°)	Described in many studies (e.g. Heubeck & Lowe 1994a, b, 1999, Heubeck 2016, Nabhan et al. 2016)	data from Heubeck & Lowe 1994, Lowe et al. 2012 and the author	Dominant feature of the western part of the BGB
Schoonoord Anticline	Onverwacht Group (Mendon Fm)	C	NW: Manzimnyama Syncline, SE Paulus Syncline	to the southeast	plunges towards NE	mentioned by Heinrichs & Reimer 1977 but no well described yet	date from Heubeck / Lowe 1994, Lowe et al. 2012 and the author	

Steynsdorp Anticline	Onverwacht Group (Hooggenoeg, Kromberg and Mendon formations)	W	N: The Heights, Manzimnyama and Paulus synclines, E: Ngwenya Syncline, S: Steynsdorp Pluton, W: Kromberg Syncline (Seperated by Kromberg Fault)	no	plunges steeply towards NE	well described by Lana et al. 2010	data from Lana et al. 2010 and Lowe et al. 2012
Stolzburg Schist Belt	Onverwacht Group	N	N: Nelshoogte Pluton, E: Stolzburg Syncline, S: Stolzburg Pluton, W: Badplaas Pluton				Synclinal structure
Stolzburg Syncline	Moodies Group (mainly quartzarenites and conglomerates and Fig Tree Group (Schoongezicht Fm)	N	N: Nelshoogte Schist Belt (seperated by Moodies Fault), E: Montrose Anticlinorium, S: Onverwacht Anticline (seperated by Inyoka Fault), W: Stolzburg Schist Belt	no	plunges towards W (50° - 60°)	original mapping by Reimer 1969	data from Lowe et al. 2012 and the author	Type section of the Schoongezicht Fm (Fig Tree Group)
Strathmore Anticline	Onverwacht Group	E	surrounded by Fig Tree Group strata	no	unknown	well described by Kohler 2003	data from Kohler 2003 and the author	
The Heights Syncline	Moodies Group (mostly quartzites and conglomerates)	C	NW: Unnamed fold defined by FT (Mapepe Fm and Minor Auber Villiers Fm), SE: Manzimnyama Syncline, SW: Steynsdorp Anticline	to the northwest	plunges NE (45° - 55°)	western part well mapped by Lowe et al. 2012	date from Lowe et al. 2012, and the author	
Three Sisters Syncline	Moodies Group (quartzarenites and thick conglomerates) and underlying Fig Tree Group (bien Venue and Belvue Road formations)	N	N: Undifferentiated Onverwacht Group rocks, SE: Ardonachi Fault, SW: Revolver Fault	to the northwest	plunges towards E (60°)	well described by Kohler 2003	data from Kohler 2003 and the author	refolded fold axis, dominant feature of the northeastern part of the BGB

Ulundi Syncline	Fig Tree Group	N	N: Eureka Syncline (seperated by Sheba Fault), E: Amo Syncline, S: Barbrook Fault, W: Moodies Hills Block (seperated by Sheba Fault)	to the northwest	plunges towards NNE (10°)in the southwest and towards W (20°) in the east	well described by Ramsey 1963 and the author	data from Ramsey 1963, Anhaeusser 1974 and the author	type section of the Ulundi Fm (Fig Tree Group)
Vooruitzicht Syncline	Moodies Group	C	N: Vooruitzicht Anticline, E. unknown, S: Fig Tree Group strata, seperated by the Songimvelo Fault, W: Makhonjwa Block	no	plunges towards NE (48°)	data from the authors		
Vooruitzicht Anticline	Moodies Group	C	N: Duurstede Syncline, S: Vooruitzicht Syncline	no	plunges towards NE (42° - 45°)	data from the authors		
Woodstock Anticline	Onverwacht Group	N	N: Jamestown Schist Belt, E: Lily Syncline, S: Eureka Syncline, W: Kaap Valley Tonalite	no	unknown	data from Anhaeusser 1969		

Table 5.2: Summary of geometry of the major folds of the BGB. For location of the respective fold, see Fig. 5.5.

Amo Syncline

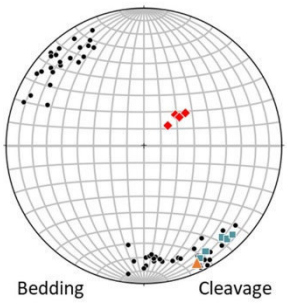

Bedding Cleavage
n = 53 n = 5

Angle Station Syncline

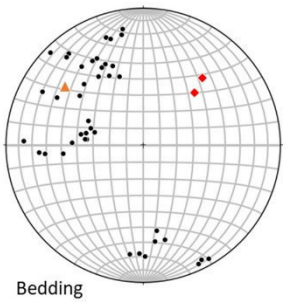

Bedding
n = 41

Big Buffalo Syncline

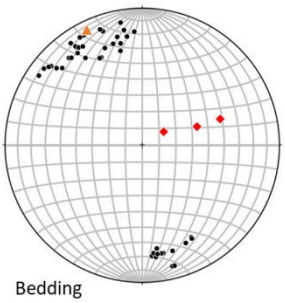

Bedding
n = 47

Brommers Syncline
Northeast

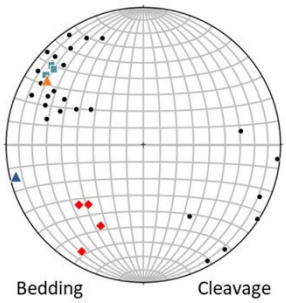

Bedding Cleavage
n = 27 n = 3

Brommers Syncline
Southwest

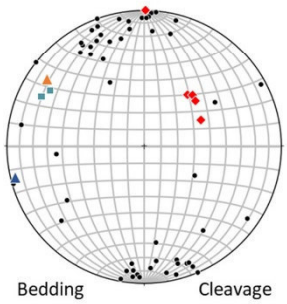

Bedding Cleavage
n = 55 n = 2

Devils Bridge Syncline

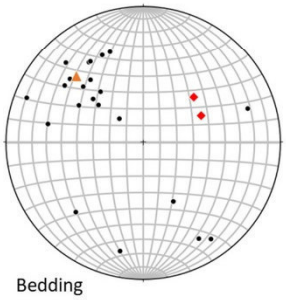

Bedding
n = 22

Duurstede Anticline

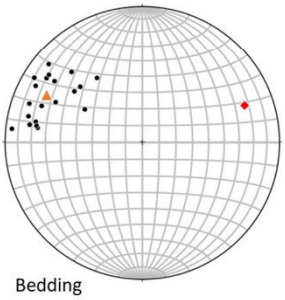

Bedding
n = 20

Duurstede Syncline

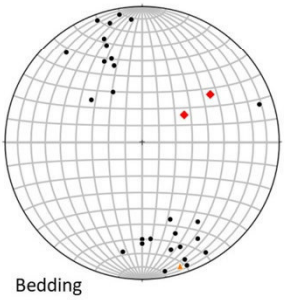

Bedding
n = 33

Dycedale Syncline

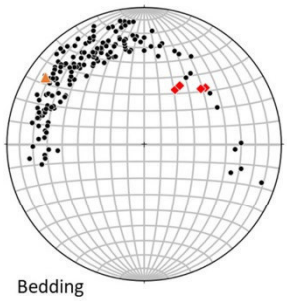

Bedding
n = 159

Eureka Syncline
Central

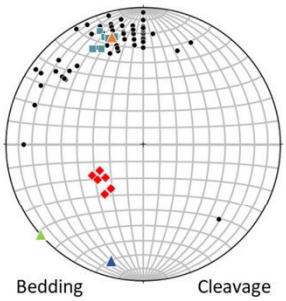

Bedding Cleavage
n = 62 n = 6

Eureka Syncline
East

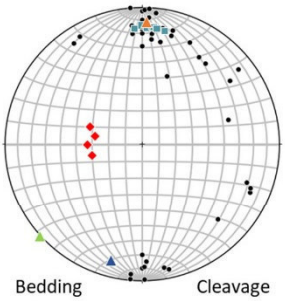

Bedding Cleavage
n = 45 n = 7

Eureka Syncline
South

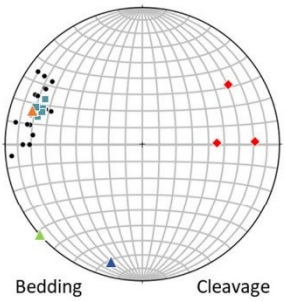

Bedding Cleavage
n = 21 n = 5

Forbes Reef Anticline
North

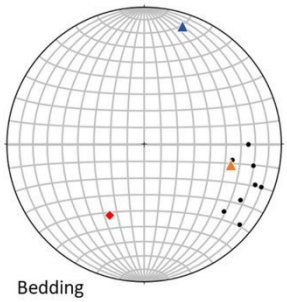

Bedding
n = 8

Forbes Reef Anticline
South

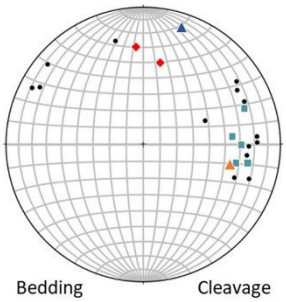

Bedding Cleavage
n = 14 n = 5

Heemstede Syncline
West

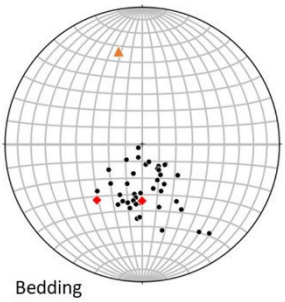

Bedding
n = 41

Heemstede Syncline
East

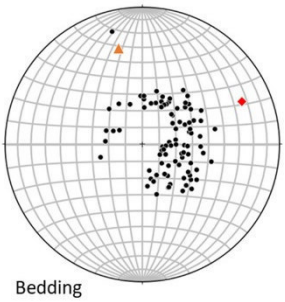

Bedding
n = 91

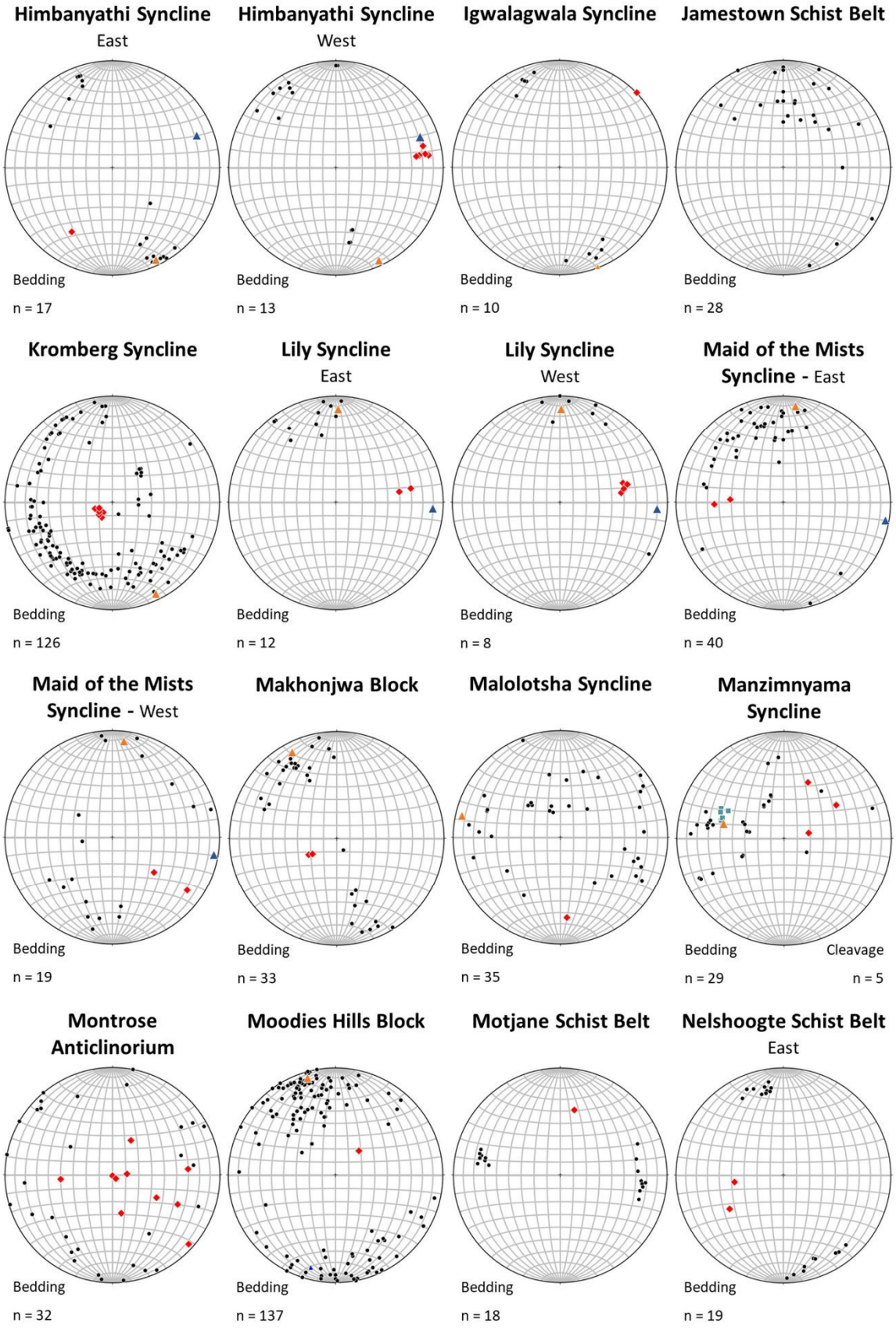
Himbanyathi Syncline
East
Bedding
n = 17
Himbanyathi Syncline
West
Bedding
n = 13
Igwalagwala Syncline
Bedding
n = 10
Jamestown Schist Belt
Bedding
n = 28
Kromberg Syncline
Bedding
n = 126
Lily Syncline
East
Bedding
n = 12
Lily Syncline
West
Bedding
n = 8
Maid of the Mists Syncline - East
Bedding
n = 40
Maid of the Mists Syncline - West
Bedding
n = 19
Makhonjwa Block
Bedding
n = 33
Malolotsha Syncline
Bedding
n = 35
Manzimnyama Syncline
Bedding
n = 29
Cleavage
n = 5
Montrose Anticlinorium
Bedding
n = 32
Moodies Hills Block
Bedding
n = 137
Motjane Schist Belt
Bedding
n = 18
Nelshoogte Schist Belt
East
Bedding
n = 19

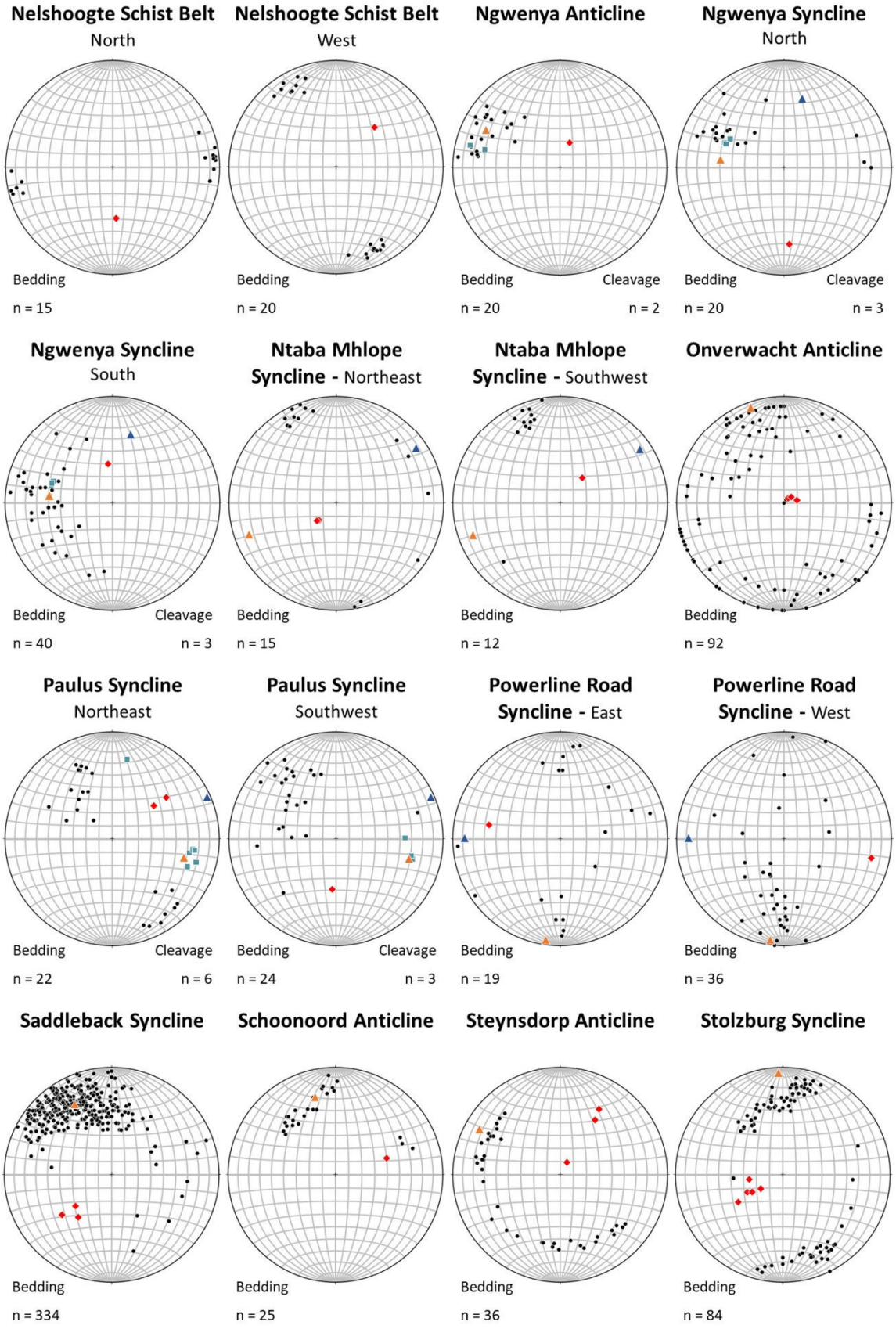
Nelshoogte Schist Belt
North
Bedding
n = 15
Nelshoogte Schist Belt
West
Bedding
n = 20
Ngwenya Anticline
Bedding
Cleavage
n = 20
n = 2
Ngwenya Syncline
North
Bedding
Cleavage
n = 20
n = 3
Ngwenya Syncline
South
Bedding
Cleavage
n = 40
n = 3
Ntaba Mhlope Syncline - Northeast
Bedding
n = 15
Ntaba Mhlope Syncline - Southwest
Bedding
n = 12
Onverwacht Anticline
Bedding
n = 92
Paulus Syncline
Northeast
Bedding
Cleavage
n = 22
n = 6
Paulus Syncline
Southwest
Bedding
Cleavage
n = 24
n = 3
Powerline Road Syncline - East
Bedding
n = 19
Powerline Road Syncline - West
Bedding
n = 36
Saddleback Syncline
Bedding
n = 334
Schoonoord Anticline
Bedding
n = 25
Steynsdorp Anticline
Bedding
n = 36
Stolzburg Syncline
Bedding
n = 84

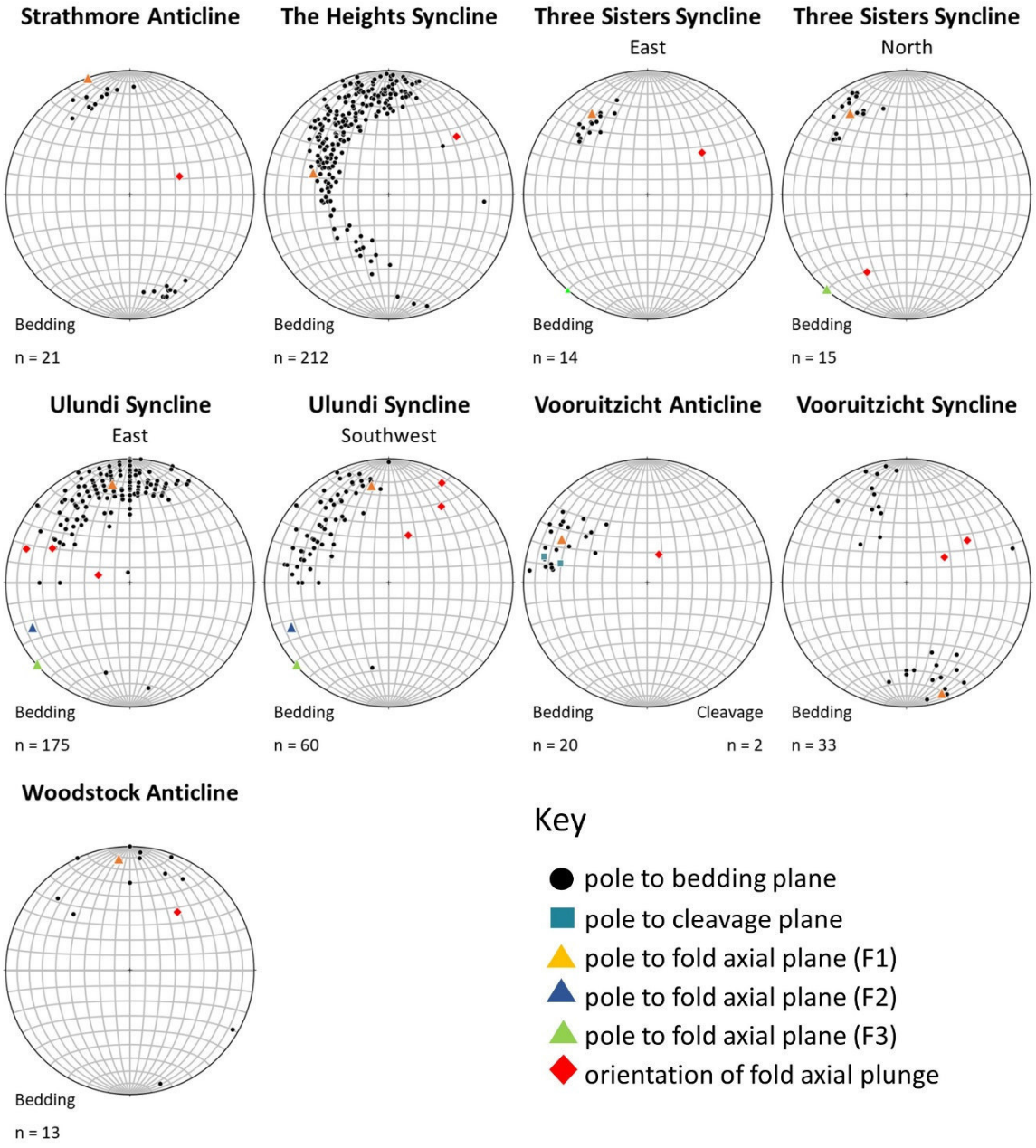

Fig. 5.3: Stereographic projections of structural features of the folds described in Table 5.2. For location of the respective fold, see Fig. 5.5.

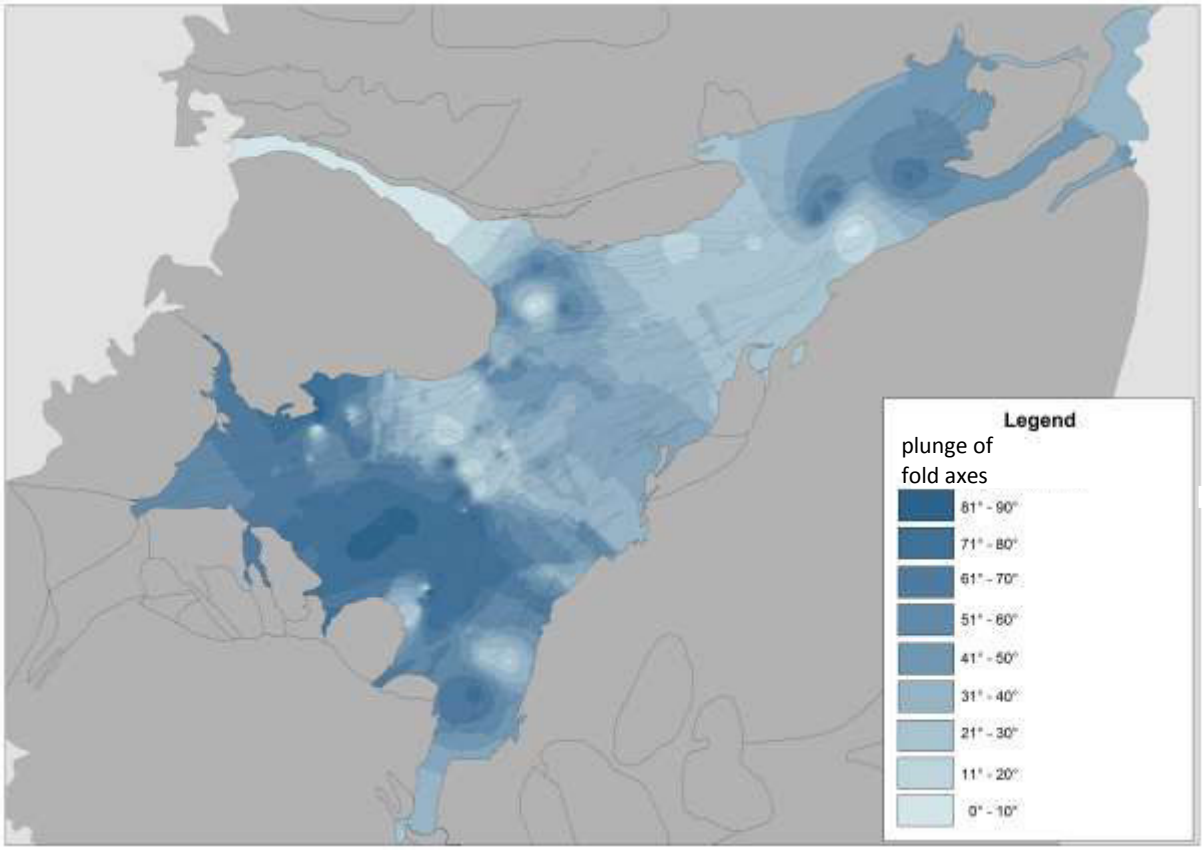

Fig. 5.4: Map of plunge variability. Colored areas represent mean regional plunge of fold axes.

5.5.3 Major faults

Faults can be subdivided into four major groups according to their orientation:

(1) Faults striking subparallel to the general trend of the greenstone belt (SW-NE) include the Inyoka Fault (IF), the Saddleback, Barbrook and Moodies faults. The Sheba, Lily and Revolver Creek faults are also attributed to the first group, even though their fold axial trace is arcuate due to later refolding around the Kaap Valley and Stentor plutons (F3), respectively. Within this group, the IF is the most important fault because it represents a major break marked by facies changes in all stratigraphic units (Heinrichs & Reimer, 1977; de Wit et al., 1992; Heubeck & Lowe, 1994a; Lowe et al., 1999; Lowe & Byerly, 1999; de Ronde & Kamo, 2000; Byerly et al., 2018). Many of these faults were reactivated during D5 as strike-slip faults with local transpressional and –tensional components (Schoene & Bowring, 2010).

(2) E-W striking faults comprise the Geluk, Granville Grove (GGF), Eucalyptus Mill (EMF) and Auber Villiers (AVF) faults in the central BGB. They show an up-to-the-south sense of displacement and generally repeat a Mendon Formation – Mapepe Formation succession north of the Onverwacht Anticline. Most faults of this group merge with the IF in the vicinity of the eastern margin of the Stolzburg Syncline.

(3) N-S striking faults include the Kromberg Fault Zone (KFZ) and the Manhaar Fault (MF). The KFZ is difficult to trace north of the The Heights Syncline but the orientation of nearby large folds suggest that it merges with the SW-NE striking faults of the first group.

Faults striking perpendicular to the general strike of the greenstone belt are restricted to the northeastern part of the BGB. Faults of this group include the Strathmore, Adamanda and Amo faults. Faults of this group truncate SW-NE-trending folds and are associated with minor dextral strike-slip offsets.

The Komati Shear Zone (KSZ) pre-dates D2 and, thus, represents the oldest major fault in the BGB. Prior to later folding during D2 to D5, it apparently showed a NW-SE strike. For its age and unusual geometry, the KSZ is not attributed to any of the fault groups described above.

5.5.4 Plutons and gneiss terranes

Ancient Gneiss Complex: The Ancient Gneiss Complex (AGC) borders locally the BGB to the southeast. It represents a chronologically complex and heterogeneous Paleoarchean crustal unit containing a variety of gneisses varying in age from c. 3666 to 3200 Ma (Hoffmann & Kröner, 2018). Over wide distances, its original contact to the BGB is obliterated by the later intrusion of the Piggs Peak and Mpuluzi batholiths at 3.1 Ga (Lana et al., 2011), but two small remnants of the AGC, the Malolotsha and Piggs Peak Inlier, remain at the southeastern margin of the greenstone belt (Chapter 4). The AGC records a complex tectono-metamorphic history with a youngest deformational event at c. 3220 Ma, coinciding with D3 deformation in the BGB (Kröner et al., 1989; Kamo & Davis, 1994; Dziggel et al., 2002; Brown, 2015). D5 caused the exhumation of the AGC at an extensional detachment along its border to the BGB (Lana et al., 2011).

Plutons adjacent to the BGB can be grouped in three generations of tonalite-trondhjemite-granodiorite plutons (Moyen et al., 2018) and two generations of younger granitic plutons.

TTG 1 series: The small Steynsdorp Pluton is located at the southern margin of the BGB and covers an area of c. 3 x 5 km. It represents the earliest generation of felsic/intermediate TTG melts in the Kaapvaal craton and is dated at 3510 ± 11 Ma, similar to a zircon crystallization age cluster in the AGC (Moyen et al., 2018). The pervasive, shallow (~35 °) gneissosity in the Steynsdorp Pluton defines a semi-concentric, outward-dipping northeasterly plunging, non-cylindrical antiform (Moyen et al., 2018) and, thus, can be regarded as a gneiss dome (Kisters & Anhaeusser, 1995; Lana et al., 2010).

TTG 2 series: The second generation of TTG plutons comprises a series of plutons along the southern margin of the greenstone belt east of the Inyoni Shear Zone (ISZ) and south of the Komati Shear Zone (KSZ). The largest and best studied of these are the Stolzburg and the Theespruit plutons, which cover areas of c. 14 x 9 and 10 x 4 km, respectively. Minor plutons of this generation include the Uitgevonden, Honigklip, Eerstehoek and Weergevonden plutons. Most of the TTG 2 plutons represent silica-rich trondhjemites and were emplaced at c. 3.45 Ga (Moyen et al., 2018), contemporaneous with upper Hooggenoeg Formation volcanism and with D1. TTG2 plutons are separated from the TTG3 plutons of the Badplaas Terrane by the ISZ.

TTG 3 series: The third generation of TTG plutons in the BGGT consists of two distinct groups: The TTG3a plutons along the northwestern margin of the BGB and TTG3b plutons in the Badplaas area to the southwest of the greenstone belt. TTG3a plutons comprise the Nelshoogte Pluton (3227 Ma), the Kaap Valley Tonalite (3229 Ma) and the Stentor Pluton (3218 Ma) (Moyen et al., 2018 and references therein). The Nelshoogte Pluton is a medium-grained trondhjemite, similar to those of the TTG2 generation, and was emplaced at mid-crustal depth at 2 – 5 kbar (Matsumura, 2014; Nedelec et al., 2012). The Kaap Valley Tonalite is a coarse-grained hornblende tonalite, which was emplaced in the upper crust at 1 – 2 kbar (Matsumura, 2014). The Stentor Pluton is a medium- to coarse-grained pinkish-grey granodiorite-adamellite, which is poorly understood with respect to age and internal phases (Kohler 2003).

TTG3b plutons of the Badplaas area comprise the Batavia, Nederland and Badplaas plutons, which range in age between 3280 and 3220 Ma (Moyen et al., 2018). These represent medium-grained

tonalites, grey trondhjemites and leucocratic granitoids, all of which are strongly foliated (Moyen et al., 2018).

Younger granitic plutons: Granitic plutons intruded the BGGT after deformation of the greenstone belt strata had ceased (e.g. Kisters & Anhaeusser, 1995). They include the sheetlike Nelspruit, Mpuluzi and Piggs Peak batholiths and the Dalmein, Salisbury Kop (Heubeck et al., 1993) Berlin, Ntonjeni, Boesmans Kop, Mbabane, Nkalengeni and Malandela plutons.

Plutons of the BGGT			
Pluton	**Age**	**Pluton**	**Age**
Ancent Gneiss Complex		**TTG3b**	
Ngwane Gneiss	3.2 - 3.66 Ga	Kaap Valley Tonalite	3.229 Ga
Dwalile Suite	3.45 Ga	Nelshoogte Pluton	3.227 Ga
Tsawela Gneiss	3.42 - 3.47 Ga	Stentor Pluton	3.218 Ga
TTG1		**Granitoid plutons**	
Steynsdorp Pluton	3.51 Ga	Nelspruit Batholith	3.22 Ga
		Dalmein Pluton	3.215 Ga
TTG2		Salisbury Kop Pluton	3.195 Ga
Stolzburg Pluton	3.45 Ga	Berlin Pluton	3.1 Ga
Uitgevonden Pluton	3.45 Ga	Ntonjeni Pluton	3.1 Ga
Honingklip Pluton	3.45 Ga	Mpuluzi Batholith	3.1 Ga
Eerstehoek Pluton	3.45 Ga	Piggs Peak Batholith	3.1 Ga
Weergevonden Pluton	3.45 Ga	Boesmanskop Pluton	3.07 Ga
Theespruit Pluton	3.44 Ga	Mbabane Pluton	2.7 Ga
		Nkalengeni Pluton	2.7 Ga
TTG3a		Malandela Pluton	2.7 Ga
Batavia Pluton	3.28 Ga		
Nederland Pluton	3.28 Ga	**Mafic plutons**	
Badplaas Pluton	3.23 Ga	Ushushwana Complex	2.671 Ga

Table 5.3: Plutons of the BGGT with approximate age of emplacement.

5.5.5 Contact relationships

BGB-internal principal contacts: The Onverwacht Group – Fig Tree Group contact is generally conformable (Byerly & Lowe, 1985; Heubeck & Lowe, 1994a; Lowe et al., 1999) and observable in numerous sections, e.g., at the base of the eastern Stolzburg Syncline and north of the Onverwacht Anticline. An unconformity within the Fig Tree Group separates the Belvue Road, Ulundi and Sheba formations from the overlying Schoongezicht Formation (north of the IF) and the Mapepe Formation from the overlying Auber Villiers Formation (south of the IF), respectively (Lowe et al., 2007; Byerly et al., 2018). The 24-Hour-Camp Fault, possibly a large normal fault in the central BGB, separates a hanging-wall assemblage of Auber Villiers Formation and Moodies Group from a footwall assemblage of Mendon Fromation and Mapepe Formations (Byerly et al., 2018).

The contact between the uppermost Fig Tree Group north of the IF (Schoongezicht Formation) and the overlying Moodies Group is gradational and conformable, which is evident at the eastern margin of the Stolzburg Syncline and along the southwestern margin of the Saddleback Syncline. No such conformable contact between Fig Tree and Moodies Group strata is known south of the IF. Between

the IF and the KFZ, Moodies Group strata occur only as tectonic klippe, bounded by faults crosscutting older units (in the Powerline Road and Maid-of-the-Mists Synclines).

BGB-external principal contacts: Along the northwestern margin of the BGB, greenstone belt strata in contact to TTG plutons show tectonically thinned contact-metamorphic aureoles (Anhaesusser, 1972; Robb et al. 1986; Heubeck et al., 2016). Synclinal fold axes adjacent to plutons are refolded around the curvature of the pluton's margin (e.g. Eureka, Ulundi and Three Sisters synclines; Fig. 5.14). Along the southwestern margin, the contact between the BGB and TTG2 plutons is marked by a D2 extensional detachment, which juxtaposes high-grade metamorphic plutons with lower-greenschist-facies greenstone belt strata (Kisters et al., 2003; Moyen et al., 2006). At the eastern margin, the contact between the BGB and the AGC is marked by a D5 extensional detachment (Lana et al., 2011). This crucial contact, however, is largely obscured by the Mpuluzi and Piggs Peak batholiths. Small remnants of the original contact of the BGB to the AGC, which are defined by the Malolotja and Phophonyane inliers, suggest, that the original contact was marked by a D5 extensional detachment (Lana et al., 2011).

Contacts between the BGB and adjacent units in the northeast are poorly studied; no qualified statement can be made.

Overall, metamorphic fabric at the pluton - BGB contacts all around the greenstone belt indicate a normal (greenstone-belt-down and plutons-up) sense of shear (Jackson & Robertson, 1983; Anhaeusser, 1984; Jackson et al., 1987; Kisters et al., 2003; Lana et al., 2010).

5.5.6 Distribution of strain indicators

Strain is distributed heterogeneously across the BGB (Fig. 5.6). The margins of the greenstone belt are strongly affected by dominantly oblate strain (Heubeck & Lowe, 1994a; Kisters & Anhaeusser, 1995) but many parts of its interior do not show any evidence of pervasive strain, which appears to be localized at major fault zones, such as the IF. The situation differs along the southeastern margin of the BGB in Eswatini, where deformed conglomerate clasts and mineral elongation lineation indicate widespread strong prolate strain (chapter 4). The Manhaar Fault may separate the low- from high-strain regime in this region.

5.6 Structural Domains

5.6.1 Subdivision into structural domains

Based on the differences in scale and geometry of folding, sense of shear and orientation of faults, timing of deformation and strain regime described above, we subdivide the BGB into five tectonic domains. While the subdivision of the west-central greenstone belt by Lowe & Byerly (1999) into four domains and by Byerly et al. (2018) into three blocks is based on tectonostratigraphic criteria, this subdivision is based on differences in deformation patterns only and covers the entire BGB.

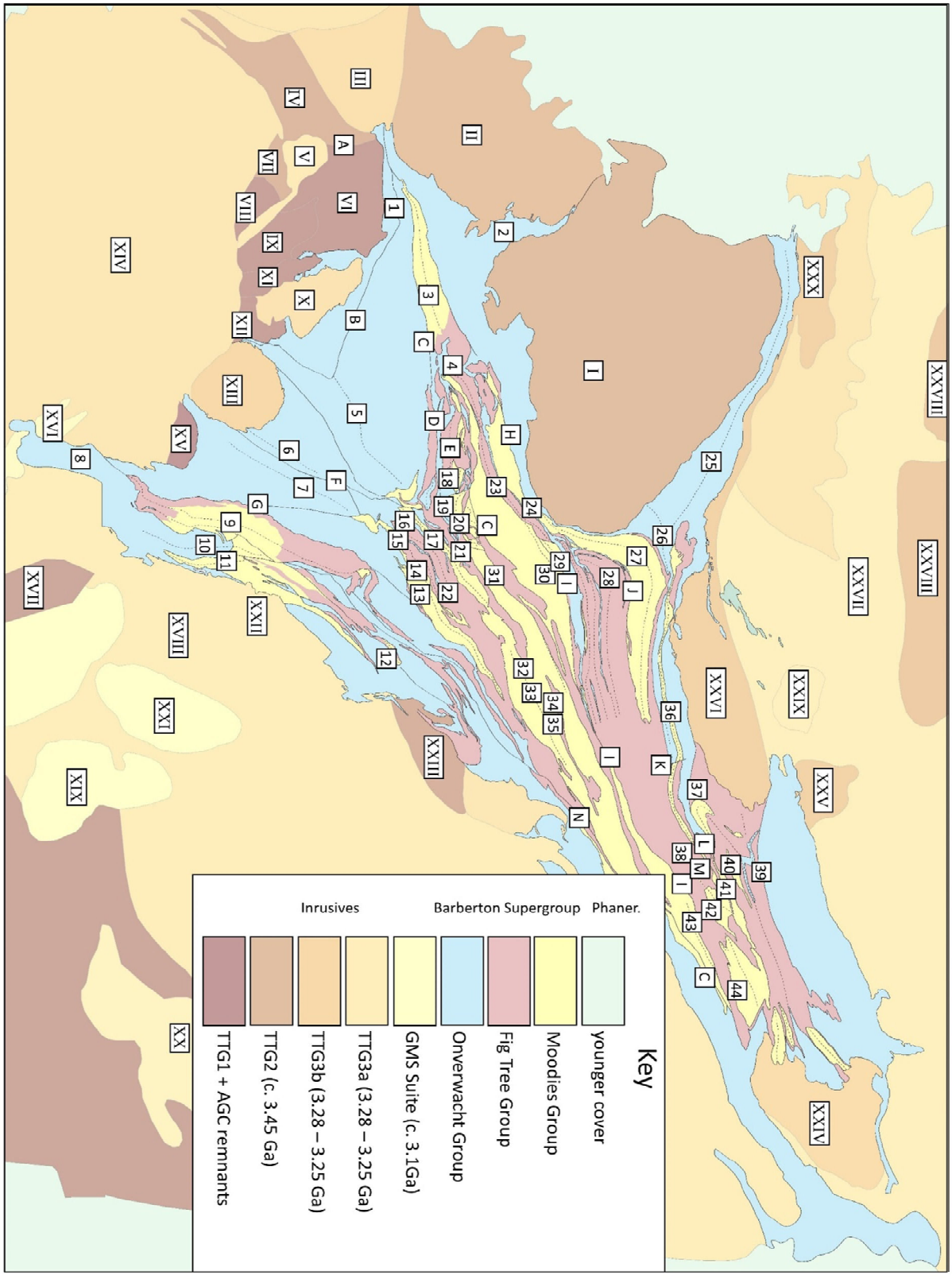

Fig. 5.5: Structural elements of the BGGT. For explanation and description see text, Tables 5.2; 5.3.

Folds

1 Stolzburg Syncline
2 Montrose Anticlinorium
3 Onverwacht Anticline
4 Kromberg Syncline
5 Steynsdorp Anticline
6 Ngwenya Syncline
7 Motjane Anticline
8 Malolotsha Syncline
9 Forbes Reef Syncline
10 Ntaba Mhlope Syncline
11 Devil's Bridge Syncline
12 Paulus Syncline
13 Schoonord Anticline
14 Manzimnyama Syncline

15 The Heights Syncline
16 Angle Station Syncline
17 Heemstede Syncline
18 Maid of the Mists Syncline
19 Powerline Road Syncline
20 Triple Point Anticline
21 Saddleback Syncline
22 Brommers Syncline
23 Sycedale Syncline
24 Moodies Hills Block
25 Eureka Syncline
26 Sheba Anticline
27 Ulundi Syncline
28 Woodstock Anticline
29 Jamestown Schist Belt
30 Lily Syncline
31 Louieville Anticline
32 Makhonjwa Block
33 Vooruitzicht Block
34 Three Sisters Syncline
35 Bien Venue Synform
36 Strathmore Anticline
37 Koede Anticline
38 Ugwalagwala Syncline
39 Amo Syncline
40 Himbanyathi Syncline
41 Big Buffalo Syncline

Faults

A Inyoka Fault
B Komati Fault
C Dunbar Fault
D Kromberg Fault
E Songimvelo Fault
F Manhaar Fault
G Mobovane Fault
H Granville Grove Fault
I Auber Villiers Fault
J Saddleback Fault
K Sheba Fault
L Moodies Fault
M Barbrook Fault
N Lily Fault
O Louieville Fault

Plutons

I Kaap Valley Pluton
II Nelshoogte Pluton
III Badplaas Pluton
IV Batavia Pluton
V Stolzburg Pluton
VI Boesmanskop Pluton
VII Nederland Pluton
VIII Weergevonden Pluton
IX Eerstehoek Pluton
X Mpuluzi Batholith
XI Honingklip Pluton
XII Theespruit Pluton
XIII Uitgevonden Pluton
XIV Dalmein Pluton
XV Steynsdorp Pluton
XVI Ushushwana Compley
XVII Ancient Gneiss Complex
XVIII Mbabane Pluton
XIX Nkalangeni Pluton
XX Malandela Pluton
XXI Milba Pluton
XXII Piggs Peak Gneiss
XXIII Ntonjeni Pluton
XXIV Piggs Peak Batholith
XXV Salisbury Kop Pluton
XXVI Stentor Pluton
XXVII Nelspruite Granite
XXVIII Berlin Pluton

Average values of measured conglomerate clasts										
Domain	Locality Name	Loc. No.	X	Y	Z	X*	Y*	Z*	X/Y	Y/Z
ND	Eureka Syncline E	1	1,38	1,34	0,54	1,00	0,97	0,39	1,03	2,48
	Eureka Syncline C	2	1,91	1,06	0,49	1,00	0,55	0,26	1,80	2,16
	Eureka Syncline S	3	1,64	0,99	0,62	1,00	0,60	0,38	1,66	1,60
	Moodies Hills Block	4	1,60	1,20	0,52	1,00	0,75	0,33	1,33	2,31
	Nelshoogte Schist Belt	5	2,49	1,13	0,35	1,00	0,45	0,14	2,20	3,23
	Saddleback Syncline	6	1,26	0,98	0,81	1,00	0,78	0,64	1,29	1,21
	Dycedale Syncline	7	1,18	0,97	0,83	1,00	0,82	0,70	1,22	1,17
	Stolzburg	8	1,02	1,00	0,98	1,00	0,98	0,96	1,02	1,02
ED	Amo Syncline	9	1,60	1,56	1,47	1,00	0,98	0,92	1,03	1,06
	Big Buffalo Syncline	10	1,30	1,28	1,29	1,00	0,98	0,99	1,02	0,99
CD	Inyoka Fault	11	1,79	1,07	0,52	1,00	0,60	0,29	1,67	2,06
	The Heights Syncline	12	1,09	1,03	0,89	1,00	0,94	0,82	1,06	1,16
	Devils Bridge Syncline	13	1,13	0,99	0,89	1,00	0,88	0,79	1,14	1,11
	Vooruitzicht Syncline	14	1,02	1,02	0,96	1,00	1,00	0,94	1,00	1,06
SD	Ntaba Mhlope Syncline	15	4,37	1,63	1,52	1,00	0,37	0,35	2,68	1,07
	Ngwenya Syncline S	16	2,05	0,98	0,88	1,00	0,48	0,43	2,09	1,11
	Ngwenya Syncline N	17	2,98	1,63	1,36	1,00	0,55	0,46	1,83	1,20
	Malolotsha Syncline	18	2,25	2,42	2,29	1,00	1,08	1,02	0,93	1,06
	Forbes Reef Syncline N	19	7,74	1,85	1,73	1,00	0,24	0,22	4,18	1,07
	Forbes Reef Syncline S	20	3,77	1,56	1,23	1,00	0,41	0,33	2,42	1,27
WD	Powerline Road Syncline	21	8,47	6,00	5,00	1,00	0,71	0,59	1,41	1,20
	Maid of the Mists Syncline	22	8,00	5,50	3,90	1,00	0,69	0,49	1,45	1,41

Table 5.4: Summary of clast axes ratios. See Appendix for measured values. Additional data are from Heubeck & Lowe (1994a).

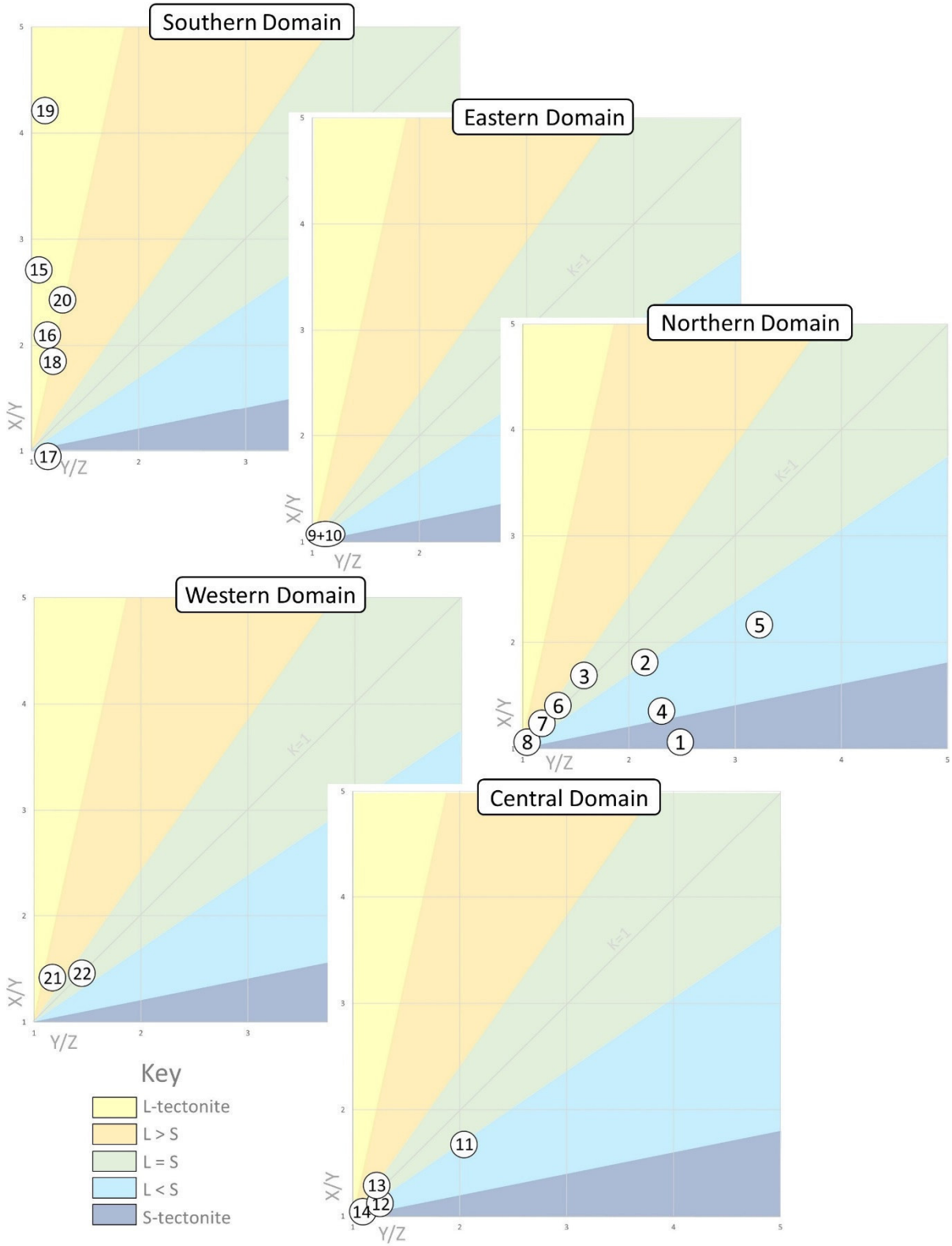

Fig. 5.6: Flinn diagrams showing strain distribution across the BGB. Number of data points refer to Table 5.4. For definition and escription of domains see text.

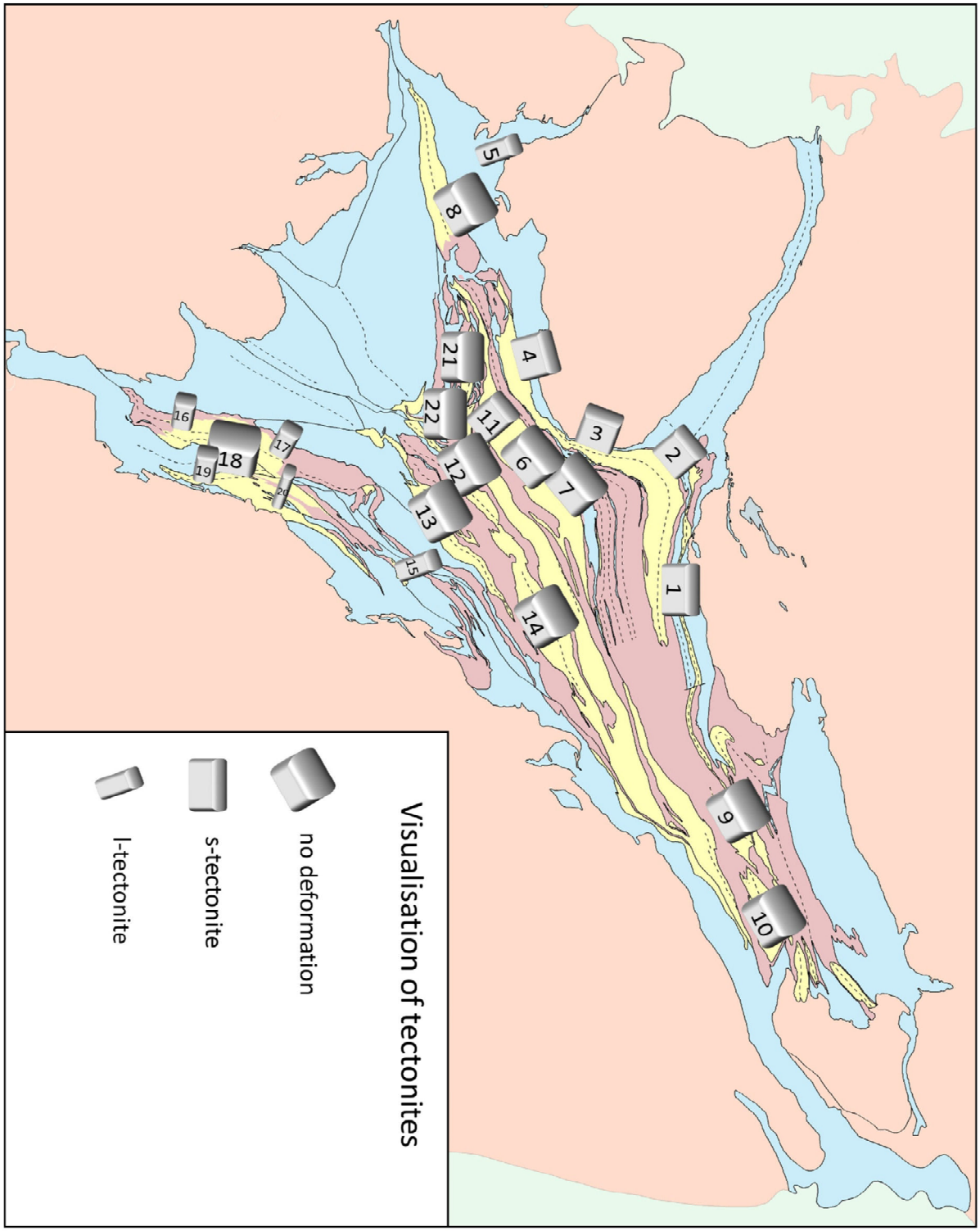

Fig. 5.7: Map showing distribution of strain indicators. Number of data points refer to Table 5.4. For legend, scale and location of the map see Fig. 5.1 or Fig. 5.8.

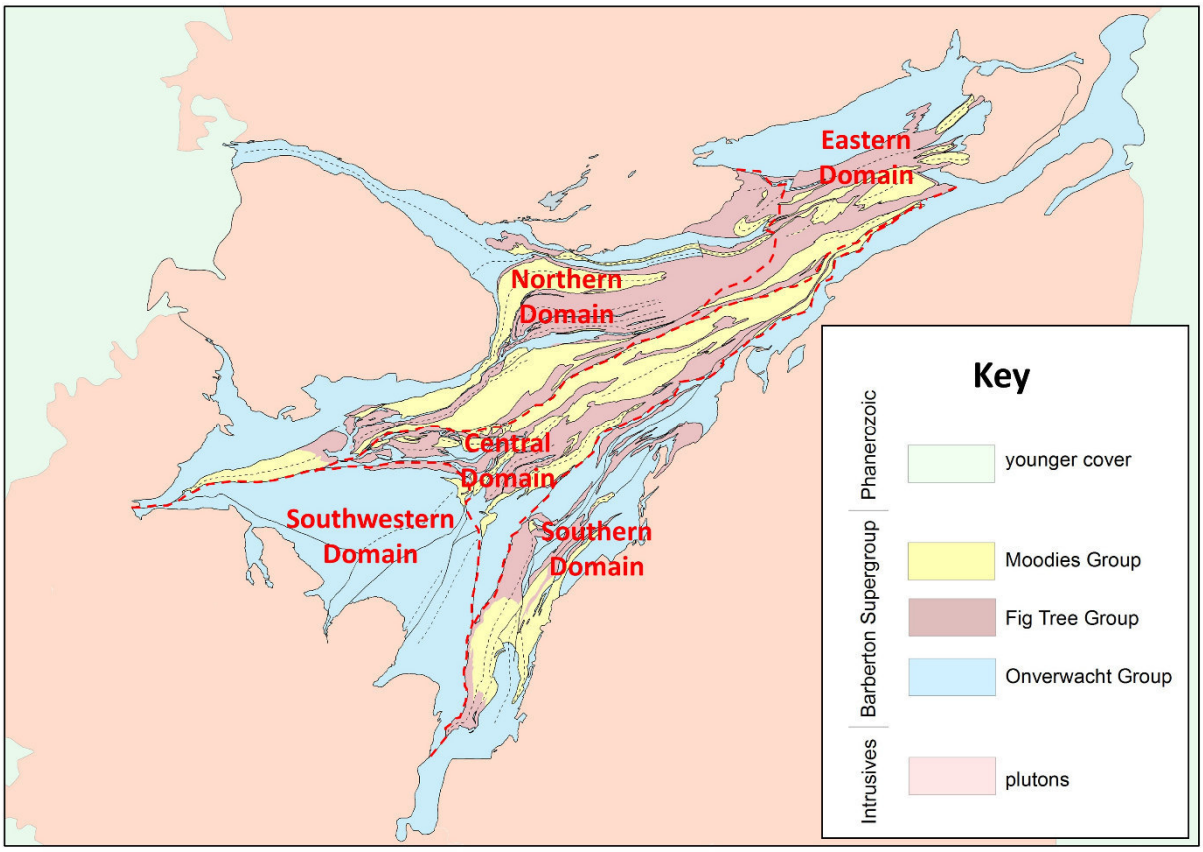

Fig. 5.8: Subdivision of the BGB into five domains.

5.6.2 Southwestern Domain

The Southwestern Domain (SWD; Fig. 5.8) is located between the IF in the north, the KFZ in the east and a series of TTG plutons in the southwest. Along the southwestern margin, the (from NW to SE) Onverwacht Anticline, Kromberg Syncline and Steynsdorp Anticline form a continuous fold train. South of the Komati Shear Zone, the oldest greenstone belt strata, assigned to the Sandspruit and Theespruit formations, are exposed. North of the Komati Shear Zone, the Onverwacht Anticline consists of the Komati, Hooggenoeg, Kromberg and Mendon Formations, while the Kromberg Syncline is filled entirely by rocks of the Kromberg Formation. The Steynsdorp Anticline consists of the Theespruit, Komati and Hooggenoeg formations. The extent of these folds along strike is c. 19 km in the Onverwacht and Steynsdorp synclines and c. 10 km in the Kromberg Syncline. The Onverwacht Anticline comprises c. 10 km of stratigraphic thickness, while the Kromberg Syncline and Steynsdorp Anticline contain strata only c. 2 – 3 km thick. These folds contain the oldest strata of the BGB. No strata >3.3 Ga occur outside the SWD (Lowe & Byerly 2007).

North of the Onverwacht Anticline, a stratigraphic succession consisting of Mendon Formation and Mapepe Formation is tectonically repeated by the (from S to N) GGF, EMF and AVF. This sequence is overlain by the fault-bounded Powerline Road and Maid-of-the-Mists Synclines, which likely represent tectonic klippen above tightly refolded normal faults. These synclines extent for c. 2.5 – 3.5 km along strike and have an exposed stratigraphic thickness of c. 600 m. With the exception of the fault-bounded synclines consisting of Moodies Group strata, fold axes in the SWD plunge subvertically. The exposed stratigraphic base of the BGB south of the KSZ is intruded by c. 3.44 Ga old plutons of TTG generation 2 (Kröner et al., 1996; Dann, 2000; Kisters et al., 2013; Anhaeusser et al., 2014).

Fig. 5.9: Stratigraphic units used in Figs. 5.10 – 5-14.

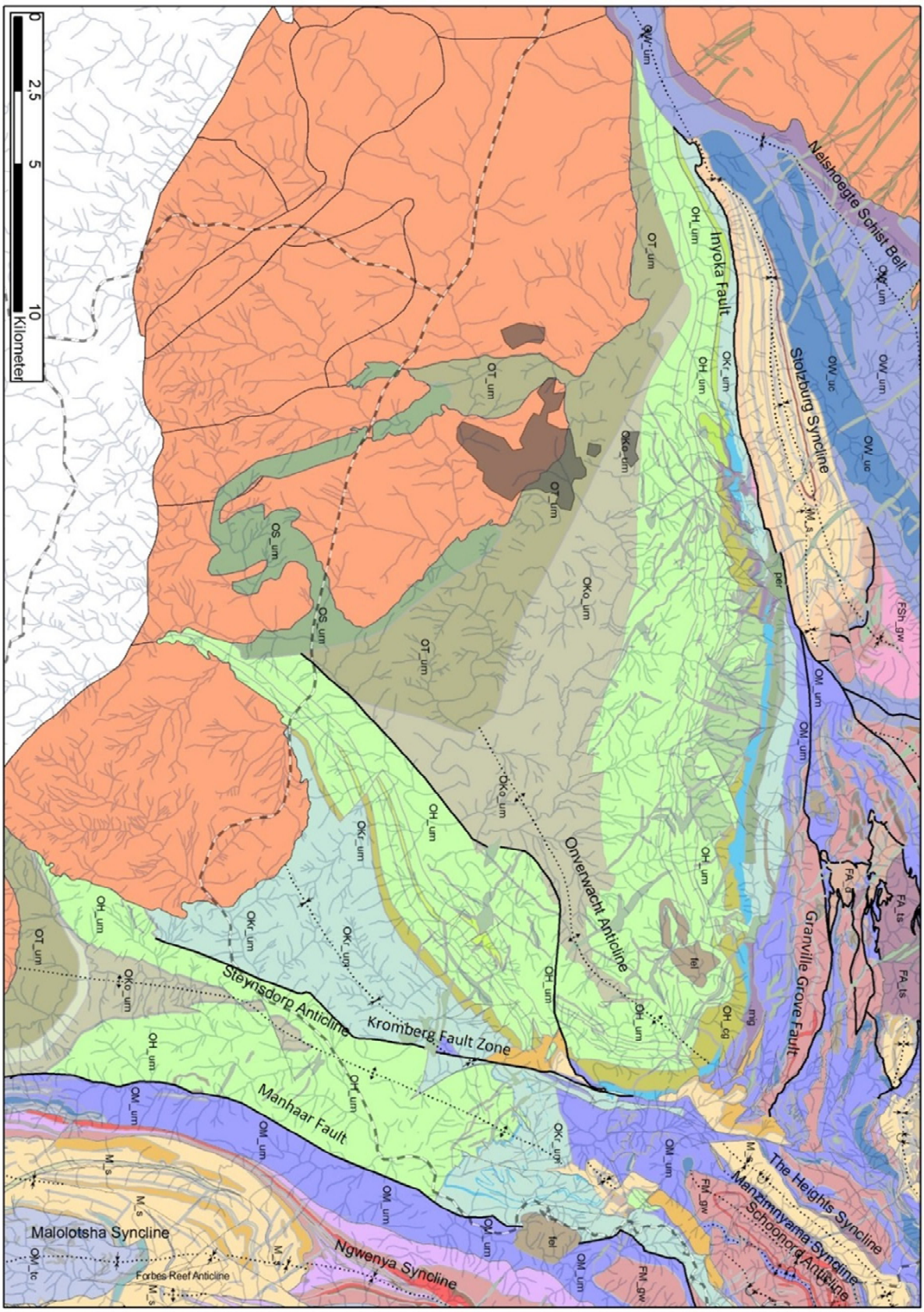

Fig. 5.10: Map of the SW domain. For key, see Fig. 5.9.

Most authors agree that folding and tilting of Onverwacht Group strata in the SWD was driven by diapiric rise of plutons (e.g. Kisters & Anhaeusser, 1995; Lana et al., 2010) comparable to the ``mantled gneiss domes´´ of Eskola (1949). Exhumation of these high-grade metamorphic terranes occurred during D2 (Kisters et al., 2003; Lana et al., 2010). The fault-bounded synclines consisting of Moodies Group strata show no evidence of having formed contemporaneously with the formation of the Onverwacht Anticline. The emplacement of the Dalmein Pluton, which sharply truncates folded strata of the Onverwacht Group, at c. 3203 ± 7 Ma postdates deformation of the SWD (Lana et al., 2011).

5.6.3 Southern Domain

The Southern Domain (SD; Fig. 5.10) is bounded by the Manhaar Fault to the west, the Mpuluzi Batholith to the south, the Piggs Peak Batholith to the east and the Songimvelo Fault to the north. The dominant geological structures in the SD include the Malolotsha Syncline and the adjacent Ngwenya and Forbes Reef Anticlines. The extent of these folds along strike is between 12 (Malolotsha Syncline) and 28 km (Ngwenya Syncline) with a maximum stratigraphic thickness of c. 2.2 km. Talcose schists, assigned to the Onverwacht Group due to their characteristic lithology, overlie strata of the Moodies Group in the core of the Malolotsha Syncline. The nature of the contact is debated and its interpretation is problematic. Various hypotheses face major shortcomings (chapter 4).

The angular unconformity within the Fig Tree Group clearly indicates D2 deformation, uplift and erosion of the Onverwacht Group and conformably overlying Mapepe Formation. Syn- and post-Moodies deformation during D3 and D4 was followed by exhumation of the AGC, probably along a ductile extensional shear zone during D5 (D4 of de Ronde and de Wit, 1994). The emplacement of the Piggs Peak Batholith at c. 3.1 Ga obscured most of the primary AGC-BGB contact (Murphy, 2015). Contact relationships between the Motjane Schist Belt and adjacent plutonic rocks indicate relative sagging of greenstone belt strata and uplift of the surrounding plutons (Jackson & Robertson 1983). The SD appears to have been affected regionally by higher strain than observed in most other parts of the BGB during late/post Moodies deformation. In particular, conglomerate clasts common in Moodies Group strata show variably high prolate strain. Their long axes are usually aligned parallel to the trend of the fold axes of the structures which contain the strata.

5.6.4 Central Domain

The Central Domain (CD; Fig 5.11) is located between the MF in the southeast, the KFZ in the west and the IF in the north. The western part of the domain consists of a series of parallel, SW-NE trending synclines consisting of Moodies and Fig Tree Group strata (Heemstede, Angle Station, The Heights, Manzimnyama, Paulus, and Devil's Bridge synclines) separated by narrow anticlines cored by Onverwacht Group strata (Schoonoord and Loenen anticlines). All folds in this part of the CD verge northwest and show a relatively low extent along strike of c. 12 km. The stratigraphic thickness exposed in the western part of the CD is c. 1 to 1.2 km in synclines and c. 150 m in anticlines. The eastern part of the domain comprises a series of synclines and anticlines expressed in Moodies Group strata (Duurstede Syncline and Anticline, Vooruitzicht Syncline and Anticline), an unusual thick occurrence of the Moodies Lava, traceable for c. 15 km along strike, and several minor folds consisting of Fig Tree Group strata. Large-scale folds in the eastern part of the CD can be traced along strike for c. 20 km and show a maximum stratigraphic thickness of c. 2.5 km. Fold axes in this area are generally moderately doubly-plunging (37-51°) and conglomerate clasts are undeformed. The Onverwacht - Fig Tree Group contact is poorly exposed in this mountainous domain due to the easily weathered talcose schists in the narrow anticlines, but there is no indication of an unconformable contact. Moodies strata appear to overlie Fig Tree strata with angular unconformity.

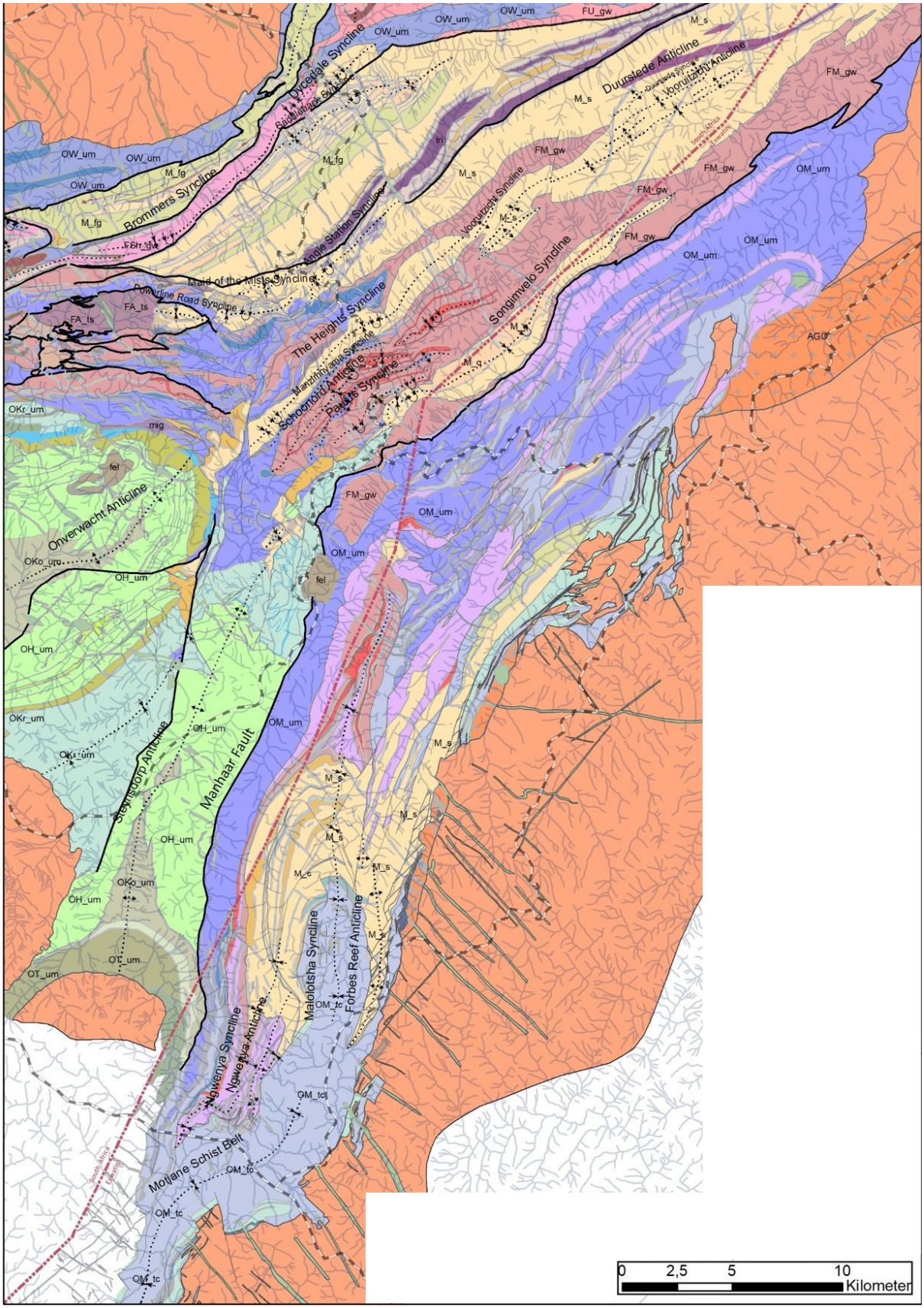

Fig. 5.11: Map of the S domain. For key, see Fig. 5.9

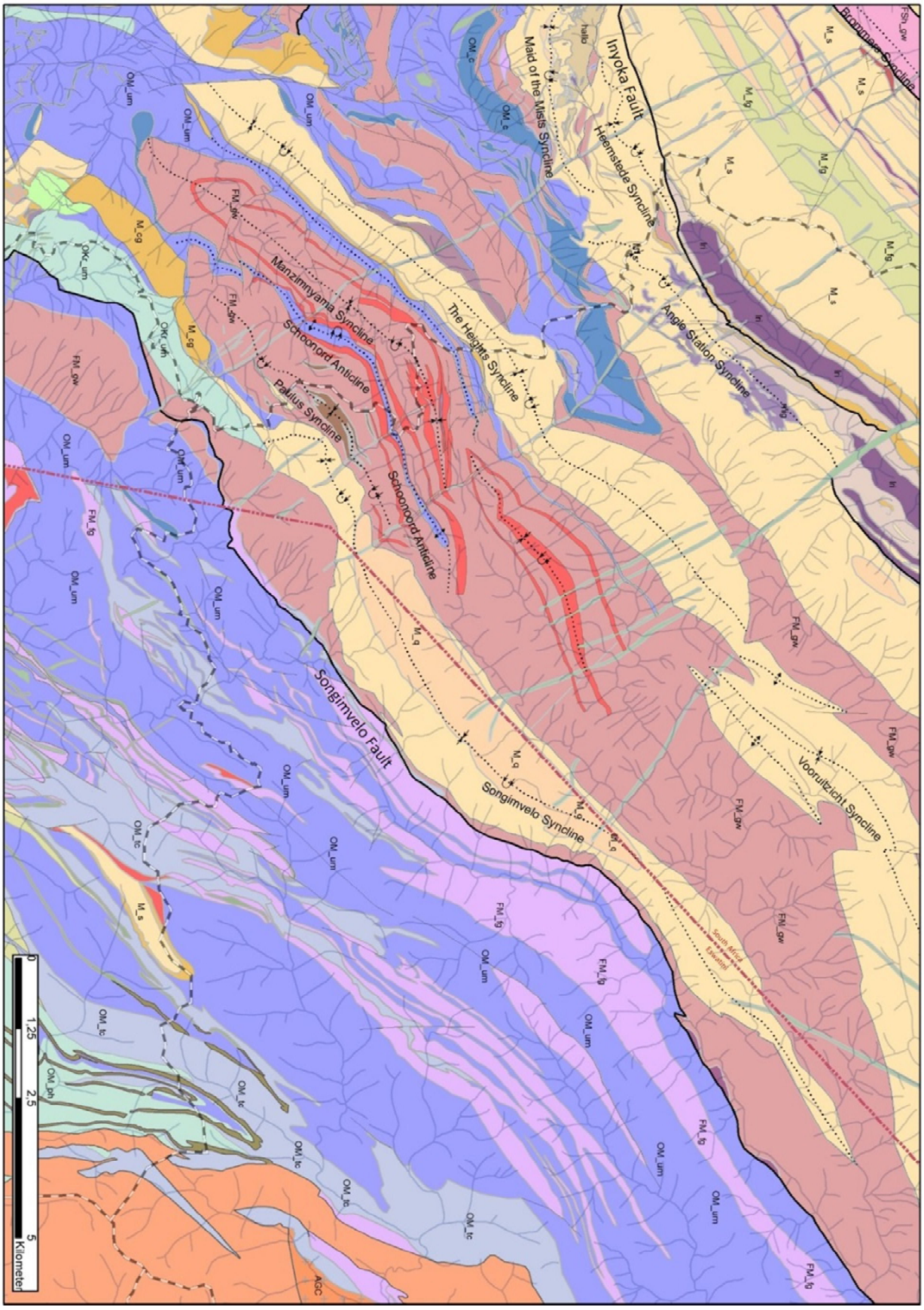
Inyoka Fault
Heemstede Syncline
Maid of the Mists Syncline
Bromman Syncline
Angle Station Syncline
The Heights Syncline
Manzimnyama Syncline
Schoonoord Anticline
Pakilus Syncline
Schoonoord Anticline
Songimvelo Fault
Songimvelo Syncline
Vooruitzicht Syncline
South Africa Eswatini
AGC
0
1.25
2.5
5
Kilometers

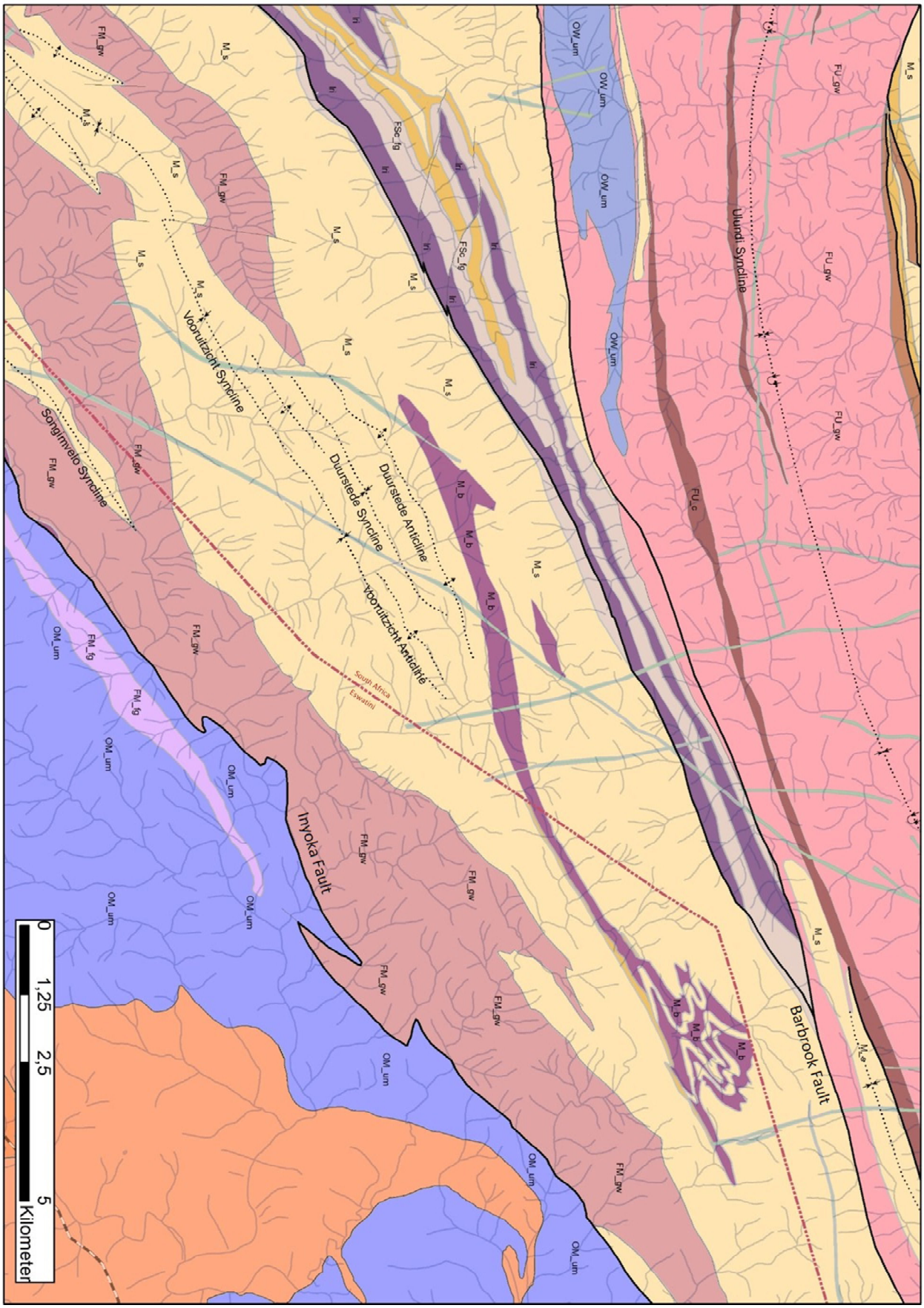

Fig. 5.12: Map of the C domain. For key, see Fig. 5.9.

5.6.5 Eastern Domain

The Eastern Domain (ED; Fig. 5.13) is located between the Strathmore and Adamanda faults in the northwest, the Nelspruit Batholith in the north, the Salisbury Kop Pluton in the east and the IF in the south. Onverwacht Group strata all appear to belong to the Weltevreden Formation (and thus are 100 to 200 Ma younger than lithologically similar units of the Onverwacht Group to the south) and are restricted to the marginal areas of this domain, where no major structures are identified. The conformably overlying Fig Tree Group crops out generally poorly in this domain and appear to make up only one major fold, the Koedoe Anticline. Most other major folds in this domain are expressed in Moodies Group strata which appear to unconformably overlie Fig Tree strata, including the Amo, Big Buffalo and Himbanyathi synclines. These reach c. 4 km, c. 8 km and c. 29 km in length, respectively. Fault-bounded elongate blocks of Moodies strata, including the Scotsman and Koedoe blocks, represent the northern (Koedoe) and southern (Scotsman) limbs of synclines, whose fold axes were truncated by faults. Not much is known about the lithologies and internal stratigraphic subdivision in this domain.

The contact between the BGB and surrounding plutons is largely obscured by the Piggs Peak and Nelspruit batholiths (to the north and south of the BGB, respectively) or younger sedimentary cover of the Karoo. The Salisbury Kop Pluton, emplaced c. 3105 ± 3 Ma ago (Heubeck et al.), sharply truncates folded strata of the Onverwacht and Moodies Group. D4 and D5 must predate its intrusion. A unique feature of this domain is the presence of a series of faults striking approximately perpendicular to the general strike of the BGB, including the (from west to east) Strathmore, Adamanda, and Amo faults.

5.6.6 Northern Domain

The Northern Domain (ND) represents the part of the BGB north of the IF and is bordered by a series of plutons along its northern margin. With few exceptions, Onverwacht Group strata are largely limited to the northern margin of the ND along the contact to the adjacent plutons. Lower (Belvue Road, Ulundi and Sheba formations) and upper (Schoongezicht Formation) Fig Tree Group is separated by an (D2) intra-Fig Tree angular unconformity. The Moodies Group defines several large folds in the ND, including the Eureka, Saddleback and Stolzburg synclines and the Moodies Hills block (which is the southern limb of the Eureka's Syncline western extension). Synclines consisting of Fig Tree and Moodies Group strata are juxtaposed with respect to each other along major upright fault planes or separated by narrow and tectonically thinned anticlines of Onverwacht Group strata. The ND between Barberton and the IF may have been affected by the highest degree of horizontal shortening in the BGB, resulting in the replacement of anticlines by major vertical fault zones and the oblique truncation of synclinal fold axes (Moodies Hills Block by the Moodies Fault, Saddleback Syncline by the Saddleback Fault, Dycedale Syncline by the Barbrook Fault). These faults include the Moodies, Saddleback, Sheba and Barbrook faults, which all show an up-to-the-north sense of displacement. It is plausible to relate the formation of the synclines to the development of the fault zones.

Fold axes in the ND can be traced for long distances. They may reach c. 20 – 30 km along strike while limbs may reach a stratigraphic thickness of up to 3.5 km. A unique feature of the ND is the continuous sequence of culminations and depression (F2) along strike of the fold axial planes (e.g, depression of the Stolzburg Syncline – culmination of the Montrose Anticline – depression between the Moodies Hills Block and the Eureka Syncline) The refolding (F3) of F1 folds around a vertical axis by the emplacement of TTG3 plutons is another unique feature of the ND (e.g., Eureka, Ulundi and Three Sisters synclines). This domain includes a major folded mafic sill, the Lomati River Sill, with a Moodies-age intrusion age of 3212±8 Ma (Fugmann et al., submitted), but has no contact with surrounding plutons.

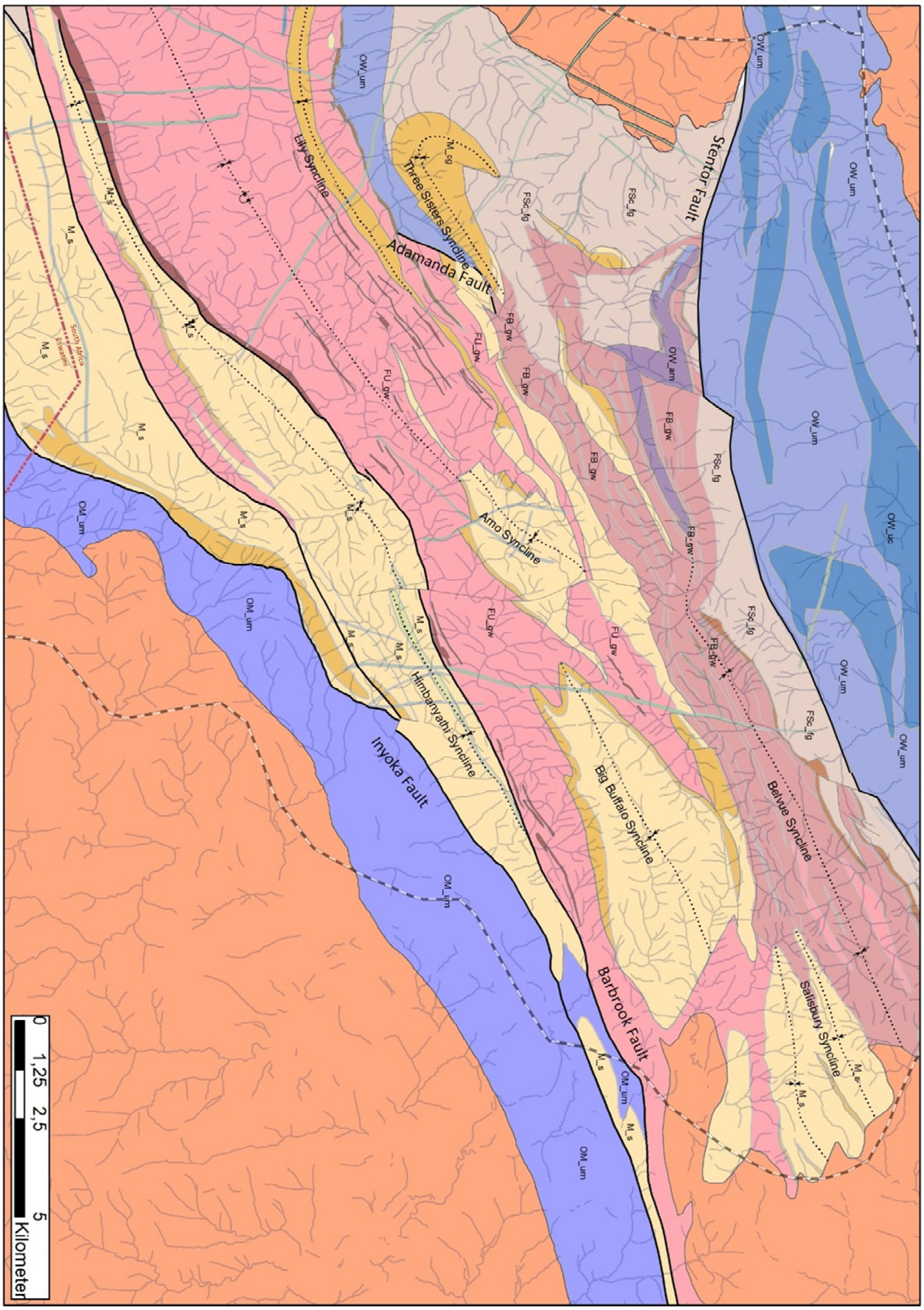

Fig. 5.13: Map of the E domain. For key, see Fig. 5.9

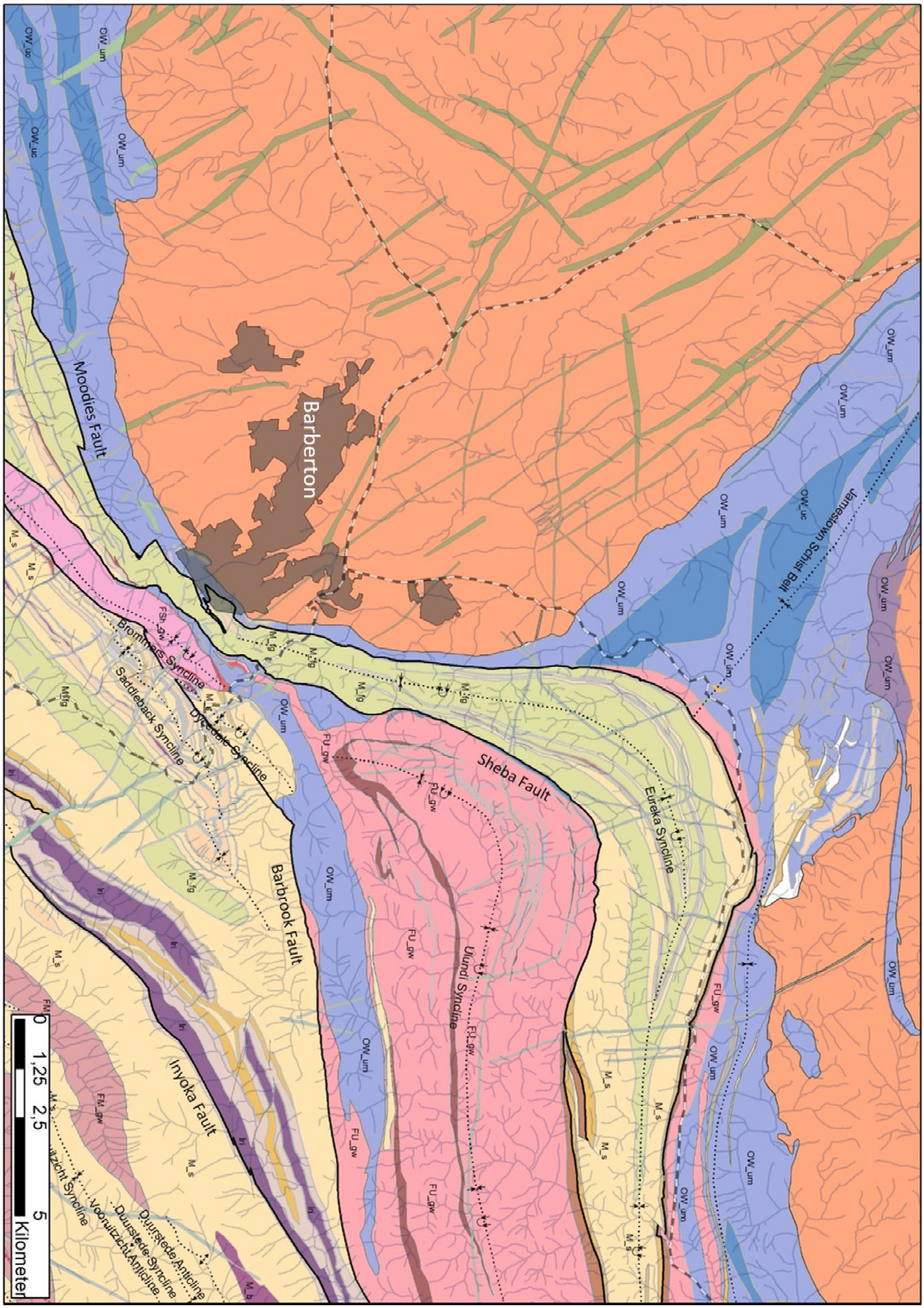
Barberton
Moodies Fault
Jamestown Schist Belt
Sheba Fault
Eureka Syncline
Barbrook Fault
Inyoka Fault
Ulundi Syncline
Bromhams Syncline
Saddleback Syncline
Dycedale Syncline
Vooruitzicht Syncline
Vooruitzicht Anticline
Duurstede Syncline
Duurstede Anticline
0 1,25 2,5 5 Kilometers

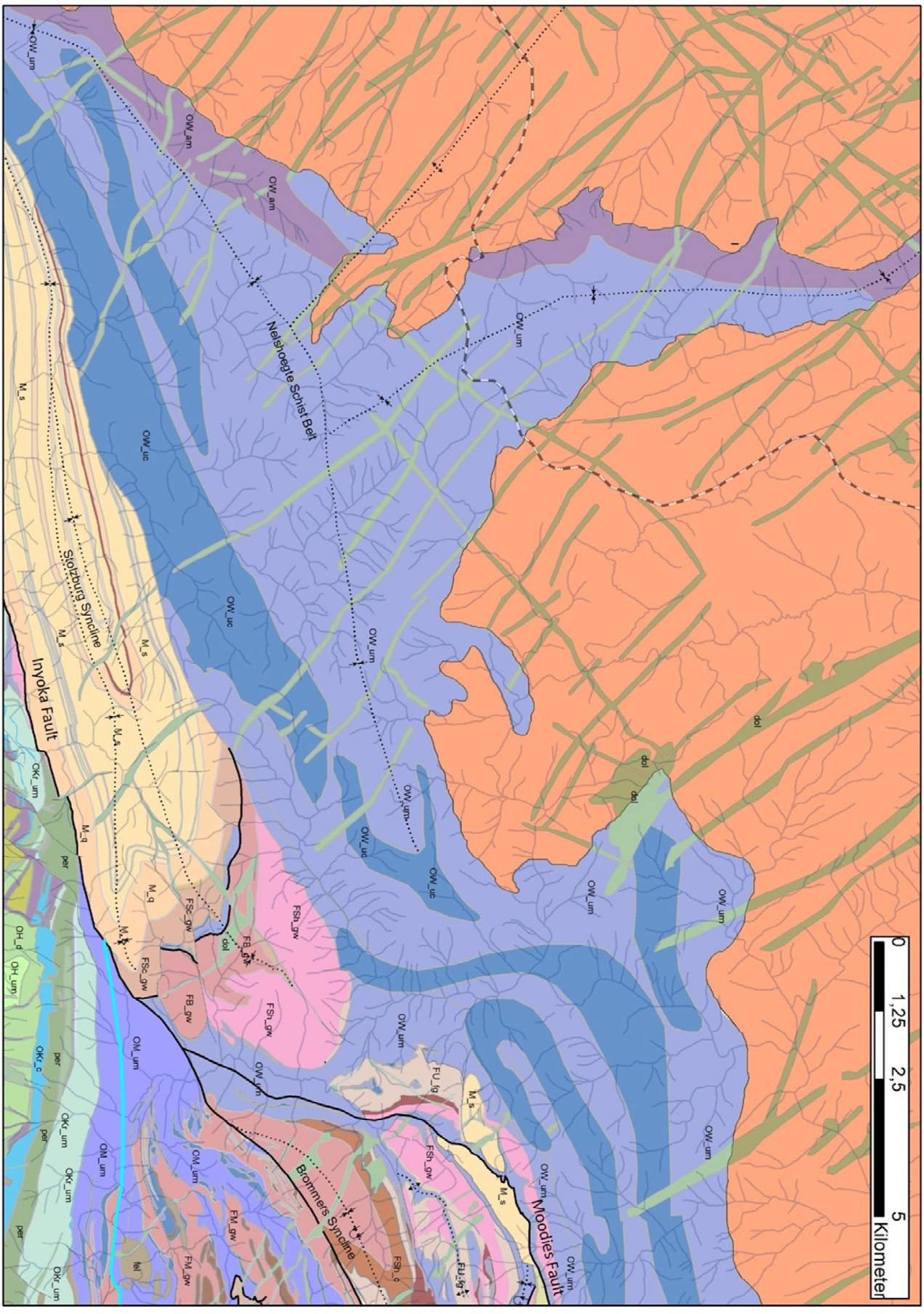

Fig. 5.14: Map of the N domain. For key, see Fig. 5.9.

5.7 Discussion

5.7.1 Synthesis

The emplacement of the Steynsdorp Pluton (a TTG1 pluton) at c. 3.51 Ga (Moyen et al., 2018 and references therein) occurred prior to any major deformation event recorded within the BGB. The plutons' gneissic fabric is mainly related to its diapiric rise and forms a gneiss dome (Kisters & Anhaeusser, 1995; Lana et al., 2010; Moyen et al., 2018). Zircons from the AGC show an age population similar to the age of the Steynsdorp Pluton, implying a linked formation of the pluton and of the gneiss terrane adjacent to the BGB (Kröner & Hoffmann, 2018). No deformational event younger than D2 is recorded within the AGC (Hoffmann & Kröner, 2018), although it was exhumed at an extensional detachment during D5, and no deformation younger than D1 is recorded within the TTG plutons of this generation (Moyen et al., 2018).

D1 at c. 3.55 - 3.45 Ga affected strata of the Onverwacht Group and TTG2 plutons to the south, for which a syndeformational emplacement is implied by their age of c. 3.45 Ga (Armstrong et al., 1990; Kröner et al., 2016; Moyen et al., 2018). In the southwestern BGB, this event uplifted and partially eroded the shallow-water volcanic platform and dacites of the upper Hooggenoeg Formation and created local accommodation space which was filled by debris flows and turbidites of H6 on the eastern limb of the Onverwacht anticline (Noisy Formation; Grosch et al., 2011). The Tsawela Gneiss, a part of the AGC to the southeast of the BGB, was formed at a similar age, indicating a linked origin of this two intrusive bodies (Moyen et al., 2018; Hoffmann & Kröner, 2018).

The extensional D2 is the first large-scale event which affected the BGB. It is associated with the emplacement of TTG3 plutons. Most of the TTG3b plutons of the Badplaas area were emplaced during D2. These plutons may have been accreted to the region dominated by TTG2 plutons to the east along the ISZ. Foliation and lineation of plutons to both sides of the shear zone steepens towards the ISZ to the vertical. The ISZ has been interpreted as subduction zone based on mineral assemblages and low dT/dP gradients (Dziggel et al., 2002; Moyen et al., 2006). However, it has to be noted that a terrane is suggested to be subducted here that formed immediately previously to the alleged subduction.

TTG2 plutons were exhumed during D2 at extensional detachments, thus juxtaposing high-grade metamorphic plutons with lower-greenschist-facies greenstone belt strata (Kisters et al., 2003). The extensional detachment, which contains mineral assemblages indicative of 6-8 kbar and 500-600°C (Moyen et al., 2006; Stevens & Moyen, 2007; Nedelec et al., 2012), separates the TTG2 plutons in the southwest from the main body of the BGB in the northeast and appears to have accommodated most of the D2 strain in the area (Dziggel et al., 2002; Stevens et al., 2002), uncoupling deformation in the BGB from the surrounding plutons. Undeformed dikes in the Stolzburg Pluton are dated at 3.38 Ga (Moyen et al., 2018) and significantly predate D2.

The formation of the main structures of the WD, including the Onverwacht Anticline, the Kromberg Syncline and the Steynsdorp Anticline, began during D2 (Lowe et al., 1999). Based on facies changes in the middle and upper Mapepe Formation north and south of the IF, Heinrichs and Reimer (1977) and Lowe et al. (1999) argued that the Proto-Inyoka-Zone formed during D2 as a topographic positive feature along the trend of the Onverwacht Anticline, breaking up the formerly uniform Mapepe basin into two distinct basins.

A controversially discussed topic in this context is the nature, timing and extent of the KSZ. Kisters et al. (2003, 2010) and Diener et al. (2005) investigated this shear zone in detail and concluded that it represents a greenstone-down, pluton-up ductile shear zone of approximately 18 km vertical displacement, juxtaposing the amphibolite-grade Sandspruit and Theespruit Formations, along with the TTG2 plutons, against lower-greenschist-facies strata of the Onverwacht Group. Because the trace

of the KSZ is clearly folded about the trace of the Onverwacht Anticline (a D2 structure, approximately 3230 - 3225 Ma), displacement must predate its formation and be associated with D1. Nevertheless, D2 to D5 rotation and tightening of that huge structure certainly contributed to its present geometry. The KSZ can be traced best along the west limb of the Onverwacht Anticline and may grade to the west into the extensional detachment separating the TTG2 plutons from the Stolzburg Schist Belt (Kisters et al., 2003). To the east, it disappears in the contact aureole of the Dalmein Pluton (3207 Ma).

South of the KSZ, D2 is recorded in the Theespruit Formation by a static metamorphic overprint indicating 6-8 kbar (van Kranendonk, 2011; Diener et al., 2005; Moyen et al., 2018). North of the KSZ, D2 is represented by deformation, uplift and erosion of the Onverwacht and (lower) Fig Tree Group (Mapepe Formation). D2 may have occurred in the ND earlier than south of the IF. An alternative scenario, suggesting that the change from Fig Tree to Moodies Group deposition occurred in the ND later than in the other domains, can be ruled out because the Schoongezicht and uppermost Mapepe Formations are both dated at 3225 Ma (Lowe & Byerly, 1999) implying a contemporaneous deposition.

The orientation of the Onverwacht Anticline, Kromberg Syncline and Steyndorp Anticline and the apparent segmentation of Fig Tree basins along the Proto-Inyoka-Zone suggests SE-NW-directed shortening. Because the preserved trace of the (extensional) D1 KSZ is orientated approximately 90° to this orientation, it conforms well to the D2 stress field.

D3 deformation occurred contemporaneously with deposition of the uppermost Fig Tree Group (Schoongezicht Formation) and lower Moodies Group (Heubeck et al., 2013; Heubeck, 2019) and may be continuous with D2. Emplacement of TTG3 (e.g. Kaap Valley and Stentor) plutons continued even though the majority of plutons had already formed by that time. No major change in stress orientation can be documented (Roering, 1965). Sedimentary facies associations of the lower Moodies Group are overall fining- and deepening-upward, suggesting an extensional tectonic regime at that time (Heubeck & Lowe 1994b).

The change to a compressional regime marks the onset of D4 (Heubeck et al., 2016; Heubeck, 2018). This likely occurred contemporaneously with the extrusion of the Moodies Lava complex at 3221 Ma (Heubeck et al., 2013), approximately in the middle of the Moodies stratigraphic succession. D4 was contemporaneous with the deposition of the upper Moodies Group; its end is not documented. The current general geometry of the BGB, dominated by large, northeast-southwest striking folds defined by all three stratigraphic groups, must have been induced during D4. It has been a matter of debate whether D4 deformation occurred by (sub-)horiztonal shortening, by differential (sub-)vertical sagging or by both processes (chapter 2). Because the BGB preserves only the basal part of an originally much larger and deeper basin (c. 5 – 15) km of overburden apparently existed, but have been removed), the original basin geometry, sediment provenance, basin margin geometry, and syndepositional deformation geometry is poorly constrained.

Heubeck & Lowe (1994a), among others, noted the absence of any strain in the folds of the central BGB despite extremely tight folding, vertically dipping strata and major horizontal shortening, and suggested that folds were formed by passive limb rotation. This observation, combined with the rapid change from an extensional to a compressional regime, is compatible with the PCO model by van Kranendonk (2011), which suggests initial extension due to local subsidence followed by compression caused by convergence of strata towards the zone of sinking.

Extensional D3 and compressional D4 may be closely related to further rotation (up-plunge uplift and down-plunge subsidence) and tightening of the Onverwacht Anticline. The tight folding of c. 10 km of stratigraphic section and the rotation of such an enormous anticline to the vertical must have created abundant nearby accommodation space while simultaneously providing significant material for erosion.

Finally, the D5 deformational event is associated with the exhumation of the AGC at an extensional detachment along the southeastern margin of the BGB (Lana et al., 2011). Itled to further modification of the folds within the BGB. D5 must have occurred following the end of Moodies Group deposition at c. 3209±14 Ma (Heubeck, 2019) and the widespread emplacement of undeformed intrusives at c. 3.1 Ga. The northwest vergence of BGB folds is restricted to an approximately NW-SE trending area including the western part of the CD and the central part of the ND (approximately from Devil's Bridge Syncline to Moodies Hills Block and the Eureka Syncline) and does not extend to folds elsewhere in the BGB. This local feature may be related to northwestward directed tectonic transport (Ramsay, 1963; Roering, 1965) in response to the exhumation of the AGC along the southeastern margin of the BGB during D5. The former extent of the AGC along strike of the BGB cannot be quantified because most of the original contact was intruded or covered by the Piggs Peak Batholith at 3.1 Ga.

The absence of two generations of crosscutting cleavage fabrics and the paucity of evidence for SW-NE-directed shortening in syn- and post-Moodies time shows that cross-folding cannot be responsible for the doubly-plunging geometry of large-scale folds of the BGB (chapter 3). The widespread lack of strain on many D3-D4 fold limbs throughout the BGB suggests that subsidence followed by passive limb rotation into the vertical was the main deformation mechanism (Heubeck & Lowe, 1994a; Kisters et al., 2003; Lana et al., 2011). This mechanism also provides the most plausible explanation for the rotation of the enormous Onverwacht Anticline to the vertical.

The absence of large-scale folds with a wavelength of c. 20 – 25 km in the eastern part of the CD and northwestern part of the WD may be the result of extensive faulting and shearing at the junction of the major fault zones of the IF and the KFZ. Because no domain besides the ND contains continuous sequences of F2 folds, SW-NE shortening may have been significantly larger south of the IF. Additionally, strike-slip movement along major fold-bounding faults dislocated culminations and depression of adjacent folds. The unusual geometry and strain indicators in the SD implies different deformation mechanisms or P-T conditions during deformation. These could be associated with the adjacent Steynsdorp Pluton and AGC.

5.7.2 Comparison of suggested tectonic settings

Any model aiming at providing a comprehensive explanation for the structural evolution of the BGB must explain the following four fundamental observations:

- The Onverwacht Anticline in the southwest of the BGB with a stratigraphic thickness of c. 10 km dominates maps and cross sections. It shows a (sub-)vertical fold axial plunge. Its size and geometry is the most powerful constraint on the depth structure of the (southwestern) BGB. Whatever mechanism created this structure must have triggered far-field effects with respect to uplift, subsidence, volcanism and metamorphism which any model must take into account.
- Large-scale folds of the BGB show a distinctive and rare three-dimensional geometry. They are characterized by steeply and doubly-plunging fold axes, subvertically dipping bedding planes and low strain (chapter 3).
- BGB strata are heterogeneous in terms of deformation geometry, facies, age and stratigraphic thickness. Major tectonostratigraphic breaks are the KFZ, the GGF and the IF. The KSZ constitutes a first-order break in metamorphic grade. Timing of the different deformation events varies across the greenstone belt.
- Even though the contact relationships between the surrounding plutons and the BGB vary across the greenstone belt, all contacts indicate relative uplift of the plutons. The metamorphic overprint alos shows a significantly higher grade than the BGB strata.

- Despite their close spatial association, deformation patterns of the BGB do not apply to the adjacent plutons, except for the plutons' marginal areas.

While virtually all tectonic models have substantial field, petrologic, geochronological or geochemical support, they also all face major shortcomings as well:

(1) Gravitational Collapse

- These early studies could not incorporate subsequent geochronological and geochemical constraints of metamorphic mineral assemblages and inferred P-T paths.
- The gravitational collapse model does not address the complex multideformation history of the BGB nor does it provide an explanation for the complex orientation, nature and timing of deformation events.
- The implied depth of the BGB stands in conflict with geophysical data suggesting a shallow BGB.
- Significant regional changes in deformation style across the BGB were not considered in this model or unknown at the time of its postulation.

(2) Doubly-vergent subduction zone

- Several of the terranes postulated by Schoene & Bowring (2010) are only a few km in width and are, thus, unreasonably small, considering the depth of subducted slabs.
- Subduction zones produce a continuous record of accretion, dewatering, deformation, magmatism and metamorphism over a long period of time. TTG plutons along the northeastern margin of the BGB have a magmatic record only from 3240-3220 Ma, incompatible with the suggested subduction zone.
- The postulated presence of other elements supporting plate-tectonic settings, such as ocean-floor alteration, ophiolite complexes, accretionary prisms with tectonic repetition etc. have been falsified (Lowe & Byerly, 2007; van Kranendonk et al., 2009).
- The Inyoni Shear Zone is the only reasonable candidate of a suture zone because of the preserved high-grade metamorphic mineral assemblage. Schoene & Bowring (2010) suggest subduction took also place at the southwestern and northeastern margin of the BGB. There is no supporting petrological or geochemical evidence for this geometry.
- Recent studies showed that high-pressure metamorphism at the ISZ, which was suggested to indicate subduction at the ISZ (Moyen et al. 2006), occurred at two distinct ages (c. 3.4 Ga and 3.2 Ga) and on both sides of the alleged subduction zone, strongly contradicting the earlier interpretation of the ISZ as a suture (Wang et al. 2019).

(3a) Foreland basins to the AGC

- Sedimentary rocks of the BGB contain no metamorphic clasts nor grains of metamorphic provenance or detrital zircons of AGC age, as one would expect in a typical foreland basin. Detrital zircons do not show AGC ages. The sedimentary facies and thickness variations are inconsistent with a provenance from the SE.
- The shortening style commonly observed in the thrust-belt segments of foreland basins DeCelles & Giles 1996) is inconsistent with the fold geometry, the heterogeneity of the deformation and the evidence for extensional detachment faulting along the margins of the BGB..

(3b) Rifts and passive continental margins

- There is no evidence for exposed basement exposed in rift shoulders or similar settings.
- Magmatic petrology in the BGB is not consistent with that expected in a rift setting.
- Rift models do not adequately explain the fold geometry nor the heterogeneity of the deformation.

(4) Fold-and-thrust belts

- Unidirectional thrusting is not an appropriate mechanism to explain the doubly-plunging folds and the variability of fold geometry across the greenstone belt.
- Fold-and-thrust-belts usually produce multiple, consistently oriented, older-over-younger displacements. However, the BGB appears to represents an overall synclinal structure, with the oldest strata exposed at its margins and younger strata in its center.

(5) Core Complex Model

- Core complex models do not explain the widespread (sub-)vertical bedding and steep fold-axial plunges. Extensional detachments exhuming core complexes are usually inclined only a few degrees.
- A shallow detachment does not provide an explanation for the vertically plunging Onverwacht Anticline. The model does not include a reasonable mechanism for later steepening of the structure.
- Large-scale normal displacement along the Komati Shear Zone must have taken place prior to folding and tilting of the Onverwacht Anticline because the Komati Fault is folded with it. Extension along the KSZ thus explains some D1 structures but cannot be responsible for subsequent Fig Tree or Moodies Group deformation.

(6) Partial Convective Overturn (PCO)

- Even though the PCO model adequately explains the large-scale fold geometry, the vertical orientation of bedding and steep plunge of fold axis in the WD, no distinct zone of sinking, as mapped in the Pilbara model, could be identified.
- The scale of F2 folding (depressions and culminations) indicates localized subsidence in a number of locations in contrast to one major zone of sinking, as described in the Pilbara.
- A general radial inward plunge predicted by the PCO model was not observed. In fact, most of the fold axial planes throughout the BGB strike SW-NE (or were subsequently refolded due to the emplacement of plutons or around the massive Onverwacht Anticline).

5.8 Conclusions

The BGGT represents a complex assemblage of tectonic domains with several deformation styles and distinct deformation phases. No single tectonic model can account for all observed features. The PCO model explains best the Western Domain because the very large, near-vertical plunging Onverwacht Anticline is best compatible with the mechanisms and processes occurring in or near a central zone of sinking. This model is also most compatible with the geometry of adjacent large synclines, which may have formed by passive limb rotation resulting from local subsidence. However, the variability of orientations of their fold axes and plunges deviates significantly from the radial arrangement observed in the Pilbara Craton; there, fold axes largely plunge towards a well-defined and mappable “central zone of sinking”.

The formation of doubly plunging folds is best explained as the result of small-scale sagging between TTG plutons or doming above serpentine diapirs. The apparent shortening in NW-SE direction suggested by the parallel arrangement of SW-NE striking synclines may be minor but not nil; it resulted largely from sagging. D5 induced some shortening and NW-directed thrusting, resulting in the NW-vergence of the fold-and-thrust belt in the central BGB.

Overall, the complexity and heterogeneity of timing and style of deformation across the BGGT is not explainable by a single model. It rather suggests a highly dynamic sequence of tectonic stress fields varying rapidly in orientation and magnitude through time, pulses in petrologically distinct magmatic activity and in sedimentation. It is striking that the BGGT's history has no major tectonic event for the initial c. 270 Ma of its recorded history. D2, D3, D4 and perhaps D5, in contrast, followed quickly upon each other and none of them lasted for longer than 30 Ma. Such a sequence of events is incompatible with modern, plate-tectonic-style tectonic processes. It rather favors the episodic overturn of metastable greenstones and associated sedimentary successions.

Acknowledgements

First, I have to thank my supervisor Christoph Heubeck for his support, encouragement, advice and trust in me for the past three years. I also owe thanks to Kamil Ustaszewski for our inspiring discussions, the opportunities to present my data to his research group and for reviewing this thesis. Special thanks go to Martin van Kranendonk for his guidance in the field, his hospitality and patience with me and for the many, many things I learned from him. This study was funded by the DFG SPP 1833 ''Building a habitable Earth''. Special thanks go to Carsten Münker and Daniela Hülle for organizing annual meetings and field workshops, which greatly enhanced the experience of this PhD project.

Furthermore, I wish to thank Linda Gorniak, Nora Bieker and Paul Fugmann for assistance in the field. This important part of my work would not have been the same without you. I am very grateful to Maik Schlimme for his assistance in compiling the geological map of the Barberton Greenstone Belt. Thanks also go to Janis Pingel and Nora Bieker for the effort they put into creating the 3D model of parts of the greenstone belt and to Nora Wassermann for preparing digital maps for our field work.

I would also like to express my gratitude to Astrid Christianson for her hospitality, her advice around Barberton and for making me feel home during my time in South Africa. Thanks also go to Tony Ferrar for his help with any legal restrictions concerning our work in Songimvelo Reserve and for sharing his incredible knowledge about the environment, we worked in. Both Astrid and Tony deserve many thanks for their endless efforts, which finally resulted in the declaration of the Barberton Greenstone Belt as a UNESCO world heritage site, which will help to protect and preserve this wonderful archive of Archean geology for the future. I owe thanks to Duwies Duvenage and Toyota Barberton for providing us with great vehicles during field work as well. Thanks also go to Barberton Mines, who provided us with crucial subsurface information and were very helpful and supportive in every respect. I would like to express my gratitude towards the Swaziland National Trust Commission for allowing and supporting our field work in the Malolotsha Nature Reserve.

I have to thank Frank Linde and Sandra Urban for processing my samples, extracting zircons for age dating and creating many interesting thin sections. I would like to extend that to the entire research group *Allgemeine und Historische Geologie* at the IGW in Jena for the discussions, talks and good times we had. I am very grateful to have shared the last three years with my fellow PhD students Benjamin Schmitz, Georg Löwe and Mauro Alivernini, who made my time as a PhD student (especially Wednesdays) a special time of my life, which I will always remember with pleasure. Last, but not least, I wish to thank my family for their support in crucial moments of my PhD. Thanks to all of you.

References

Alsop, G. I., & Holdsworth, R. E. (1999). Vergence and facing patterns in large-scale sheath folds. *Journal of Structural Geology*, *21*, 1335-1349.

Alsop, G. I., & Holdsworth, R. E. (2006). Sheath folds as discriminators of bulk strain type. *Journal of Structural Geology*, *28*, 1588-1606.

Anhaeusser, C. R. (1969). A comparison of pebble and fold deformations in the Nelspruit Granite contact aureole, Barberton Mountain Land. *South African Journal of Geology*, *72*, 49-60.

Anhaeusser, C. R. (1972). The geology of the Jamestown Hills area of the Barberton Mountain Land, South Africa. *South African Journal of Geology*, *75*, 225-263.

Anhaeusser, C. R. (1975). The geological evolution of the primitive earth: evidence from the Barberton Mountain Land. *Evolution of the crust,* 1, 71-106

Anhaeusser, C. R. (1976). The geology of the Sheba Hills area of the Barberton Mountain Land, South Africa, with particular reference to the Eureka Syncline. *South African Journal of Geology*, *79*, 253-280.

Anhaeusser, C. R. (1981). Geotectonic evolution of the Archaean successions in the Barberton Mountain land, South Africa. In *Developments in Precambrian Geology, 4*, 137-160

Anhaeusser, C. R. (1984). Structural elements of Archaean granite-greenstone terranes as exemplified by the Barberton Mountain Land, southern Africa. *Precambrian tectonics illustrated*, 57-78.

Anhaeusser, C. R. (1986). Archaean gold mineralization in the Barberton Mountain Land. *Mineral deposits of southern Africa*, *1*, 359-375.

Anhaeusser, C. R. (2014). Archaean greenstone belts and associated granitic rocks–a review. *Journal of African Earth Sciences*, *100*, 684-732.

Armstrong, R. A., Compston, W., De Wit, M. J., & Williams, I. S. (1990). The stratigraphy of the 3.5-3.2 Ga Barberton Greenstone Belt revisited: a single zircon ion microprobe study. *Earth and Planetary Science Letters*, *101*, 90-106.

Avigad, D., Ziv, A., & Garfunkel, Z. (2001). Ductile and brittle shortening, extension-parallel folds and maintenance of crustal thickness in the central Aegean (Cyclades, Greece). *Tectonics*, *20*, 277-287.

Barley, M. E., & Groves, D. I. (1990). Deciphering the tectonic evolution of Archaean greenstone belts: the importance of contrasting histories to the distribution of mineralization in the Yilgarn Craton, Western Australia. *Precambrian Research*, *46*, 3-20.

Barton Jr, J. M., Hunter, D. R., Jackson, M. P. A., & Wilson, A. C. (1983). Geochronologic and Sr-isotopic studies of certain units in the Barberton granite-greenstone terrane, Swaziland. *South African Journal of Geology*, *86*, 71-80.

Bédard J. H. (2018). Stagnant lids and mantle overturns: implications for Archaean tectonics, magmagenesis, crustal growth, mantle evolution, and the start of plate tectonics. *Geosci. Front. 9*, 19–49.

Bennett, J. A. E. (1971). Geological map series (1: 25,000) Sheet 4, Motshane. *Swaziland Geol Surv Mines Dept (Mbabane)*.

Bickle, M. J., Bettenay, L. F., Boulter, C. A., Groves, D. I., & Morant, P. (1980). Horizontal tectonic interaction of an Archean gneiss belt and greenstones, Pilbara block, Western Australia. *Geology*, *8*, 525-529.

Bontognali, T. R., Fischer, W. W., & Föllmi, K. B. (2013). Siliciclastic associated banded iron formation from the 3.2 Ga Moodies group, Barberton greenstone belt, South Africa. *Precambrian Research*, *226*, 116-124.

Brown, M. (2015). Paleo- to Mesoarchean polymetamorphism in the Barberton Granite-Greenstone Belt, South Africa: Constraints from U-Pb monazite and Lu-Hf garnet geochronology on the tectonic processes that shaped the belt: Discussion. *Bulletin*, *127*, 1550-1557.

Brown, M., Johnson, T. (2018). Secular change in metamorphism and the onset of global plate tectonics. *Am. Mineral., 103*, 181–196

Byerly, G. R., & Lowe, D. R. (1985). Late-Stage Komatiitic and Dacitic Volcanism in the Early Archean Barberton Greenstone Belt, South Africa.

In *Lunar and Planetary Science Conference, 16*, 101-102).

Byerly, G. R., Kröner, A., Lowe, D. R., Todt, W., & Walsh, M. M. (1996). Prolonged magmatism and time constraints for sediment deposition in the early Archean Barberton greenstone belt: evidence from the Upper Onverwacht and Fig Tree groups. *Precambrian Research*, *78*, 125-138.

Byerly, G. R., Lowe, D. R., & Heubeck, C. (2018). Geologic evolution of the Barberton Greenstone Belt–a unique record of crustal development, surface processes, and early life 3.55 to 3.20 Ga. *Earth's oldest rocks, 2nd edn. Elsevier, Berlin*.

Cabral, A. R., Zeh, A., Koglin, N., Gomes Jr, A. A. S., Viana, D. J., & Lehmann, B. (2012). Dating the Itabira iron formation, Quadrilátero Ferrífero of Minas Gerais, Brazil, at 2.65 Ga: depositional U–Pb age of zircon from a metavolcanic layer. *Precambrian Research*, *204*, 40-45.

Canfield, D. E., & Raiswell, R. (1999). The evolution of the sulfur cycle. *American Journal of Science*, *299*, 697-723.

Canfield, D. E., Habicht, K. S., & Thamdrup, B. O. (2000). The Archean sulfur cycle and the early history of atmospheric oxygen. *Science*, *288*, 658-661.

Carlson, R. W., Hunter, D. R., & Barker, F. (1983). Sm–Nd age and isotopic systematics of the bimodal suite, Ancient Gneiss Complex, Swaziland. *Nature*, *305*, 701.

Catling, D. C., Zahnle, K. J., & McKay, C. P. (2001). Biogenic methane, hydrogen escape, and the irreversible oxidation of early Earth. *Science*, *293*, 839-843.

Cawood, P. A., Kröner, A. & Pisarevsky, S. (2006). Precambrian plate tectonics: criteria and evidence. GSA Today 16, 4–11

Cawood, P. A., Hawkesworth, C. J., Pisarevsky, S. A., Dhuime, B., Capitanio, F. A., & Nebel, O. (2018). Geological archive of the onset of plate tectonics. *Philosophical Transactions of the Royal Society A: Mathematical, Physical and Engineering Sciences*, *376*, 593.

Chadwick, O. A., Derry, L. A., Vitousek, P. M., Huebert, B. J., & Hedin, L. O. (1999). Changing sources of nutrients during four million years of ecosystem development. *Nature*, *397*, 491-497.

Chardon, D., Choukroune, P., & Jayananda, M. (1996). Strain patterns, décollement and incipient sagducted greenstone terrains in the Archaean Dharwar craton (south India). *Journal of Structural Geology*, *18*, 991-1004.

Choukroune, P., Ludden, J. N., Chardon, D., Calvert, A. J., & Bouhallier, H. (1997). Archaean crustal growth and tectonic processes: a comparison of the Superior Province, Canada and the Dharwar Craton, India. *Geological Society, London, Special Publications*, *121*, 63-98.

Cnossen, I., Sanz-Forcada, J., Favata, F., Witasse, O., Zegers, T., & Arnold, N. F. (2007). Habitat of early life: Solar X-ray and UV radiation at Earth's surface 4–3.5 billion years ago. *Journal of Geophysical Research: Planets*, *112*. doi:10.1029/2006JE002784

Cobbold, P. R., & Quinquis, H. (1980). Development of sheath folds in shear regimes. *Journal of structural geology*, *2*, 119-126.

Cockell, C. S., & Horneck, G. (2001). The History of the UV Radiation Climate of the Earth—Theoretical and Space-based Observations. *Photochemistry and Photobiology*, *73*, 447-451.

Collins, W. J., Van Kranendonk, A. M., & Teyssier, C. (1998). Partial convective overturn of Archaean crust in the east Pilbara Craton, Western Australia: driving mechanisms and tectonic implications. *Journal of Structural Geology*, *20*, 1405-1424.

Compston, W., & Kröner, A. (1988). Multiple zircon growth within early Archaean tonalitic gneiss from the Ancient Gneiss Complex, Swaziland. *Earth and Planetary Science Letters*, *87*, 13-28.

Condie, K. C. (1986). Origin and early growth rate of continents. *Precambrian Research*, *32*, 261-278.

Condie, K. C. (2000). Episodic continental growth models: afterthoughts and extensions. *Tectonophysics*, *322*, 153-162.

Condie, K. C., Bickford, M. E., Aster, R. C., Belousova, E., & Scholl, D. W. (2011). Episodic zircon ages, Hf isotopic composition, and the preservation rate of continental crust. Geol. Soc. Am. *Bulletin*, *123*, 951-957.

Condie, K. C., & Benn, K. (2006). Archean geodynamics: similar to or different from modern geodynamics? *Geophysical Monograph – American Geophysical Union*, *164*, 47.

Condie, K. C., & Pease, V. (Eds.). (2008). *When did plate tectonics begin on planet Earth?* (Vol. 440). Geological Society of America.

Condie, K. C. (2018). A planet in transition: the onset of plate tectonics on Earth between 3 and 2 Ga? *Geoscience Frontiers*, *9*, 51-60.

Dahlstrom, C. D. A. (1969). Balanced cross sections. *Canadian Journal of Earth Sciences*, *6*(4), 743-757

Dahlstrom, C. D. (1990). Geometric Constraints Derived from the Law of Conservation of Volume and Applied to Evolutionary Models for Detachment Folding: Geologic Note:(1). *AAPG Bulletin*, *74*, 336-344.

Damasceno, D. R., Eckert, A., & Liu, X. (2017). Flexural-slip during visco-elastic buckle folding. *Journal of Structural Geology*, *100*, 62-76.

Daneel, G.J. (1987). The Structural Controls of Gold Mineralization in the Moodies Hills which surround the Agnes Gold Mine, Barberton Greenstone Belt. M.Sc. Thesis (unpublished), *University of Natal, Durban*, 129 pp..

Dann, J. C. (2000). The 3.5 Ga Komati Formation, Barberton greenstone belt, South Africa, part I: new maps and magmatic architecture. *South African Journal of Geology*, *103*, 47-68.

Darracott, B. W. (1975). The interpretation of the gravity-anomaly over the Barberton Mountain Land, South Africa. *South African Journal of Geology*, *78*, 123-128.

Debaille, V., O'Neill, C., Brandon, A. D., Haenecour, P., Yin, Q. Z., Mattielli, N., & Treiman, A. H. (2013). Stagnant-lid tectonics in early Earth revealed by 142Nd variations in late Archean rocks. *Earth and Planetary Science Letters*, *373*, 83-92.

De Beer, J. H., & Stettler, E. H. (1988). Geophysical characteristics of the southern African continental crust. *Journal of Petrology*, 1, 163-184.

De Beer, J., & Stettler, E. (2009, September). Geophysics and the deep structure of the barberton belt: a review. In *11th SAGA Biennial Technical Meeting and Exhibition*.

DeCelles, P. G., & Giles, K. A. (1996). Foreland basin systems. *Basin research*, *8*, 105-123.

De Ronde, C. E. J., Kamo, S., Davis, D. W., De Wit, M. J., & Spooner, E. T. C. (1991). Field, geochemical and U-Pb isotopic constraints from hypabyssal felsic intrusions within the Barberton greenstone belt, South Africa: Implications for tectonics and the timing of gold mineralization. *Precambrian Research*, *49*, 261-280.

De Ronde, C. E. J., Spooner, E. T. C., de Wit, M. J., & Bray, C. J. (1992). Shear zone-related, Au quartz vein deposits in the Barberton greenstone belt, South Africa; field and petrographic characteristics, fluid properties, and light stable isotope geochemistry. *Economic Geology*, *87*, 366-402.

De Ronde, C. E., & de Wit, M. J. (1994). Tectonic history of the Barberton greenstone belt, South Africa: 490 million years of Archean crustal evolution. *Tectonics*, *13*, 983-1005.

De Ronde, C. E., & Kamo, S. L. (2000). An Archean arc-arc collisional event: a short-lived (ca 3 Myr) episode, Weltevreden area, Barberton greenstone belt, South Africa. *Journal of African Earth Sciences*, *30*, 219-248.

De Wit, M. J. (1982). Gliding and overthrust nappe tectonics in the Barberton Greenstone Belt. *Journal of Structural Geology*, *4*, 117-136.

De Wit, M. J., Fripp, R. E. P., & Stanistreet, I. G. (1983). Tectonic and stratigraphic implications of new field observations along the southern part of the Barberton greenstone belt. *Spec. Publ. Geol. Soc. S. Afr.*, *9*, 21-29.

De Wit, M. J., Hart, R. A., & Hart, R. J. (1987). The Jamestown Ophiolite Complex, Barberton mountain belt: a section through 3.5 Ga oceanic crust. *Journal of African Earth Sciences (1983)*, *6*, 681-730.

De Wit, M. J. (1991). Archaean greenstone belt tectonism and basin development: some insights from the Barberton and Pietersburg greenstone belts, Kaapvaal Craton, South Africa. *Journal of African Earth Sciences (and the Middle East)*, *13*, 45-63.

De Wit, M. J., de Ronde, C. E., Tredoux, M., Roering, C., Hart, R. J., Armstrong, R. A., Green, R. W. E., Peberdy, E. & Hart, R. A. (1992). Formation of an Archaean continent. *Nature*, *357*, 553.

De Wit, M. J., & Hart, R. A. (1993). Earth's earliest continental lithosphere, hydrothermal flux and crustal recycling. *Lithos*, *30*, 309-335.

De Wit, M. J., Furnes, H., & Robins, B. (2011). Geology and tectonostratigraphy of the Onverwacht Suite, Barberton greenstone belt, South Africa. *Precambrian Research*, *186*, 1-27.

De Wit, M., Furnes, H., MacLennan, S., Doucouré, M., Schoene, B., Weckmann, U., Martinez, U., & Bowring, S. (2018). Paleoarchean bedrock lithologies across the Makhonjwa Mountains of South Africa and Swaziland linked to geochemical, magnetic and tectonic data reveal early plate tectonic genes flanking subduction margins. *Geoscience Frontiers*, *9*, 603-665.

Dhuime, B., Hawkesworth, C. J., Cawood, P. A., & Storey, C. D. (2012). A change in the geodynamics of continental growth 3 billion years ago. *Science*, *335*, 1334-1336.

Diener, J. F., Stevens, G., Kisters, A. F., & Poujol, M. (2005). Metamorphism and exhumation of the basal parts of the Barberton greenstone belt, South Africa: Constraining the rates of Mesoarchaean tectonism. *Precambrian Research*, *143*, 87-112.

Dirks, P. H. G. M., Charlesworth, E. G., & Munyai, M. R. (2009). Cratonic extension and Archaean gold mineralisation in the Sheba-Fairview mine, Barberton greenstone belt, South Africa. *South African Journal of Geology*, *112*, 291-316.

Dirks, P. H., Charlesworth, E. G., Munyai, M. R., & Wormald, R. (2013). Stress analysis, post-orogenic extension and 3.01 Ga gold mineralisation in the Barberton Greenstone Belt, South Africa. *Precambrian Research*, *226*, 157-184.

Dong, C., Xie, H., Kröner, A., Wang, S., Liu, S., Xie, S., Song, Z., Ma, M., Liu, D. & Wan, Y. (2017). The complexities of zircon crystllazition and overprinting during metamorphism and anatexis: An example from the late Archean TTG terrane of western Shandong Province, China. *Precambrian Research*, *300*, 181-200.

Drabon, N., Galić, A., Mason, P. R., & Lowe, D. R. (2019). Provenance and tectonic implications of the 3.28–3.23 Ga Fig Tree Group, central Barberton greenstone belt, South Africa. *Precambrian Research*, *325*, 1-19.

Drummond, B. J., Goleby, B. R., & Swager, C. P. (2000). Crustal signature of Late Archaean tectonic episodes in the Yilgarn craton, Western Australia: evidence from deep seismic sounding. *Tectonophysics*, *329*, 193-221.

Duebendorfer, E. M., & Wallin, E. T. (1991). Basin development and syntectonic sedimentation associated with kinematically coupled strike-slip and detachment faulting, southern Nevada. *Geology*, *19*, 87-90.

Dumoulin, C., Doin, M. P., & Fleitout, L. (1999). Heat transport in stagnant lid convection with temperature-and pressure-dependent Newtonian or non-Newtonian rheology. *Journal of Geophysical Research: Solid Earth*, *104*, 12759-12777.

Dziggel, A., Stevens, G., Poujol, M., Anhaeusser, C. R., & Armstrong, R. A. (2002). Metamorphism of the granite–greenstone terrane south of the Barberton greenstone belt, South Africa: an insight into the tectono-thermal evolution of the 'lower'portions of the Onverwacht Group. *Precambrian Research*, *114*, 221-247.

Dziggel, A., Knipfer, S., Kisters, A. F., & Meyer, F. M. (2006). P–T and structural evolution during exhumation of high-T, medium-P basement rocks in the Barberton Mountain Land, South Africa. *Journal of Metamorphic Geology*, *24*, 535-551.

Dziggel, A., Poujol, M., Otto, A., Kisters, A. F., Trieloff, M., Schwarz, W. H., & Meyer, F. M. (2010). New U–Pb and 40Ar/39Ar ages from the northern margin of the Barberton greenstone belt, South Africa: implications for the formation of Mesoarchaean gold deposits. *Precambrian Research*, *179*, 206-220

Eglington, B. M., & Armstrong, R. A. (2004). The Kaapvaal Craton and adjacent orogens, southern Africa: a geochronological database and overview of the geological development of the craton. *South African Journal of Geology*, *107*, 13-32.

Engelhardt, J. (2012). Constraints from high-resolution zircon geochronology on age and provenance of the Archean Moodies Group, Barberton Greenstone Belt, South Africa. M.Sc. thesis (unpublished), *Freie Universität Berlin, 82 pp*.

Eriksson, K. A. (1977). A paleoenvironmental analysis of the Archaean Moodies Group. Barberton Mountain Land, South Africa. Ph. D. thesis (unpublished) *Johannesburg, University of the Witwatersrand*.

Eriksson, K. A. (1979). Marginal marine depositional processes from the Archaean Moodies group, Barberton Mountain land, South Africa: evidence and significance. *Precambrian Research*, *8*, 153-182.

Eriksson, K. A. (1980). Transitional sedimentation styles in the Moodies and Fig Tree Groups, Barberton mountain land, South Africa: evidence favouring an Archean continental margin. *Precambrian Research*, *12*, 141-160.

Eriksson, K. A. (1982). Sedimentation patterns in the Barberton Mountain Land, South Africa, and the Pilbara Block, Australia: evidence for Archean rifted continental margins. *Tectonophysics*, *81*, 179-193.

Eriksson, K. A., Krapez, B., & Fralick, P. W. (1994). Sedimentology of Archean greenstone belts: signatures of tectonic evolution. *Earth-Science Reviews*, *37*, 1-88.

Ernst, W. G. (2009). Archean plate tectonics, rise of Proterozoic supercontinentality and onset of regional, episodic stagnant-lid behavior. *Gondwana Research*, *15*, 243-253.

Eskola, P. E. (1949). The problem of mantled gneiss domes. *Geological Society of London Quarterly Journal, 104.*

Evans, D. A. D., Pisarevsky, S. A. (2008). Plate tectonics on early Earth? Weighing the paleomagnetic evidence. In When did plate tectonics begin on planet earth? (eds Condie KC, Pease V.), pp. 249–263. Boulder, CO: Geological Society of America

Farquhar, J., Bao, H., & Thiemens, M. (2000). Atmospheric influence of Earth's earliest sulfur cycle. *Science*, *289*, 756-758.

Fischer, W. W., Schroeder, S., Lacassie, J. P., Beukes, N. J., Goldberg, T., Strauss, H., Horstmann, U. E., Schrag, D. P. & Knoll, A. H. (2009). Isotopic constraints on the Late Archean carbon cycle from the Transvaal Supergroup along the western margin of the Kaapvaal Craton, South Africa. *Precambrian Research*, *169*, 15-27.

Fischer, M. P., & Jackson, P. B. (1999). Stratigraphic controls on deformation patterns in fault-related folds: a detachment fold example from the Sierra Madre Oriental, northeast Mexico. *Journal of Structural Geology*, *21*, 613-633.

Fischer, R., & Gerya, T. (2016a). Early Earth plume-lid tectonics: A high-resolution 3D numerical modelling approach. *Journal of Geodynamics*, *100*, 198-214.

Fischer, R., & Gerya, T. (2016b). Regimes of subduction and lithospheric dynamics in the Precambrian: 3D thermomechanical modelling. *Gondwana Research*, *37*, 53-70.

Friend, C. R. L., & Nutman, A. P. (2001). U–Pb zircon study of tectonically bounded blocks of 2940–2840 Ma crust with different metamorphic histories, Paamiut region, South-West Greenland: implications for the tectonic assembly of the North Atlantic craton. *Precambrian Research*, *105*, 143-164.

Fripp, R. E. P., Van Nierop, D. A., Callow, M. J., Lilly, P. A., & Du Plessis, L. U. (1980). Deformation in part of the Archaean Kaapvaal craton, South Africa. *Precambrian Research*, *13*, 241-251.

Gay, N. C. (1969). The analysis of strain in the Barberton Mountain Land, Eastern Transvaal, using deformed pebbles. *The Journal of Geology*, *77*, 377-396.

Gerya, T. (2014). Precambrian geodynamics: concepts and models. *Gondwana Res*., *25*, 442–463

Gibson, R. G., & Gray, D. R. (1985). Ductile-to-brittle transition in shear during thrust sheet emplacement, Southern Appalachian thrust belt. *Journal of structural geology*, *7*, 513-525.

Glikson, A. Y. & Pirajno, F. (2018). Asteroids and Crustal Evolution. In *Asteroids Impacts, Crustal Evolution and Related Mineral Systems with Special Reference to Australia* (pp. 157-171). Springer, Cham.

Goodwin, A. M. (2016). Precambrian geology: the dynamic evolution of the continental crust. *Elsevier.*

Griffin, W. L., Belousova, E. A., Shee, S. R., Pearson, N. J., & O'reilly, S. Y. (2004). Archean crustal evolution in the northern Yilgarn Craton: U–Pb and Hf-isotope evidence from detrital zircons. *Precambrian Research*, *131*, 231-282.

Grosch, E., McLoughlin, N., de Wit, M., & Furnes, H. (2009). Drilling for the Archean roots of life and tectonic Earth in the Barberton Mountains. *Scientific Drilling*, 8, 24-28.

Grosch, E. G., Kosler, J., McLoughlin, N., Drost, K., Slama, J., & Pedersen, R. B. (2011). Paleoarchean detrital zircon ages from the earliest tectonic basin in the Barberton Greenstone Belt, Kaapvaal craton, South Africa. *Precambrian Research*, *191*, 85-99.

Grosch, E. G., Vidal, O., Abu-Alam, T., & McLoughlin, N. (2012). P–T constraints on the metamorphic evolution of the Paleoarchean Kromberg type-section, Barberton Greenstone Belt, South Africa. *Journal of Petrology*, *53*, 513-545.

Grosch, E. G., & McLoughlin, N. (2013). Paleoarchean sulfur cycle and biogeochemical surface conditions on the early Earth, Barberton,

South Africa. *Earth and Planetary Science Letters*, *377*, 142-154.

Grosch, E. G., & Slama, J. (2017). Evidence for 3.3-billion-year-old oceanic crust in the Barberton greenstone belt, South Africa. *Geology*, *45*, 695-698.

Gumsley, A. P., Chamberlain, K. R., Bleeker, W., Söderlund, U., de Kock, M. O., Larsson, E. R., & Bekker, A. (2017). Timing and tempo of the Great Oxidation Event. *Proceedings of the National Academy of Sciences*, *114*, 1811-1816.

Hall, A. L. (1918). The geology of the Barberton gold mining district, including adjoining portions of Northern Swaziland. *Geological Society of South Africa, Memoir No. 16.*

Harris, P. O., Robb, L. J., & Tomkinson, M. J. (1995). The nature and structural setting of rare-element pegmatites along the northern flank of the Barberton greenstone belt, South Africa. *South African Journal of Geology*, *98*, 82-94.

Hawkesworth, C., Cawood, P., & Dhuime, B. (2013). Continental growth and the crustal record. *Tectonophysics*, *609*, 651-660.

Heam, M. G. (1943). A study of the working properties of the chief gold producer of the Barberton district, eastern Transvaal. D. Sc. Thesis (unpublished). *University of the Witwatersrand, Johannesburg.*

Heinrichs, T. K., & Reimer, T. O. (1977). A sedimentary baryte deposit from the Archean Fig Tree Group of the Barberton Mountain Land (South Africa). *Economic Geology, 72*, 1426-1441.

Hessler, A. M., & Lowe, D. R. (2006). Weathering and sediment generation in the Archean: an integrated study of the evolution of siliciclastic sedimentary rocks of the 3.2 Ga Moodies Group, Barberton Greenstone Belt, South Africa. *Precambrian Research*, *151*, 185-210.

Heubeck, C., Wendt, J. I., Toulkeridis, T., Kröner, A., & Lowe, D. R. (1993). Timing of deformation of the Archaean Barberton greenstone belt, South Africa: Constraints from zircon dating of the Salisbury Kop pluton. *South African Journal of Geology*, *96*, 1-8.

Heubeck, C., & Lowe, D. R. (1994a). Late syndepositional deformation and detachment tectonics in the Barberton Greenstone Belt, South Africa. *Tectonics*, *13*, 1514-1536.

Heubeck, C., & Lowe, D. R. (1994b). Depositional and tectonic setting of the Archean Moodies Group, Barberton greenstone belt, South Africa. *Precambrian Research*, *68*, 257-290.

Heubeck, C., Engelhardt, J., Byerly, G. R., Zeh, A., Sell, B., Luber, T., & Lowe, D. R. (2013). Timing of deposition and deformation of the Moodies Group (Barberton Greenstone Belt, South Africa): Very-high-resolution of Archaean surface processes. *Precambrian Research*, *231*, 236-262.

Heubeck, C. (2019). The Moodies Group—a High-Resolution Archive of Archaean Surface Processes and Basin-Forming Mechanisms. In *The Archaean Geology of the Kaapvaal Craton, Southern Africa* (pp. 133-169). Springer, Cham.

Heubeck, C., Biasing, S., Grund, M., Drabon, N., Homann, M., & Nabhan, S. (2016). Geological constraints on Archean (3.22 Ga) coastal-zone processes from the Dycedale Syncline, Barberton greenstone belt. *South African Journal of Geology 2016*, *119*, 495-518.

Hofmann, A. (2005). The geochemistry of sedimentary rocks from the Fig Tree Group, Barberton greenstone belt: implications for tectonic, hydrothermal and surface processes during mid-Archaean times. *Precambrian Research*, *143*, 23-49.

Hoffmann, J. E., & Kröner, A. (2018). Early Archaean crustal evolution in southern Africa—an updated record of the Ancient Gneiss Complex of Swaziland. *Earth's oldest rocks, 2nd edn. Elsevier, Amsterdam*, 553-567.

Homann, M., Heubeck, C., Airo, A., & Tice, M. M. (2015). Morphological adaptations of 3.22 Ga-old tufted microbial mats to Archean coastal habitats (Moodies Group, Barberton Greenstone Belt, South Africa). *Precambrian Research*, *266*, 47-64.

Hunter, D. R. (1957). The geology, petrology and classification of the Swaziland granites and gneisses. *South African Journal of Geology*, *60*, 85-120.

Hunter, D. R. (1961). The geological evolution of Swaziland during the Precambrian. *Bull. Geol. Surv*, *1*, 29-32.

Hunter, D. R., & Jones, D. H. (1969). Geological map of Swaziland, 1**:** 25,000, series, Sheet 2 Piggs Peak.

Hunter, D. R. (1970). The ancient gneiss complex in Swaziland. *South African Journal of Geology*, *73*, 107-150.

Hunter, D. R., Barker, F., & Millard Jr, H. T. (1978). The geochemical nature of the Archean Ancient Gneiss Complex and Granodiorite Suite, Swaziland: a preliminary study. *Precambrian Research*, *7*, 105-127.

Hunter, D. R., & Wilson, A. H. (1988). A continuous record of Archaean evolution from 3, 5 Ga to 2, 6 Ga in Swaziland and northern Natal. *South African Journal of Geology*, *91*, 57-74.

Jackson, M. P. A., & Robertson, D. I. (1983). Regional implications of Early Precambrian strains in the Onverwacht Group adjacent to the Lochiel granite, north-west Swaziland. *Contributions to the Geology of the Barberton Mountain Land. Special Publication of the Geological Society of South Africa*, *9*, 45-62.

Jackson, M. P. A., Kröner, A., & Greiling, R. (1984). Archaean structural styles in the Ancient Gneiss Complex of Swaziland, southern Africa. *Precambrian Tectonics Illustrated*, 1-18

Jackson, M. P. A., Eriksson, K. A., & Harris, C. W. (1987). Early Archean foredeep sedimentation related to crustal shortening: a reinterpretation of the Barberton Sequence, southern Africa. *Tectonophysics*, *136*, 197-221.

Johnson, A. M., & Pfaff, V. J. (1989). Parallel, similar and constrained folds. *Engineering Geology*, *27*, 115-180.

Kamo, S. L., & Davis, D. W. (1994). Reassessment of Archean crustal development in the Barberton Mountain Land, South Africa, based on U-Pb dating. *Tectonics*, *13*, 167-192

Kay, M. (1951). North American geosynclines: Geol. Soc. *Am, Mem, 48: 1*, *143*.

Keller, B., & Schoene, B. (2018). Plate tectonics and continental basaltic geochemistry throughout Earth history. *Earth Planet. Sci. Lett., 481*, 290–304

King, L. H., & Young, I. F. (1977). Paleocontinental slopes of east coast geosyncline (Canadian Atlantic margin). *Canadian Journal of Earth Sciences*, *14*, 2553-2564

Kisters, A. F., & Anhaeusser, C. R. (1995). Emplacement features of Archaean TTG plutons along the southern margin of the Barberton greenstone belt, South Africa. *Precambrian Research*, *75*, 1-15.

Kisters, A. F., Stevens, G., Dziggel, A., & Armstrong, R. A. (2003). Extensional detachment faulting and core-complex formation in the southern Barberton granite–greenstone terrain, South Africa: evidence for a 3.2 Ga orogenic collapse. *Precambrian Research*, *127*, 355-378.

Kisters, A. F., Belcher, R. W., Poujol, M., & Dziggel, A. (2010). Continental growth and convergence-related arc plutonism in the Mesoarchaean: Evidence from the Barberton granitoid-greenstone terrain, South Africa. *Precambrian Research*, *178*, 15-26.

Klein, B. Z., Jagoutz, O., & Behn, M. D. (2017). Archean crustal compositions promote full mantle convection. *Earth and Planetary Science Letters*, *474*, 516-526.

Kohler, E.A. (2003). The geology of the Archaean granitoid-greenstone terrane in the vicinity of Three Sisters, Barberton Greenstone Belt: report on mapping and geological studies between 1990 and 1994. Council for Geoscience, 2003 Physical description: vi, 150 p.: ill. (some col.), maps; 30 cm. Series Bulletin (Council for Geoscience (South Africa)); 133.

Kröner, A., Compston, W., Tegtmeyer, A., Milisenda, C., & Liew, T. C. (1988). Growth of early Archaean crust in the Ancient Gneiss Complex of Swaziland and adjacent Barberton greenstone belt, southern Africa. In *Workshop on the Growth of Continental Crust* (p. 85).

Kröner, A., Compston, W., & Williams, I. S. (1989). Growth of early Archaean crust in the Ancient Gneiss Complex of Swaziland as revealed by single zircon dating. *Tectonophysics*, *161*, 271-298.

Kröner, A. (1991). Tectonic evolution in the Archaean and Proterozoic. *Tectonophysics*, *187*, 393-410.

Kröner, A., & Layer, P. W. (1992). Crust formation and plate motion in the early Archean. *Science*, *256*, 1405-1411.

Kröner, A., Hegner, E., Wendt, J. I., & Byerly, G. R. (1996). The oldest part of the Barberton granitoid-greenstone terrain, South Africa: evidence for crust formation between 3.5 and 3.7 Ga. *Precambrian Research*, *78*, 105-124.

Kröner, A., Anhaeusser, C. R., Hoffmann, J. E., Wong, J., Geng, H., Hegner, E., Xie, H., Yang, J. & Liu, D. (2016). Chronology of the oldest supracrustal sequences in the Palaeoarchaean Barberton Greenstone Belt, South Africa and Swaziland. *Precambrian Research*, *279*, 123-143.

Kröner, A., Hoffmann, J. E., Wong, J. M., Geng, H. Y., Schneider, K. P., Xie, H., Yang, J. H., & Nhleko, N. (2019). Archaean Crystalline Rocks of the Eastern Kaapvaal Craton. In *The Archaean Geology of the Kaapvaal Craton, Southern Africa*. Springer, Cham.

Lamb, S. H. (1984). Structures on the eastern margin of the Archaean Barberton greenstone belt, northwest Swaziland. *Precambrian Tectonics Illustrated*, 19-39.

Lamb, S. H., & Paris, I. (1988). Post-onverwacht group stratigraphy in the SE part of the Archaean Barbeton greenstone belt. *Journal of African Earth Sciences (and the Middle East)*, *7*, 285-306.

Lana, C., Kisters, A., & Stevens, G. (2010). Exhumation of Mesoarchean TTG gneisses from the middle crust: Insights from the Steynsdorp core complex, Barberton granitoid-greenstone terrain, South Africa. *Bulletin*, *122*, 183-197.

Lana, C., Buick, I., Stevens, G., Rossouw, R., & De Wet, W. (2011). 3230–3200 Ma post-orogenic extension and mid-crustal magmatism along the southeastern margin of the Barberton Greenstone Belt, South Africa. *Journal of Structural Geology*, *33*, 844-858.

Laurent, O., Martin, H., Moyen, J. F., & Doucelance, R. (2014). The diversity and evolution of late-Archean granitoids: Evidence for the onset of "modern-style" plate tectonics between 3.0 and 2.5 Ga. *Lithos*, *205*, 208-235.

Layer, P. W., Kröner, A., McWilliams, M., & York, D. (1989). Elements of the Archean thermal history and apparent polar wander of the eastern Kaapvaal Craton, Swaziland, from single grain dating and paleomagnetism. *Earth Planet. Sci. Lett.* 93, 23–34

Lin, S. (2005). Synchronous vertical and horizontal tectonism in the Neoarchean: Kinematic evidence from a synclinal keel in the northwestern Superior craton, Canada. *Precambrian Research*, *139*, 181-194.

Lowe, D. R., Byerly, G. R., Ransom, B. L., & Nocita, B. W. (1985). Stratigraphic and sedimentological evidence bearing on structural repetition in early Archean rocks of the Barberton greenstone belt, South Africa. *Precambrian research*, *27*, 165-186.

Lowe, D. R. (1994). Accretionary history of the Archean Barberton greenstone belt (3.55-3.22 Ga), southern Africa. *Geology*, *22*, 1099-1102.

Lowe, D.R. (1999). Geologic evolution of the Barberton greenstone belt and vicinity. In: Lowe, D.R. and Byerly, G.R. (eds.), Geologic Evolution of the Barberton Greenstone Belt, South Africa. Special Paper, Geological Society of America 329, 287-312.

Lowe, D. R., & Byerly, G. R. (1999). Stratigraphy of the west-central part of the Barberton Greenstone Belt, South Africa. *Special Papers-Geological Society of America*, 1-36.

Lowe, D. R., Byerly, G. R., & Heubeck, C. (1999). Structural divisions and development of the west-central part of the Barberton Greenstone Belt. *Special Papers-Geological Society of America*, 37-82.

Lowe, D. R., & Byerly, G. R. (2007). An overview of the geology of the Barberton Greenstone Belt and vicinity: implications for early crustal development. *Developments in Precambrian Geology*, *15*, 481-526.

Lowe, D. R., Byerly, G. R., & Heubeck, C. (2012). Geologic map of the west-central Barberton Greenstone Belt, South Africa. *Geological Society of America.*

Lowe, D. R., Byerly, G. R., & Kyte, F. T. (2014). Recently discovered 3.42–3.23 Ga impact layers, Barberton Belt, South Africa: 3.8 Ga detrital zircons, Archean impact history, and tectonic implications. *Geology*, *42*, 747-750.

Lowe, D. R., & Byerly, G. R. (2018). The terrestrial record of Late Heavy Bombardment. *New Astronomy Reviews*, 81, 39-61.

Lüning, S., Marzouk, A. M., Morsi, A. M., & Kuss, J. (1998). Sequence stratigraphy of the Upper Cretaceous of central-east Sinai, Egypt. *Cretaceous Research*, *19*, 153-196.

Lyons, T. W., Reinhard, C. T., & Planavsky, N. J. (2014). The rise of oxygen in Earth's early ocean and atmosphere. *Nature*, *506*, 307.

Macgregor, A. M. (1951). Some milestones in the Precambrian of Southern Rhodesia. *Proceedings of the Geological Society of South Africa*, *54*, 27-71.

Martin, H. (1986). Effect of steeper Archean geothermal gradient on geochemistry of subduction-zone magmas. *Geology*, *14*, 753-756.

Matsumura, R. (2014). The petrogenesis of the Nelshoogte pluton: The youngest and most compositionally variable TTG pluton in the Barberton Granite-Greenstone Terrain. Doctoral Thesis (unpublished) *Stellenbosch University, Stellenbosch.*

Moresi, L., & Solomatov, V. (1998). Mantle convection with a brittle lithosphere: thoughts on the global tectonic styles of the Earth and Venus. *Geophys. J. Int., 133*, 669–682.

Moyen, J. F., Stevens, G., & Kisters, A. (2006). Record of mid-Archaean subduction from metamorphism in the Barberton terrain, South Africa. *Nature*, *442*, 559.

Moyen, J. F., Stevens, G., Kisters, A. F., & Belcher, R. W. (2007). TTG plutons of the Barberton granitoid-greenstone terrain, South Africa. *Developments in Precambrian Geology*, *15*, 607-667.

Moyen, J.-F., Stevens, G., Kisters, A. F. M. & Belcher, B. L. (2018). TTG plutons of the Barberton Granitoid-Greenstone Terrain, South Africa. *Earth's oldest rocks, 2nd edn. Elsevier, Berlin*.

Munyai, M. R., Dirks, P. H. G. M., & Charlesworth, E. G. (2011). Archaean gold mineralisation during post-orogenic extension in the New Consort gold mine, Barberton greenstone belt, South Africa. *South African Journal of Geology*, *114*, 121-144.

Murphy, R. C. L. (2015). Stabilising a Craton: The origin and emplacement of the 3.1 Ga Mpuluzi Batholith. PhD thesis (unpublished) *Macquarie University, Sydney*

Nabhan, S., Luber, T., Scheffler, F., & Heubeck, C. (2016). Climatic and geochemical implications of Archean pedogenic gypsum in the Moodies group (~ 3.2 Ga), Barberton Greenstone Belt, South Africa. *Precambrian Research*, *275*, 119-134.

Nédélec, A., Chevrel, M. O., Moyen, J. F., Ganne, J., & Fabre, S. (2012). TTGs in the making: Natural evidence from Inyoni shear zone (Barberton, South Africa). *Lithos*, *153*, 25-38.

Nelson, D. R., Trendall, A. F., & Altermann, W. (1999). Chronological correlations between the Pilbara and Kaapvaal cratons. *Precambrian Research*, *97*, 165-189.

Nicoli, G., Stevens, G., Buick, I., & Moyen, J. F. (2014). A comment on ultrahigh-temperature metamorphism from an unusual corundum+ orthopyroxene intergrowth bearing Al–Mg granulite from the Southern Marginal Zone, Limpopo Complex, South Africa, by Belyanin et al. *Contributions to mineralogy and petrology*, *167*, 1022.

Nocita, B. W., & Lowe, D. R. (1990). Fan-delta sequence in the Archean Fig Tree Group, Barberton Greenstone Belt, South Africa. *Precambrian Research*, *48*, 375-393.

Nutman, A. P., & Collerson, K. D. (1991). Very early Archean crustal-accretion complexes preserved in the North Atlantic craton. *Geology*, *19*, 791-794

Olsson, J. R., Söderlund, U., Klausen, M. B., & Ernst, R. E. (2010). U–Pb baddeleyite ages linking major Archean dyke swarms to volcanic-rift forming events in the Kaapvaal craton (South Africa), and a precise age for the Bushveld Complex. *Precambrian Research*, *183*, 490-500.

Otto, A., Dziggel, A., Kisters, A. F. M., & Meyer, F. M. (2007). The New Consort Gold Mine, Barberton greenstone belt, South Africa: orogenic gold mineralization in a condensed metamorphic profile. *Mineralium Deposita*, *42*, 715-735.

Pearce, J. A. (2008). Geochemical fingerprinting of oceanic basalts with applications to ophiolite classification and the search for Archean oceanic crust. *Lithos, 100*, 14–48.

Peck, W. H., Valley, J. W., Wilde, S. A., & Graham, C. M. (2001). Oxygen isotope ratios and rare earth elements in 3.3 to 4.4 Ga zircons: Ion microprobe evidence for high δ18O continental crust and oceans in the Early Archean. *Geochimica et Cosmochimica Acta*, *65*, 4215-4229.

Percival, J. A., Stern, R. A., Skulski, T., Card, K. D., Mortensen, J. K., & Begin, N. J. (1994). Minto block, Superior province: Missing link in deciphering assembly of the craton at 2.7 Ga. *Geology*, *22*, 839-842.

Percival, J. A., McNicoll, V., Brown, J. L., & Whalen, J. B. (2004). Convergent margin tectonics, central Wabigoon subprovince, Superior Province, Canada. *Precambrian Research*, *132*, 213-244.

Pierson, B. K., Mitchell, H. K., & Ruff-Roberts, A. L. (1993). Chloroflexus aurantiacus and ultraviolet radiation: implications for Archean shallow-water

stromatolites. *Origins of Life and Evolution of the Biosphere*, *23*, 243-260.

Piper, J. D. (2013). A planetary perspective on Earth evolution: lid tectonics before plate tectonics. *Tectonophysics*, *589*, 44-56.

Pollack, H. N. (1986). Cratonization and thermal evolution of the mantle. *Earth and Planetary Science Letters*, *80*, 175-182.

Ramsay, J. G. (1963). Structural investigations in the Barberton Mountian land, Eastern Transvaal. *South African Journal of Geology*, *66*, 353-401.

Ramsay, J. G. (1967). Folding and fracturing of rocks. *Mc Graw Hill Book Company*.

Reese, C. C., Solomatov, V. S., & Moresi, L. N. (1998). Heat transport efficiency for stagnant lid convection with dislocation viscosity: Application to Mars and Venus. *Journal of Geophysical Research: Planets*, *103*, 13643-13657.

Reimer, T.O. (1967). Die Geologie der Stolzburg-Synklinale im Barberton Bergland (Transvaal-Südafrika). Ph.D. Thesis (unphblished) *Goethe-Universität, Frankfurt am Main*.

Reimer, T.O. (1971). Kanu-Falten - ein ungewöhnlicher Faltentyp aus geringmetamorphen präkambrischen Sedimenten. *Neues Jahrbuch für Geologie und Paläontologie, Monatshefte*, 1971, 489-495.

Robb, L. J., Barton Jr, J. M., Kable, E. J. D., & Wallace, R. C. (1986). Geology, geochemistry and isotopic characteristics of the Archaean Kaap Valley pluton, Barberton mountain land, South Africa. *Precambrian Research*, *31*, 1-36.

Roering, C. (1965). The tectonics of the main gold-producing area of the Barberton Mountain Land. *University of the Witwatersrand, Economic Geology Research Unit*.

S.A.C.S. (South African Committee for Stratigraphy). 1980. Stratigraphy of South Africa. part 1. Litho-stratigraphy of the Republic of South Africa, South West Africa Namibia, and the Republics of Bophuthatswana, Transkei and Venda. *S. Afr. Geol. Surv. Handbook. No. 8*.

Schoene, B., de Wit, M. J., & Bowring, S. A. (2008). Mesoarchean assembly and stabilization of the eastern Kaapvaal craton: A structural-thermochronological perspective. *Tectonics*, *27*, TC5010.

Schoene, B., Dudas, F. O., Bowring, S. A., & De Wit, M. (2009). Sm–Nd isotopic mapping of lithospheric growth and stabilization in the eastern Kaapvaal craton. *Terra Nova*, *21*, 219-228.

Schoene, B., & Bowring, S. A. (2010). Rates and mechanisms of Mesoarchean magmatic arc construction, eastern Kaapvaal craton, Swaziland. Geol. Soc. Am. *Bull.*, *122*, 408-429.

Shirey, S. B., Kamber, B. S., Whitehouse, M. J., Mueller, P. A., & Basu, A. R. (2008). A review of the isotopic and trace element evidence for mantle and crustal processes in the Hadean andArchean: Implications for the onset of plate tectonic subduction. *When did plate tectonics begin on planet Earth?*, *440*, 1.

Sizova, E., Gerya, T., Brown, M., & Perchuk, L. L. (2010). Subduction styles in the Precambrian: Insight from numerical experiments. *Lithos*, *116*, 209-229.

Sizova, E., Gerya, T., Brown, M., & Stüwe, K. (2018). What drives metamorphism in early Archean greenstone belts? Insights from numerical modeling. *Tectonophysics*, *746*, 587-601.

Skjernaa, L. (1989). Tubular folds and sheath folds: definitions and conceptual models for their development, with examples from the Grapesvare area, northern Sweden. *Journal of Structural Geology*, *11*, 689-703.

Sleep, N. H. (2018). Geological and geochemical constraints on the origin and evolution of life. *Astrobiology*, *18*, 1199-1219.

Solomatov, V. S., & Moresi, L. N. (1997). Three regimes of mantle convection with non-Newtonian viscosity and stagnant lid convection on the terrestrial planets. *Geophys. Res. Lett., 24*, 1907–1910.

Stern, R. J. (2007). When and how did plate tectonics begin? Theoretical and empirical considerations. *Chinese Science Bulletin*, *52*, 578-591.

Stern, R. J. (2008). Modern-style plate tectonics began in Neoproterozoic time: An alternative interpretation of Earth's tectonic history. *When did plate tectonics begin on planet Earth*, *440*, 265-280.

Stettler, J. H., & Plessis, H, D. (1988). The structure of the Pietersburg greenstone belt, South Africa, as

derived from geophysics. *South African journal of geology*, *91*, 292-303.

Stevens, G., Droop, G. T. R., Armstrong, R. A., & Anhaeusser, C. R. (2002). Amphibolite facies metamorphism in the Schapenburg schist belt: A record of the mid-crustal response to~ 3.23 Ga terrane accretion in the Barberton greenstone belt. *South African Journal of Geology*, *105*, 271-284.

Stevens, G., & Moyen, J. F. (2007). .7 Metamorphism in the Barberton Granite Greenstone Terrain: A Record of Paleoarchean Accretion. *Developments in precambrian geology*, *15*, 669-698.

Stutenbecker, L., Heubeck, C., & Zeh, A. (2019). The Lomati Delta Complex: A prograding tidal delta in the Archean Moodies Group, Barberton Greenstone Belt. *South African Journal of Geology, 122, 17-38.*

Sundquist, E. T., & Broecker, W. S. (1985). The carbon cycle and atmospheric CO2: Natural variations archean to present; Proceedings of the Chapman Conference on Natural Variations in Carbon Dioxide and the Carbon Cycle, Tarpon Springs, FL, January 9-13, 1984. *Washington DC American Geophysical Union Geophysical Monograph Series*, *32*.

Tankard, A. J., Jackson, M. P. A., Eriksson, K. A., Hobday, D. K., Hunter, D. R., & Minter, W. E. L. (1982). Granite-Greenstone Terrane: Kaapvaal Province. In *Crustal Evolution of Southern Africa* (pp. 21-86). Springer, New York, NY.

Tackley, P. J. (1998). Self-consistent generation of tectonic plates in three-dimensional mantle convection. *Earth Planet. Sci. Lett., 157,* 9–22.

Teson, E., & Teixell, A. (2008). Sequence of thrusting and syntectonic sedimentation in the eastern Sub-Atlas thrust belt (Dades and Mgoun valleys, Morocco). *International Journal of Earth Sciences*, *97*, 103-113.

Tian, F., Toon, O. B., Pavlov, A. A., & De Sterck, H. (2005). A hydrogen-rich early Earth atmosphere. *Science*, *308*, 1014-1017.

Toulkeridis, T., Goldstein, S. L., Clauer, N., Kröner, A., Todt, W., & Schidlowski, M. (1998). Sm–Nd, Rb–Sr and Pb–Pb dating of silicic carbonates from the early Archaean Barberton Greenstone Belt, South Africa: evidence for post-depositional isotopic resetting at low temperature. *Precambrian Research*, *92*, 129-144.

Urie, J. G. (1965). A reconnaissance structural investigation in the Forbes Reef area, Swaziland. In *Presented at 8th Ann. Congr. Geol. Soc.*.

Urie, J. G. (1970). Geological map series (1: 25,000) Sheet 3, Forbes Reef. *Swaziland Geol Surv Mines Dept (Mbabane)*.

Van Eeden, O. R. (1941). Die Geologie van die Shebarante en Omstreke, Distrik Barberton. Doctoral Thesis (unpublished), *University of Stellenbosch, Stellenbosch*.

Van Kranendonk, M. J., & Collins, W. J. (1998). Timing and tectonic significance of late Archaean, sinistral strike-slip deformation in the central Pilbara structural corridor, Pilbara Craton, Western Australia. *Precambrian Research*, *88*, 207-232.

Van Kranendonk, M. J., Hickman, A. H., Smithies, R. H., Nelson, D. R., & Pike, G. (2002). Geology and tectonic evolution of the archean North Pilbara terrain, Pilbara Craton, Western Australia. *Economic Geology*, *97*, 695-732.

Van Kranendonk, M. J., Collins, W. J., Hickman, A., & Pawley, M. J. (2004). Critical tests of vertical vs. horizontal tectonic models for the Archaean East Pilbara granite–greenstone terrane, Pilbara craton, western Australia. *Precambrian Research*, *131*, 173-211.

Van Kranendonk, M. J., Hugh Smithies, R., Hickman, A. H., & Champion, D. C. (2007). secular tectonic evolution of Archean continental crust: interplay between horizontal and vertical processes in the formation of the Pilbara Craton, Australia. *Terra Nova*, *19*, 1-38.

Van Kranendonk, M. J., Kröner, A., Hegner, E., & Connelly, J. (2009). Age, lithology and structural evolution of the c. 3.53 Ga Theespruit Formation in the Tjakastad area, southwestern Barberton Greenstone Belt, South Africa, with implications for Archaean tectonics. *Chemical Geology*, *261*, 115-139.

Van Kranendonk, M. J. (2010). Two types of Archean continental crust: Plume and plate tectonics on early Earth. *American Journal of Science*, *310*, 1187-1209.

Van Kranendonk, M. J. (2011). Onset of plate tectonics. *Science*, *333*, 413-414.

Van Kranendonk, M. J., Ivanic, T. J., Wingate, M. T., Kirkland, C. L., & Wyche, S. (2013). Long-lived, autochthonous development of the Archean

Murchison Domain, and implications for Yilgarn Craton tectonics. *Precambrian Research*, *229*, 49-92.

Van Kranendonk, M. J., Kröner, A., Hoffmann, J. E., Nagel, T., & Anhaeusser, C. R. (2014). Just another drip: Re-analysis of a proposed Mesoarchean suture from the Barberton Mountain Land, South Africa. *Precambrian Research*, *254*, 19-35.

van Schijndel, V., Stevens, G., Zeh, A., Frei, D., & Lana, C. (2017). Zircon geochronology and Hf isotopes of the Dwalile Supracrustal Suite, Ancient Gneiss Complex, Swaziland: Insights into the diversity of Palaeoarchaean source rocks, depositional and metamorphic ages. *Precambrian Research*, *295*, 48-66.

Viljoen, M. J., & Viljoen, R. P. (1969). The Barberton Mountain Land: Geol. *Soc. South Africa Spec. Pub*, 2, 9-304.

Viljoen, R. P., Saager, R., & Viljoen, M. J. (1969). Metallogenesis and ore control in the Steynsdorp goldfield, Barberton mountain land, South Africa. *Economic Geology*, *64*, 778-797.

Visser, D.J.L. (comp., with reports by Eeden, O.R. van, Joubert, G.K., Söhnge, A.P.G., Zyl,J.S. van, Rossouw, J., Taljaard, J.J., and Visser, D.J.L.) (1956). The geology of the Barberton area. Geological Survey of South Africa Special Publication 15, 253 p.

Walraven, F., & Pape, J. (1994). U/ Pb whole-rock ages for the Pongola supergroup and the Usushwana Complex, South Africa. *Journal of African Earth Sciences*, *18*, 297-308.

Wassmann, M., Moeller, R., Reitz, G., & Rettberg, P. (2010). Adaptation of Bacillus subtilis cells to Archean-like UV climate: relevant hints of microbial evolution to remarkably increased radiation resistance. *Astrobiology*, *10*, 605-615.

Windley, B. F., & Garde, A. A. (2009). Arc-generated blocks with crustal sections in the North Atlantic craton of West Greenland: crustal growth in the Archean with modern analogues. *Earth-Science Reviews*, *93*, 1-30.

Xie, X., Byerly, G. R., & Ferrell Jr, R. E. (1997). IIb trioctahedral chlorite from the Barberton greenstone belt: crystal structure and rock composition constraints with implications to geothermometry. *Contributions to Mineralogy and Petrology*, *126*, 275-291.

Zeh, A., Gerdes, A., Klemd, R., & Barton Jr, J. M. (2008). U–Pb and Lu–Hf isotope record of detrital zircon grains from the Limpopo Belt–evidence for crustal recycling at the Hadean to early-Archean transition. *Geochimica et Cosmochimica Acta*, *72*, 5304-5329.

Zeh, A., & Gerdes, A. (2012). U–Pb and Hf isotope record of detrital zircons from gold-bearing sediments of the Pietersburg Greenstone Belt (South Africa)—Is there a common provenance with the Witwatersrand Basin?. *Precambrian Research*, *204*, 46-56.

Zeh, A., Gerdes, A., & Heubeck, C. (2013). U–Pb and Hf isotope data of detrital zircons from the Barberton Greenstone Belt: constraints on provenance and Archaean crustal evolution. *Journal of the Geological Society*, *170*, 215-223.

Appendix

Appendix 1: Measured orientations of bedding planes (Dip / Azimuth)

Amo Syncline	
85	135
85	330
70	359
85	335
73	355
83	332
69	357
83	139
81	136
82	147
66	142
81	156
71	355
70	354
74	343
80	328
87	335
78	334
75	346
74	351
83	124
83	134
77	130
73	134
72	140
72	151
77	311
68	328
72	334
81	322
88	332
76	359
72	352
78	000
83	007
75	342
73	317
71	355
73	005
62	009
68	356
70	123
75	153
79	114
81	126
75	153
74	129
65	113
67	146
69	153
75	135
82	110
74	147

Angle Station Syncline	
50	147
30	105
35	102
55	155
49	128
36	114
49	084
34	096
61	119
61	085
43	092
60	347
53	351
69	007
75	141
74	139
76	092
72	118
61	152
72	161
75	170
62	142
44	161
52	159
85	135
85	330
70	359
85	335
35	096
33	108
47	154
70	163
61	149
52	136
68	002
60	353
83	333
38	100
54	152
71	169
65	086

Big Buffalo Syncline	
70	355
80	150
80	145
80	346
65	147
80	170
80	124
70	353
80	152
80	150
65	332
80	345
65	147
80	128
60	167
60	155
69	349
67	336
69	344
71	353
65	352
69	350
69	352
68	354
69	352
66	332
65	159
71	145
77	131
72	140
70	167
72	176
77	161
75	146
78	130
76	146
66	164
74	171
79	160
74	147
71	141
70	134
60	154
65	168
69	172
73	149
73	132

Brommers Syncline NE	
82	294
86	322
52	327
78	132
72	159
76	121
65	121
56	120
78	114
66	112
89	303
77	143
55	112
86	146
67	117
88	276
62	105
86	331
77	152
87	134
83	125
71	135
80	135
46	118
38	124
83	125
61	262

Brommers Syncline SW	
72	146
76	149
80	340
64	325
75	344
90	128
78	149
84	159
60	353
84	338
83	3
78	357
81	305
73	354
85	2
35	300
83	350
83	156
60	155
70	168
85	194
74	193
82	173
81	8
76	173
51	238
89	185
84	179
74	184
80	5
85	5
88	183
75	6
85	169
88	10
86	346
85	182
80	339
90	337
90	337
72	152
74	156
90	160
78	344
84	181
44	152
67	150
70	162
80	100
70	48
58	55
54	85
89	74
86	242
77	159

Devil's Bridge Syncline	
80	111
60	101
60	131
70	12
40	333
60	146
50	133
60	126
70	136
60	147
40	131
45	120
70	330
60	160
60	155
50	140
20	135
75	325
35	130
40	140
69	252
60	44

Duurstede Syncline	
80	175
70	340
60	340
85	350
85	340
85	160
60	000
70	160
40	130
75	140
70	330
60	340
82	330
85	170
63	000
70	010
50	160
60	355
80	165
50	340
55	160
70	345
35	150
60	355
60	355
65	160
80	340
70	345
55	160
70	340
55	155
60	325
79	252

Dycedale Syncline	
74	150
78	170
83	157
73	125
53	086
79	288
56	288
71	109
65	112
62	111
62	121
59	129
58	147

61	131
72	113
69	126
62	140
59	151
58	158
64	141
65	109
66	106
67	100
66	093
68	106
71	135
68	160
62	143
68	104
68	105
75	131
57	161
57	162
59	133
66	109
77	125
67	157
65	169
64	178
55	189
48	212
50	243
56	273
62	284
60	269
51	232
52	213
58	180
68	176
64	190
62	208
60	201
76	169
77	145
72	133
65	108
62	094
62	084
62	082
61	103
62	133
62	098
59	087
61	101
69	117
64	139
65	164
65	156
68	118
69	107
74	130
69	158
69	161
70	146
65	137
65	155
69	147
63	155
61	151
63	150
64	151
67	144
67	139
66	125
65	118
69	127

70	131
72	101
70	089
65	079
60	112
65	138
66	156
74	166
74	154
74	152
69	174
73	083
69	104
81	136
80	142
80	148
79	139
75	115
61	097
65	110
76	134
80	156
80	171
81	169
76	153
76	155
78	165
78	163
73	128
71	123
67	136
67	154
69	167
67	170
61	184
67	180
77	171
60	169
59	172
66	175
79	173
79	175
72	184
61	198
62	189
68	167
62	143
64	163
64	135
61	113
62	112
59	148
56	154
55	140
57	122
57	121
58	171
62	169
82	139
71	126
65	148
65	152
71	136
64	169
66	169
66	151
60	158
61	160
66	159
73	134
72	133
71	141
58	117

Eureka Syncline C

73	110
64	140
64	130
67	155
60	180
70	180
75	175
78	155
70	180
85	125
66	130
63	130
80	125
75	120
72	130
65	135
76	135
64	130
60	160
76	160
71	165
66	160
67	170
67	170
62	175
62	200
67	180
70	175
76	175
82	170
75	180
72	170
70	185
64	180
87	150
75	180
80	180
80	160
80	180
73	175
66	175
80	165
77	170
67	315
71	205
72	180
66	180
64	165
81	160
64	180
86	180
86	155
73	180
78	165
75	165
87	165
60	160
71	170
60	165
62	165
76	90
74	180

Eureka Syncline E

67	315
71	205
87	180
90	175
76	180
76	175
61	180
66	185
70	185
73	180
71	175
44	200
75	180
65	190
75	180
70	0
80	0
80	150
80	180
75	195
70	175
70	180
75	294
74	292
70	290
82	183
55	254
68	234
64	218
65	213
78	232
71	195
75	190
75	180
81	350
78	146
83	348
89	5
85	5
88	181
89	359
79	359
75	358
89	183
86	186

Eureka Syncline S

83	100
71	120
76	90
85	85
73	105
76	125
82	125
73	110
70	120
75	115
73	105
70	110
60	110
73	115
64	110
72	100
69	125
76	90
71	90
69	95
74	100

Forbes Reef Syncline N

70	281
55	280
80	310
65	310
75	290
65	270
80	290
70	300

Forbes Reef Syncline S

40	249
67	165
69	247
65	276
71	236
70	288
80	117
66	271
72	269
75	119
72	266
80	130
68	240
60	290

Heemstede Syncline E

21	346
20	309
20	335
16	314
30	329
25	353
29	325
31	344
16	345
74	165
23	111
19	115
16	122
29	137
22	95
26	73
28	150
29	178
26	198
30	212
34	229
38	248
37	278
25	299
13	287
16	265
22	245
25	226
28	204
27	182
25	163
31	203
36	234
37	278
36	295
40	312
36	306
25	288
25	271
29	255
34	245
35	262
35	272
30	257
22	235
28	211
25	192
22	183

27	209
37	229
41	240
45	258
43	284
39	303
31	291
27	272
28	245
25	224
25	207
29	182
33	195
41	217
40	223
36	226
26	239
30	252
24	283
17	272
31	245
30	224
32	211
20	262
12	276
12	287
15	293
22	297
28	282
34	303
32	301
25	281
20	270
14	273
13	283
12	300
24	321
37	319
36	313
32	309
22	323
23	343
30	328

Heemstede Syncline W

51	3
46	13
346	27
4	45
329	46
327	65
324	16
338	30
323	16
17	18
21	25
310	18
323	70
337	23
331	27
328	17
24	33
9	30
7	32
329	40
17	8
350	12
311	28
339	11
312	18
327	18
329	21
345	39
2	29
19	36
2	44
9	34
2	35
6	36
347	54
39	30
14	36
22	39
11	39
53	25
44	39

Himbanyathi Syncline E

75	161
85	330
85	332
80	159
85	337
80	161
70	160
80	335
65	340
80	160
84	322
79	339
88	329
40	313
62	334
59	124
65	148

Himbanyathi Syncline W

85	181
50	346
80	151
60	349
60	131
80	126
80	140
70	150
75	150
60	350
80	145
50	345
85	180

Igwalagwala Syncline

81	165
78	157
67	149
75	159
76	158
74	341
76	356
80	338
67	329
75	333

Jamestown Schist Belt

46	270
54	135
71	135
72	200
35	180
52	175
52	180
39	200
53	190
40	185
80	180
83	180
43	215
47	210
52	160
46	230
51	190
70	240
60	180
90	155
80	180
78	175
76	325
78	175
84	345
85	300
74	210
87	200

Kromberg Syncline

30	227
70	142
20	275
65	173
70	008
79	161
70	334
10	332
50	309
40	338
60	338
80	176
80	150
70	346
85	170
70	305
80	176
80	174
50	159
70	129
80	325
40	353
20	263
70	143
30	258
80	149
70	293
80	152
70	176
80	233
70	061
30	290
90	076
90	075
61	036
64	031
63	024
62	023
62	031
72	054
68	032
68	026
68	015
68	001
81	335
67	305
69	303
59	316
56	337
53	001
53	026
56	051
56	062
55	064
55	071
54	090
61	124
79	100
65	087
53	065
56	038
58	013
66	349
60	325
67	309
58	326
57	008
59	019
65	046
65	048
64	056
64	062
65	061
64	051
60	037
59	024
58	035
57	046
58	054
59	060
60	071
58	079
60	074
59	059
64	028
58	015
58	005
61	350
61	340
63	331
64	315
60	308
54	315
51	339
52	355
59	028
63	045
67	070
67	079
66	081
65	092
64	112
79	144
75	138
66	118
62	091
64	072
65	049
61	025
61	350
66	323
56	346
60	044
59	068
64	087
62	114
75	139
76	155
74	134
68	103
71	071
71	044
29	220
34	220
32	224
33	219

Lily Syncline E

80	177
65	166
75	169
85	173
70	180
85	144
85	143
85	173
85	183
61	144
54	168
71	148

Lily Syncline W

85	300
74	210
87	200
85	185
90	180
78	200
85	170
65	175

Louieville Anticline

82	161
78	155
74	161
70	160
69	172
80	163

Maid of the Mists Syncline E

87	345
74	321
78	193
81	167
80	171
75	189
63	197
65	173
56	184
31	174
68	160
75	179
64	164
49	172
63	166
49	180
65	167
73	180
75	153
79	160
51	173
64	161
70	129
65	142
65	122

72 141
85 156
76 60
65 103
62 101
72 135
64 117
55 157
64 146
51 134
70 179
55 138
64 161
67 138
57 187

Maid of the Mists Syncline W

60 56
23 83
45 44
64 228
31 124
55 44
55 22
85 194
67 17
66 9
77 12
85 174
70 249
85 254
64 355
70 200
85 174
80 176
55 353

Masenjane Block

60 117
70 142
60 159
88 328
66 152
79 143
71 145
62 112
78 133
69 118
63 134
71 149
66 149
69 151
65 178
80 345
80 335
55 155
75 150
65 150
70 350
75 335
80 340
75 150
10 330
45 345
55 345
50 155
55 335
43 340
73 175
85 170

78 165

Malolotsha Syncline

20 164
25 164
30 223
75 240
25 195
35 135
61 288
45 186
50 170
55 199
62 110
62 111
69 290
67 266
33 139
22 158
35 140
70 119
65 094
75 298
50 307
68 249
68 297
51 280
84 232
54 091
75 098
87 159
44 323
64 285
80 238
56 212
72 077
49 058
54 032

Manzimnyama Syncline

61 102
61 168
34 068
34 163
63 064
76 251
76 093
71 099
76 065
61 098
66 109
34 112
29 148
27 101
29 101
65 176
35 067
63 064
75 064
61 102
30 149
35 163
60 104
62 100
57 101
32 110
31 158
20 301
47 218

Montrose Anticlinorium

58 055
89 074
90 120
71 085
72 064
86 242
67 235
90 191
74 189
88 354
87 335
75 347
87 006
83 008
70 028
54 328
69 156
65 025
76 024
82 131
90 101
61 037
65 263
80 133
90 140
39 124
56 254
78 237
74 290
83 341
85 136
90 191

Motjane Schist Belt

57 98
61 101
65 104
61 103
67 98
66 102
67 108
67 105
69 275
65 281
66 287
65 274
66 276
67 278
62 267
62 258
67 248

Moodies Hill Block

86 000
88 359
82 000
90 018
65 168
60 009
71 164
90 149
80 176
74 188
59 149
69 133
90 144

58 145
84 169
80 054
88 348
81 169
89 164
79 157
71 171
53 175
65 165
65 337
74 338
55 143
84 164
88 337
84 341
82 163
66 007
71 177
67 296
85 026
77 031
90 027
82 026
76 024
84 008
85 193
75 193
82 221
71 189
66 348
50 167
77 009
31 124
30 143
84 351
73 223
56 161
55 154
80 184
78 166
81 354
78 164
77 001
52 140
90 349
82 044
79 162
84 155
78 161
89 166
72 352
83 164
77 177
84 160
82 162
59 174
76 157
82 338
82 160
74 154
84 152
76 145
85 154
76 332
65 182
74 172
52 148
84 149
84 154
46 170
39 167
87 147

88 334
88 350
71 314
78 296
80 213
46 139
48 130
84 283
65 203
52 327
88 165
84 138
69 174
65 170
84 323
56 157
62 327
65 323
63 323
78 156
68 136
72 152
74 135
73 118
89 117
79 092
56 189
57 173
46 169
78 161
60 067
80 160
85 342
68 156
85 160
70 152
60 153
84 156
90 165
82 159
90 129
64 348
90 170
58 226
82 003
87 008
84 017
85 135
84 300
72 157
66 112

Nelshoogte Schist Belt E

76 157
74 161
77 171
67 165
71 172
73 168

69 169
68 171
67 168
70 152
82 354

76 347
71 340
72 339
85 358
80 348

77 324
76 318
76 326

Nelshoogte Schist Belt N

86 264
87 259

86 266

84 271
84 263
84 265
81 278
76 248
76 264
81 78
75 81
84 88
76 74

87 77
86 75

Nelshoogte Schist Belt W

77 139

78 145
81 157
74 154
71 149
65 157
71 150
82 148
77 161
77 332
75 329

75 341
74 336

73 335
79 341
76 334
74 329
68 336
69 328
72 352

Ngwenya Anticline

85 096
48 145
40 120
76 109
66 098
74 103
68 101
59 115
72 099
73 124
52 127
67 110
67 099
62 135
51 132
73 126
77 118

81 121
67 125
78 130

Ngwenya Syncline

60 049
65 101
58 102
80 106
85 096
65 096
50 086
45 112
55 082
70 099
66 078
65 083
65 059
46 125
76 109
66 098
74 103
65 101
58 102
80 106
49 097
54 103
42 091
72 141
54 142
54 158
60 018
55 041
60 018
55 041
56 114
39 087
31 055
46 066
45 086

48 102
56 058
41 051
45 061
54 007

Nwenya Syncline N (Masali Syncline)

40 117
35 123
60 117
35 140
70 270
55 165
55 165
75 110
57 112
59 113
52 125
63 121
71 114
64 266
64 132
78 141
53 123
64 118
63 246
54 117

Ntaba Mhlope Syncline NE

88 160
75 148
76 156
82 305
75 264
69 237
70 224
87 155
73 149
88 350
84 346
78 166
79 154
82 149
83 162

Ntaba Mhlope Syncline SW

82 162
88 170
65 044
83 158
79 152
66 149
76 162
65 158
70 160
72 156

71 163
68 156

Onverwacht Anticline

75 352
68 027
51 340
37 134
63 333
85 356
40 187
52 173
82 048
40 154
45 115
60 131
45 145
65 315
80 338
68 331
87 317
85 146
60 171
70 152
60 153
80 163
70 164
70 140
80 159
70 139
80 145
80 144
80 094
70 079
60 153
70 177
60 161
80 296

80 146
80 154
80 174
80 333
85 161
70 159
70 109
60 109
50 131
42 097
70 278
80 288
70 271
80 151
70 282
80 276
80 100
80 210
70 076
80 203
60 198
80 169
40 120
70 047
70 006
70 181
70 000
70 326
80 171
70 017
80 354
80 180
80 179
60 167
80 178
70 220
90 006
90 037
90 348
90 039
90 022
90 000
90 316
90 001
90 014
90 067
90 058
90 057
90 069
90 074
90 076
90 310
0 000
90 072
90 064
90 067
3 234
3 209

Paulus Syncline NE

60 160
63 157
60 155
61 154
50 140
56 117
54 321
20 135
63 311
75 325
54 163
76 318

35 130
38 112
40 140
41 153
43 148
75 340

78 337
80 330
66 154
75 315

Paulus Syncline SW

77 127
60 146
69 145
50 133
48 127
45 100
63 85
71 136
34 92
52 167
23 96
64 147
77 147
42 103
40 131
45 120
53 161
62 136
85 138
62 140
58 160
37 140
69 252
60 44

Powerline Road Syncline E

65 358
35 261
34 308
80 359
65 3
45 359
75 358
85 86
50 17
76 254
85 56
76 188
54 179
62 167

78 192
66 182
56 223
61 248
54 182

Powerline Road Syncline W

32 98
35 59
50 180
58 469
45 12
48 22

40	8	50	160	62	179	82	133	81	145
21	29	57	160	60	160	74	118	66	148
30	20	50	192	58	179	74	133	87	135
29	22	40	187	67	168	86	126	71	132
62	15	40	185	55	192	73	113	60	140
72	0	40	176	57	194	83	145	64	146
75	27	63	164	57	159	83	126	76	146
65	358	60	159	47	190	81	135	76	144
55	359	75	145	55	180	76	130	85	145
42	46	65	152	50	209	80	134	81	153
72	160	55	150	55	182	76	146	81	140
89	203	65	162	68	161	77	125	71	133
24	171	40	165	40	170	72	146	77	159
44	227	60	156	55	171	71	133	68	135
35	261	53	184	35	175	72	166	88	145
34	308	70	170	50	160	81	122	74	145
65	3	78	150	57	164	47	146	61	151
45	359	70	112	45	163	48	165	66	146
62	359	85	140	55	152	59	130	73	151
87	348	37	198	65	158	58	130	59	151
30	32	85	147	65	153	56	163	74	151
52	6	75	133	72	178	52	165	70	159
85	185	62	122	83	250	58	152	74	159
55	349	58	110	55	214	55	152	68	146
56	8	70	159	50	137	67	166	59	134
75	358	50	174	80	167	55	182	69	151
70	2	45	165	65	148	76	160	71	159
85	4	52	163	77	151	83	133	71	160
90	5	50	181	44	154	74	140	74	139
80	14	60	147	71	134	82	147	63	141
		53	185	65	122	79	139	68	138
Saddleback		72	165	71	256	62	145	65	151
Syncline		55	158	45	161	64	145	72	151
		50	199	57	142	77	141	81	146
72	188	57	162	65	246	71	146	71	152
45	202	60	158	60	275	78	146	70	146
35	190	78	143	58	309	64	138	79	134
45	168	60	170	51	133	67	146	77	160
55	140	65	163	61	154	82	130	63	140
45	218	52	176	63	344	66	130	79	140
40	237	78	143	37	328	69	146	75	140
35	257	81	131	42	167	75	139	54	181
45	180	87	155	58	125	78	134	73	151
50	182	70	138	49	152	84	125	73	168
60	145	72	145	71	147	76	114	63	159
45	177	80	138	48	154	88	117	66	159
35	169	45	170	49	156	84	129	66	173
65	115	45	166	49	162	80	118	41	151
70	120	65	154	58	160	66	103	71	193
35	240	62	160	44	165	79	122	67	141
47	97	80	150	58	287	68	126	68	151
87	128	70	130	69	134	56	136	65	145
80	125	70	154	57	140	79	131	42	159
85	126	50	172	68	125	76	125	62	159
50	181	40	199	70	145	84	135	65	146
60	160	45	201	70	152	54	130	65	167
63	150	57	171	85	155	76	130	75	146
75	145	50	170	87	162	65	117	74	165
60	146	45	144	66	183	63	125	85	178
67	153	50	169	46	163	75	139	65	145
55	173	52	160	59	131	79	132	80	180
45	180	60	153	63	133	77	125	68	139
60	183	77	157	52	160	80	146	60	168
50	195	75	148	63	143	77	146	60	153
35	192	65	153	68	148	67	140	73	140
57	147	70	187	67	133	80	131	89	161
55	157	79	182	83	123	78	131	62	171
65	157	80	156	75	126	85	140	77	161
77	148	85	145	85	140	76	145	86	180
80	128	70	145	81	165	69	160	70	140
45	175	63	157	87	146	70	135	67	135
50	186	75	170	81	145	78	146	72	160
48	177	65	167	72	146	71	125	82	150

45 160
85 170
65 170

Schoonoord Anticline

56 157
70 171
65 174
53 164
52 152
54 142
72 172
70 178
67 179
82 176
76 181
64 164
60 148
60 140
57 136
50 129
49 144
54 161
59 141
54 135
53 130
51 139
65 251
58 245
59 240

Steynsdorp Anticline

60 312
57 329
52 351
55 015
59 035
55 063
62 101
64 116
69 102
61 085
65 057
61 044
65 307
60 317
60 332
61 342
59 001
57 006
55 014
54 005
58 344
64 318
65 310
66 120
68 112
67 098
63 101
54 121
62 104
62 094
65 129
63 119
66 133
66 138
62 126
61 120

Stolzburg Syncline

40 147
80 193
50 187
70 189
70 354
70 185
80 015
90 334
70 340
70 324
60 171
60 344
80 203
80 188
74 007
66 000
65 348
64 346
72 000
82 012
76 011
76 339
64 326
64 335
68 341
64 332
72 329
78 332
69 334
68 329
70 341
75 335
72 327
70 323
62 311
60 296
55 274
64 249
71 202
66 195
54 174
53 173
74 188
81 198
77 197
66 191
54 185
50 177
47 140
53 160
61 183
71 198
72 196
64 187
53 169
45 150
45 148
47 136
54 140
59 160
71 173
73 192
59 189
38 087
38 086
54 149
54 168
61 179
58 171
49 150
58 181

72 194
73 186
63 172
57 165
65 187
71 189
76 194
58 181
52 180
56 158
48 141
49 154
59 186

Strathmore Anticline

76 168
75 156
76 182
78 149
65 156
67 155

67 159
66 143
71 164
72 167
74 173
75 342
72 338
68 352
69 346
72 337
68 338
71 327
76 341
75 335
76 340

The Heights Syncline

55 171
41 070
49 228
41 028
41 012
66 274
32 020
50 157
71 176
70 172
57 157
54 150
60 161
63 168
59 162
50 156
65 179
76 180
78 163
64 145
57 132
49 121
56 145
59 162
55 156
51 143
48 129
47 125
58 157
61 180

67 181
71 183
68 174
58 150
48 135
56 148
63 166
70 178
70 177
68 170
64 158
55 139
63 150
71 167
74 177
75 171
66 147
57 129
49 116
63 131
68 148
74 162
79 172
81 172
82 164
80 166
79 183
73 187
68 188
55 179
53 163
49 139
36 115
40 097
47 118
60 150
53 128
44 083
43 030
33 052
36 104
52 144
65 164
61 143
48 112
45 094
51 113
62 130
70 143
78 164
83 173
82 181
78 182
74 182
57 173
57 183
72 192
73 189
72 178
70 167
60 145
57 128
53 118
52 115
55 119
61 128
66 141
71 155
74 169
74 178
70 181
59 181
54 152

48 135
47 140
47 156
42 132
41 098
43 102
42 121
43 125
48 107
45 085
43 058
45 025
38 035
36 050
39 026
38 075
39 107
51 132
60 158
64 174
70 184
71 190
70 191
61 189
70 196
81 189
81 184
69 159
54 139
41 084
62 130
66 136
69 140
72 131
72 137
76 145
75 156
75 164
75 158
47 113
73 135
67 125
56 110
39 084
39 099
46 122
52 117
49 101
62 119
63 129
88 165
85 176
87 179
80 192
82 194
83 194
85 187
85 181
86 182
87 179
76 165
60 143
53 115
45 050
55 012
71 355
79 347
46 015
33 034
47 359
84 341
84 161
84 158

74	145
64	134
53	125
42	109
39	098
42	088
44	114
46	144
59	177
69	190
84	195
83	188
69	174
59	148
43	115
41	101
41	096
57	125
68	136
77	153
83	165
89	158
82	146
69	132
71	145
74	166
66	158
53	138
54	171
63	178
63	169
42	117
40	093
48	121
62	154
67	171

Three Sisters Syncline E

60	130
65	150
63	131
59	128
63	149
60	158
63	142
64	136
68	136
61	145
58	137
62	142
69	162
53	143

Three Sisters Syncline N

60	130
80	154
62	128
63	127
64	131
79	149
78	153
82	152
76	148
65	153
66	149
63	152
75	137
77	144
61	165

Ulundi Syncline E

47	90
57	130
60	120
80	145
74	165
56	115
52	120
62	130
45	125
70	145
74	170
74	170
70	165
86	130
87	130
82	155
66	145
80	165
51	130
60	150
56	140
52	145
65	175
71	150
65	150
74	140
61	135
55	145
75	160
50	160
7	170
62	90
70	155
59	120
81	175
54	135
65	160
66	160
51	140
67	185
73	180
65	175
60	175
50	180
63	145
81	180
70	185
66	160
87	180
88	155
60	175
84	170
77	152
75	160
72	120
55	120
60	165
63	170
75	155
90	180
79	180
80	165
80	175
78	168
76	175
85	165
69	135
49	165
62	160
75	180

65	145
68	180
75	180
74	142
72	160
69	160
66	155
72	170
40	160
64	170
79	170
64	170
60	185
60	170
71	180
66	165
60	175
80	165
77	160
85	160
80	170
60	165
72	180
83	180
80	185
60	170
64	15
56	180
57	175
70	190
60	180
46	180
76	180
85	180
77	180
64	175
70	185
78	180
81	180
84	180
89	180
88	180
77	170
90	200
74	180
70	180
69	180
72	180
90	185
67	180
77	205
87	175
80	190
72	180
74	200
80	183
87	200
60	180
71	195
64	185
61	183
76	183
50	180
73	190
62	185
70	190
71	190
70	180
72	180
62	185
70	185
63	195
68	195

62	195
70	192
70	200
66	200
70	180
72	200
64	180
80	190
65	200
67	195
63	205
64	200
84	210
80	205
81	210
67	195
74	200
63	190
74	195
67	190
60	180
78	185
75	180
65	180
85	170
85	175
80	175
75	180
80	170
80	170
80	180
75	350

Ulundi Syncline SW

74	100
74	160
82	160
63	110
62	105
64	110
72	100
75	120
64	100
67	95
54	100
60	105
60	130
59	90
56	120
47	90
57	130
60	120
80	145
74	165
70	170
71	110
42	115
56	115
52	120
62	130
45	125
70	145
74	170
74	170
70	165
86	130
87	130
82	155
66	145
80	165
51	130

66	150
56	140
52	145
65	175
71	150
65	150
74	140
61	135
55	145
75	160
57	110
61	135
65	120
68	140
59	11
50	160
72	170
62	90
70	155
59	120
66	160
87	180
88	155

Vooruitzicht Syncline

80	175
70	340
60	340
85	350
85	340
85	160
60	000
70	160
40	130
75	140
70	330
60	340
82	330
85	170
63	000
70	010
50	160
60	355
80	165
50	340
55	160
70	345
35	150
60	355
60	355
65	160
80	340
70	345
55	160
70	340
55	155
60	325
79	252

Woodstock Anticline

54	135
71	135
72	200
60	180
90	155
78	175
84	345
85	300
74	210

87	200	85	185	90	180	80	185

Appendix II: Measured orientations of cleavage planes (Dip & Azimuth)

Amo Syncline				74	182	67	251	50	108
		73	116	73	191	66	280		
80	315	69	121	75	185			Ngwenya Anticline	
76	320			74	187	Manzimnyama			
78	330	Eureka Syncline C				Syncline		75	104
				Eureka Syncline S				61	102
81	334	68	152			48	116		
		70	165	66	110	51	108	Paulus Syncline	
79	318	71	162	68	105	51	106		
		78	159	66	108	55	115	65	278
Brommers		65	156	67	115	54	112	62	281
Syncline NE		72	160	71	109			64	191
						Ngwenya Syncline		70	286
78	131	Eureka Syncline E		Forbes Reef				66	278
76	126			Syncline		47	118	64	291
74	130	76	180			50	112	62	285
		74	176	58	281	49	112	61	283
Brommers		75	186	61	270	49	110		
Syncline SW				55	265	50	106	54	270

Appendix III: Measured and calculated fold axial plunges (plunge / trend)

Amo Syncline		Duurstede		30	356			87	133
		Syncline				30	080	34	114
72	049			Heemstede		40	080	05	132
59	052	40	55	Syncline E				30	085
63	051	60	57			Lily Syncline W		79	087
64	046			22	067			50	266
		Dycedale Syncline				80	42	52	118
Angle Station				Heemstede		73	38	60	167
		52	029	Syncline W		75	35	90	000
72	049	48	031			78	39	61	029
59	052	41	045	219	46				
63	051	39	047	180	56	Maid of the Mists		Moodies Hills	
64	046					Syncline E		Block	
		Eureka Syncline C		Himbanyathi					
Big Buffalo				Syncline E		36	269	64	044
Syncline		229	60			49	272		
		238	59	30	212			Motjane Schist	
40	071	232	55			Maid of the Mists		Belt	
56	071	238	54	Himbanyathi		Syncline W			
75	057	216	57	Syncline W				37	12
		217	51			48	130		
Brommers				81	13	16	125	Nelshoogte Schist	
Syncline NE		Eureka Syncline E		76	17			Belt E	
				81	21	Masenjane Block			
210	11	279	61	81	24			52	261
208	34	288	56	81	16	68	238	41	238
227	36	269	57			65	241		
223	41	256	58	Igwalagwala				Nelshoogte	
				Syncline		Malolotsha		Syncline N	
Brommers		Eureka Syncline S				Syncline			
Syncline SW				00	046			51	176
		45	088			25	175		
64	52	19	088					Nelshoogte Schist	
48	48	25	055	Kromberg Syncline		Manzimnyama		Belt W	
42	46					Syncline			
39	49	Forbes Reef		242	79			47	43
		Anticline N		219	79	71	078		
Devil's Bridge				229	76	42	058	Ngwenya Anticline	
Syncline		42	206	245	75				
				231	77	43	023	70	22
51	066	Forbes Reef		226	76				
49	048	Anticline S		216	76	Montrose			
						Anticlinorium		Ngwenya Syncline	
		40	012	Lily Syncline E				N (Masali Syncline)	

30 176

Ngwenya Syncline S

60 354

Ntaba Mhlope Syncline NE

71 226
70 225

Ntaba Mhlope Syncline SW

65 42

Onverwacht Anticline

80 080

85 043
90 046
83 054

Paulus Syncline NE

49 051
37 053

Paulus Syncline SW

50 184

Powerline Road Syncline E

33 281

Powerline Road Syncline W

18 102

Saddleback Syncline

40 230
53 228
48 218

Schoonoord Anticline

49 072

Steynsdorp Anticline

30 031
40 033

80 030

Stolzburg Syncline

64 261
70 238

59 244
63 241
50 239

Strathmore Anticline

55 070

The Heights Syncline

29 50

Three Sisters Syncline E

44 53

Three Sisters Syncline N

31 207

Ulundi Syncline E

69 281
32 294
14 288

Ulundi Syncline SW

56 023
26 035
10 028

Vooruitzicht Syncline

40 55
60 57

Woodstock Anticline

40 040

Appendix IV: Calculated orientations of fold axial planes (dip / azimuth / fold generation)

Amo Syncline

82 336 F1

Angle Station Syncline

61 127 F1

Big Buffalo Syncline

83 154 F1

Brommers Syncline NE

74 124 F1
86 076 F2

Brommers Syncline SW

74 124 F1
86 076 F2

Devil's Bridge Syncline

57 135 F1

Dycedale Syncline

75 124 F1

Duurstede Syncline

84 343 F1

Eureka Syncline C

71 164 F1
78 015 F2
90 048 F3

Eureka Syncline E

79 182 F1
78 015 F2
90 048 F3

Eureka Syncline S

73 107 F1
78 015 F2
90 048 F3

Forbes Reef Anticline N

55 284 F1
79 198 F2

Forbes Reef Anticline S

55 284 F1
79 198 F2

Heemstede Syncline E

60 166 F1

Heemstede Syncline W

60 166 F1

Himbanyathi Syncline E

85 335 F1
72 250 F2

Himbyanathi Syncline W

85 335 F1
72 250 F2

Igwalagwala Syncline

89 339 F1

Kromberg Syncline

85 335 F1

Lily Syncline E

76 181 F1
80 274 F2

Lily Syncline W

76 181 F1
80 274 F2

Maid of the Mists Syncline E

80 187 F1
86 280 F2

Maid of the Mists Syncline W

80 187 F1
86 280 F2

Masenjane Block

79 152 F1

Malolotsha Syncline

83 102 F1

Manzimnyama Syncline

49 103 F1

Moodies Hills Block

82 164 F1
78 015 F2

Ngwenya Anticline

66 116 F1

Ngwenya Syncline S

50 096 F1
56 195 F2

Ngwenya Syncline N (Masali Syncline)

50 096 F1
56 195 F2

Ntaba Mhlope Syncline NE

76 069 F1
79 236 F2

Ntaba Mhlope Syncline SW

79 236 F1
79 236 F2

Onverwacht Anticline

84 161 F1

Paulus Syncline NE

59 286 F1
86 247 F2

Paulus Syncline SW

59 286 F1
86 247 F2

Powerline Road Syncline E

86 008 F1
78 090 F2

Powerline Road Syncline W

86 008 F1
78 090 F2

Saddleback Syncline

63	152	F1
Schoonoord Anticline		
63	164	F1
Steynsdorp Anticline		
75	119	F1
Stolzburg Syncline		
83	177	F1
Strathmore Anticline		
89	160	F1
Strathmore Anticline		
53	105	F1
Three Sisters Syncline E		
68	145	F1
90	040	F3
Three Sisters Syncline N		
68	145	F1
90	040	F3
Ulundi Syncline E		
68	170	F1
76	065	F2
90	048	F3
Ulundi Syncline SW		
68	170	F1
76	065	F2
90	048	F3
Vooruitzicht Syncline		
84	343	F1
Woodstock Anticline		
79	174	F1

Appendix V: Uncorrected measurements of foresets (measured plane / azimuth / dip)

Clutha Creek		
bed	198	62
for	228	69
for	210	63
for	207	62
for	169	62
for	204	49
bed	212	76
for	49	60
for	48	66
bed	206	78
for	206	56
for	196	55
for	191	61
bed	192	88
for	30	76
for	24	74
for	39	85
for	34	90
for	18	90
bed	228	74
for	245	82
bed	218	70
for	212	81
Dycedale Syncline		
bed	167	56
for	181	42
for	178	45
for	176	37
for	180	34
for	139	55
for	180	35
for	152	58
for	199	35
for	195	40
for	153	52
for	144	57
for	192	38
for	189	37
for	148	46
bed	170	62
for	167	81
for	201	57
for	89	54
for	229	50
for	183	50
for	197	43
for	143	51
for	219	54
for	185	61
bed	162	65
for	137	56
for	139	41
for	143	40
for	167	43
for	134	41
for	149	40
for	148	40
for	110	50
for	114	43
bed	164	51
for	196	45
for	208	44
for	166	44
for	194	41
for	188	65
for	197	52
for	185	50
for	213	45
for	212	46
for	148	72
for	215	57
for	147	63
for	154	72
bed	156	63
for	202	61
for	203	50
for	160	48
for	185	44
for	162	80
for	220	54
for	219	52
for	173	54
for	203	52
for	221	55
for	167	60
for	171	76
bed	184	53
for	173	41
for	195	37
for	199	27
for	186	23
for	190	40
for	147	45
for	209	22
for	149	44
for	149	28
for	143	49
for	129	40
for	204	27
for	139	57
bed	155	46
for	137	39
for	142	57
for	143	42
for	173	21
for	188	46
for	192	19
for	164	55
for	148	32
for	209	37
for	159	35
for	139	39
for	140	60
for	161	60
Elephant's Kloof		
bed	130	78
for	116	88
for	306	90
for	134	85
for	132	80
bed	158	65
for	125	67
for	118	72
for	113	69
bed	160	67
for	179	46
for	169	41
for	172	48
bed	185	75
for	172	75
for	224	75
for	178	71
for	215	71
for	176	71
for	209	69
for	208	70
for	174	68
for	174	71
for	208	77
for	207	69
for	177	70
for	207	78
for	206	79
for	209	75
for	210	59
for	174	70
for	172	62
for	199	75
for	174	65
for	178	81
for	220	62
for	214	65
for	178	88
for	207	64
for	170	72
for	200	53
for	168	64
for	194	65
for	198	59
for	197	65
for	178	64
for	205	68
for	172	71
for	177	69
for	200	70
for	200	60
for	167	85
for	166	72
for	167	75
for	179	80
for	206	74
for	172	74
for	208	73
for	171	65
for	198	71
for	169	71
for	209	84
for	201	84
for	194	72
for	171	79
for	201	68
for	211	78
for	181	81
for	182	83
for	179	84
for	181	77
for	186	86
for	179	79
for	209	74
for	170	71
for	203	70
for	200	84
for	210	79
for	168	70
for	176	73
for	212	79
for	169	75
for	202	69
for	206	73
for	166	71
for	209	76
for	202	61
for	203	74
for	171	71
for	173	80
for	208	70
for	175	70
for	166	67
for	171	66
for	165	68
for	167	65
for	173	70
for	199	55
for	194	52

for	177	68
for	162	60
for	196	55
for	195	60
for	170	67
for	174	65
for	204	65
for	167	65
for	202	71
for	168	70
for	204	68
for	170	62
for	176	59
for	178	59
for	210	60
for	175	60
for	173	60
for	164	70
for	200	76
for	169	70
for	172	70
for	207	71
for	197	50
for	198	50
for	164	60
for	202	60
for	166	55
for	162	65
for	206	60
for	179	59
for	177	49
for	178	69
for	180	69
for	180	61
for	180	61
for	178	65
for	170	65
for	169	69
for	173	59
for	168	70
for	168	74
for	168	79
for	170	73
for	172	61
for	182	66
for	179	71
for	173	67

for	168	67
for	213	62
for	173	81
for	202	86
for	199	86
for	198	80
for	162	86
for	178	82
for	200	81
for	150	79
for	173	71
for	194	72
for	186	90
for	172	74
for	176	81
for	180	80
for	165	84
for	172	81
for	166	88
for	168	81
for	169	76
for	170	76
for	162	76
for	173	79
for	161	76
for	164	80
for	169	76
for	169	76
for	159	77
for	170	70
for	168	72
for	156	75
for	205	82
for	173	52
for	198	76
for	214	75
for	169	78
for	164	90
for	159	89
for	154	85
for	166	90
for	178	58
for	158	87
for	183	69
for	168	74
for	167	69

bed	188	79
for	204	80
for	201	75
for	211	76
for	196	71
bed	175	81
for	150	71
for	161	59
for	156	71
bed	196	75
for	214	68
bed	275	86
for	95	75
for	294	82
bed	278	81
for	116	76
for	136	84
for	113	80
bed	131	68
for	149	76
for	154	71
for	156	70
bed	121	74
for	100	75
for	104	76
for	108	77
for	96	72
for	97	73
for	94	69
for	277	84
for	102	56
for	106	72
bed	119	77
for	102	88
for	108	89
for	96	85
for	142	64
for	133	69
for	152	72
bed	133	70
for	157	71
for	147	62
for	150	60
for	101	41
for	112	41
for	125	39
bed	140	55

for	152	75
for	144	77
for	166	69
bed	130	46
for	102	40
for	104	46
for	87	46
for	134	66
for	130	63
for	151	53
bed	130	55
for1	128	70
for1	118	74
for1	135	72
for2	113	36
for2	120	41
for2	119	37
bed	140	65
for	157	58
for	147	56
for	162	56

Fairview Mine

bed	122	75
for	117	57
for	120	59
for	131	75
for	148	80
for	158	81
bed	122	82
for	141	80
for	105	85
for	126	80
bed	120	80
for	138	85
bed	128	73
for	128	65
bed	152	74
for	155	63
for	162	60
bed	138	10
for	156	65
bed	136	69
for	128	52
bed	139	75
for	142	54

Appendix VI: Measured axes of conglomerate clasts (long, middle, short axis)

Forbes Reef Anticline N

1,9	1,5	1
10,5	4	3,2
2	0,5	0,4
15	4	3,2
7,1	1,4	1
14,5	2	1,6
9,6	1,4	1
12,1	1,8	1,3
9,7	0,9	0,4
10,4	1,9	1,2
7,8	2,4	2,1
8,1	1,6	1,2
9,8	1,4	1,1
13,1	2,6	2
6,8	0,8	0,3
9,7	1,1	0,7
6,30	1,10	0,50
7,40	1,20	0,60
7,60	1,10	0,40
9,20	1,30	0,60

Forbes Reef Anticline S

1,55	1	0,44
11,7	2	1,5
9	1	0,5
4,5	1,5	1,1
6	1	0,6
5	1,5	0,9
8	4	2,6
2,5	1	0,6
3	1	0,5
3,5	0,5	0,2
6,5	1	0,6
4	1	0,7
2	0,5	0,3
5,5	2	1,2
3,5	1	0,6
3	1	0,5
4	2	1,2
5	1,5	0,8
4	3	2,3
3,5	1	0,4
3	0,5	0,3
9	3,5	2,6
3,5	1	0,4
6	2	1,2
2,5	1	0,5
7	2	1,3
3	1	0,6
4	1,5	1,1
11	3	2,1
8	1,5	0,9
3	1	0,6
5,5	2,5	1,6
3,5	2	1,6
3,5	2	1,4
6	2,5	1,9
5	1,5	1,1
2	0,5	0,3
3,5	1,5	0,9
3	1,5	0,8
3	2	1,5
3	1	0,7
3	1	0,6
4,5	2	1,2
4,5	1,2	1,1
5	1,3	1,2
2	0,5	0,3

Maid of the Mists Syncline

11	5	2
14	8	4,5
7,5	4,5	3
9	6	3,5
6	3,5	2,5
12	7	5,5

12	5,5	2,5
11	6	3
11,5	6	3
11,5	6	3
6	3	2,5

Malolotsha Syncline

0,9	0,2	0,1
2,4	1,9	1,4
1,2	0,9	0,9
1,1	1	0,7
2,3	1,9	1,8
3,7	3	2,2
3,5	2,8	2,7
2,4	1,9	1,3
1,4	1,2	1,1
1,6	1,3	0,9
2,5	2,1	2
2,7	2,2	1,5
3,5	3,3	3,1
2,1	1,8	1,3
2,2	1,7	1,2
2,8	2,2	2,2
3,6	3,2	2,2
1,2	0,7	0,5
2,2	1,6	1,5
3,1	1,9	1,4
4,8	3,7	2,8
8,5	7,6	4,7
2,3	1,9	1,4
2,3	1,6	1,2
1,4	4	3
2,5	2,4	1,5
1,9	1,5	1,1
1,9	1,4	1,1
7,2	6,7	4,6
2,3	1,9	1,4
2,4	1,9	1,3

Ngwenya Syncline S

7	1,8	1,4
1,9	0,4	0,3
1,3	0,4	0,2
3	1,2	0,7
1	0,2	0,1
5,6	2,2	1,8
1,4	0,3	0,2
2,4	0,4	0,4
1,9	0,3	0,2
2,5	0,8	0,4
2,2	0,4	0,3
2,8	1,8	1,4
1,8	0,4	0,3
1,2	0,4	0,3
2,7	1,2	0,9
7	3,5	2,8
1,8	0,9	0,3
2,4	0,9	0,4
3,1	0,5	0,4
1,5	0,4	0,2
5,3	1,9	1,5
1,2	0,4	0,32
1,7	1,1	0,8
3,4	2,3	1,8
1,8	0,3	0,2
3,2	1,5	1,1
3,6	0,9	0,7
3,6	1,3	1

Ngwenya Syncline N (Masali Syncline)

2,1	1	0,69
8,2	2,6	2,1
0,6	0,3	0,2
0,5	0,2	0,1
0,8	0,3	0,1
1,2	0,4	0,2
0,4	0,2	0,1
5	1	1,2
12	8,1	5,9
7,1	5	2,6
1,5	0,3	0,2
1,2	0,9	0,4
6,4	2,3	1,4
8,6	2	1,3
0,5	0,3	0,2
1	0,3	0,2

Ntaba Mhlope Syncline

13	3	2,4
2	0,5	0,4
1,2	0,3	0,2
1,2	0,4	0,3
1	0,2	0,1
1,8	0,7	0,5
5,7	2,2	1,7
3	1,2	0,7
1,8	0,4	0,3
1,9	0,4	0,3
2,2	0,8	0,6
3,5	0,9	0,7
2,8	1,9	1,4
2,4	0,5	0,4
1,7	0,4	0,3
1,2	0,3	0,2
1,2	0,5	0,4
1,3	0,4	0,3
3,2	1,5	1,1
3,3	0,5	0,4
3,2	1,8	1,4
1,5	0,9	0,6
2,4	0,8	0,6
1,7	1,2	0,9
3,5	2,3	1,8
7	3,4	2,8
5,1	1,9	1,4
2,5	0,7	0,5
3,7	1,3	1
2,5	1,2	0,8
2	1,2	0,9
1,2	0,6	0,6
1,4	0,4	0,3
3,4	0,9	0,7
2,6	0,6	0,5
1,7	0,4	0,3
1	0,3	0,2
2,9	1,9	1,5
0,7	0,5	0,4
1,3	0,4	0,3
0,6	0,4	0,3
0,6	0,2	0,1
0,8	0,2	0,1
0,8	0,2	0,1
0,4	0,3	0,2
1	0,3	0,2
1,2	0,9	0,5
1	0,2	0,15
8	3	2,4
13	8,5	6,8
0,5	0,3	0,2
9	2	1,5
6	2,5	1,5
7	5	3,5
5	1,5	1,2
4	1	0,7
1,7	0,5	0,3
1,3	0,3	0,2
1	0,5	0,4
0,8	0,2	0,1
0,9	0,3	0,2
0,9	0,2	0,1
1,4	0,2	0,1
1,7	1,5	1,1
1	0,2	0,1
6,5	1	0,5
1,1	0,3	0,2
2,8	0,6	0,4
1,1	0,2	0,1
1,2	0,2	0,2
1,1	0,4	0,3
1,3	0,4	0,3
1,2	0,4	0,3
1,1	0,1	0,1
1,6	1,5	1,2
0,4	0,1	0,1
0,5	0,2	0,1
1,2	0,8	0,4
0,6	0,2	0,1
6,5	2	1,7
6,5	1	0,6
8,5	2,4	1,9
7	1,3	1
8	2,3	1,5
6	1,5	1,1
7	2	1,3
9,5	3	2,4
5	0,5	0,3
7	1,5	1,1
15	2,5	1,8
26	4	3,2
11	2,5	2
6	3	2,2
10	4,5	3,5
17	5,5	4
6,5	4	3,2
7	3	2,3
7,5	2,5	1,9
5	2,2	1,6
6,5	2	1,5
6	1,6	1,2
8	1,7	1,2
16	2	1,6
10,5	1,6	1,2
13	4	3,2
24	2,5	1,8
7	1,4	1
19,5	3,4	2,8
8	3	2,1
11,5	2,5	1,8
4	1,2	0,7
9,5	3	2,2
8,5	2,7	2,1
9,5	2	1,4
10,5	4	3,4
13,5	3	2,3
19	7	5,4
15	4	3,2
5	1,5	1
7,5	2,7	2,1
4,5	2	1,4
14	2	1,5
3,5	0,5	0,3
6	1,2	0,9
5,5	1	0,7
8	1,5	1,1
2	0,5	0,4
7	2,5	2
6	2	1,4
5,3	2,8	2,3
5,5	1,7	1,1
12	2,5	1,8
6	2	1,5
10	4	3,1
7,5	1,2	0,7
5	2	1,5
6,5	2	1
9	3,5	2,7
4	1,1	0,7
5	1,5	1
7	2,5	2
5,5	1,7	1,2
11	3	2,3
3,7	0,9	0,6
6	1	0,7
12	4,5	3
8,5	4	3,5
4,3	0,8	0,5
11,7	2	1,5

Powerline Road Syncline

8	4	3
6	3	1,5
12	8	6
14	8	6
18	9	5
6	4	2,5

Appendix VII: Measured orientation of long axes of conglomerate clasts

Forbes Reef Anticline N

48	213
51	212
51	208
57	210

Forbes Reef Anticline S

42	019
37	021
38	020
35	017
33	025

Maid of the Mists Syncline E

36	269
49	272

Maid of the Mists Syncline W

48	130
16	125

Malolotsha Syncline

33	189
27	168
29	171

Ngwenya Anticline

70	22

Ngwenya Syncline N (Masali Syncline)

37	196
44	205
45	197
31	201
38	203

Ngwenya Syncline S

56	334
58	348
36	018
42	022
51	014

Ntaba Mhlope Syncline

68	261
50	220
53	253
60	220
61	220
59	225
40	210
51	218
60	23ß

65	243
59	232
54	233
65	245
43	233
65	244

Powerline Road Syncline E

33	281

Powerline Road Syncline W

18	102

Appendix VIII: Results of U/Pb age dating of sample 15-213:

	Agedisplay		16A		105																			cum.
Spot	Age	1s	conc.	conc. = 105 / 240	grain	7/35r	2s%	6/38r	2s%	corr	7/6r	2s%	207/235	2s	206/238	2s	207/206	2s	conc%	Th/U	age	Th/U	prob.
A-6	3232,56	16,75	106,54	A-267	A-267	21,12	9,22	0,66	8,92	0,97	0,23	2,35	3144,22	89,40	3248,46	227,51	3078,33	37,58	105,53	1,65	3078,33	1,65	0,01
A-7	3472,72	15,67	108,77	A-15	A-15	17,95	6,68	0,55	6,18	0,92	0,24	2,55	2986,99	64,29	2836,79	141,84	3089,73	40,61	91,81	0,50	3089,73	0,50	0,02
A-8	592,56	94,83	633,33	A-117	A-117	17,95	8,91	0,54	8,63	0,97	0,24	2,20	2987,21	85,66	2802,43	196,14	3114,07	35,01	89,99	0,65	3114,07	0,65	0,03
A-9	3260,54	20,29	122,43	A-290	A-290	22,95	8,00	0,68	7,78	0,97	0,24	1,87	3224,70	77,82	3349,27	203,12	3148,12	29,74	106,39	0,34	3148,12	0,34	0,04
A-10	3171,66	17,60	99,53	A-70	A-70	23,91	7,71	0,70	6,09	0,79	0,25	4,73	3264,59	75,12	3421,53	161,55	3169,57	74,98	107,95	1,25	3169,57	1,25	0,05
A-11	3295,78	18,20	61,31	A-10	A-10	21,60	6,43	0,63	6,04	0,94	0,25	2,22	3165,89	62,44	3156,80	150,73	3171,66	35,19	99,53	0,43	3171,66	0,43	0,06
A-12	2644,36	42,26	210,28	A-47	A-47	19,88	6,54	0,58	6,21	0,95	0,25	2,04	3085,44	63,24	2950,74	147,15	3174,32	32,36	92,96	0,58	3174,32	0,58	0,07
A-13	3246,41	23,90	111,85	A-275	A-275	21,69	8,25	0,62	7,94	0,96	0,25	2,23	3169,90	80,07	3107,60	195,86	3209,57	35,19	96,82	1,37	3209,57	1,37	0,08
A-14	3433,25	16,89	98,04	A-239	A-239	21,75	8,33	0,62	8,11	0,97	0,25	1,90	3172,76	80,89	3110,77	200,18	3212,20	30,08	96,84	1,40	3212,20	1,40	0,09
A-15	3089,73	20,30	91,81	A-163	A-163	22,65	8,13	0,64	7,91	0,97	0,26	1,86	3211,90	79,03	3192,58	199,21	3223,99	29,33	99,03	0,46	3223,99	0,46	0,10
A-16	868,79	25,86	137,03	A-61	A-61	24,43	7,35	0,69	7,18	0,98	0,26	1,55	3285,72	71,65	3385,28	189,07	3225,53	24,51	104,95	0,77	3225,53	0,77	0,10
A-17	798,15	25,56	65,13	A-265	A-265	23,61	7,95	0,67	7,70	0,97	0,26	1,97	3252,25	77,41	3294,83	198,58	3226,10	31,14	102,13	0,24	3226,10	0,24	0,11
A-18	3408,82	19,68	88,41	A-132	A-132	25,06	8,24	0,71	8,10	0,98	0,26	1,50	3310,59	80,42	3451,63	216,42	3226,27	23,69	106,98	1,01	3226,27	1,01	0,12
A-19	3373,25	22,19	91,01	A-240	A-240	23,76	8,14	0,67	7,95	0,98	0,26	1,73	3258,46	79,29	3309,00	205,78	3227,50	27,35	102,52	0,73	3227,50	0,73	0,13
A-20	3439,87	18,34	110,79	A-137	A-137	23,29	7,72	0,66	7,61	0,99	0,26	1,29	3239,13	75,16	3256,65	194,63	3228,31	20,29	100,88	0,58	3228,31	0,58	0,14
A-21	3420,94	21,24	105,26	A-162	A-162	24,06	8,29	0,68	8,09	0,98	0,26	1,82	3270,70	80,85	3335,70	210,73	3231,09	28,68	103,24	0,99	3231,09	0,99	0,15
A-22	3301,74	20,19	115,24	A-109	A-109	21,75	9,20	0,61	8,84	0,96	0,26	2,56	3172,83	89,30	3079,61	216,36	3232,32	40,33	95,28	0,47	3232,32	0,47	0,16
A-23	3416,89	21,85	106,30	A-6	A-6	25,09	6,62	0,71	6,27	0,95	0,26	2,12	3311,64	64,61	3443,87	167,18	3232,56	33,50	106,54	1,15	3232,56	1,15	0,17
A-24	3454,95	17,29	108,32	A-124	A-124	23,09	8,24	0,65	7,88	0,96	0,26	2,42	3230,66	80,17	3222,47	199,73	3235,74	38,09	99,59	1,42	3235,74	1,42	0,18
A-25	3438,35	18,01	93,61	A-116	A-116	22,74	9,09	0,64	8,91	0,98	0,26	1,81	3215,93	88,46	3174,78	223,42	3241,70	28,59	97,94	0,96	3241,70	0,96	0,19
A-31	3275,47	22,76	75,05	A-32	A-32	25,91	6,97	0,72	6,41	0,92	0,26	2,73	3342,99	68,12	3509,62	173,48	3244,56	43,03	108,17	0,71	3244,56	0,71	0,20
A-32	3244,56	21,52	108,17	A-266	A-266	20,87	8,54	0,58	8,19	0,96	0,26	2,43	3132,36	82,75	2954,48	194,04	3248,43	38,28	90,95	0,56	3248,43	0,56	0,21
A-33	3449,72	11,04	117,55	A-63	A-63	22,23	6,62	0,62	6,30	0,95	0,26	2,05	3193,93	64,34	3104,32	155,10	3250,72	32,33	95,50	0,74	3250,72	0,74	0,22
A-34	3559,78	11,43	99,24	A-141	A-141	21,38	8,13	0,59	7,89	0,97	0,26	1,95	3156,13	78,84	3007,02	189,63	3252,36	30,64	92,46	0,91	3252,36	0,91	0,23
A-35	8332,85	33,74	29,60	A-87	A-87	21,23	11,41	0,59	10,20	0,89	0,26	5,12	3149,36	110,64	2989,82	243,94	3252,66	80,59	91,92	0,09	3252,66	0,09	0,24
A-36	3426,36	20,21	102,58	A-62	A-62	21,33	6,92	0,59	6,35	0,92	0,26	2,76	3153,69	67,16	2999,52	152,34	3253,32	43,42	92,20	1,25	3253,32	1,25	0,25
A-37	947,70	121,41	28,60	A-260	A-260	24,14	8,29	0,67	8,04	0,97	0,26	2,01	3274,13	80,78	3307,60	207,99	3253,69	31,60	101,66	1,29	3253,69	1,29	0,26
A-38	3264,20	18,02	51,14	A-96	A-96	23,03	8,28	0,64	8,03	0,97	0,26	2,02	3228,04	80,57	3186,28	201,83	3254,08	31,84	97,92	1,56	3254,08	1,56	0,27
A-39	2859,76	20,74	96,38	A-187	A-187	22,97	7,92	0,64	7,68	0,97	0,26	1,96	3225,56	77,10	3174,75	192,46	3257,31	30,88	97,47	0,72	3257,31	0,72	0,28
A-40	3435,79	19,56	108,20	A-248	A-248	20,65	8,31	0,57	8,00	0,96	0,26	2,26	3122,43	80,49	2934,93	187,51	3258,70	35,65	89,45	1,56	3258,70	1,56	0,29
A-41	3423,33	16,98	105,57	A-131	A-131	24,51	8,34	0,68	7,90	0,95	0,26	2,67	3288,81	81,35	3331,62	205,51	3262,81	42,02	102,11	0,84	3262,81	0,84	0,30

A-42	3375,66	20,74	101,31	A-269	A-269	23,65	8,13	0,65	7,71	0,95	0,26	2,60	3253,94	79,24	3229,09	195,73	3269,28	40,95	98,77	1,09	3269,28	1,09	0,30
A-43	2992,17	24,78	50,15	A-97	A-97	22,72	8,22	0,62	7,98	0,97	0,26	1,99	3215,00	79,94	3127,29	197,64	3270,19	31,23	95,63	1,12	3270,19	1,12	0,31
A-44	3449,77	17,90	82,77	A-181	A-181	22,21	8,49	0,61	8,22	0,97	0,26	2,10	3192,99	82,48	3069,07	200,82	3271,80	33,09	93,80	0,60	3271,80	0,60	0,32
A-45	3432,95	10,25	112,12	A-110	A-110	22,67	7,92	0,62	7,64	0,96	0,26	2,09	3212,93	77,00	3114,70	188,64	3274,84	32,88	95,11	1,38	3274,84	1,38	0,33
A-46	3382,38	21,60	103,13	A-262	A-262	24,72	8,25	0,68	7,85	0,95	0,26	2,51	3297,09	80,47	3333,62	204,43	3274,96	39,49	101,79	0,51	3274,96	0,51	0,34
A-47	3174,32	16,18	92,96	A-291	A-291	24,80	7,98	0,68	7,83	0,98	0,26	1,54	3300,40	77,84	3341,59	204,05	3275,48	24,23	102,02	0,65	3275,48	0,65	0,35
A-48	8332,85	42,14	36,61	A-164	A-164	25,60	7,95	0,70	7,77	0,98	0,27	1,68	3331,56	77,71	3424,00	206,46	3276,42	26,48	104,50	0,66	3276,42	0,66	0,36
A-49	2786,34	47,71	83,12	A-282	A-282	24,25	7,95	0,66	7,72	0,97	0,27	1,92	3278,41	77,54	3280,05	198,35	3277,40	30,20	100,08	0,80	3277,40	0,80	0,37
A-50	2851,55	26,65	77,27	A-283	A-283	24,66	7,94	0,67	7,60	0,96	0,27	2,31	3294,89	77,48	3312,99	196,81	3283,89	36,28	100,89	0,62	3283,89	0,62	0,38
A-56	3312,17	17,77	48,65	A-156	A-156	25,19	8,10	0,69	7,88	0,97	0,27	1,90	3315,44	79,12	3367,56	206,59	3284,07	29,81	102,54	1,54	3284,07	1,54	0,39
A-57	3447,14	19,95	78,54	A-263	A-263	21,93	8,16	0,59	7,88	0,97	0,27	2,11	3180,42	79,27	3003,03	189,26	3294,33	33,18	91,16	0,48	3294,33	0,48	0,40
A-58	3414,94	17,37	42,10	A-186	A-186	23,52	8,26	0,62	7,94	0,96	0,27	2,25	3248,56	80,41	3129,61	196,95	3322,84	35,21	94,18	0,81	3322,84	0,81	0,41
A-59	3426,37	15,67	103,70	A-215	A-215	27,69	8,86	0,72	8,58	0,97	0,28	2,20	3408,25	86,84	3495,90	231,63	3357,12	34,37	104,13	0,77	3357,12	0,77	0,42
A-60	3405,83	17,11	95,34	A-206	A-206	25,18	8,27	0,65	8,10	0,98	0,28	1,63	3315,06	80,73	3219,79	205,38	3373,18	25,44	95,45	0,86	3373,18	0,86	0,43
A-61	3225,53	12,26	104,95	A-19	A-19	23,71	7,56	0,61	7,01	0,93	0,28	2,84	3256,36	73,70	3069,93	171,20	3373,25	44,38	91,01	1,39	3373,25	1,39	0,44
A-62	3253,32	21,71	92,20	A-42	A-42	27,24	6,69	0,70	6,14	0,92	0,28	2,66	3392,03	65,55	3419,80	162,99	3375,66	41,48	101,31	0,37	3375,66	0,37	0,45
A-63	3250,72	16,17	95,50	A-46	A-46	28,06	6,95	0,72	6,37	0,92	0,28	2,77	3421,36	68,10	3488,31	171,60	3382,38	43,20	103,13	1,04	3382,38	1,04	0,46
A-64	3458,11	22,58	73,59	A-86	A-86	25,34	8,49	0,64	7,79	0,92	0,29	3,37	3321,49	82,93	3200,88	196,61	3395,10	52,48	94,28	0,45	3395,10	0,45	0,47
A-65	3449,64	13,29	84,38	A-67	A-67	26,55	7,17	0,67	6,70	0,93	0,29	2,54	3367,02	70,15	3315,38	173,72	3397,91	39,63	97,57	0,96	3397,91	0,96	0,48
A-66	8332,85	21,91	50,61	A-261	A-261	28,67	8,08	0,72	7,81	0,97	0,29	2,06	3442,38	79,24	3509,19	211,30	3403,72	32,08	103,10	0,58	3403,72	0,58	0,49
A-67	3397,91	19,81	97,57	A-60	A-60	25,99	6,75	0,65	6,38	0,95	0,29	2,20	3346,07	65,96	3247,20	162,70	3405,83	34,21	95,34	0,88	3405,83	0,88	0,50
A-68	3416,98	14,27	88,47	A-214	A-214	28,19	7,85	0,71	7,69	0,98	0,29	1,57	3425,75	76,95	3459,18	205,84	3406,26	24,42	101,55	0,64	3406,26	0,64	0,50
A-69	3419,15	15,88	79,84	A-120	A-120	26,40	8,23	0,66	7,97	0,97	0,29	2,04	3361,64	80,54	3284,23	205,20	3408,12	31,82	96,36	0,80	3408,12	0,80	0,51
A-70	3169,57	37,49	107,95	A-294	A-294	24,58	8,34	0,62	8,15	0,98	0,29	1,78	3291,71	81,39	3103,23	200,71	3408,60	27,72	91,04	0,82	3408,60	0,82	0,52
A-71	3391,25	19,33	80,66	A-93	A-93	25,46	8,68	0,64	8,38	0,97	0,29	2,26	3326,02	84,78	3183,70	210,51	3412,93	35,13	93,28	0,95	3412,93	0,95	0,53
A-72	3436,99	17,61	86,62	A-223	A-223	25,43	8,00	0,64	7,85	0,98	0,29	1,55	3325,05	78,13	3177,18	196,80	3415,44	24,08	93,02	0,94	3415,44	0,94	0,54
A-73	-5385,23	#WERT!	-86,90	A-268	A-268	30,64	8,03	0,77	7,79	0,97	0,29	1,97	3507,69	79,00	3671,28	218,04	3415,56	30,59	107,49	0,67	3415,56	0,67	0,55
A-74	3222,83	16,56	84,48	A-23	A-23	30,24	6,71	0,76	6,10	0,91	0,29	2,81	3494,72	65,99	3632,09	169,31	3416,89	43,69	106,30	1,09	3416,89	1,09	0,56
A-75	3456,25	13,45	78,61	A-200	A-200	27,59	8,18	0,69	8,07	0,99	0,29	1,34	3404,57	80,17	3382,73	212,44	3417,45	20,84	98,98	0,88	3417,45	0,88	0,57
A-81	3415,66	13,57	78,41	A-297	A-297	29,82	7,89	0,75	7,78	0,99	0,29	1,27	3480,74	77,48	3590,71	214,32	3418,04	19,69	105,05	0,30	3418,04	0,30	0,58
A-82	3445,41	17,92	86,87	A-21	A-21	29,98	6,56	0,75	5,96	0,91	0,29	2,73	3486,25	64,45	3601,03	164,50	3420,94	42,48	105,26	0,64	3420,94	0,64	0,59
A-83	3464,22	18,25	91,15	A-233	A-233	28,89	8,56	0,72	8,26	0,96	0,29	2,27	3449,92	84,06	3499,90	223,04	3421,03	35,30	102,31	2,36	3421,03	2,36	0,60
A-84	2935,74	30,33	37,24	A-115	A-115	28,43	8,27	0,71	7,89	0,95	0,29	2,48	3434,16	81,08	3454,98	210,94	3422,04	38,48	100,96	0,15	3422,04	0,15	0,61

A-85	3462,92	22,25	93,63	A-273	A-273	28,74	9,40	0,72	9,24	0,98	0,29	1,71	3444,73	92,23	3483,02	248,72	3422,54	26,56	101,77	0,89	3422,54	0,89	0,62
A-86	3395,10	26,24	94,28	A-41	A-41	30,17	6,81	0,75	6,45	0,95	0,29	2,19	3492,36	66,89	3613,96	178,32	3423,33	33,97	105,57	0,48	3423,33	0,48	0,63
A-87	3252,66	40,29	91,92	A-207	A-207	30,94	8,13	0,77	7,89	0,97	0,29	1,97	3517,14	80,01	3681,56	221,33	3424,78	30,68	107,50	0,87	3424,78	0,87	0,64
A-88	8339,04	35,10	22,98	A-293	A-293	26,78	8,69	0,67	8,49	0,98	0,29	1,88	3375,54	85,10	3291,54	218,80	3425,78	29,25	96,08	1,01	3425,78	1,01	0,65
A-89	3435,05	36,38	93,64	A-36	A-36	29,15	6,93	0,73	6,42	0,93	0,29	2,60	3458,72	68,03	3514,87	174,03	3426,36	40,42	102,58	0,68	3426,36	0,68	0,66
A-90	3470,87	22,08	95,33	A-59	A-59	29,57	7,06	0,74	6,77	0,96	0,29	2,02	3472,59	69,33	3553,29	184,80	3426,37	31,34	103,70	1,08	3426,37	1,08	0,67
A-91	2829,18	22,23	66,84	A-161	A-161	24,79	8,03	0,62	7,82	0,97	0,29	1,84	3300,12	78,37	3093,80	192,05	3427,96	28,58	90,25	0,68	3427,96	0,68	0,68
A-92	3463,25	37,66	92,70	A-175	A-175	29,72	8,04	0,74	7,84	0,97	0,29	1,81	3477,74	79,00	3563,19	214,47	3428,89	28,13	103,92	0,83	3428,89	0,83	0,69
A-93	3412,93	17,57	93,28	A-211	A-211	26,82	8,31	0,67	8,04	0,97	0,29	2,09	3376,85	81,30	3286,55	206,97	3430,88	32,47	95,79	1,15	3430,88	1,15	0,70
A-94	3270,75	14,46	78,47	A-234	A-234	29,56	7,93	0,73	7,71	0,97	0,29	1,86	3472,19	77,90	3543,05	210,16	3431,57	28,87	103,25	0,61	3431,57	0,61	0,70
A-95	3456,15	18,83	98,71	A-14	A-14	27,69	6,49	0,69	6,11	0,94	0,29	2,17	3408,31	63,59	3366,04	160,31	3433,25	33,77	98,04	2,03	3433,25	2,03	0,71
A-96	3254,08	15,92	97,92	A-258	A-258	29,38	7,98	0,73	7,75	0,97	0,29	1,89	3466,39	78,35	3522,60	210,40	3434,07	29,28	102,58	1,10	3434,07	1,10	0,72
A-97	3270,19	15,61	95,63	A-89	A-89	26,17	10,12	0,65	8,97	0,89	0,29	4,69	3352,73	99,01	3216,75	227,28	3435,05	72,76	93,64	0,82	3435,05	0,82	0,73
A-98	3448,75	18,95	94,12	A-272	A-272	25,00	8,43	0,62	8,13	0,97	0,29	2,21	3308,02	82,27	3102,45	200,26	3435,07	34,26	90,32	1,17	3435,07	1,17	0,74
A-99	3203,05	13,44	64,58	A-232	A-232	29,07	8,56	0,72	8,14	0,95	0,29	2,65	3455,85	84,04	3491,80	219,50	3435,08	41,13	101,65	0,85	3435,08	0,85	0,75
A-100	3170,05	17,39	65,60	A-160	A-160	28,57	8,10	0,71	7,96	0,98	0,29	1,52	3438,77	79,49	3443,92	212,37	3435,77	23,58	100,24	0,64	3435,77	0,64	0,76
A-106	3396,62	14,58	83,47	A-40	A-40	31,56	6,67	0,78	6,17	0,93	0,29	2,52	3536,69	65,62	3717,56	174,38	3435,79	39,13	108,20	0,75	3435,79	0,75	0,77
A-107	3339,02	18,05	53,92	A-182	A-182	31,79	8,35	0,79	8,12	0,97	0,29	1,94	3543,82	82,20	3737,35	230,35	3436,19	30,13	108,76	1,04	3436,19	1,04	0,78
A-108	3482,69	13,64	58,24	A-25	A-25	26,24	6,92	0,65	6,52	0,94	0,29	2,32	3355,49	67,70	3218,52	165,23	3438,35	36,02	93,61	1,89	3438,35	1,89	0,79
A-109	3232,32	20,17	95,28	A-238	A-238	24,99	8,66	0,62	8,35	0,96	0,29	2,31	3307,64	84,56	3095,63	205,21	3438,77	35,84	90,02	1,02	3438,77	1,02	0,80
A-110	3274,84	16,44	95,11	A-296	A-296	25,05	8,25	0,62	8,09	0,98	0,30	1,59	3310,23	80,51	3094,25	198,81	3443,76	24,75	89,85	0,99	3443,76	0,99	0,81
A-111	2939,42	18,60	69,27	A-119	A-119	27,66	8,18	0,68	7,81	0,96	0,30	2,41	3407,26	80,12	3340,28	203,69	3446,89	37,36	96,91	0,69	3446,89	0,69	0,82
A-112	2087,72	68,03	79,10	A-98	A-98	26,70	8,21	0,65	7,84	0,95	0,30	2,44	3372,60	80,34	3245,93	199,84	3448,75	37,89	94,12	1,06	3448,75	1,06	0,83
A-113	8339,04	56,68	22,63	A-236	A-236	25,37	8,47	0,62	8,05	0,95	0,30	2,62	3322,61	82,70	3116,23	198,93	3449,58	40,64	90,34	0,95	3449,58	0,95	0,84
A-114	3403,10	15,97	86,07	A-235	A-235	26,95	8,28	0,66	7,88	0,95	0,30	2,55	3381,60	81,08	3265,93	201,84	3450,87	39,63	94,64	0,97	3450,87	0,97	0,85
A-115	3422,04	19,24	100,96	A-148	A-148	29,32	8,05	0,72	7,80	0,97	0,30	2,01	3464,32	79,04	3485,82	209,92	3451,92	31,10	100,98	0,82	3451,92	0,82	0,86
A-116	3241,70	14,30	97,94	A-24	A-24	32,24	6,63	0,79	6,24	0,94	0,30	2,23	3557,51	65,30	3742,49	177,27	3454,95	34,58	108,32	0,71	3454,95	0,71	0,87
A-117	3114,07	17,50	89,99	A-95	A-95	28,59	8,15	0,70	7,78	0,95	0,30	2,43	3439,71	79,99	3411,56	206,17	3456,15	37,67	98,71	0,57	3456,15	0,57	0,88
A-118	3439,64	14,10	42,99	A-188	A-188	30,89	8,25	0,75	7,92	0,96	0,30	2,29	3515,56	81,10	3616,91	219,25	3458,31	35,53	104,59	0,99	3458,31	0,99	0,89
A-119	3446,89	18,68	96,91	A-299	A-299	26,05	8,28	0,63	7,92	0,96	0,30	2,42	3348,23	81,01	3162,02	198,00	3461,66	37,55	91,34	0,86	3461,66	0,86	0,90
A-120	3408,12	15,91	96,36	A-85	A-85	26,91	8,62	0,65	8,13	0,94	0,30	2,87	3380,10	84,38	3242,17	207,05	3462,92	44,51	93,63	0,43	3462,92	0,43	0,90
A-121	3013,32	20,50	73,18	A-92	A-92	26,58	9,06	0,65	7,64	0,84	0,30	4,86	3368,14	88,61	3210,60	193,22	3463,25	75,32	92,70	0,75	3463,25	0,75	0,91
A-122	3419,38	17,61	84,51	A-83	A-83	26,04	8,25	0,63	7,90	0,96	0,30	2,36	3348,14	80,62	3157,66	197,27	3464,22	36,50	91,15	0,98	3464,22	0,98	0,92

A-123	3281,28	14,21	61,00	A-174	A-174	30,86	8,11	0,75	7,84	0,97	0,30	2,08	3514,73	79,74	3602,02	216,28	3465,35	32,15	103,94	1,05	3465,35	1,05	0,93
A-124	3235,74	19,05	99,59	A-285	A-285	28,39	8,00	0,69	7,84	0,98	0,30	1,61	3432,50	78,51	3370,94	205,81	3468,62	24,95	97,18	1,32	3468,62	1,32	0,94
A-125	3182,60	15,25	71,93	A-90	A-90	27,76	8,64	0,67	8,15	0,94	0,30	2,85	3410,51	84,66	3308,70	211,03	3470,87	44,15	95,33	0,75	3470,87	0,75	0,95
A-131	3262,81	21,01	102,11	A-7	A-7	33,01	6,38	0,80	6,05	0,95	0,30	2,02	3580,84	62,91	3777,27	173,07	3472,72	31,33	108,77	1,00	3472,72	1,00	0,96
A-132	3226,27	11,85	106,98	A-242	A-242	28,92	8,11	0,69	7,74	0,95	0,30	2,41	3450,70	79,56	3391,94	204,09	3484,99	37,35	97,33	0,56	3484,99	0,56	0,97
A-133	3116,01	16,10	80,06	A-241	A-241	28,63	8,33	0,68	8,05	0,97	0,30	2,15	3440,93	81,72	3359,27	210,65	3488,82	33,31	96,29	1,08	3488,82	1,08	0,98
A-134	3226,03	14,94	86,92	A-271	A-271	28,57	8,66	0,66	8,33	0,96	0,31	2,34	3438,72	84,93	3260,18	213,26	3544,45	36,10	91,98	0,96	3544,45	0,96	0,99
A-135	3259,48	17,47	88,69	A-34	A-34	31,99	6,02	0,73	5,84	0,97	0,32	1,49	3549,98	59,30	3532,64	158,73	3559,78	22,87	99,24	0,67	3559,78	0,67	1,00

Geological Map of the Barberton Granitoid-Greenstone Terrane

Institut für Geowissenschaften
Friedrich-Schiller-Universität Jena

Editor: M. Schmitz

Cartography: M. Schmitz and M. Schlimme

Geological consultation:

C. Heubeck and J.-F. Moyen

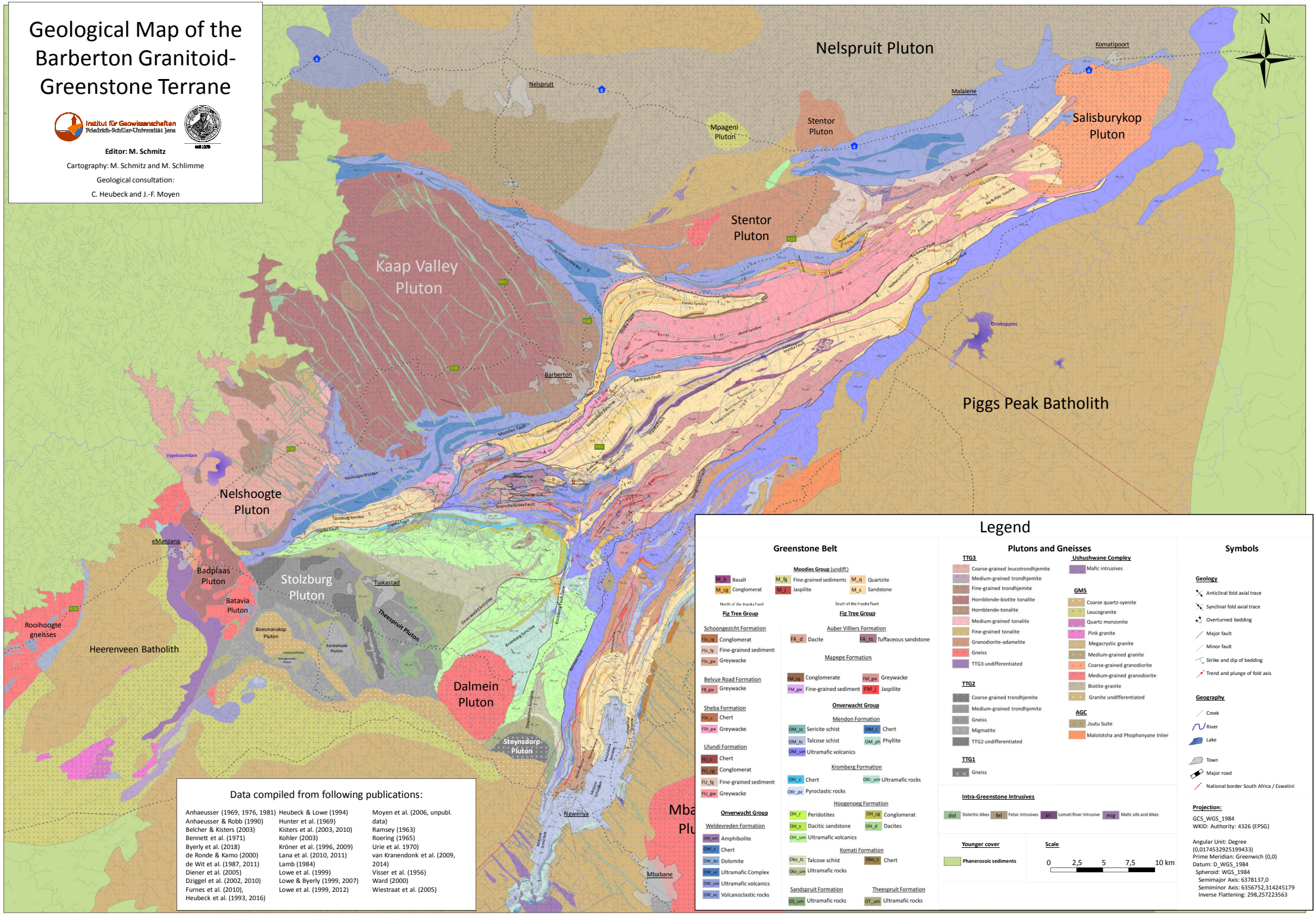

Legend

Greenstone Belt

Moodies Group (undiff.)
M_b Basalt; M_cg Conglomerat; M_fg Fine-grained sediments; M_j Jaspilite; M_q Quartzite; M_s Sandstone

North of the Inyoka Fault

Fig Tree Group

Schoongezicht Formation: FSc_cg Conglomerat; FSc_fg Fine-grained sediment; FSc_gw Greywacke

Belvue Road Formation: FB_gw Greywacke

Sheba Formation: FSh_c Chert; FSh_gw Greywacke

Ulundi Formation: FU_c Chert; FU_cg Conglomerat; FU_fg Fine-grained sediment; FU_gw Greywacke

Onverwacht Group

Weldevreden Formation: OW_am Amphibolite; OW_c Chert; OW_do Dolomite; OW_ud Ultramafic Complex; OW_um Ultramafic volcanics; OW_vc Volcanoclastic rocks

South of the Inyoka Fault

Fig Tree Group

Auber Villiers Formation: FA_d Dacite; FA_ts Tuffaceous sandstone

Mapepe Formation: FM_cg Conglomerate; FM_fg Fine-grained sediment; FM_gw Greywacke; FM_j Jaspilite

Onverwacht Group

Mendon Formation: OM_sc Sericite schist; OM_tc Talcose schist; OM_um Ultramafic volcanics; OM_c Chert; OM_ph Phyllite

Kromberg Formation: OKr_c Chert; OKr_pc Pyroclastic rocks; OKr_um Ultramafic rocks

Hoogenoeg Formation: OH_f Peridotites; OH_s Dacitic sandstone; OH_um Ultramafic volcanics; OH_cg Conglomerat; OH_d Dacites

Komati Formation: Oko_tc Talcose schist; Oko_um Ultramafic rocks; Oko_c Chert

Sandspruit Formation: OS_um Ultramafic rocks

Theespruit Formation: OT_um Ultramafic rocks

Plutons and Gneisses

TTG3
Coarse-grained leucotrondhjemite; Medium-grained trondhjemite; Fine-grained trondhjemite; Hornblende-biotite tonalite; Hornblende-tonalite; Medium-grained tonalite; Fine-grained tonalite; Granodiorite-adamelite; Gneiss; TTG3 undifferentiated

TTG2
Coarse-grained trondhjemite; Medium-grained trondhjemite; Gneiss; Migmatite; TTG2 undifferentiated

TTG1
Gneiss

Ushushwane Complex
Mafic intrusives

GMS
Coarse quartz-syenite; Leucogranite; Quartz monzonite; Pink granite; Megacrystic granite; Medium-grained granite; Coarse-grained granodiorite; Medium-grained granodiorite; Biotite-granite; Granite undifferentiated

AGC
Jsutu Suite; Malolotsha and Phophonyane Inlier

Intra-Greenstone Intrusives
dol Doleritic dikes; fel Felsic intrusives; lri Lomati River Intrusive; mig Mafic sills and dikes

Younger cover
Phanerozoic sediments

Scale
0 2,5 5 7,5 10 km

Symbols

Geology
Anticlinal fold axial trace; Synclinal fold axial trace; Overturned bedding; Major fault; Minor fault; Strike and dip of bedding; Trend and plunge of fold axis

Geography
Creek; River; Lake; Town; Major road; National border South Africa / Eswatini

Projection:
GCS_WGS_1984
WKID: Authority: 4326 (EPSG)

Angular Unit: Degree (0,0174532925199433)
Prime Meridian: Greenwich (0,0)
Datum: D_WGS_1984
Spheroid: WGS_1984
Semimajor Axis: 6378137,0
Seminor Axis: 6356752,314245179
Inverse Flattening: 298,257223563

Data compiled from following publications:

Anhaeusser (1969, 1976, 1981)
Anhaeusser & Robb (1990)
Belcher & Kisters (2003)
Bennett et al. (1971)
Byerly et al. (2018)
de Ronde & Kamo (2000)
de Wit et al. (1987, 2011)
Diener et al. (2005)
Dziggel et al. (2002, 2010)
Furnes et al. (2010),
Heubeck et al. (1993, 2016)
Heubeck & Lowe (1994)
Hunter et al. (1969)
Kisters et al. (2003, 2010)
Kohler (2003)
Kröner et al. (1996, 2009)
Lana et al. (2010, 2011)
Lamb (1984)
Lowe et al. (1999)
Lowe & Byerly (1999, 2007)
Lowe et al. (1999, 2012)
Moyen et al. (2006, unpubl. data)
Ramsey (1963)
Roering (1965)
Urie et al. 1970)
van Kranendonk et al. (2009, 2014)
Visser et al. (1956)
Ward (2000)
Wiestraat et al. (2005)